ISSN: 2408-2384 (Online)

# Environment and Natural Resources Journal

Volume 22, Number 1, January - February 2024

# Environment and Natural Resources Journal (EnNRJ)
Volume 22, Number 1, January - February 2024 ISSN: 2408-2384 (Online)

## AIMS AND SCOPE

The Environment and Natural Resources Journal is a peer-reviewed journal, which provides insight scientific knowledge into the diverse dimensions of integrated environmental and natural resource management. The journal aims to provide a platform for exchange and distribution of the knowledge and cutting-edge research in the fields of environmental science and natural resource management to academicians, scientists and researchers. The journal accepts a varied array of manuscripts on all aspects of environmental science and natural resource management. The journal scope covers the integration of multidisciplinary sciences for prevention, control, treatment, environmental clean-up and restoration. The study of the existing or emerging problems of environment and natural resources in the region of Southeast Asia and the creation of novel knowledge and/or recommendations of mitigation measures for sustainable development policies are emphasized.

The subject areas are diverse, but specific topics of interest include:

- Biodiversity
- Climate change
- Detection and monitoring of polluted sources e.g., industry, mining
- Disaster e.g., forest fire, flooding, earthquake, tsunami, or tidal wave
- Ecological/Environmental modelling
- Emerging contaminants/hazardous wastes investigation and remediation
- Environmental dynamics e.g., coastal erosion, sea level rise
- Environmental assessment tools, policy and management e.g., GIS, remote sensing, Environmental Management System (EMS)
- Environmental pollution and other novel solutions to pollution
- Remediation technology of contaminated environments
- Transboundary pollution
- Waste and wastewater treatments and disposal technology

**Schedule**
Environment and Natural Resources Journal (EnNRJ) is published 6 issues per year in January-February, March-April, May-June, July-August, September-October, and November-December.

**Publication Fees**
There is no cost of the article-processing and publication.

**Ethics in publishing**
EnNRJ follows closely a set of guidelines and recommendations published by Committee on Publication Ethics (COPE).

# Environment and Natural Resources Journal (EnNRJ)
Volume 22, Number 1, January - February 2024 ISSN: 2408-2384 (Online)

**Editorial Office Address**
Research Management and Administration Section,
Faculty of Environment and Resource Studies, Mahidol University
999, Phutthamonthon Sai 4 Road, Salaya, Phutthamonthon, Nakhon Pathom, Thailand, 73170
Phone +662 441 5000 ext. 2108 Fax. +662 441 9509-10
Website: https://ph02.tci-thaijo.org/index.php/ennrj/index
E-mail: ennrjournal@gmail.com

# Environment and Natural Resources Journal (EnNRJ)

Volume 22, Number 1, January - February 2024 ISSN: 2408-2384 (Online)

## CONTENT

# Biosorption of Toxic Reactive Blue Textile Dye from Effluent Water Using Immobilized Biomass Based Adsorbent

**Tanjore Ramachandran Sundararaman[1], Sivamani Sivalingam[1*], Melvin Millicent Mabel[2], and Trisha Gobinath[2]**

*[1]Department of Chemical Engineering, Rajalakshmi Engineering College, Thandalam, Chennai-602105, Tamilnadu, India*
*[2]Department of Biotechnology, Rajalakshmi Engineering College, Thandalam, Chennai-602105, Tamilnadu, India*

**ARTICLE INFO**

Received: 20 Jul 2023
Received in revised: 4 Nov 2023
Accepted: 10 Nov 2023
Published online: 13 Dec 2023
DOI: 10.32526/ennrj/22/20230192

**Keywords:**
Biosorption/ Reactive blue dye/ Immobilization/ *Canna indica* beads/ Isotherms/ Kinetics

*** Corresponding author:**
E-mail: sivamchem@gmail.com; sivamani.s@rajalakshmi.edu.in

**ABSTRACT**

The present research employed immobilized *Canna indica* beads (CIBs) to obtain maximum degradation of highly toxic Reactive Blue Dye (RBD), predominantly used in textile industry. The CIBs were characterized using FTIR and SEM-EDX analysis. A batch adsorption study was conducted to measure the removal of harmful RBD dye. Different factors were examined in the biosorption technique to achieve the maximum level of toxic dye elimination, such as adsorbent-solute interaction time (5-120 min), solution pH (2-10), adsorbent dose (25 to 250 mg/100 mL), RBD concentration (50-250 mg/L), and temperature (30-60°C). Removal of 99.96% of RBD was successfully achieved at the optimum pH 7, RBD concentration of 50 mg/L, adsorbent dosage of 150 mg/100 mL, a temperature of 303 K, and 60 min of interaction time. The Langmuir isotherm and pseudo-second-order (PSO) kinetic model data have been found to be an ideal match compared to the Freundlich isotherm and pseudo-first-order (PFO) kinetic model. The maximum adsorption capacity onto CIBs biosorbent was found to be 70.49 mg/g. It was noticed that the chemical reaction occurred naturally and released heat during the process which denoted an exothermic reaction. These results shown that the adsorption of RBD removal is efficient using prepared adsorbent from *Canna indica* root tubers. Therefore, these CIBs could be used for other toxic dyes and heavy metals from industrial wastewater.

## 1. INTRODUCTION

Water is a precious resource that supports human progress and all living microorganisms life on Earth. Aquatic organisms are depend on water bodies for survival. Textile industry dyes are incredibly poisonous to aquatic environments, which prevent light and oxygen from reaching the water and it can reduce photosynthesis (Sivalingam et al., 2019; Sivalingam and Sen, 2019). The textile business is massive, employing around 35 million people throughout the globe, and earns almost $1 trillion in sales annually (Desore and Narula, 2018). Discharging untreated effluents from textile industries into water bodies is one example of anthropogenic activities that pollute and make water unusable (Bhatia et al., 2017). Fabric, paint, and pigment dyes have been used over millennia in the textile industries, and they have many more uses outside just coloring the fabric (Kosaiyakanon et al., 2020). Around one million distinct varieties of dyes are available in the market, and they are crucial in the production of textiles, paints, and pigments (Ali, 2010). Dyes are partially or entirely saturated chemical substances that absorb light to generate color. As much as 50% of the colors used never make it onto the fiber and act as contaminants in the liquid phase (Rehman et al., 2020; Yuan et al., 2020). Hence need to purify the dye-colored industry water that can be used as treated water for industry and humans' day-to-day activities.

Several methods for removing pollutants from effluents are available including adsorption, cementation, ion exchange, membrane filtration, precipitation, solvent extraction, evaporation, chemical oxidation, and electrochemical processes and so on. From these methods, adsorption is highly effective one for effective wastewater treatment since

**Citation:** Sundararaman TR, Sivalingam S, Mabel MM, Gobinath T. Biosorption of toxic reactive blue textile dye from effluent water using immobilized biomass based adsorbent. Environ. Nat. Resour. J. 2024;22(1):1-12. (https://doi.org/10.32526/ennrj/22/20230192)

adsorbents are inexpensive and available easily (Kyzas and Kostoglou, 2014; Midha and Dey, 2008). Adsorption is used for a large-scale method of separation, purification, and detoxification process which has been increasing significantly last few decades; and also it removes impurities from gasses and liquids with their color, odor, and isolation (Wang et al., 2018). The interaction force of affinity between adsorbent and adsorbate in the adsorption is most significant in this ternary system (Gunarathne et al., 2018; Sivalingam and Sen, 2019). Biosorbents can refer to either living or non-living biomass, including plants, algae (cyanobacteria, unicellular and multicellular microalgae), bacteria, and fungi. A few examples of dead biomass are forest by-products, fibers, peat, rice hulls, chitosan polymer, and agro-food waste. Most places have access to biosorbents, inexpensive filter materials with excellent binding capacity and selectivity (Gupta et al., 2015).

Commercial activated carbons (CAC) are generated from agro-industry waste and by products from different industry, whereas commercial ion-exchange resins are made from natural substances such as clays and red mud. These commercial substances are the traditional preferable adsorbents for pollutant degradation, but their cost-effectiveness limits to use huge amount in industry level. Commercial carbons manufactured from more expensive feedstocks that are often not worth to expense, even though they could be effective in specific pollution control and environmental applications. Because of their low-cost and incredible efficiency, developing the green adsorbents from waste sources like industrial, agricultural, and forest product (Bhatia et al., 2017; Rehman et al., 2020).

Sodium alginate is a brown algal polymer that occurs naturally, and it is unique because of its high biocompatibility, biodegradability, and renewability. High adsorption affinity is another feature since it has numerous hydroxyl and carboxyl groups. It has been demonstrated that sodium alginate's carboxyl and pyranose oxygen atoms may form stable five-membered chelates rings, which could be exploited as requisite sites in adsorption process (Paudyal et al., 2013). Sodium alginate has weak mechanical power, poor thermal stability, and short shelf life (Wang et al., 2018). Plants can aid in the breakdown of human and animal wastewater and removal of disease-causing germs and contaminants. Their potent to adsorb various contaminants has been acknowledged globally in water treatment sector (Ansari et al., 2020). *Canna indica*, also known as Indian shot, is a native of America and a member of the Cannaceae family. *Canna indica* is widely used as an adsorbent, food, and medicine and is available in abundance. When it is grown on a microscopic scale, this plant can absorb heavy metals, including lead, chromium, zinc, nickel, and cadmium (Dixit et al., 2014).

The naturally occurring bioplastics, and chitin are nearly equal to the cellulose characteristics. It has several valuable properties for modification during derivative synthesis because of its lengthy polymeric chain as a polysaccharide. N-acetyl-D-glucosamine is associated by b-1, 4 units that share many chemical characteristics with cellulose, exception of the acetamido group at carbon-2 in cellulose (Karthikeyan et al., 2005). Crustacean exoskeletons, especially those of shrimp and crabs, are rich in chitin (Gonzalez et al., 2018). It has several eco-friendly qualities, such as biodegradable, biocompatible, non-toxic, porous, and light respectively. Shrimp shells are considered large-scale waste worldwide, and many developing countries dump them directly into the sea. Chitin can be extracted directly from these shells in large quantities using a simple and cost-effective process (Elieh-Ali-Komi and Hamblin, 2016). However, the inability of chitin to dissolve in water limits their use on a large scale (Hamed et al., 2016). This study aims to prepare CIBs from *Canna indica* root tuber as an adsorbent and analyse with FTIR and SEM techniques. The prepared adsorbent will use to produce clean water from RBD dye contained wastewater.

## 2. METHODOLOGY

### 2.1 Chemicals and materials used

Reactive Blue Dye was procured from Sigma-Aldrich. All other essential chemicals used in this study, including HCl and NaOH, were procured from HiMedia Laboratories Pvt. Ltd., Mumbai, India. To produce immobilized beads, *Canna indica* plant saplings were sourced from the Kaivalya Garden Center located in Anna Nagar, Chennai, Tamil Nadu, India. *Canna indica* is a frequently employed plant for the remediation of industrial wastewater.

### 2.2 RBD aqueous solution preparation

RBD is one of the toxic dye present in textile industry, with a 637.43 g/mol molecular weight and $C_{23}H_{14}Cl_2N_6O_8S_2$ molecular formula. The RBD stock solution of 1.0 L was set by dissolving 1.0 g of dye in of double-distilled water. The stock solution was

diluted to the appropriate working solution concentration (between 10 and 100 mg/L) in double-distilled water for the batch adsorption experiment. 0.1 N HCl and 0.1 M NaOH were used to modify the pH of the working solutions.

### 2.3 Adsorbent preparation

The tubers of the *canna indica* plant were dried for three hours at 80°C after peeling. It was grounded using a mortar and pestle to make a fine powder and stored under sterile conditions for later use. 1.0 g to 4.0 g powder was combined with 3% sodium alginate and chitin, respectively, dissolved in acetic acid. The required 2-3 mm size of the immobilized *Canna indica* root tuber beads was achieved by slowly infusing sodium alginate and chitin in a 4% (w/v) of calcium chloride solution. To enhance the mechanical stability, CIBs were applied in curing process with 4% of calcium chloride solution for 4 h. The beads were continuously washed in double distilled water and filtered using Whatman 42 size filter paper up to reaching pH 7. Later, the characterization and adsorption process was carried out with prepared immobilized beads.

### 2.4 Adsorbent characterization

The different analysis methods are used to identify the properties of prepared CIBs adsorbent. FTIR (Fourier Transform Infrared) spectroscopy techniques are used to find the availability of various functional groups present in the adsorbent and using SEM (Scanning Electron Microscopy) techniques the surface morphology of the immobilized beads were investigated.

### 2.5 Batch adsorption

The adsorption process of RBD was performed in a batch experiments. The several parameters are influencing adsorption technique, including pH, RBD concentration, CIBs dose, contact time, adsorbent dose, and temperature were examined in a series of adsorption trials. This adsorption was performed with varying one parameter to evaluate and rest of the parameter has been fixed. Numerous experimental conditions were used to check the optimum results as follows: initial RBD dye concentration: 50 to 250 mg/L, adsorbent dosage: 25 to 250 mg/100 mL, the solution pH: 2 to 10, temperature: 303 to 333 K, contact time: 5 to 120 min. The required amount of immobilized beads were added in 100 mL of RBD solution which placed in the incubator shaker at the speed of 120 rpm. Supernatant solution was collected using Whatman 42 filter paper after the stipulated time, and dye removal was calculated by measuring the absorbance value of 580 nm (Shimadzu: UV-1900i double-beam spectrophotometer). The percentage of RBD removal was calculated using the following Equation (1),

$$\% \text{ Removal} = \frac{C_o - C_e}{C_o} \times 100 \quad (1)$$

Where; $C_0$ and $C_e$ are RBD's initial and final solution (mg/L), respectively.

### 2.6 Equilibrium adsorption isotherm

The batch adsorption experiment was conducted between 50 to 250 mg/L RBD concentration. 100 mg/100 mL of immobilized beads were placed in each flask, then incubated in the shaker incubator at 303 K temperature for 60 min. Following the specified incubation period, the supernatant solution was collected from filteration process and measured UV Vis-spectroscopy by 580 nm absorbance. The equilibrium adsorption of RBD onto the immobilized beads can be calculated using Equation (2) (Gonzalez et al., 2018):

$$q_e = (C_i - C_e)\, V/m \quad (2)$$

Where; $q_e$ is the capacity of adsorption (mg/g), $C_i$ and $C_e$ are initial and equilibrium RBD concentrations (mg/L), V is volume of RBD solution (L), and M is the weight of CIBs used (g) (Assimeddine et al., 2021). Equilibrium isotherms are commonly employed for assessing an adsorbent's capacity, surface characteristics, and binding affinity. Langmuir and Freundlich isotherm models were utilized to know monolayer (homogeneious) and multilayer (heterogeneous) sites on the immobilized beads. The adsorption isotherm parameters, adsorption capacity (mg/g) and correlation coefficient [$R^2$], were calculated using a non-regression analysis in ORIGINPRO 9.0 software.

### 2.7 Adsorption kinetics study

The adsorption kinetic study reports the uptake of RBD from aqueous solutions with constant concentration. Adsorption kinetics were carried out in RB flasks containing 100 mL of 100 mg/L RBD concentration along with 100 mg/100 mL of immobilized CIB at 303 K in a shaking incubator for

60 min. After 60 min, the solution was filtered, and a colorimeter was used to measure the absorbance of the dye on the immobilized beads at 580 nm. The quantity of RBD adsorbed on the immobilized beads was determined using Equation 2 (Katheresan et al., 2018). The adsorption rate can be expressed as PFO, PSO and mixed adsorption kinetic models.

### 2.8 Thermodynamic study

The adsorption of RBD onto immobilized CIBs was subjected to thermodynamic investigation. At 303 to 333 K temperatures, the thermodynamic study was conducted with 100 mL of 100 mg/L RBD concentration and immobilized CIBs. Gibbs free energy (ΔG°), change in enthalpy (ΔH°), and change in entropy (ΔS°) are the crucial thermodynamic factors could be calculated using the given equation in Table 3.

## 3. RESULTS AND DISCUSSION

### 3.1 Immobilized CIBs characterization

The CIBs adsorbent analysis of before and after adsorption process is important to get the changes occurred on the prepared adsorbent. The FTIR analysis was conducted with wavenumber from 400 to 4,000 1/cm region, as shown in Figure 1. Figure 1(a) can be seen that there are four significant peaks formed at different wavenumbers (1,087, 1,621, 3,102, and 3,840 1/cm). The C-O stretching in ether is formed at 1,087 and 1,032 1/cm peaks. Because of C=O stretching vibration, the peaks at 1,621 are produced (Amide I). Figure 1(b) shows distinct significant peaks at various wavenumbers: 1,032, 1,612, and 3,514 1/cm. The vibration mode of the strong hydrogen-bonded O-H stretching of the alcohol is seen at 3,514 1/cm, similar spectra has been reported by Venkatesh and Arutchelvan (2020).

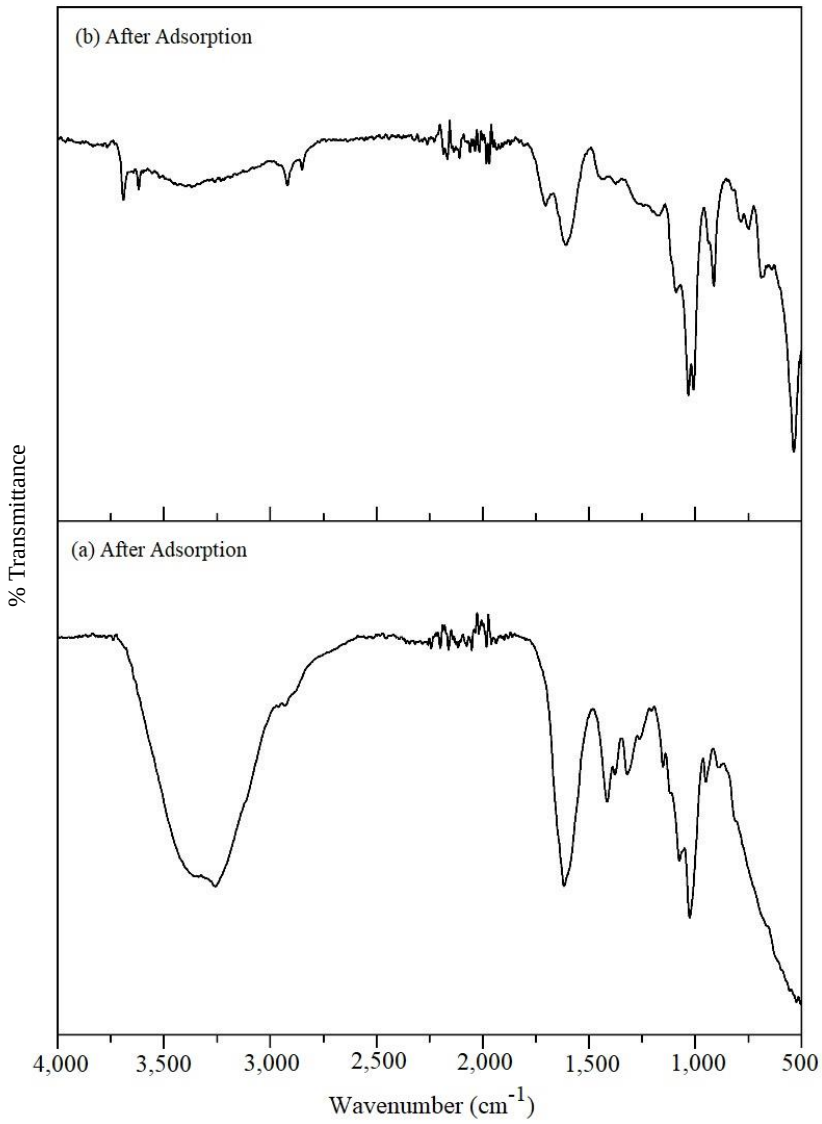


**Figure 1.** FTIR spectra of CIBs (a) before adsorption, (b) after adsorption

As adsorption process takes place at the surface of an adsorbent, its very sensitive to surface features, such as the pore size distribution. Figure 2(a-b) displays the morphology images of SEM analysis for immobilized CIBs taken prior to adsorption. Figure 2(c-d) shows the morphology images of the SEM study of immobilized CIBs after adsorption. The SEM images captured the both before and after adsorption process to find the changes in the CIBs surfaces clearly and distinctly (Wang et al., 2018). When the surface smoothness is examined, can be seen from Figure 2(a-b) possessing more pores, bigger cavities, and nonporous solid material. During the adsorption process the RBD molecules were fills out in fewer pores and reduces pore size, as demonstrated in Figure 2(c-d). These results are accepted that the immobilized CIBs have prevalent adsorption limits concerning the adsorption of RBD molecules. Elemental analysis also obtained from SEM where can be found the weight and atomic % of various elements. Figure 2 clearly depicting the Ca, Cl, and Na percentage changes after the adsorption process which has confirming the RBD dye molecule interaction and CIBs particle.

### 3.2 Optimization of adsorption process

In adsorption process, the contact time is a crucial parameter since it provides insights on the kinetics required to complete interaction with the CIBs surface. All other factors were held constant while the impact of contact time was examined by varying the intervals from 5 to 120 min at room temperature with a pH of 7 in a rotary shaker at 120 rpm and 150 mg/100 mL adsorbent dose, can be seen in Figure 3(a). Figure 3(a) illustrates the removal percent of RBD dye at various contact time. The adsorption increased to a more significant proportion as the interating duration has been monitored between 5 to 120 min, and observed that after 60 min there was no changes occured. At 60 min of treatment the RBD removal from an aqueous solution was adsorbed 99.20%. This is caused by the early presence of highly active sites and the destabilization of the driving force. As the duration rises, the dye's ability to bind to the active sites becomes less and less until it reaches the equilibrium (Venkatesh and Arutchelvan, 2020; Sun et al., 2013).

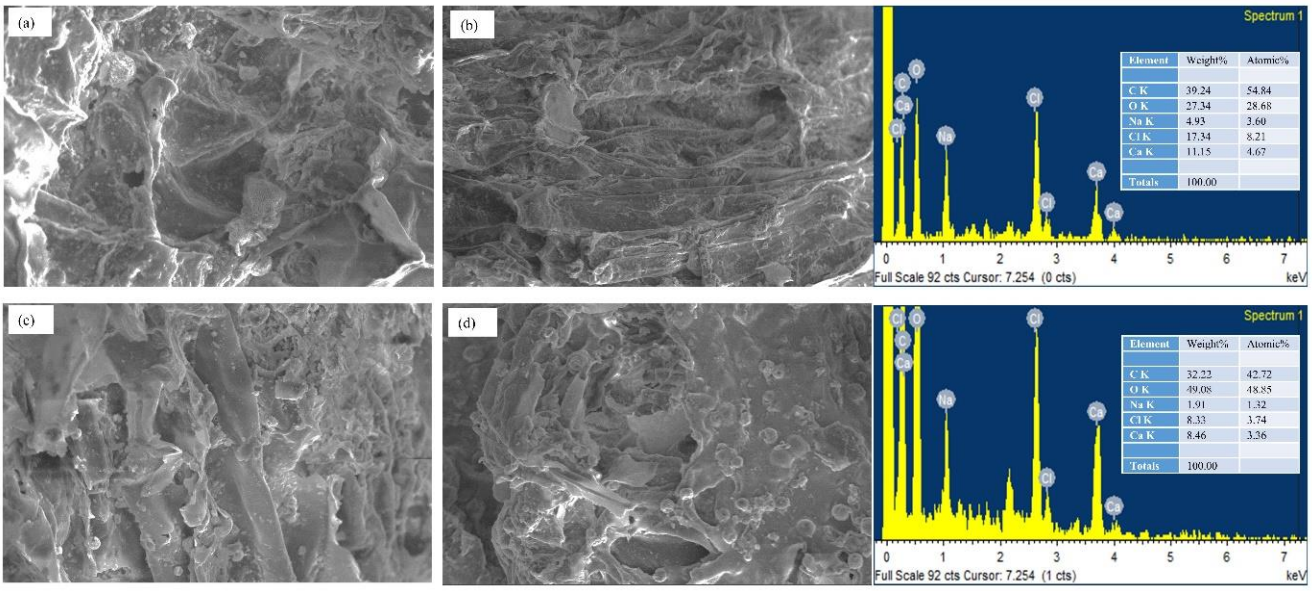


**Figure 2.** Surface morphology results of immobilized CIBs (a-b) before adsorption, (c-d) after adsorption

The removal of RBD varies dosages of suspended CIBs is shown in Figure 3(b).The amount of the adsorbent used has a significant impact on the method used to calculate an adsorbent capacity for a certain amount of adsorbent. The working experiment is done at room temperature at pH 7 in a rotary shaker operating at 120 rpm. This condition is ideal for the thorough distribution of particles and molecules in an aqueous solution. For the analysis, various adsorbent dosages ranging from 25 to 250 mg/100 mL. The adsorbent dosage with a 150 mg/100 ml yielded of 99.96% RBD dye adsorption because of availability of vast pores, adsorbent's capacity, and surface characteristics (Sivalingam and Sen, 2019). The % removal of dye that is adsorbed onto immobilized CIBs is significantly influenced by the RBD's initial

concentration, as shown in Figure 3(c). Optimal results were obtained when the process was performed at standard working settings of 303 K, pH 7, 120 rpm agitation, and 60 min of contact time. From 25 to 250 mg/L RBD concentrations were accounted to conduct the experiment with an intervals 50 mg/L. As shown in Figure 3(c) RBD removal has achieved of 99.04% at 50 mg/L solution. Additionally, it was noted that the original dye concentration increases the rate of RBD removal from an aqueous solution got reduced (Venkatesh and Arutchelvan, 2020).

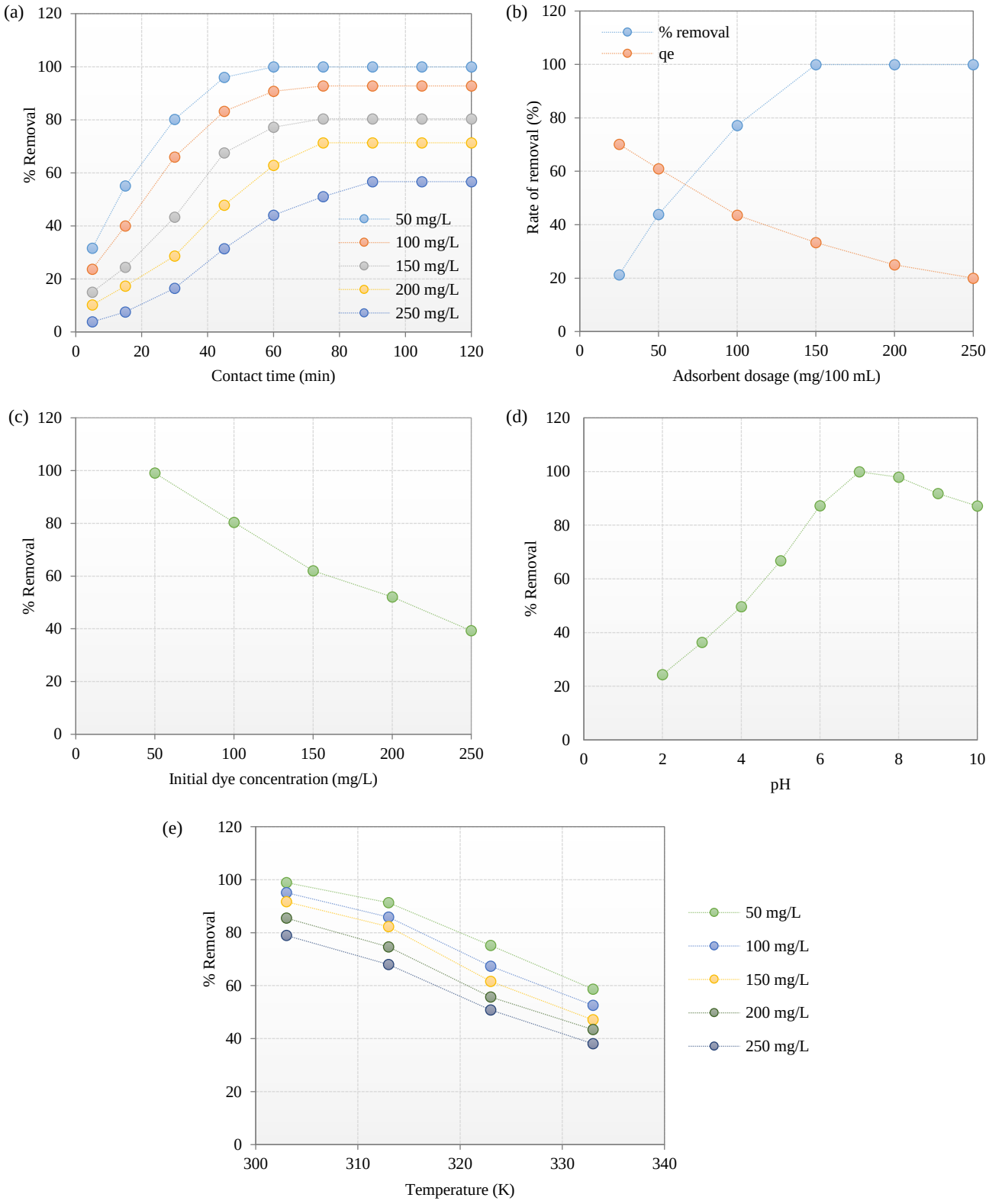


**Figure 3.** Removal of RBD, (a) contact time, (b) biosorbent dosage, (c) dye concentration, (d) pH, (e) temperature

Figure 3(d) shows the study of pH optimization for dye removal. The RBD concentration in the aqueous solution was studied by varying the pH from 2 to 10 at 303 K, 120 rpm, with the optimized dosage of adsorbent and contact time. As the pH of the solution increased from 2 to 7, the proportion of adsorbed dye increased, and the final removal was 98.88% at the optimum pH of 7. The CIB-stabilized RBD adsorption temperature dependence is shown in Figure 3(e). Varying temperatures such as 303, 313, 323, and 333 K were used for the analysis. As shown in Figure 3(e), a minimum quantity of the RBD was adsorbed by the immobilized CIBs as the temperature increased. This is due to the fading attraction between the dye and the immobilized beads, and the process suggests that it is exothermic nature (Kosaiyakanon et al., 2020).

### 3.3 Adsorption isotherm

The isotherm study giving better clarity as interaction occurs between the immobilized CIBs and the RBD in the liquid medium. Adsorption isotherms, often expressed as the ratio of the amount adsorbed to the amount still in solution, describe the equilibrium connection between an adsorbent and an adsorbate at a specific temperature. Two different models were used to examine the equilibrium adsorption isotherm, namely Langmuir and Freundlich which often called the two-parameter adsorption isotherms (Venkatesh and Arutchelvan, 2020). The correlation coefficient ($R^2$), extreme monolayer ability of adsorption ($q_m$), and error values like SSE and RMSE were assessed using the ORIGINPRO 9.0 software utilizing the experimental data and non-linear equation (Table 1).

**Table 1.** The adsorption results of isotherm models, kinetic models, and thermodynamic study

| Isotherm models | Formula | Parameters | Values |
|---|---|---|---|
| Langmuir isotherm | $q_e = \frac{q_m K_L C_e}{1 + K_L C_e}$ | $Q_m$ (mg/g) | 70.49 |
| | | $K_L$ (L/mg) | 2.104 |
| | | $R^2$ | 0.988 |
| Freundlich isotherm | $q_e = K_F C_e^{1/n}$ | $K_F$ ((mg/g (L/mg)$^{1/n}$) | 6.328 |
| | | n | 0.476 |
| | | $R_L$ | 0.0094 |
| | | $R^2$ | 0.939 |

The isotherm study demonstrates the adsorbate adsorbed by CIBs adsorbent is directly proportional to the equilibrium RBD adsorbate in the solution. The effectiveness of adsorption isotherm was analyzed by calculating the dimensionless constant RL. The known linear growth of the Langmuir isotherm (Figure 4) is obtained by the values for the (Langmuir constant: L/mg) $k_L$, (maximum sorption capacity: mg/g) $q_m$, and (equilibrium concentration of RBD solution: mg/L) $C_e$. Freundlich isotherm graph of adsorption capacity vs. adsorption intensity is shown in Figure 4. $K_F$ and n are determined from the $q_e$ vs. $C_e$ plot (intercept and slope). The separation factor ($R_L$) is calculated, for 50 mg/L (0.0094), 100 mg/L (0.0047), 150 mg/L (0.0031), 200 mg/L (0.0023), and 250 mg/L (0.0018). The $R_L$ value gives feasibility, which can be either $R_L$>1 shows unfavorable condition, $R_L$=1 means linear, 0 < $R_L$ <1 ensure favorable situation, or $R_L$=0 confirms the process is favourable, these all condition indicates the form of the isotherm (Venkatesh and Arutchelvan, 2020). *Canna indica* has a linear Laungmuir isotherm with a high value of $R^2$ ($R^2$=0.988), indicating the adsorption of RBD (Table 1).

### 3.4 Adsorption kinetics

The various parameters such as changing the contact period from 5 to 120 min, RBD solution from 25 to 250 mg/L, temperature (303K), and the number of immobilized CIBs respectively, were studied. The removal rate of RBD from prepared solution was calculated using adsorption kinetic models, including a PFO model and a PSO model (Kosaiyakanon et al., 2020). The values of numerous adsorption kinetic model parameters like rate constant (k), correlation coefficient ($R^2$), and equilibrium adsorption capacity ($q_e$) etc were calculated using ORIGINPRO 9.0 software.

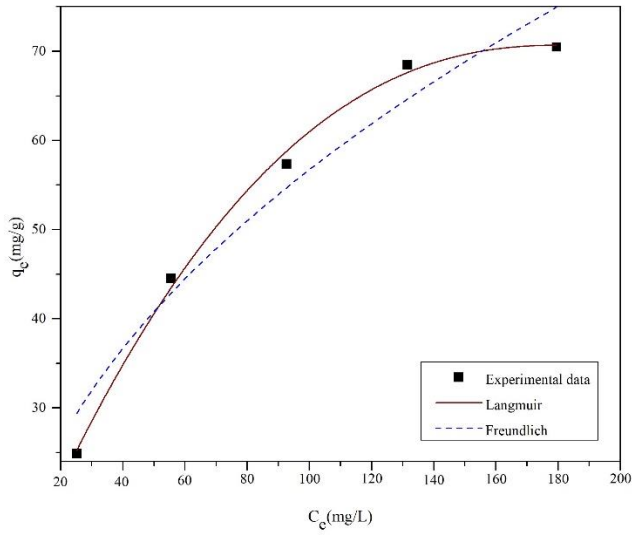


**Figure 4.** RBD adsorption isotherm model of Langmuir, and Freundlich model

The value of first-order rate constant is 0.1006 1/min (Figure 5(a) and Table 2) and second-order rate constant value of 0.0056 1/min (Figure 5(b) and Table 2) are determined onto immobilized CIB adsorbent. According to the rate constant values, the RBD varied for more active positions on the surface of the immobilized CIBs as the initial RBD concentration and contact duration grew (Riyanti et al., 2023). The equilibrium adsorption capacity ($q_e$(exp)) of CIBs used to eliminate RBD from the prepared solution was related with the estimated adsorption capacity ($q_e$(cal)) values using the ORIGINPRO 9.0 software. The type of adsorption kinetic model was best explained by evaluating the $q_e$ and the correlation coefficient (Yuan et al., 2020). Adsorption capacity ($q_e$) values derived from experiments at equilibrium ($q_e$(exp)) are more closely correlated with values obtained from the PSO model ($q_e$). The findings showed that the PSO model provided the best match compared to the PFO model when CIBs were used to remove RBD from an aqueous environment. The physisorption process has described using both the kinetic models (Venkatesh and Arutchelvan, 2020). RBD was adsorbed onto immobilized CIBs, and the more significant correlation coefficient ($R^2$) value between the PFO and PSO models proved that physisorption takes place in the reaction.

### 3.5 Thermodynamic study

In a study of the spontaneousness, unpredictability, feasibility, and nature of the adsorption of RBD onto immobilized CIBs, thermodynamic metrics, including ΔG° (Gibbs free energy), ΔS° (change in entropy), and ΔH°(change in enthalpy) are used to characterize the process. Immobilized CIB thermodynamic data for RBD removal are shown in Figure 6.

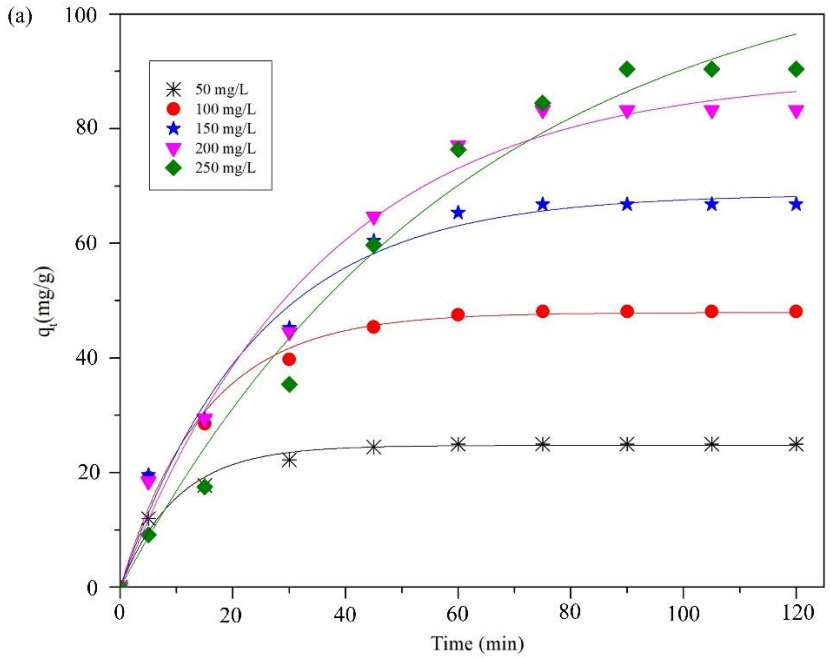


**Figure 5.** The toxic RBD adsorption kinetic study (a) PFO kinetics, (b) PSO kinetics

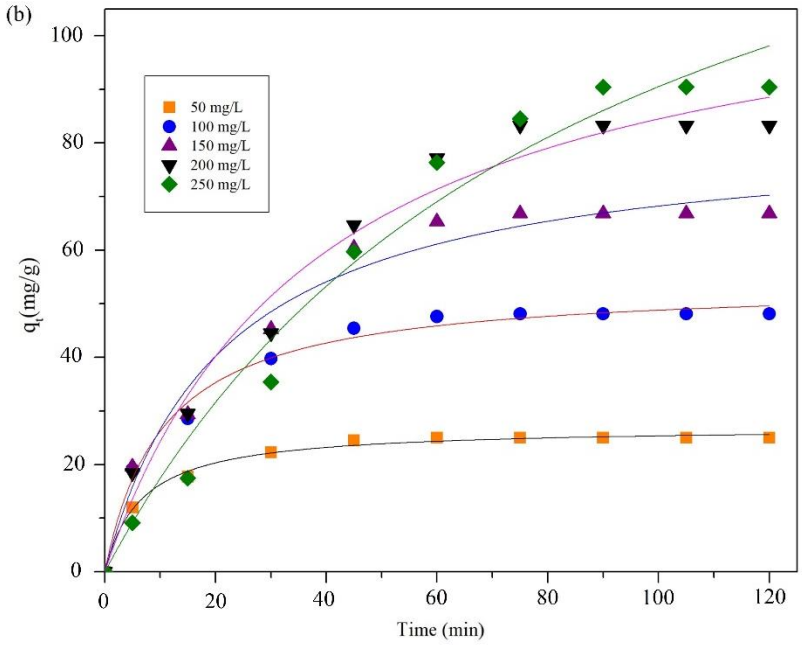


**Figure 5.** The toxic RBD adsorption kinetic study (a) PFO kinetics, (b) PSO kinetics (cont.)

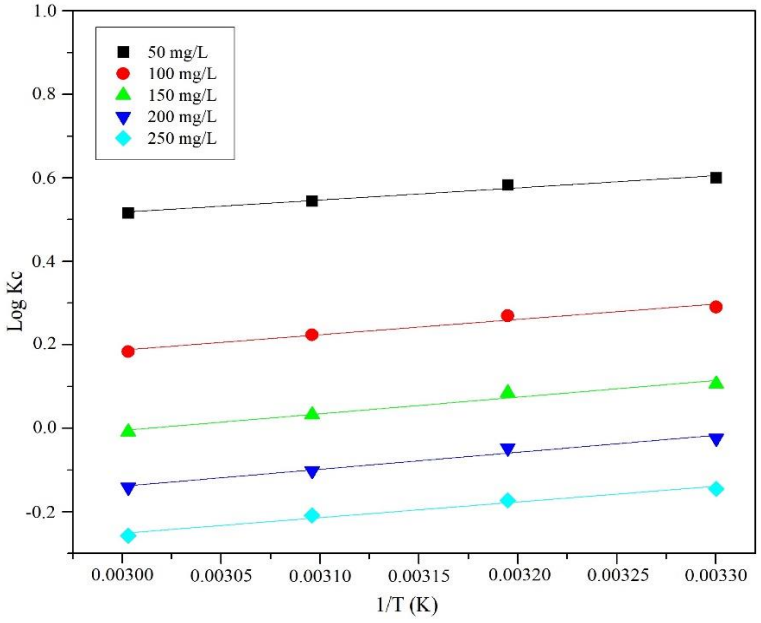


**Figure 6.** Thermodynamic analysis of Reactive Blue Dye removal from *Canna indica* bead entrapment

**Table 2.** Adsorption kinetic fit for the RBD onto CIBs

| $C_0$ mg/L | $q_e$ exp (mg/g) | Pseudo First Order $[q_t = q_e (1-\exp(-k_1 t))]$ | | | Pseudo Second order $(q_t = \frac{(q_e^2 k_2 t)}{(1+q_e k_2 t)})$ | | |
|---|---|---|---|---|---|---|---|
| | | $q_e$ (mg/g) | $k_1$ (1/min) | $R^2$ | qe (mg/g) | $k_2$ (1/min) | $R^2$ |
| 50 | 24.99 | 24.71 | 0.1006 | 0.9833 | 26.99 | 0.0056 | 0.9944 |
| 100 | 48.12 | 47.90 | 0.0682 | 0.9827 | 53.93 | 0.0017 | 0.9895 |
| 150 | 66.84 | 68.58 | 0.0420 | 0.9832 | 72.57 | 0.00057 | 0.9777 |
| 200 | 83.26 | 89.49 | 0.0282 | 0.9820 | 106.53 | 0.00022 | 0.9760 |
| 250 | 98.42 | 112.37 | 0.0163 | 0.9779 | 129.39 | 0.00067 | 0.9722 |

The other thermodynamic parameters were calculated using the graph of the logarithm of entropy (S°) versus the logarithm of enthalpy (H°) at constant temperature (1/T). Each temperature was given a calculated ΔG°. RBD adsorption onto immobilized CIBs from the aqueous solution resulted in an adverse ΔS° values, indicating that the process was enthalpy-driven. During dye adsorption, negative values of ΔG° and ΔH° were also noticed, demonstrating the feasibility, serendipity, and exotherms of the process can be seen in Table 3 (Venkatesh and Arutchelvan, 2020).

Table 4 shows various adsorbents that has been used for removal of reactive blue dye. This result confirmed the capability of the prepared immobilized Canna indica beads to effectively remove reactive blue dye from the aqueous solution. This biosorbent also a potential candidature for elimination of organic and toxic contaminants from water.

**Table 3.** Thermodynamic parameters for the biosorption of RBD onto immobilized *Canna indica* beads

| Thermodynamic parameter | $C_0$ (mg/L) | ΔH° (kJ/mol) | ΔS° (J/mol/K) | ΔG° (kJ/mol) | | | |
|---|---|---|---|---|---|---|---|
| | | | | 303 K | 313 K | 323 K | 333 K |
| $\Delta G° = - RT \ln Kc$ | 50 | -2.4301 | -2.9830 | -1.5105 | -1.5163 | -1.4623 | -1.3885 |
| $\mathrm{Log}K_c = \frac{\Delta S°}{2.303R} - \frac{\Delta H°}{2.303RT}$ | 100 | -3.040 | -7.6131 | -0.7311 | -0.7003 | -0.6004 | -0.5080 |
| | 150 | -3.3203 | -10.0075 | -0.2680 | -0.2204 | -0.0867 | 0.0236 |
| $K_c = \frac{C_{Ae}}{C_e}$ | 200 | -3.3854 | -11.3095 | 0.0824 | 0.1532 | 0.2919 | 0.3999 |
| | 250 | -3.1240 | -11.4675 | 0.3659 | 0.4495 | 0.5898 | 0.7137 |

**Table 4.** Comparison of maximum adsorption of capacity of various adsorbent materials for RBD removal

| S. No | Adsorbents for RBD removal | $q_m$ (mg/g) | References |
|---|---|---|---|
| 1 | Activated carbon (*Enteromorpha prolifera*) | 71.94 | Sun et al. (2013) |
| 2 | Bagasse beads | 3.17 | Ngamsurach et al. (2022) |
| 3 | Chicken eggshell beads | 24.10 | Praipipat et al. (2022a) |
| 4 | Duck eggshell beads | 12.63 | Praipipat et al. (2022a) |
| 5 | Lemon peel beads-doped iron (III) oxide-hydroxide | 3.23 | Praipipat et al. (2022b) |
| 6 | Lemon peel beads-doped zinc oxide | 2.59 | Praipipat et al. (2022b) |
| 7 | Immobilized Canna indica beads | 70.49 | This study |

### 3.7 Desorption study

To perform the desorption of immobilized CIBs beads that have adsorbed a RBD, was chosen three different desorbing solutions namely ethanol, acetic acid, and sodium hydroxide. From Figure 7 can be seen that acetic acid show better desorption capacity than ethanol, and sodium hydroxide. Up to 4 cycles the acitic acid treated CIBs has better desorption of 72% whereas ethanol, and sodium hydroxide could desorb of 39% and 46% only. Therefore acitic acid has chosen for other consecutive cycles.

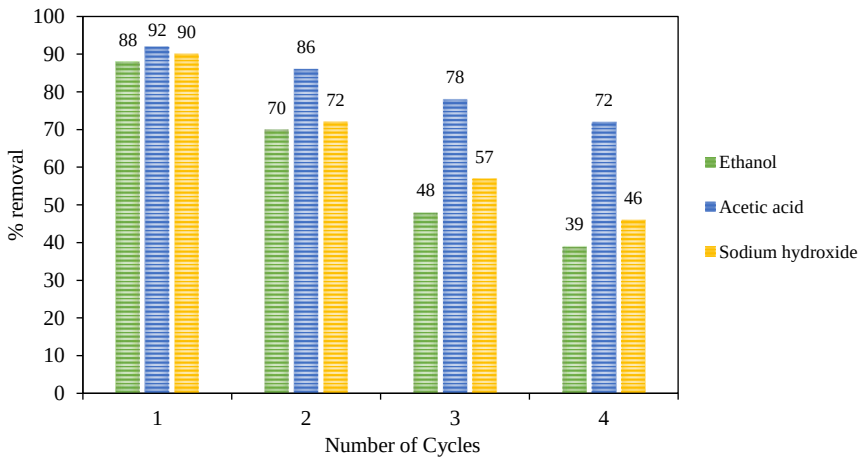


**Figure 7.** Desorption study of CIBs with different solutions

## 4. CONCLUSION

*Canna indica* root tubers were used to obtain the immobilized CIBs for adsorption of RBD from water. The biosorption test has beed carried out using several parameters, such as RBD concentration, pH, immobilized CIBs dose, contact period, and temperature. The maximum dye removal efficiency was found 99.20% at 303 K, 60 min, pH 7, with an adsorbent dosage of 150 mg/100 mL and 150 mg/L of RBD. The maximum adsorption capacity was found to be 70.49 mg/g. With various adsorption isotherm models, it is concluded that the Laungmuir model fitted well in this adsorption process. The adsorption kinetic data is consistent with a PSO kinetic model. The sorption of RBD onto the immobilized CIBs was feasible, spontaneous, exothermic, and enthalpy driven as confirmed by thermodynamic study. Based on the results, this experiment concluded that immobilized CIBs is proved to be a cost-effective and reusable adsorbent material for biosorption of RBD and also can be used for removal of other toxic dyes and heavy metal from real waters.

## ACKNOWLEDGEMENTS

Authors are wish to acknowledge their sincere thanks to Rajalakshmi Engineering College (Autonomous), Thandalam, Chennai, India, for giving all kind of support.

## REFERENCES

Ali H. Biodegradation of synthetic dyes: A review. Water Air Soil Pollution 2010;213:251-73.

Ansari MA, Murali M, Prasad D, Alzohairy MA, Almatroudi A, Alomary MN, et al. Cinnamomum verum bark extract mediated green synthesis of ZnO nanoparticles and their antibacterial potentiality. Biomolecules 2020;10:Article No. 336.

Assimeddine M, Abdennouri M, Barka N, Elmoubarki R, Sadiq M. Natural phosphates characterization and evaluation of their removal efficiency of methylene blue and methyl orange from aqueous media. Environment and Natural Resources Journal 2021;20(1):29-41.

Bhatia D, Sharma NR, Singh J, Kanwar RS. Biological methods for textile dye removal from wastewater: A review. Critical Reviews Environmental Science and Technology 2017; 47(19):1836-76.

Desore A, Narula SA. An overview on corporate response towards sustainability issues in textile industry. Environment Development and Sustainability 2018;20(4):1439-59.

Elieh-Ali-Komi D, Hamblin MR. Chitin and chitosan: Production and application of versatile biomedical nanomaterials. International Journal of Advanced Research 2016;4(3):411-27.

Gonzalez JA, Bafico JG, Villanueva ME, Giorgieri SA, Copello GJ. Continuous flow adsorption of ciprofloxacin by using a nanostructured chitin/graphene oxide hybrid material. Carbohydrate Polymers 2018;188:213-20.

Gunarathne V, Ashiq A, Ginige MP. Adsorption-oriented processes using conventional and non-conventional adsorbents for wastewater treatment. Green Adsorbents for Pollutant Removal 2018;18:23-71.

Gupta VK, Nayak A, Agarwal S. Bioadsorbents for remediation of heavy metals: Current status and their future prospects. Environmental Engineering Research 2015;20(2):163-9.

Hamed I, Ozogul F, Regenstein JM. Industrial applications of crustacean by-products (chitin, chitosan, and chitooligosaccharides): A review. Trends in Food Science and Technology 2016;48:40-50.

Karthikeyan G, Muthulakshmi Andal N, Anbalagan K. Adsorption studies of iron(III) on chitin. Journal of Chemical Sciences 2005;117(6):663-72.

Katheresan V, Kansedo J, Lau SY. Efficiency of various recent wastewater dye removal methods: A review. Journal of Environmental Chemical Engineering 2018;6(4):4676-97.

Kosaiyakanon C, Kungsanant S. Adsorption of reactive dyes from wastewater using cationic. Environment and Natural Resources Journal 2020;18(1):21-32.

Kyzas GZ, Kostoglou M. Green adsorbents for wastewaters: A critical review. Materials 2014;7(1):333-64.

Midha V, Dey A. Biological treatment of tannery wastewater for sulfide removal. International Journal of Chemical Science 2008;6(2):472-86.

Ngamsurach P, Nemkhuntod S, Chanaphan P, Praipipat P. Modified beaded materials from recycled wastes of bagasse and bagasse fly ash with iron (III) oxide-hydroxide and zinc oxide for the removal of reactive blue 4 dye in aqueous solution. ACS Omega 2022;7:34839-57.

Paudyal H, Pangeni B, Inoue K, Kawakita H, Ohto K, Ghimire KN, et al. Preparation of novel alginate based anion exchanger from Ulva japonica and its application for the removal of trace concentrations of fluoride from water. Bioresource Technology 2013;148:221-7.

Praipipat P, Ngamsurach P, Saekrathok C, Phomtai S. Chicken and duck eggshell beads modified with iron (III) oxide-hydroxide and zinc oxide for reactive blue 4 dye removal. Arabian Journal of Chemistry 2022a;15:Article No. 104291.

Praipipat P, Ngamsurach P, Prasongdee V. Comparative reactive blue 4 dye removal by lemon peel bead doping with iron (III) oxide-hydroxide and zinc oxide. ACS Omega 2022b;7: 41744-58.

Rehman A, Usman M, Bokhari TH, Haq A ul, Saeed M, Rahman HMAU, et al. The application of cationic-nonionic mixed micellar media for enhanced solubilization of Direct Brown 2 dye. Journal of Molecular Liquids 2020;301:Article No. 112408.

Riyanti F, Nurhidayah N, Purwaningrum W, Yuliasari N, Hariani PL. $MgFe_2O_4$ magnetic catalyst for photocatalytic degradation of congo red dye in aqueous solution under visible light irradiation. Environment and Natural Resources Journal 2023;21(4):322-32.

Dixit A, Dixit S, Goswami CS. Study on the assessment of adsorption potential of dry biomass of *Canna indica* with reference to heavy metal ions from aqueous solutions. Journal of Chemical Engineering Process Technology 2014;5(3):10-2.

Sivalingam S, Kella T, Maharana M, Sen S. Efficient sono-sorptive elimination of methylene blue by fly ash-derived

nano-zeolite X: Process optimization, isotherm and kinetic studies. Journal of Cleaner Production 2019;208:1241-54.

Sivalingam S, Sen S. Efficient removal of textile dye using nanosized fly ash derived zeolite-x: Kinetics and process optimization study. Journal of Taiwan Institute of Chemical Engineering 2019;96:305-14.

Sun D, Zhang Z, Wang M, Wu Y. Adsorption of reactive dyes on activated carbon developed from *Enteromorpha prolifera*. American Journal of Analytical Chemistry 2013;4(7A):17-26.

Venkatesh S, Arutchelvan V. Biosorption of alizarin red dye onto immobilized biomass of *Canna indica*: Isotherm, kinetics, and thermodynamic studies. Desalination and Water Treatment 2020;196:409-21.

Wang S, Vincent T, Faur C, Guibal E. A comparison of palladium sorption using polyethylenimine impregnated alginate-based and carrageenan-based algal beads. Applied Science 2018;8(2):Article No. 264.

Yuan H, Chen L, Cao Z, Hong FF. Enhanced decolourization efficiency of textile dye Reactive Blue 19 in a horizontal rotating reactor using strips of BNC-immobilized laccase: Optimization of conditions and comparison of decolourization efficiency. Biochemical Engineering Journal 2020;156:Article No. 107501.

# Microbes Isolated from Landfill Soil Utilize Polyethylene Terephthalate (PET) as Their Sole Source of Carbon: An Unexplored Possibility of Bioremediation in Bangladesh

**Sudipta Kundu Swarna[1], Mehmud Al Muntasir[1], M Murshida Mahbub[1*], Suraia Nusrin[1], and Jesmin[2]**

*[1]Department of Genetic Engineering and Biotechnology, East West University, Dhaka-1212, Bangladesh*
*[2]Department of Genetic Engineering and Biotechnology, University of Dhaka, Dhaka-1000, Bangladesh*

**ARTICLE INFO**

Received: 26 May 2023
Received in revised: 14 Nov 2023
Accepted: 16 Nov 2023
Published online: 8 Jan 2024
DOI: 10.32526/ennrj/22/20230124

**Keywords:**
Plastic pollution/ PET/ Biodegradation/ Microalgae/ PETase

*** Corresponding author:**
E-mail: murshida@ewubd.edu

**ABSTRACT**

Plastic products are so extensively used that they continue to strain the already overburdened waste management system and, inevitably, the global climate. Biodegradation is a sustainable remedy. Here, we report a few microorganisms isolated from landfill soil near Dhaka that thrive especially on polyethylene terephthalate (PET) polymers. Soil samples were subjected to three enrichment cycles that contained no carbon except PET. Pure isolates were recovered and incubated on minimal agar containing PET as the sole carbon. A morphological examination was carried out. Potential PET-degrading enzyme sequences from the isolates and other microalgae were analyzed for homology using BLASTP and TBLASTN, and multiple sequence alignment (MSA) was performed to assess conserved domains. Six isolates were obtained. Two isolates grew around the PET film but did not grow sufficiently in other areas of the minimal agar. Two other isolates with greenish pigmentation flourished around the PET film as well as on other areas of the agar. One of the green cells resembled *Aphanocapsa*, with irregular shapes and occasionally brown dense bodies, while the others looked round like *Microcystis*. Homology analysis revealed the hypothetical PETases in green cells contained the highly conserved catalytic triad (Ser-His-Asp) at the active site, as always found in alpha-beta hydrolase fold containing enzymes. Microbes isolated from two landfill sites in the vicinity of Dhaka have been adapted to utilize PET as a carbon source. In the future, sequencing and further characterization would be necessary to validate the findings. Microalgal systems demand increased focus, given their potential to offer valuable resources for bioremediation.

## 1. INTRODUCTION

Polyethylene terephthalate (PET or PETE) is one of the most used types of plastic for many attractive features. Aromatic terephthalic acid and ethylene glycol give rise to this linear polymer with excellent mechanical and thermal properties. Oftentimes, we use the single-use versions of it for its appealing qualities. However, the same appears as a curse as piled-up plastics in the natural ecosystem continuously pose a threat to our earth, including clogging issues, habitat ruining, animal entrapment, and microplastic-mediated toxicity to the nervous and reproductive system (Barnes et al., 2009; Waring et al., 2018). The difficulties in the degradation of PET arise from its molecular weight (Urbanek et al., 2021) high degree of crystallinity, failure to act as substrate, and high Tg (glass transition temperature) (Mohanan et al., 2020; Brott et al., 2022). Part of the ecological burden has been attempted to solve by taking recycling initiatives. Recycling, which may take many forms, is currently practiced mainly through melt extrusion and glycolysis (Park et al., 2014). However, these processes are not cheap or efficient, let alone eco-friendly. Biodegradation is an extremely desirable alternative. Nature has excellent capacity by dint of its collection of microbes to adapt and tweak its existing enzyme pool to create a new variety that can degrade new substrates. Past attempts to find enzymes that can degrade PET provide evidence

**Citation:** Swarna SK, Muntasir MA, Mahbub MM, Nusrin S, Jesmin. Microbes isolated from landfill soil utilize polyethylene terephthalate (PET) as their sole source of carbon: An unexplored possibility of bioremediation in Bangladesh. Environ. Nat. Resour. J. 2024;22(1):13-25. (https://doi.org/10.32526/ennrj/22/20230124)

of microorganisms or their enzymes' ability to break down these notoriously resilient synthetic chemicals (Malafatti-Picca et al., 2019; Carniel et al., 2017; Gamerith et al., 2017; Yang et al., 2013). *Ideonella sakaiensis* PETase (IsPETase) isolated from Japan has been one of the top-performing mesophilic PET metabolizing enzymes (Yoshida et al., 2016; Samak et al., 2020; Carr et al., 2020). The enzyme is secreted when the substrate is available after which it breaks down the PET into MHET (mono-2-hydroxyethyl terephthalate), BHET (bis-hydroxyethyl terephthalate-late), TPA (terephthalic acid), and EG (ethylene glycol) along with MHETase. PETases are enzymes similar to cutinase, and they have been demonstrated to possess the ability to biodegrade PET. Similar to cutinase, other hydrolases such as lipase and carboxylesterase have previously been reported to exhibit biodegradation activity on PET (Han et al., 2017). Studies have revealed that these enzymes share a common characteristic: they all contain the typical serine hydrolase fold at their active sites, along with the Ser-His-Asp catalytic triad (Wei et al., 2016; Han et al., 2017; Joo et al., 2018; Austin et al., 2018). Other PET degradation activities with the same catalytic elements have been reported in fungi such as *Fusarium* and *Humicola* cutinases, *Candida antarctica* lipase CalB as well as *Aspergillus* and *Penicillium* sp., etc. (Carniel et al., 2017) and in bacteria such as *Thermobifida* cutinases (Barth et al., 2016; Silva et al., 2011; Wei et al., 2016) and *Saccharomonospora viridis* cutinase type polyesterase (Kawai et al., 2014). Most of the reports on plastic biodegradation in Bangladesh have been on LDPE (Low-Density Polyethylene) (Hossain et al., 2019; Biki et al., 2021) where isolates such as *Ralstonia* sp. strain SKM2 and *Bacillus* sp. strain SM1 were found to exhibit plastic breakdown activity.

Our study aims to isolate strains from the natural microbial community evolving to utilize PET in landfill soil near Dhaka through enrichment culturing. A variety of PET utilization abilities if found in the current study would add to the existing handful list of enzymatic systems. Moreover, it is always desirable to find an alternative option or outperformer in terms of activity and/or other characteristics that are biotechnologically promising such as cheaper feedstock and thermal stability.

## 2. METHODOLOGY

### 2.1 Sample collection

Garbage soil samples were collected along with dumped plastic from Matuail and Aminbazar, the two landfills serving the capital city of Bangladesh (Figure 1). The sampling was performed in rounds: At first, in December 2020, and then in April 2022. Matuail, with a 100-acre area located in Demra (south of Dhaka), serves as the city's garbage dump. It is an aged landfill (26 years old) (Akter et al., 2021). Since there is no segregation and recycling facility, with a daily load of 2,500 tons of solid waste from Dhaka's south city corporation areas, it is a place where massive mounds of plastic waste deposition take place (Chandan, 2021). The Aminbazar landfill is l km away from the capital and has been serving mostly the northern part of Dhaka since 2007 (Urme et al., 2021). So, both areas have the potential to facilitate the evolution of enzymes that degrade plastic.

For sampling, we used sterile containers to collect the soil samples at a depth of 9-10 cm. Around 10 g of soil were collected into a sterile Ziplock bag and transported to the laboratory, the temperature was also recorded.

### 2.2 Preparation of PET strips as the sole source of carbon and for the PET utilization test

The polyethylene terephthalate (PET) sheet (HS Code: 3920.62.90) used in this study was a generous gift from Arbab Poly Pack Ltd. (Bangladesh) (https://www.arbabpolypackltd.com). These PET sheets were 100% Food grade and have been imported from India. PET film was sectioned into 2×3 cm rectangular-shaped pieces of PET strips which were used as the sole source of carbon in the liquid enrichment medium or minimal agar medium. All PET strips were disinfected by autoclaving at 121°C for at least 30 min under 15 psi of pressure. These PET strips were further used in enrichment culturing or performing PET-utilizing tests.

### 2.3 Inoculum preparation, screening using enrichment medium, pure culture isolation and characterization

One gram of the soil sample along with dumped plastic was dipped into 90 mL NaCl Solution (0.85%) and gently shaken to mix (Jangra et al., 2020). This plastic-associated environment, known as the plastisphere, was used as an enrichment source for plastic utilizing microorganisms (as described by Rüthi et al., 2023). The suspended soil samples were kept for 2 days in a shaker incubator at 120 rpm and at room temperature, and 1 mL of this suspension was used as an inoculum for the enrichment medium (Figure 1).

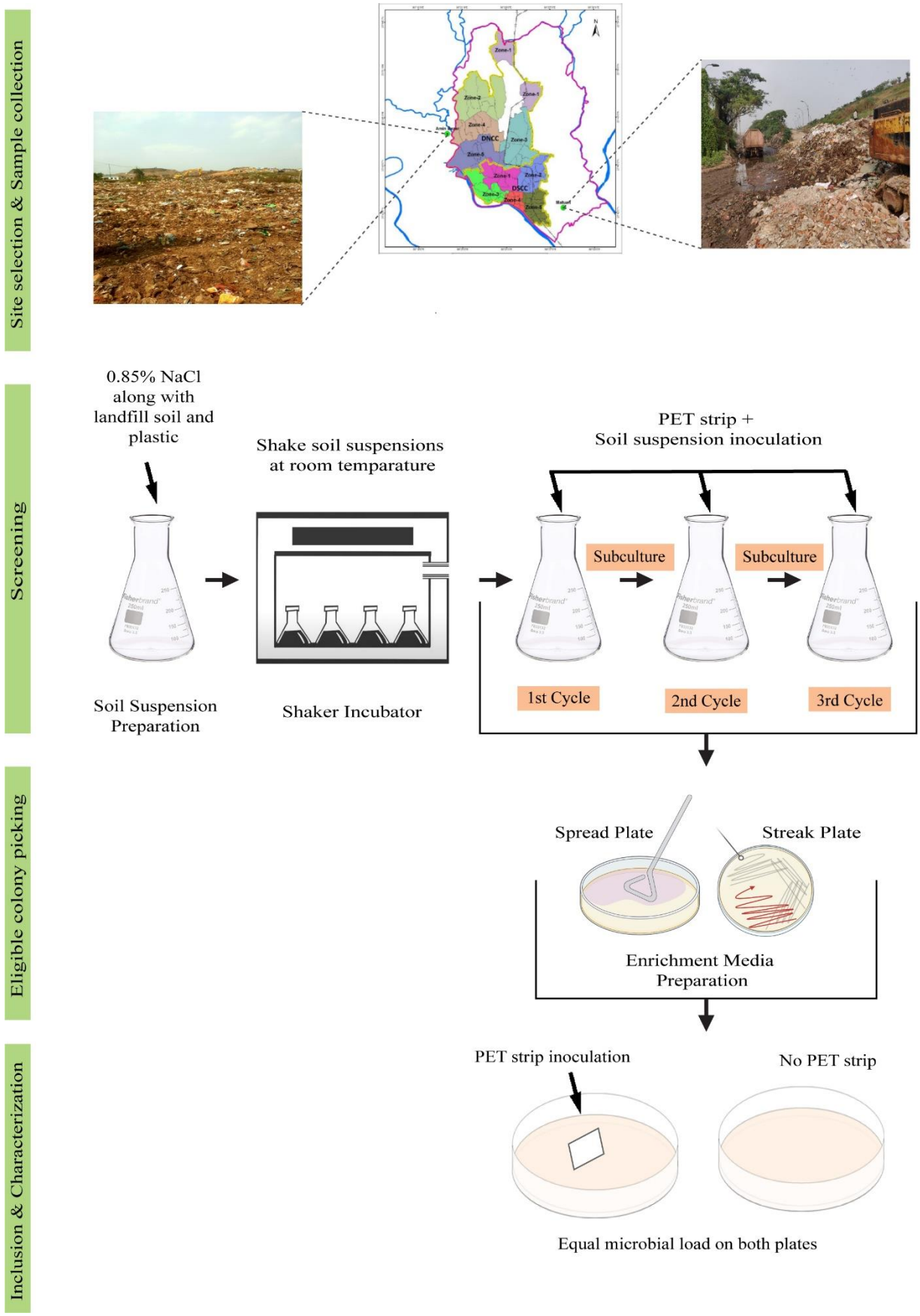


**Figure 1.** Flow diagram of site selection, sampling, screening, isolation, and characterization of plastic (PET) utilizing microbes from Matuail (left) and Aminbazar (right) landfill soil

For screening, 100 mL of enrichment medium was prepared following Skariyachan et al. (2015) with slight modifications. The enrichment broth contained 1 g/L $NaNO_3$, 0.2 g/L $MgSO_4.7H_2O$, 0.05 g/L $FeCl_3$, 0.02 g/L $CaCl_2$, 1 g/L $KH_2PO_4$, 1 g/L $K_2HPO_4$, 1 g/L $(NH_4)_2SO_4$ at pH 7 supplemented with one PET strip (2 × 3 cm rectangular shaped) as the sole source of carbon in a 250 mL Erlenmeyer flask (Figure 1). One mL of the inoculum (prepared soil suspension) was added and then the flasks were incubated for 15 days at ambient temperature in the presence or absence of light (not shown). Negative control was also incorporated into the experiment. It contained the enrichment broth with the PET strip that did not receive any inoculum. After 15 days of incubation, 1 mL of the first enrichment culture was transferred along with the PET strip from the first cycle to a second enrichment broth for another 15 days at ambient temperature. The third round of enrichment also followed in the same way for an additional 15 days. After three cycles of enrichment, 50 µL from both the Matuail and Aminbazar flasks were placed on minimal agar (the same composition as the enrichment broth but supplemented with 1.5% agar) by the spread plate technique. Plates were incubated at 37°C for those that did not receive any light in the enrichment cycles. Another group of plates was incubated at an ambient temperature where there was an ample amount of light. Obtained colonies were isolated by the streak plate method and subcultured repeatedly for pure isolates (Figure 1).

These isolates were further characterized by the PET-utilizing test following the plate test described by Urbanek et al. (2017) with modification. In this study, we designed and performed the PET-utilizing test, by growing individual isolates first in liquid enrichment broth with PET strips as the sole source of carbon and then a hundred microliters of the resulting cultures were dropped and spread on the solid enrichment (minimal) agar plates. The experiment was conducted in parallel using two sets: In one set: an agar plate was overlaid with PET film as the sole organic carbon source while a control plate was set without any carbon source, and both plates were incubated at 37°C (Figure 1). For the second set: two plates were set one with PET films as the carbon source and another without, just like mentioned above, but with different incubation conditions including ambient temperature and sufficient light. After four days of incubation, all plates were checked and growth was compared between the two sets. For both of these sets, a third plate was also incorporated that received no inoculum.

A smear of the isolated pure culture was made on a fresh grease-free slide with a sterile loop. The slide was checked under a microscope to determine the morphology of isolated strains based on shape, size, and color (Sugoro et al., 2022; Najeeb et al., 2022, Badr and Fouad, 2021; Bellinger and Sigee, 2015). Otherwise, a drop of culture was placed under a cover slip and directly observed without stain.

### 2.4 Glycerol stock preparation

Five hundred microliter overnight cultures of each of the isolates were added in 50% (v/v) glycerol, gently mixed and the tube was frozen at -20°C.

### 2.5 *In silico* bioinformatics analysis

A homology search utilizing BLASTP and TBLASTN (Basic Local Alignment Search Tool Program and Protein-nucleotide 6-frame translation) was conducted to select potential PETase-like microalgal proteins (performed on 19 October 2022) by selecting the following organisms such as algae (taxid: 3041), green algae (taxid: 3041), red algae (taxid: 2763), blue-green algae (taxid: 1117), yellow-green algae (taxid: 2833), brown algae (taxid: 2870), Shewanella algae (taxid: 38313), *Chlamydomonas reinhardtii* (taxid: 3055), *Dunaliella salina* (taxid: 3046), Chlorella (taxid: 3071), *Botrycoccus braunii* (taxid: 38881), *Phaeodactylum tricornutum* (taxid: 2850), *Thalassiosira pseudonana* (taxid: 35128), *Isochrysis* (taxid: 37098), and *Nannochloropsis* (taxid: 5748). Multiple sequence alignments were conducted using PROMALS3D (http://prodata.swmed.edu/promals3d/promals3d.php) (Pei et al., 2008) on the amino acid sequences of enzymes obtained from the abovementioned searches in addition to previously known PETase enzymes preferably with known structures. The Phyre2.0 fold recognition server (Kelley et al., 2015) was used for protein modeling (normal mode and default parameters). Docking of the substrate against the model proteins was performed using AutoDock Vina (Trott and Olson, 2010) accessible via PyRx (Dallakyan and Olson, 2015).A grid box was specified mainly around the substrate binding and active sites with dimensions (25.0-X, 28.54-Y, 21.45-Z for cyanobacterial enzyme and 25.30-X, 26.05-Y, 23.47-Z for pycnococcal protein) Å and centered at (0.0, -1.77, 2.47 for cyanobacterial protein and -13.24, 30.11, 5.27 for pycnococcal protein) Å. The ligand was docked to the protein with

a default exhaustiveness of 8. The model with the lowest binding energy was chosen. The BIOVIA Discovery Studio Visualizer (Biovia, 2021) was used for model visualization and representation of the intermolecular interactions, and to create a 2D diagram of ligand binding site atoms.

## 3. RESULTS AND DISCUSSION

### 3.1 Microorganisms from Aminbazar and Matuail dumpsites showed growth in the enrichment broth utilizing PET film as the sole source of carbon

Enrichment culturing has been previously used for the isolation of microorganisms with novel metabolic capacity (Tortora et al., 2007). The design of the enrichment medium tells which metabolic type is going to be favored. Usually, no selective agent is used in this type of nutritional material; but omission/incorporation of a metabolic condition results in the selection of a specific type of microbe that possesses the desired metabolic trait, and by the same mechanism it does not allow other types of microbes to grow (Tortora et al., 2007).

The enrichment medium used in our study did not contain any organic carbon source except the PET film. Soil samples collected from Aminbazar and Matuail dumpsites were inoculated into the enrichment medium. Enrichment of PET-degrading microbes was carried out in three consecutive 15-day-long subculture screens both in the presence and/ or absence of sunlight. Growth and greenish appearance were noticed at the end of each subculture for cycles that were exposed to light, which were more evident in further subcultures (Figure 2). Quicker growth in the subsequent subcultures and slow response in the first few days after soil samples were introduced in the enrichment medium may represent the lag phase (Rolfe et al., 2012) when the microbes were preparing and acclimatizing with the nutrient and other conditions.

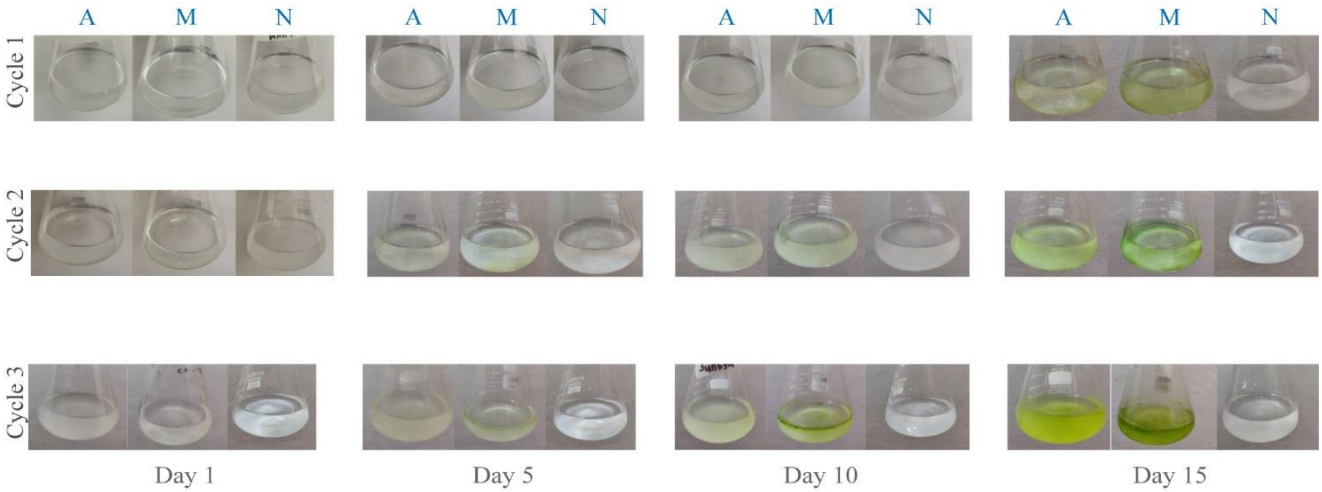


**Figure 2.** Enrichment analysis of PET utilizing microorganisms in three consecutive 15-day-long subculture stages showing growth and green appearances. 1st cycle: the first 15 days; 2nd cycle: from the 16-30th day; 3rd cycle: 31st- 45th day. M: Matuail; A: Aminbazar; and N=Negative control with PET strip but no inoculum

### 3.2 PET as the sole organic carbon source for individual isolates on minimal (enrichment) agar plate

Since the liquid enrichment medium contained no other carbon source except plastic film, the growth in the enrichment medium indicates two possibilities: (a) autotrophic growth or (b) growth using PET film as a carbon source. We recovered six pure isolates after repeated streaking and microscopic observations. To test if their growth is the result of either of the two above reasons, equal amounts of the pure cultures were used to make a lawn on two minimal agar plates one of which was laid over with PET films, but the other plate was not (Figure 1).

Both plates were examined on the 4th day of incubation. Two of the isolates showed growth at the edges of the PET film and only scarcely or no growth was observed on the rest of the agar surface. The other four isolates (M2, M4, A1, and A2) were different and showed growth both at the edges of the plastic and all over the agar plates. All isolates, except A2, appeared pleomorphic/irregular, under the microscope while A2 had a round appearance (Figure 3).

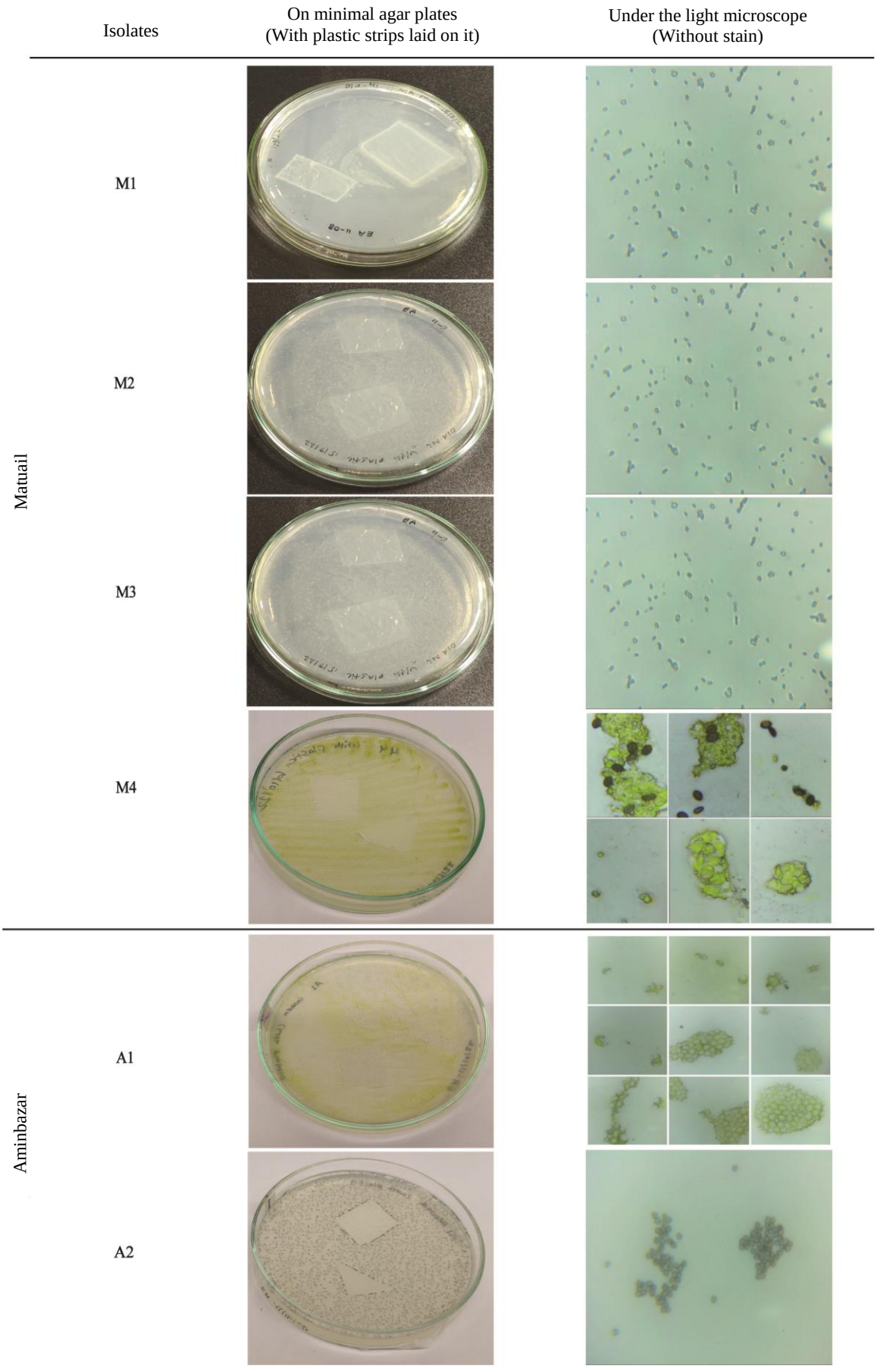


**Figure 3.** Isolated microbes on minimal agar plates with PET film as the sole organic carbon source and their microscopic observation at 100X (oil immersion) under the light microscope

Apart from the occasional isolated green cells, there were brown dense structures in the M4 micrograph. The irregularly shaped colonial form of M4 resembled amorphous gelatinous colonies of *Aphanocapsa* (Bellinger and Sigee, 2015; Felisberto and Souza, 2014; Gama et al., 2014 and Supplementary Table S1). Although A1 individual cells were sometimes spheroidal, the colonial form of A1 was largely irregular and looked like mucilage-producing *Microcystis* (Bellinger and Sigee, 2015; Pereira and Portillo, 2018; Pham et al., 2021 and Supplementary Table S2). To test if *Aphanocapsa* or *Microcystis* contain any sequence homologous to PETase, we performed BLASTP using *Aphanocapsa* and *Microcystis* as organisms but no homology was found. However, when we searched for esterase sequences in these two types of microbes using simple text mining at the NCBI Protein database, we retrieved three esterases from *Aphanocapsa* (Apest) and many from *Microcystis* (Mcest). Using the three Apest and randomly selected two Mcest sequences along with the IsPETase, we performed an MSA using the align tab of the UniProt toolbar, which revealed the three catalytic Ser-His-Asp triad typical of alpha-beta hydrolases (Consortium, 2023 and Supplementary Figure S1). PET degrading activity has been reported previously in different enzymes like cutinase, lipase, esterase (Joo et al., 2018; Carr et al., 2020; Maurya et al., 2020) or PETase (an alpha-beta hydrolase fold family member) that act along with MHETase (Palm et al., 2019). These enzymes have been primarily described in bacteria or fungi (Carr et al., 2020; Qi et al., 2021). Although scarce in reports, PET degrading activities are also present in microalgae (Chia et al., 2020). The isolates for this study were green in appearance, and their characteristics under the microscope (Figure 3) resembled much to an extent, the previously reported plastic biodegradation by green photosynthetic microalgae capable of plastic biodegradation (Kumar et al., 2017). Microalgae have been demonstrated with plastic degradation capacity by synthesizing toxins or enzymes while using plastic polymers as carbon sources (Chia et al., 2020).

To assess the ability of isolated green microbes to utilize heat-treated PET films, we subjected them to sodium dodecyl sulfate (SDS) washing to eliminate attached cells before examining them under a light microscope. Despite the SDS wash, both M4 and A2 isolates displayed green growth in connection with PET, indicating growth within the PET films (see Supplementary Table S3). This finding aligns with recent studies that used SEM to demonstrate microalgae adherence to PET surfaces, with alterations noted even after physical and/or chemical pretreatment of PET (Falah et al., 2020, Supplementary Table S3). Interestingly, another study highlighted a preference for nylon over PET, suggesting PET's resistance to biological attachment (Demirkan et al., 2020). Our study involved a comparison of our 400X light microscopy images with previously published SEM scans, revealing green growth within PET films by the isolated green microorganisms (Supplementary Table S3).

PET is a manmade product unlike cellulose or other plant or animal-derived polymers. So, nature needs more time to train its enzyme pool to attack PET; this makes PETases very rare (Carr et al., 2020). Only a handful of reports highlight and mention the PETase enzymes and their activity. A global investigation discovered a significant presence of PET hydrolases in regions with crude oil, underscoring the importance of natural selection (Danso et al., 2018). The current study's enrichment and isolation of PET-utilizing microorganisms suggest that the sampled soils in this research contain life forms adapting to PET consumption.

Nature currently lacks the maturity to efficiently handle manmade PET using microbial enzymes as tools, so a complete understanding of pathways for PET degradation in microbes remains a challenge. Some studies propose the collaboration of microbial consortiums comprising various bacteria, protozoa, and yeast-like cells, which collectively break down PET into TPA and EG. This breakdown allows the cells in the consortium to metabolize these components (Taniguchi et al., 2019). In another study, it was reported that the bacterium *I. sakaensis* can convert PET into $CO_2$ using two enzymes namely, IsPETase and IsMHETase (Yoshida et al., 2016). Prior to these findings, the fungus *Humicola insolens* cutinase (HiC) demonstrated a preference for producing MHET from BHET. When combined with *Candida antarctica* lipase B (CALB), this system could digest the MHETs into TPA (Carniel et al., 2017). Consequently, there are variations in the breakdown products and the routes that microbes take to degrade PET for utilization. In the future, further biochemical degradation analysis may provide insights into the metabolic routes our isolates are using to utilize PET as their carbon substrate.

### 3.3 Model of hypothetical protein from *Pycnococcus provasolii* and *Cyanobacterium* TDX16 alpha/beta hydrolase contain active and substrate binding sites for PET hydrolysis

Microalgal PET degradation activity is promising because industrial production of bacterial degrader is costlier than microalgae as the latter do not require organic carbon sources for growth (Moog et al., 2019; Hempel and Maier, 2016). Moreover, endotoxins are absent in algae (Akram et al., 2023). So, PET remediation approaches using algal systems are more appealing than bacterial counterparts. Due to their attractiveness, several works reported the endeavor of heterologous expression of PETase in the microalgal system (Almeida et al., 2019; Moog et al., 2019; Kim et al., 2020) (Table 1). However, naturally occurring microalgal PETases rarely appeared in the literature. Our current report highlights two natural microalgal systems (*Aphanocapsa* and *Microcystis*) with PET-associated growth, which may harbor PETase-like activity. As microalgae offer promise in various aspects, we attempted to explore the presence of naturally occurring PETase genes within microalgae. Our searches were performed by using both BLASTP and TBLASTN (Figure 4). One originates from the organism *Pycnococcus provasolii*, a species of green algae and is a hypothetical protein of 335 amino acids. The solitary, spherical, 1.5-4.0 mm in diameter, resistant, sporopollenin-free, and ultrastructurally close to green algal cells of *Pycnococcus provasolii* are hardly identifiable from the cells of other coccoid planktonic creatures under the light microscope (Guillard et al., 1991).

The other one is cyanobacterium TDX16 alpha/beta hydrolase protein containing 175 amino acids. According to Dong and Xing (2020) the first origin-known alga, TDX16-DE, is synthesized via de novo organelle biogenesis from the *Chroococcidiopsis*-like endosymbiotic cyanobacterium TDX16 after acquiring the DNA of its host green alga, *Haematococcus pluvialis*. With a diameter of 2.0-3.6 m, TDX16-DE is spherical or oval. The strain has 99.7% identity to *Chlorella vulgaris*, according to 18S rRNA sequencing. However, based on several characteristics, including size, membrane-bound organelles, and cyanobacterial origin, scientists established TDX16-DE as a new genus and species, *Chroococcidiorella tianjinensis* (Dong and Xing, 2020).

The TBLASTN search also discovered two nucleotide sequences. *Pycnococcus provasolii* genome assembly chromosome 12 is one of them. This gene repertoire, which has 65 protein genes, and 33 RNA genes is comparable in size to that found in *Chlorophyceae* green algae (Turmel et al., 2009). The other one is a partial mRNA of *Emiliania huxleyi* CCMP1516 triacylglycerol lipase 1 (LIP1). Sequencing of CCMP1516 genome revealed its proportion of repetitive components (64%), which is substantially higher than that of sequenced diatoms (Read et al., 2013).

**Table 1.** Plastic degradation activity in microalgae from literature mining

| Organism name | Species name | Detection method | Reference |
|---|---|---|---|
| Green algae | Functional expression of *Ideonella sakaiensis* PETase in *Chlamydomonas Reinhardtii* CC-124 | High-performance liquid chromatography (HPLC), Scanning electron microscopy (SEM) | Kim et al. (2020) |
| Blue-green algae (Cyanobacteria) | Biological degradation of LDPE by *Anabaena spiroides*, and *Navicula pupula* | Weight loss method | Barone et al. (2020) |
| Microalgae (Single-celled green algae) | PET Degradation by *Chlorella vulgaris* with pre-treatment | Compound microscopy (CM), SEM, Fourier transformed infrared spectroscopy (FTIR), and Gas chromatography-mass spectrometry (GCMS) | Falah et al. (2020) |
| Mesophilic marine photosynthetic microalga | Expression of PETase in *Phaeodactylum tricornutum* | SDS-PAGE, Western blot, PNGase F assay, SEM, and Ultra high-performance liquid chromatography (UHPLC) | Moog et al. (2019) |
| Marine sponge-derived strain | Heterologous expression of IsPETase-like gene *Streptomyces* sp. SM14 isolated from the sponge *Haliclona simulans* | *In silico* analysis, polycaprolactone (PCL) plate-clearing assay | Kennedy et al. (2009) and Almeida et al. (2019) |

(a)

| Description | Total score | Query coverage | E-value | Percentage identity | Accession length | Accessions ID |
|---|---|---|---|---|---|---|
| Alpha/beta hydrolase, partial [*Cyanobacterium* TDX16] | 128 | 62% | 3e-34 | 42.54% | 175 | OWY58880.1 |
| Hypothetical protein [*Pycnococcus provasolii*] | 65.9 | 73% | 6e-10 | 26.69% | 335 | GHP05201.1 |

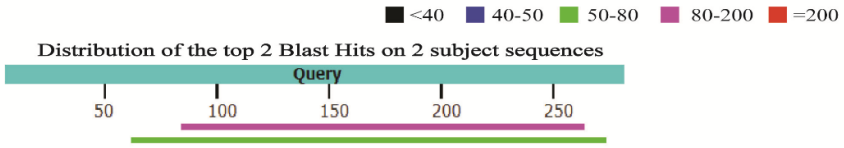


(b)

| Description | Total score | Query coverage | E-value | Percentage identity | Accession length | Accessions ID |
|---|---|---|---|---|---|---|
| *Emiliania huxleyi* CCMP1516 triacylglycerol lipase 1 (LIP1) Partial mRNA | 66.2 | 67% | 2e-10 | 25.98% | 946 | XM_005780464.1 |
| *Pycnococcus provasolii* genome assembly, chromosome: 12 | 65.1 | 72% | 1e-09 | 26.75% | 879559 | OW568872.1 |

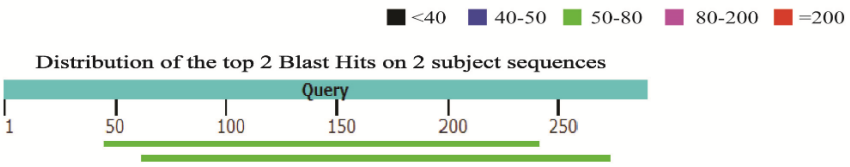


**Figure 4.** Sequence similarity analysis using BLASTP and TBLASTN for microalgal genes/proteins with PETase-like characteristics using IsPETase protein as the query

In PETase, the catalytic triad comprising Ser160, His237, and Asp206 (Figure 5) indicates a charge-relay mechanism system like that found in other α/β-fold hydrolases. From multiple sequence alignment, a similar active site is found in both microalgal proteins found in the BLASTP/TBLASTN search (Figure 4).

The hydrolytic enzymes of distant phylogenetic origin have been found to contain the alpha/beta hydrolase fold that contains eight beta sheets connected by alpha helices, with a highly conserved catalytic triad than the substrate binding sites. The model of a hypothetical protein from *Pycnococcus provasolii* constructed in this work (Figure 5(c)) also exhibits eight beta sheets that are connected by alpha helices. The Cyanobacterium TDX16 alpha/beta hydrolase model does not show eight beta sheets, which is due to the truncated amino acid sequence (175 AA long) used as a query in the Phyre2.0 server. When fed into the MSA program (Figure 5(b)), both sequences show conservation of the active sites (AS) and substrate binding sites (SBS). Among the nucleophile (serine)-histidine-aspartate loop of the catalytic triad, the histidine does not accommodate any change (Ollis et al., 1992). The substrate binding site has been found to accommodate different amino acids like Phe-Met-(Trp/Tyr/Ala) in Bacteroidetes PET hydrolyzing enzymes (Zhang et al., 2022) whereas Tyr-Met-Trp in *Ideonella sakaensis* (IsPETase) and the leaf compost cutinase (LCC) PETase, etc. In the current MSA analysis, the cyanobacterial protein contains Phe-Met-Trp but the *Pycnococcus provasolii* has Trp-Leu-Asn (Figure 5(b)).

The Cyanobacterium TDX16 alpha/beta hydrolase and *Pycnococcus provasolii* hypothetical protein models shown in Figure 5(c) (i and ii, respectively) were docked with BHET (bis 2-hydroxyethyl terephthalate) dimer. The amino acids predicted to form the SBS and AS are shown in yellow in the ribbon diagram of the models. The binding affinity for BHET dimer against the cyanobacterial protein was -4.9 Kcal/mol whereas for BHET dimer against the pycnococcal protein was -6.5 Kcal/mol. Both of the protein models demonstrate a cleft for binding BHET dimer. A 2D diagram of ligand binding site atoms shows possible interactions including pi-sigma, van der Waals, and H-bonding.

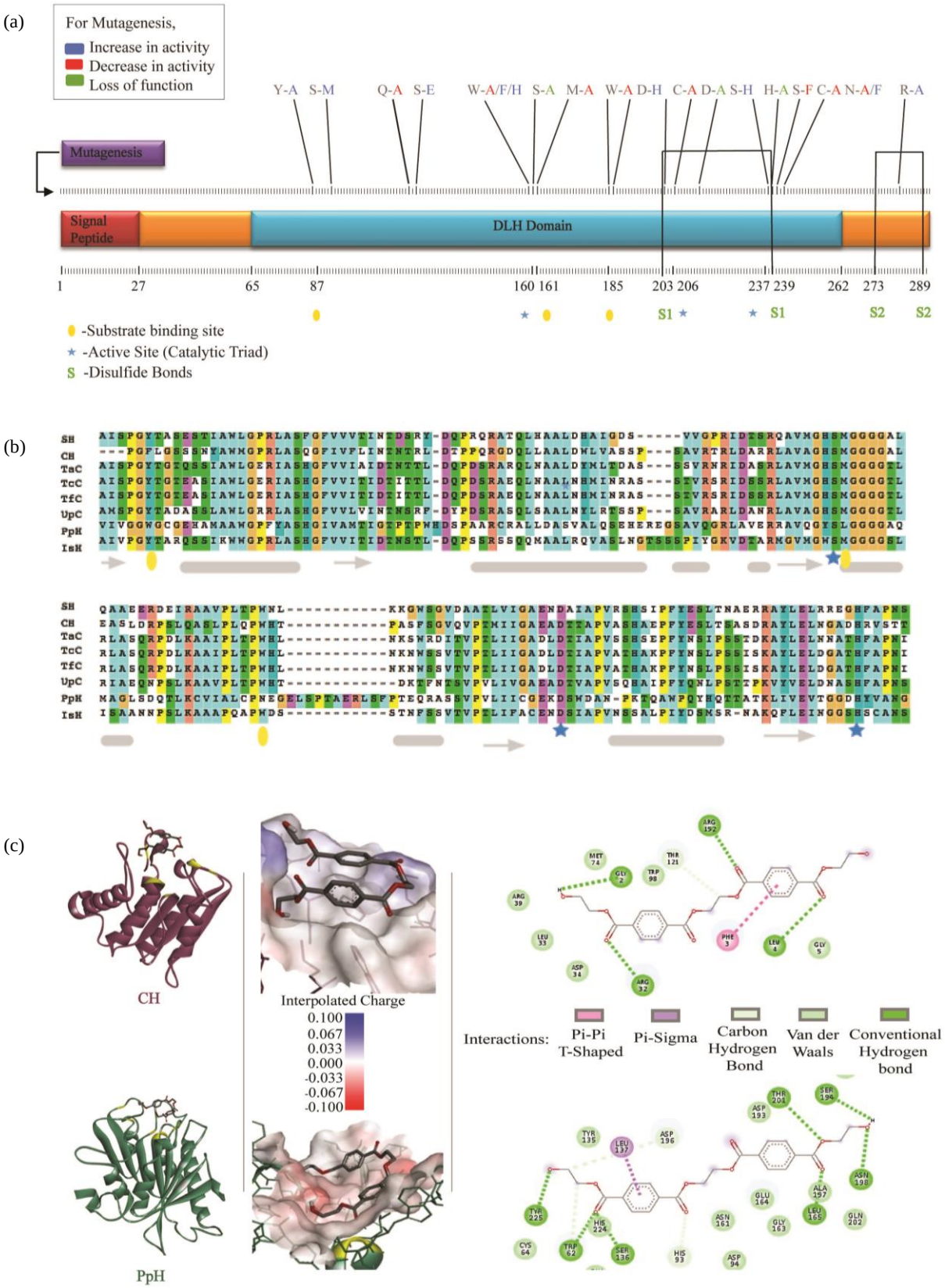


**Figure 5.** (a) Domain structure of IsPETase showing the highly conserved catalytic triad, substrate binding sites, and (b) disulfide bridges as well as previous mutagenesis effects Homology analysis building MSA. For MSA, eight sequences were used: SH: *Streptomyces* sp. SM14 alpha/beta hydrolase; CH: cyanobacterium TDX16 alpha/beta hydrolase; TaC: *Thermobifida alba* cutinase est1; TcC: *Thermobifida cellulolytica* cutinase 1; TfC: *Thermobifida fusca* Cutinase; UpC: Unknown prokaryotic cutinase; PpH: *Pycnococcus provasalii* hypothetical protein; and IsH: *Ideonella sakaiensis* PET hydrolase. All sequences share the same active site (Ser160, Asp206, and His237) also the SBSs were highly conserved. (c) Model of Cyanobacterium TDX16 alpha/beta hydrolase (i) and *Pycnococcus provasolii* hypothetical protein (ii). The ASs and SBSs are shown in yellow.

## 4. CONCLUSION

Stopping the immediate use of plastics is highly unlikely, which means we are likely to witness an increasing accumulation of plastic waste over the next decade. Plastics such as PET are commonly used in packaging industries and the production of synthetic fabrics, and their natural resistance to biodegradation has led to a rapid buildup of plastic waste which in turn poses a major threat to various forms of life and, ultimately, to the global climate. This is why it is essential to explore methods for bioremediation of plastics. The issue of plastic waste is a global problem, and it is of particular concern for densely populated delta regions like Bangladesh, which is surrounded by water. Unfortunately, the waste management systems in such areas pay limited attention to and make little effort to address the issue of plastic pollution.

In this study, we explored the garbage disposal site and isolated a few potential PET-utilizing microbes from their natural habitat, the garbage disposal site. In the lab, we screened, cultured and tested their growth utilizing PET as the sole source of carbon at defined conditions, and on synthetic enrichment media. An initial examination and characterization using light microscopy and in silico bioinformatics analysis identified two microalgal isolates with the potential capacity to degrade PET (polyethylene terephthalate). Additionally, when searching protein sequence databases for microalgal PETases, there were indications of possible PETase activity within the microalgal gene pool. However, further genomic and molecular investigations are required for taxonomic classification and to confirm their ability to biodegrade PET. Nevertheless, this study underscores the importance of exploring natural habitats to isolate promising candidates, such as green microalgal cells, with bioremediation capabilities, which could potentially lead the way to a more environmentally sustainable solution for the worldwide plastic crisis in the near future.

## ACKNOWLEDGEMENTS

This work was supported by the EWUCRT grant (Research Proposal No: Round-13, No-5; Ethical Clearance No. EWUCRT-REC-10/2021).

## AUTHORS' CONTRIBUTION

Jesmin and MMM conceptually designed the research; SKS and MAM collected, screened and analyzed the data. SKS, SN, MMM, and Jesmin, validate the interpretation and drafted and revised the manuscript. All authors have read and approved the final manuscript.

## REFERENCES

Akram M, Khan MA, Ahmed N, Bhatti R, Pervaiz R, Malik K, et al. Cloning and expression of an anti-cancerous cytokine: Human IL-29 gene in *Chlamydomonas reinhardtii*. AMB Express 2023;13:Aticle No. 23.

Akter S, Shammi M, Jolly YN, Sakib AA, Rahman MM, Tareq SM. Characterization and photodegradation pathway of the leachate of Matuail sanitary landfill site, Dhaka South City Corporation, Bangladesh. Heliyon 2021;7(9):e07924.

Almeida EL, Carrillo Rincón AF, Jackson SA, Dobson ADW. In silico screening and heterologous expression of a polyethylene terephthalate hydrolase (PETase)-like enzyme (SM14est) with polycaprolactone (PCL)-degrading activity, from the marine sponge-derived strain *Streptomyces* sp. SM14. Frontiers in Microbiology 2019;10:Article No. 2187.

Austin HP, Allen MD, Donohoe BS, Rorrer NA, Kearns FL, Silveira RL, et al. Characterization and engineering of a plastic-degrading aromatic polyesterase. Proceedings of the National Academy of Sciences of the United States of America 2018;115(19):4350-7.

Badr AA, Fouad WM. Identification of culturable microalgae diversity in the River Nile in Egypt using enrichment media. African Journal of Biological Sciences 2021;3(2):Article No. 50.

Barnes DKA, Galgani F, Thompson RC, Barlaz M. Accumulation and fragmentation of plastic debris in global environments. Philosophical Transactions of the Royal Society B 2009; 364:1985-98.

Barone GD, Ferizovi´ D, Biundo A, Lindblad P. Hints at the applicability of microalgae and Cyanobacteria for the biodegradation of plastics. Sustainability 2020;12(24):Article No. 10449.

Barth M, Honak A, Oeser T, Wei R, Belisário-Ferrari MR, Then J, et al. A dual enzyme system composed of a polyester hydrolase and a carboxylesterase enhances the biocatalytic degradation of polyethylene terephthalate films. Biotechnology Journal 2016;11(8):1082-7.

Bellinger EG, Sigee DC. Freshwater Algae: Identification, Enumeration and Use as Bioindicators. 2nd ed. John Wiley and Sons; 2015.

Biki SP, Mahmud S, Akhter S, Rahman Md J, Rix JJ, Bachchu Md AA, et al. Polyethylene degradation by *Ralstonia* sp. strain SKM2 and *Bacillus* sp. strain SM1 isolated from land fill soil site. Environmental Technology and Innovation 2021; 22:Article No. 101495.

Biovia DS. Discovery Studio Visualizer [Internet]. 2021 [cited 2022 Dec 3]. Available from: https://discover.3ds.com/discovery-studio-visualizer-download.

Brott S, Pfaff L, Schuricht J, Schwarz JN, Böttcher D, Badenhorst CPS, et al. Engineering and evaluation of thermostable IsPETase variants for PET degradation. Engineering in Life Sciences 2022;22(3-4):192-203.

Carniel A, Valoni É, Junior JN, Gomes ADC, Castro AMD. Lipase from *Candida antarctica* (CALB) and cutinase from *Humicola insolens* act synergistically for PET hydrolysis to terephthalic acid. Process Biochemistry 2017;59:84-90.

Carr CM, Clarke DJ, Dobson ADW. Microbial polyethylene terephthalate hydrolases: Current and future perspectives. Frontiers in Microbiology 2020;11:Article No. 571265.

Chandan MSK. A tale of a landfill and its ravages [Internet]. 2021 [cited 2022 Feb 12]. Available from: https://www.thedailystar.net/news/bangladesh/news/tale-landfill-and-its-ravages-2144066.

Chia WY, Tang DYY, Khoo KS, Lup ANK, Chew KW. Nature's fight against plastic pollution: Algae for plastic biodegradation and bioplastics production. Environmental Science and Ecotechnology 2020;4:Article No. 100065.

Consortium TU. UniProt: The universal protein knowledgebase in 2023. Nucleic Acids Research 2023;51(D1):523-31.

Dallakyan S, Olson AJ. Small-molecule library screening by docking with PyRx. Methods in Molecular Biology 2015; 1263:243-50.

Danso D, Schmeisser C, Chow J, Zimmermann W, Wei R, Leggewie C, et al. New insights into the function and global distribution of polyethylene terephthalate (PET)-degrading bacteria and enzymes in marine and terrestrial metagenomes. Applied and Environmental Microbiology 2018;84(8): e02773-17.

Demirkan E, Güler BE, Sevgi T. Analysis by scanning electron microscopy of polyethylene terephthalate and nylon biodegradation abilities of *Bacillus* sp. strains isolated from soil. Journal of Biological and Environmental Sciences 2020;14(42):107-14.

Dong Q, Xing X. *Chroococcidiorella tianjinensis* gen. et sp. nov. (Trebouxiophyceae, Chlorophyta), a green alga arises from the Cyanobacterium TDX16. American Journal of Plant Sciences 2020;11(11):1814-26.

Falah W, Chen FJ, Zeb BS, Hayat MT, Mahmood Q, Ebadi A, et al. Polyethylene terephthalate degradation by microalga *Chlorella vulgaris* along with pretreatment. Materiale Plastice 2020;57(3):260-70.

Felisberto S, Souza D. Characteristics and diversity of Cyanobacteria in periphyton from lentic tropical ecosystem, Brazil. Advances in Microbiology 2014;4(15):1076-87.

Gama WJ, Laughinghouse HD, St Anna CL. How diverse are coccoid cyanobacteria? A case study of terrestrial habitats from the Atlantic Rainforest (Sao Paulo, Brazil). Phytotaxa 2014;178(2):61-97.

Gamerith C, Vastano M, Ghorbanpour SM, Zitzenbacher S, Ribitsch D, Zumstein MT, et al. Enzymatic degradation of aromatic and aliphatic polyesters by *P. pastoris* expressed cutinase 1 from *Thermobifida cellulosilytica*. Frontiers in Microbiology 2017;8:Article No. 938.

Guillard RRL, Keller MD, O'Kelly CJ, Floyd GL. *Pycnococcus provasolii* gen. et sp. nov., a coccoid prasinoxanthin-containing phytoplankter from the Western North Atlantic and Gulf of Mexico. Journal of Phycology 1991;27(1):39-47.

Han X, Liu W, Huang JW, Ma J, Zheng Y, Ko TP, et al. Structural insight into catalytic mechanism of PET hydrolase. Nature Communications 2017;8:Article No. 2106.

Hempel F, Maier UG. Microalgae as solar-powered protein factories. Advances in Experimental Medicine and Biology 2016;896:241-62.

Hossain KS, Das S, Kundu S, Afrin S, Nurunnabi TR, Rahman SMM. Isolation and characterization of polythene degrading bacteria from garbage soil. International Journal of Agriculture, Environment and Bioresearch 2019;4(5):254-63.

Jangra MR, Nehra KS, Garima, Kajal, Monika, Sonia, et al. Assessment of plastic degrading ability of microbes isolated from local plastic dumping sites. Bioscience Biotechnology Research Communications 2020;13(4):1668-72.

Joo S, Cho IJ, Seo H, Son HF, Sagong HY, Shin TJ, et al. Structural insight into molecular mechanism of poly(ethylene terephthalate) degradation. Nature Communications 2018; 9:Article No. 382.

Kawai F, Oda M, Tamashiro T, Waku T, Tanaka N, Yamamoto M, et al. A novel $Ca^{2+}$-activated, thermostabilized polyesterase capable of hydrolyzing polyethylene terephthalate from *Saccharomonospora viridis* AHK190. Applied Microbiology and Biotechnology 2014;98(24):10053-64.

Kelley LA, Mezulis S, Yates CM, Wass MN, Sternberg MJE. The Phyre2 web portal for protein modeling, prediction and analysis. Nature Protocols 2015;10:845-58.

Kennedy J, Baker P, Piper C, Cotter PD, Walsh M, Mooij MJ, et al. Isolation and analysis of bacteria with antimicrobial activities from the marine sponge *Haliclona simulans* collected from Irish Waters. Marine Biotechnology 2009;11:384-96.

Kim JW, Park SB, Tran QG, Cho DH, Choi DY, Lee YJ, et al. Functional expression of polyethylene terephthalate-degrading enzyme (PETase) in green microalgae. Microbial Cell Factories 2020;19:Article No. 97.

Kumar RV, Kanna GR, Elumalai S. Biodegradation of polyethylene by green photosynthetic microalgae. Journal of Bioremediation and Biodegradation 2017;8(1):Article No. 381.

Malafatti-Picca L, Chaves MRDB, Castro AMD, Valoni É, Oliveira VMD, Marsaioli AJ, et al. Hydrocarbon-associated substrates reveal promising fungi for poly (ethylene terephthalate) (PET) depolymerization. Brazilian Journal of Microbiology 2019;50(3):633-48.

Maurya A, Bhattacharya A, Khare SK. Enzymatic Remediation of polyethylene terephthalate (PET)-based polymers for effective management of plastic wastes: An overview. Frontiers in Bioengineering and Biotechnology 2020;8:Article No. 602325.

Mohanan N, Montazer Z, Sharma PK, Levin DB. Microbial and enzymatic degradation of synthetic plastics. Frontiers in Microbiology 2020;11:Article No. 580709.

Moog D, Schmitt J, Senger J, Zarzycki J, Rexer KH, Linne U, et al. Using a marine microalga as a chassis for polyethylene terephthalate (PET) degradation. Microbial Cell Factories 2019;18:Article No. 171.

Najeeb MI, Ahmad MD, Anjum AA, Maqbool A, Ali MA, Nawaz M, et al. Distribution, screening and biochemical characterization of indigenous microalgae for bio-mass and bio-energy production potential from three districts of Pakistan. Brazilian Journal of Biology 2022;84:e261698.

Ollis DL, Cheah E, Cygler M, Dijkstra B, Frolow F, Franken SM, et al. The α/β hydrolase fold. Protein Engineering 1992; 5(3):197-211.

Palm GJ, Reisky L, Böttcher D, Müller H, Michels EAP, Walczak MC, et al. Structure of the plastic-degrading *Ideonella sakaiensis* MHETase bound to a substrate. Nature Communications 2019;10:Article No. 1717.

Park H, Park J, Lin SH, Boorady LM. Assessment of Firefighters' needs for personal protective equipment. Fashion and Textiles 2014;1:Article No. 8.

Pei J, Kim BH, Grishin NV. PROMALS3D: A tool for multiple protein sequence and structure alignments. Nucleic Acids Research 2008;36(7):2295-300.

Pereira VL, Portillo ER. Isolation, culture and morphological characterization of *Microcystis* sp. toxic strain from the tacuary reservoir. International Journal of Advanced Research 2018; 6:387-93.

Pham TL, Tran THY, Shimizu K, Li Q, Utsumi M. Toxic cyanobacteria and microcystin dynamics in a tropical reservoir: Assessing the influence of environmental variables. Environmental Science and Pollution Research 2021;28(45):63544-57.

Qi X, Yan W, Cao Z, Ding M, Yuan Y. Current advances in the biodegradation and bioconversion of polyethylene terephthalate. Microorganisms 2021;10(1):Article No. 39.

Read BA, Kegel J, Klute MJ, Kuo A, Lefebvre SC, Maumus F, et al. Pan genome of the phytoplankton *Emiliania* underpins its global distribution. Nature 2013;499:209-13.

Rolfe MD, Rice CJ, Lucchini S, Pin C, Thompson A, Cameron ADS, et al. Lag phase is a distinct growth phase that prepares bacteria for exponential growth and involves transient metal accumulation. Journal of Bacteriology 2012;194(3):686-701.

Rüthi J, Cerri M, Brunner I, Stierli B, Sander M, Frey B. Discovery of plastic-degrading microbial strains isolated from the alpine and Arctic terrestrial plastisphere. Frontiers in Microbiology 2023;14:Article No. 1178474.

Samak NA, Jia Y, Sharshar MM, Mu T, Yang M, Peh S, et al. Recent advances in biocatalysts engineering for polyethylene terephthalate plastic waste green recycling. Environment International 2020;145:Article No. 106144.

Silva C, Da S, Silva N, Matamá T, Araújo R, Martins M, et al. Engineered *Thermobifida fusca* cutinase with increased activity on polyester substrates. Biotechnology Journal 2011;6(10):1230-9.

Skariyachan S, Megha M, Kini MN, Mukund KM, Rizvi A, Vasist K. Selection and screening of microbial consortia for efficient and ecofriendly degradation of plastic garbage collected from urban and rural areas of Bangalore, India. Environmental Monitoring and Assessment 2015;187(1):Article No. 4174.

Sugoro I, Pikoli MR, Rahayu DS, Puspito MJ, Shalsabilla SE, Ramadhan F, et al. Microalgae diversity in interim wet storage of spent nuclear fuel in Serpong, Indonesia. International Journal of Environmental Research and Public Health 2022;19(22):Article No. 15377.

Taniguchi I, Yoshida S, Hiraga K, Miyamoto K, Kimura Y, Oda K. Biodegradation of PET: Current status and application aspects. ACS Catalysis 2019;9(5):4089-105.

Tortora GJ, Funke BR, Case CL. Microbiology: An Introduction. 9th ed. San Francisco: Pearson Benjamin Cummings; 2007.

Trott O, Olson AJ. AutoDock Vina: Improving the speed and accuracy of docking with a new scoring function, efficient optimization, and multithreading. Journal of Computational Chemistry 2010;31(2):455-61.

Turmel M, Gagnon MC, O'Kelly CJ, Otis C, Lemieux C. The chloroplast genomes of the green algae *Pyramimonas*, *Monomastix*, and *Pycnococcus* shed new light on the evolutionary history of Prasinophytes and the origin of the secondary chloroplasts of euglenids. Molecular Biology and Evolution 2009;26(3):631-48.

Urbanek AK, Kosiorowska KE, Mirończuk AM. Current knowledge on polyethylene terephthalate degradation by genetically modified microorganisms. Frontiers in Bioengineering and Biotechnology 2021;9:Article No. 771133.

Urbanek AK, Rymowicz W, Strzelecki MC, Kociuba W, Franczak L, Mirończuk AM. Isolation and characterization of Arctic microorganisms decomposing bioplastics. AMB Express 2017;7:Article No. 148

Urme SA, Radia MA, Alam R, Chowdhury MU, Hasan S, Ahmed S, et al. Dhaka landfill waste practices: Addressing urban pollution and health hazards. Buildings and Cities 2021; 2(1):700-16.

Waring RH, Harris RM, Mitchell SC. Plastic contamination of the food chain: A threat to human health? Maturitas 2018;115:64-8.

Wei R, Oeser T, Schmidt J, Meier R, Barth M, Then J, et al. Engineered bacterial polyester hydrolases efficiently degrade polyethylene terephthalate due to relieved product inhibition. Biotechnology and Bioengineering 2016;113(8):1658-65.

Yang S, Xu H, Yan Q, Liu Y, Zhou P, Jiang Z. A low molecular mass cutinase of *Thielavia terrestris* efficiently hydrolyzes poly(esters). Journal of Industrial Microbiology and Biotechnology 2013;40(2):217-26.

Yoshida S, Hiraga K, Takehana T, Taniguchi I, Yamaji H, Maeda Y, et al. A bacterium that degrades and assimilates poly (ethylene terephthalate). Science 2016;351(6278):1196-9.

Zhang H, Perez-Garcia P, Dierkes RF, Applegate V, Schumacher J, Chibani CM, et al. The bacteroidetes *Aequorivita* sp. and *Kaistella jeonii* produce promiscuous esterases with PET-hydrolyzing activity. Frontiers in Microbiology 2022;12: Article No. 803896.

# Effect of Seed Pelleting Application of Plant Growth Promoting Bacteria on Germination and Growth of Lettuce (*Lactuca sativa*)

**Phetcharat Jeephet[1], Nararat Thawong[1], Chuthamat Atnaseo[1,2], Sutheera Hermhuk[1,2] and Jakkrapong Kangsopa[1,2*]**

*[1]Division of Agronomy, Faculty of Agricultural Production, Maejo University, Chiang Mai 50290, Thailand*
*[2]Modern Seed Technology Research Center, Faculty of Agricultural Production, Maejo University, Chiang Mai 50290, Thailand*

**ARTICLE INFO**

Received: 7 Jul 2023
Received in revised: 16 Nov 2023
Accepted: 22 Nov 2023
Published online: 4 Jan 2024
DOI: 10.32526/ennrj/22/20230176

**Keywords:**
Seed enhancement/ Seed germination/ Carboxymethyl cellulose/ Plant growth promoting bacteria

*** Corresponding author:**
E-mail: jakkrapong_ks@mju.ac.th

**ABSTRACT**

Plant growth-promoting bacteria (PGPB) are commonly used to pellet seeds. Different bacterial strains affect germination and plant growth in varying ways. The objective of this experiment was to study the effects of seed pelleting with three strains of bacteria on changes in germination, vigor, seedling growth, and the plant growth of lettuce. The experiment followed a completely randomized design with four repetitions and five treatments: without pelleting (T1), pelleting with $CaSO_4$-zeolite only (T2), pelleting with $1\times10^7$ CFU/mL *Stenotrophomonas* sp. strain sk3 (T3), pelleting with $1\times10^8$ CFU/mL *Burkholderia* sp. strain 3-DB05 (T4), and pelleting with $1\times10^8$ CFU/mL *Enterobacter* sp. strain 4-RB05 (T5). *Burkholderia* sp. and *Enterobacter* sp. were more effective in producing indole-3-acetic acid (IAA), and pelleting seeds with these strains resulted in higher germination rates and seedling growth compared to unpelleted seeds when tested in both laboratory and greenhouse conditions. Seed pelleting with $1\times10^8$ CFU/mL *Enterobacter* sp. promoted plant growth and resulted in significantly higher leaf and root weight. Therefore, seed pelleting with $1\times10^8$ CFU/mL *Enterobacter* sp. strain 4-RB05 is recommended to improve the germination and plant growth of Red Oak Leaf lettuce seeds.

## 1. INTRODUCTION

Red oak leaf lettuce (*Lactuca sativa* L.) is a globally popular salad plant, experiencing increasing demand due to the growing emphasis on promoting health. This has elevated lettuce to a key vegetable in constant demand throughout the year (Kim et al., 2016). However, meeting market demands poses challenges, particularly in large-scale production under soilless systems using seeding machines. Lettuce seeds, with their small size, flat shape, and light weight, present difficulties for seeding machines, leading to issues, such as inconsistent germination rates, uneven growth, and low seedling vigor (Damrosch, 2016).

To address these challenges, seed pelleting technology emerges as a promising solution. Seed pelleting involves adding materials to seeds to increase weight and size, and to alter their shape, facilitating their uses with seeding machines (Taylor and Harman, 1990; Pedrini et al., 2017). Beyond enhancing practicality for seeding machines, seed pelleting provides protection against adverse environmental conditions (Siri, 2015) and offers an avenue to improve seed quality. This improvement is achieved by incorporating substances that promote plant growth into the seed, including plant nutrients, hormones, fungicides, biopesticides, and plant growth-promoting bacteria (Taylor and Harman, 1990; Wurr and Fellows, 1985; Contreras et al., 2008).

The focus of this study was to assess the impact of seed pelleting on the quality of red oak leaf lettuce seeds concerning plant growth-promoting bacteria (PGPB). Specifically, *Stenotrophomonas* sp., *Burkholderia* sp., and *Enterobacter* sp. were chosen for their roles in enhancing plant growth through nitrogen fixation, phosphate solubilization, and the production of growth-promoting substances (Kumar et al., 2023). *Stenotrophomonas* sp., recognized for its versatility, contributes to plant growth by aiding nutrient uptake and boosting stress tolerance (Kumar

**Citation:** Jeephet P, Thawong N, Atnaseo C, Hermhuk S, Kangsopa J. Effect of seed pelleting application of plant growth promoting bacteria on germination and growth of lettuce (*Lactuca sativa*). Environ. Nat. Resour. J. 2024;22(1):26-33. (https://doi.org/10.32526/ennrj/22/20230176)

et al., 2023). *Burkholderia* sp. and *Enterobacter* sp. share similar mechanisms, providing protection against pathogens and improving stress tolerance (dos Santos et al., 2022; Roslan et al., 2020). The incorporation of PGPB through seed pelleting aligns with well-established strategies, as seen in previous studies (Rocha et al., 2019).

Therefore, the objective of this research was to determine the effect of lettuce seed quality after seed pelleting on plant growth-promoting bacteria. Germination and vigor tests were conducted in both laboratory and greenhouse conditions. Ultimately, the implementation of this technology aims to promote self-sufficiency by enabling the development and in-country production of seed pelleting methods. This shift would significantly reduce dependence on imports, fostering a more sustainable and resilient agricultural system.

## 2. METHODOLOGY

### 2.1 Information of bacterial isolates

Three bacterial isolates used in this work were previously isolated, tested for IAA production and phosphate solubilization, and identified based on 16S rRNA gene as explained in Jomkhame and Atnaseo (2021). Two of these isolates were from forest soils in the Huai Hong Khrai Royal Development Study Center (Jomkhame and Atnaseo, 2021) and the 16s RNA of strains 3-DB05 and 4-RB05 were best matched to *Burkholderia* sp. (GenBank: KY048279.1) and *Enterobacter* sp. (GenBank: MN400348.1), respectively. Another strain sk3 was from Chinese kale (*Brassica oleracea* L.) rhizosphere in a farmer plots in the San Sai District of Chiang Mai Province, Thailand (Jeephet, 2022), which matched best to *Stenotrophomonas* sp. (GenBank: NR_118008.1). Essays for plant growth promoting activity of these bacteria were repeated prior to the start of this work whereby IAA production were quantified by colorimetric method using Salkowski's reaction, while phosphate solubilization index (PSI) was used to indicate level of phosphate solubility, which was calculated by dividing the diameter of the clear zone by that of the colony (Paul and Sinha, 2017) after 7 days of growth on Pikovskaya's agar (Jomkhame and Atnaseo, 2021). Plant growth promoting activity of the three isolate is summarized on Table 1.

**Table 1.** Phosphate solubilization index and indole-3-acetic acid (IAA) production (µg/mL) of *Stenotrophomonas* sp., *Burkholderia* sp., and *Enterobacter* sp.

| Bacterium | Phosphate solubilization index | IAA production (µg/mL) |
|---|---|---|
| *Stenotrophomonas* sp. | - | 1.46 |
| *Burkholderia* sp. | 2.80 | 6.98 |
| *Enterobacter* sp. | 3.94 | 9.28 |

### 2.2 Microbes preparation

Bacterial isolates were cultured in 50% TSB (Trypticase Soy Broth) (Himedia®, India) for 24 h, suspended in 0.85% NaCl solution, and adjusted concentrations to $1\times10^7$ CFU/mL for *Stenotrophomonas* sp., $1\times10^8$ CFU/mL for *Burkholderia* sp., and $1\times10^8$ CFU/mL for *Enterobacter* sp. These bacterial concentrations were selected based on data from our previous work (Jeephet, 2022). Each bacterial suspension was mixed with a binding material (0.4% CMC carboxymethyl cellulose (CMC)) at the ratio of 1 mL bacterial culture: 99 mL of 0.4% CMC.

### 2.3 Pelleting lettuce seeds

The surface of the Red Oak leaf lettuce seeds was sterilized with 1% sodium hypochlorite (NaOCl) for 1 min, washed with sterilized distilled water three times, and dried with sterilized tissue paper. For each treatment, 10 g of lettuce seeds was pelleted with the bilayer matrix contained in the inner layer was 40 g calcium sulfate ($CaSO_4$) and in the outer layer was 90 g zeolite determined previously in Jeephet et al. (2022) using a rotary drum (SKK12, CERES International Ltd., Bangkok, Thailand) at spinning rate of 40 rpm. Each layer of the matrix was cemented by the binding material-bacteria mixture prepared as mentioned in 2.1 (Figure 1). Five treatments, which were without pelleting (T1), pelleting with $CaSO_4$-zeolite only (T2), pelleting with $1\times10^7$ CFU/mL *Stenotrophomonas* sp. (T3), pelleting with $1\times10^8$ CFU/ml *Burkholderia* sp. (T4), and pelleting with $1\times10^8$ CFU/mL *Enterobacter* sp. (T5) were applied to Red Oak leaf lettuce seeds. After receiving treatment, seeds were left at room temperature for 48 h to reduce the seed moisture to 7%.

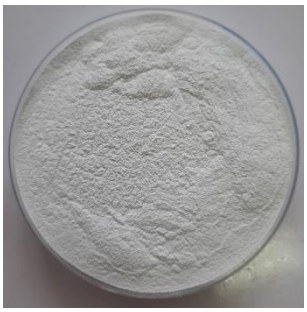

(a) Calcium sulfate powder ($CaSO_4$)

(b) Zeolite powder

(c) Carboxylmethyl cellulose binding agent

(d) Pelleting machine

(e) Lettuce seeds

(f) Lettuce pelleted seeds

**Figure 1.** Characteristic of filler types (a-b), binder type (c), pelleting machine (d), Lettuce seeds (e), and Lettuce pelleted seeds (f)

## 2.4 Evaluation of seed quality

*2.4.1 Seed quality examination under laboratory conditions*

Treated seeds were germinated using the top of paper method with 50 seeds per replication and a total of 4 replications. A germination boxes were placed in a germinator under 25°C, 80% relative humidity, 180 µE light intensity, and 24-h lighting condition. Different data on seed quality was recorded using various methods, as described below.

For the first three days, the speed of radicle emergence was evaluated by counting the number of seeds for which there were appearances of radicle length of at least 2 mm (Mis et al., 2022). Sum of the ratio of numbers of seed with radicle to the total number of tested seeds from each of the first three days were recorded as the speed of radicle emergence. On the third day of seeding, radicle emergence percentage was recorded as a percentage of seeds with apparent radicle.

Similarly, the speed of germination was recorded as a sum of the ratio of numbers of germinated seeds to the total number of tested seeds of each day from the forth to the seventh day of seeding (Czabator, 1962). Germinated seeds were those seeds which developed into normal seedlings. Germination percentage was determined by counting the number of normal seedlings four days (first count) and seven days (final count) after seeding (ISTA, 2013).

On the seventh day of seeding, ten seedlings were randomly selected for evaluating shoot and root lengths. Shoot length was measured from the base of the shoot to the tip of the longest leaf, while the root length was measured from the base of the shoot to the end of the longest root (Baki and Anderson, 1973). The seedling length was measured from the root tip to the tip of the longest leaf. All measurements were aided by a ruler and expressed in millimeter.

*2.4.2 Seed quality examination under greenhouse conditions*

Treated seeds were sawn in a nursery tray using peat moss as media. For this test 50 seeds were used per treatment per replication with a total of four replications.

For the first three days, the speed of cotyledon emergence was evaluated by observing numbers of visibly emerged seedlings (Jeephet et al., 2022). Sum of the ratio of numbers of emerging seed to the total number of tested seeds from each of the first three days were recorded as the speed of cotyledon emergence. On the third day of seeding, cotyledon emergence percentage was recorded as a percentage of emerging seeds.

Assessments of the germination percentage and the speed of germination were identical to those in laboratory conditions. Ten randomly selected seedlings were used for measuring shoot length seven days after planting. Shoot length was assessed from media surface to the tip of the leaf.

### 2.5 Evaluating the effect of seed pelleting on plant growth under non-circulating hydroponic system

One seeds for each treatment was sown in 10 cm pots supported by perlite and vermiculite (70:30). Six pots containing seed undergone the same treatment were placed in a 35 × 50 × 8 cm tray containing 1 L of 10% plant nutrient solution prepared according to the method described by Colmer et al. (2006). The total of 5 trays were used, one for each treatment. The solution in each tray was changed every 3 days, and the experiment was conducted for 45 days. The plant height was evaluated on day 7, 14, 21, 28, 35, 42, and 45 after sowing. At 45 days after sowing, leaf and root fresh weights were assessed. Then, leaf and root were oven dried at 60°C for 72 h before dry weights measurements were taken.

### 2.6 Data analysis

The percentage of germination was arcsine-transformed to normalize the data before statistical analysis. All data were analyzed by one-way analysis of variance (ANOVA, complete randomized design), and the difference between the treatments was tested using Duncan's multiple range test (DMRT).

## 3. RESULTS AND DISCUSSION

### 3.1 Seed quality

After a three-day evaluation in the laboratory, there was no difference in the radicle emergence rate. None of the three bacteria isolates increased the radicle emergence rate of lettuce seeds. Seeds that were not pelleted had a higher radicle emergence rate compared to other methods, but there was no difference between pelleting seeds with $1\times10^8$ CFU/mL *Burkholderia* sp. and $1\times10^8$ CFU/mL *Enterobacter* sp.. Pelleting seeds with $1\times10^8$ CFU/mL *Burkholderia* sp. and $1\times10^8$ CFU/mL *Enterobacter* sp. resulted in a significantly higher germination rate compared to other methods (Table 2).

In greenhouse conditions, a 3-day evaluation after testing revealed that unpelleted seeds had a higher cotyledon emergence rate and speed of cotyledon emergence compared to other methods but did not differ from seeds pelleted with $1\times10^8$ CFU/mL *Burkholderia* sp. and $1\times10^8$ CFU/mL *Enterobacter* sp. There was no significant effect on emergence and vigor in the 3-day period. Seeds pelleted with $1\times10^8$ CFU/mL *Burkholderia* sp. and $1\times10^8$ CFU/mL *Enterobacter* sp. showed significantly higher germination rates of 10% and 14%, respectively, compared to unpelleted seeds. The speed of germination showed results similar to those of the germination test (Table 2).

This result showed that pelleting seeds with plant growth promoting bacteria could enhance germination of lettuce seeds by increasing germination rate both in laboratory and greenhouse conditions and by increasing speed of germination under greenhouse condition. Increasing germination rate and speed of germination was more pronounced when using isolates with higher level of IAA production (*Burkholderia* sp. and *Enterobacter* sp.) suggesting that IAA produced by these isolates contributed to the enhancement of germination. This may be attributed to the influence of IAA on accelerating seed germination through the regulation of endogenous hormones and sucrose metabolism (Zhao et al., 2020). Sucrose metabolism is crucial for the germination process, providing energy for emerging seedlings. Enzymes break down sucrose into glucose and fructose, fueling glycolysis to generate ATP. Additionally, sucrose metabolism contributes to the synthesis of essential molecules—nucleic acids, proteins, and lipids—necessary for building cell structures and supporting overall plant growth during germination (Weber et al., 1997; Xu et al., 2010; Hao et al., 2022).

### 3.2 Seedling growth

In laboratory conditions, the shoot length, root length, and seedling length were greater when seeds were pelleted with $1\times10^8$ CFU/mL *Burkholderia* sp. and $1\times10^8$ CFU/mL *Enterobacter* sp. compared to the other treatments but were not significantly different from $1\times10^7$ CFU/mL *Stenotrophomonas* sp. (Table 3). In greenhouse conditions, seed pelleting with $1\times10^8$ CFU/mL *Enterobacter* sp. resulted in significantly

higher seedling length compared to unpelleted seeds and seeds pelleted with pelleting materials only (Table 3). The experimental results clearly showed that seed pelleted with the 3 bacterial isolates promoted seedling growth in both test conditions, particularly pelleting with *Enterobacter* sp. Enhancement of seedling growth was observed in treatments with plant growth-promoting bacteria, suggesting that these bacteria play a role in this process. The IAA produced by these bacteria stimulates cell expansion, enhancing cell wall flexibility by breaking bonds between cellulose molecules, thereby influencing the permanent stretching of the cell wall. Additionally, IAA reduces cell turgor pressure, promoting increased water influx into the cells and facilitating cell expansion (Cosgrove, 2000). Therefore, it is anticipated that the IAA produced by both types of bacteria contributes significantly to the growth and development of vegetable seedlings compared to unpelleted seeds. Moreover, *Burkholderia* sp. and *Enterobacter* sp. have been reported to promote plant growth by influencing shoot and root length, producing phytohormones, and releasing siderophores. *Burkholderia* sp. produces auxins, cytokinins, and siderophores (Pal et al., 2022), while *Enterobacter* sp. produces auxins, cytokinins, and gibberellins, and facilitates nitrogen fixation (Roslan et al., 2020).

**Table 2.** Radicle emergence (RE), speed of radicle emergence (SRE), germination percentage (GE), speed of germination (SGE), cotyledon emergence percentage (COT), and speed of cotyledon emergence (SCOT) of lettuce after pelleting seeds with *Stenotrophomonas* sp., *Burkholderia* sp., and *Enterobacter* sp., tested under laboratory and greenhouse conditions.

| Treatment[1] | Laboratory condition | | | | Greenhouse condition | | | |
|---|---|---|---|---|---|---|---|---|
| | RE (%) | SRE (root/day) | GE (%) | SGE (seedling/day) | COT (%) | SCOT (root/day) | GE (%) | SGE (seedling/day) |
| T1 | 85[2] | 43.80[a3] | 89[bc] | 21.40[a] | 54[a 2/3] | 9.08[a] | 83[b] | 10.27[c] |
| T2 | 82 | 32.02[b] | 85[c] | 19.82[bc] | 39[b] | 6.50[b] | 90[ab] | 11.07[b] |
| T3 | 83 | 31.76[b] | 92[ab] | 19.03[c] | 41[b] | 6.83[b] | 91[ab] | 11.09[b] |
| T4 | 85 | 34.37[ab] | 94[a] | 20.17[ab] | 43[ab] | 7.17[ab] | 92[a] | 11.62[ab] |
| T5 | 86 | 34.44[ab] | 94[a] | 20.01[ab] | 48[ab] | 8.07[ab] | 95[a] | 12.11[a] |
| F-test | ns | ** | * | ** | * | ** | * | ** |
| CV (%) | 14.01 | 13.82 | 5.89 | 6.73 | 10.02 | 13.62 | 11.79 | 8.94 |

ns, *, **: Non-significantly different and significantly different at $p \leq 0.05$ and $p \leq 0.01$, respectively.
[1]T1=Unpelleted seeds, T2=$CaSO_4$-zeolite, T3=$CaSO_4$-zeolite + $1\times10^7$ CFU/mL *Stenotrophomonas* sp., T4=$CaSO_4$-zeolite + $1\times10^8$ CFU/mL *Burkholderia* sp., and T5=$CaSO_4$-zeolite + $1\times10^8$ CFU/mL *Enterobacter* sp.
[2]Data were transformed by the arcsine before statistical analysis, and back-transformed data are presented.
[3]Means within a column followed by the same letter are not significantly at $p \leq 0.05$ by DMRT.

**Table 3.** Shoot length, root length, and seedling length of lettuce seeds after pelleting seeds with *Stenotrophomonas* sp., *Burkholderia* sp., and *Enterobacter* sp., tested under laboratory and greenhouse conditions.

| Treatment | Laboratory condition | | | Greenhouse condition |
|---|---|---|---|---|
| | Shoot length (mm) | Root length (mm) | Seedling length (mm) | Shoot length (mm) |
| Unpelleted seeds | 10.5[c1] | 54.5[bc] | 65.0[bc] | 10.2[bc] |
| $CaSO_4$-zeolite (P) | 11.3[b] | 47.7[c] | 59.0[c] | 11.0[c] |
| (P) + $1\times10^7$ CFU/mL *Stenotrophomonas* sp. | 13.5[ab] | 59.6[ab] | 73.1[ab] | 15.0[ab] |
| (P) + $1\times10^8$ CFU/mL *Burkholderia* sp. | 17.1[a] | 60.0[a] | 77.1[a] | 15.4[ab] |
| (P) + $1\times10^8$ CFU/mL *Enterobacter* sp. | 17.7[a] | 60.2[a] | 77.9[a] | 16.1[a] |
| F-test | ** | ** | ** | ** |
| CV (%) | 8.44 | 14.21 | 10.59 | 8.41 |

**: Significantly different at $p \leq 0.01$.
[1]Means within a column followed by the same letter are not significantly at $p \leq 0.05$ by DMRT.

The good performance of both types of bacteria has led to studies that align with the findings of this experiment, as follows: Studies indicate that *Burkholderia* sp. enhances the growth of maize, while *Enterobacter* sp. promotes the growth of wheat (Glick, 2012; Kundan et al., 2015). This enhancement in plant

growth is attributed to increased shoot and root length, as well as improved nutrient uptake and utilization efficiency. Several investigations have explored the impact of *Burkholderia* sp. and *Enterobacter* sp. on plant growth through phosphate solubilization. Liu et al. (2018) discovered that *Enterobacter* sp. significantly increased shoot and root length, as well as phosphate uptake in wheat plants. These bacteria also produce other growth-promoting substances, such as phytohormones and siderophores, further contributing to plant growth and development (Glick, 2012). However, research on the phosphate-solubilizing ability of *Stenotrophomonas* sp. has yielded mixed results. Gholami et al. (2009) observed that *Stenotrophomonas* sp. can solubilize phosphate and enhance plant growth. Further investigations are needed to determine the potential of *Stenotrophomonas* sp. as a phosphate-solubilizing bacterium, as its efficacy seems to be strain-dependent and influenced by environmental factors.

### 3.3 Plant height and yield components under non-circulating hydroponic system

During the 7-day assessment period, the plant height of seeds pelleted with bacteria (T3-T5) was higher than that of unpelleted seeds. At 21-45 days after planting, seed pelleting with bacteria led to a significant increase in plant height compared to unpelleted seeds. During the 28-45-day period, seed pelleting with $1\times10^8$ CFU/mL *Enterobacter* sp. resulted in a significantly higher plant height than all other treatments. When comparing the height differences of plants at 7 and 45 days using different methods, seed pelleting with all methods (T2-T5) resulted in significantly higher plants than unpelleted seeds. In particular, seed pelleting with $1\times10^8$ CFU/mL *Enterobacter* sp. showed the most significant increase in plant height compared to the other treatments. However, seed pelleting with all bacterial methods increased plant height compared to the unpelleted seeds (Table 4).

**Table 4.** Plant height of lettuce seeds after pelleting with *Stenotrophomonas* sp., *Burkholderia* sp., and *Enterobacter* sp. tested under non-circulating hydroponic conditions.

| Treatment | Plant height (cm) | | | | | | |
|---|---|---|---|---|---|---|---|
| | 7 days | 14 days | 21 days | 28 days | 35 days | 42 days | 45 days |
| Unpelleted seeds | $1.10^{b1}$ | $6.50^{b}$ | 12.14 | $14.56^{b}$ | $16.84^{c}$ | $18.12^{d}$ | $18.21^{d}$ |
| $CaSO_4$-zeolite (P) | $1.15^{ab}$ | $6.48^{b}$ | 11.21 | $15.17^{ab}$ | $17.77^{bc}$ | $19.18^{c}$ | $19.22^{c}$ |
| (P) + $1\times10^7$ CFU/mL *Stenotrophomonas* sp. | $1.23^{a}$ | $7.11^{ab}$ | 12.08 | $15.89^{ab}$ | $18.24^{b}$ | $20.09^{bc}$ | $20.15^{b}$ |
| (P) + $1\times10^8$ CFU/mL *Burkholderia* sp. | $1.26^{a}$ | $7.32^{a}$ | 12.41 | $15.98^{ab}$ | $18.59^{ab}$ | $20.11^{b}$ | $20.18^{b}$ |
| (P) + $1\times10^8$ CFU/mL *Enterobacter* sp. | $1.25^{a}$ | $7.01^{ab}$ | 12.33 | $16.41^{a}$ | $19.87^{a}$ | $22.21^{a}$ | $22.26^{a}$ |
| F-test | ** | * | ns | ** | * | * | * |
| CV (%) | 8.32 | 13.82 | 15.89 | 16.23 | 17.21 | 17.98 | 19.21 |

ns, *, **: Non-significantly different and significantly different at $p\leq0.05$ and $p\leq0.01$ respectively.
[1]Means within a column followed by the same letter are not significantly at $p\leq0.05$ by DMRT.

This experiment tested lettuce growth under a non-circulating hydroponic system with a 10% nutrient solution concentration, restricting its growth parameters. The outcomes revealed a height and growth boost in lettuce when seeds were pelleted with three types of bacteria. The seed pelleting method proved effective in enhancing seed conditioning by preventing bacteria adherence to the seeds. This technique exhibited advantages over conventional seed planting. Shahab et al. (2009) and Weyens et al. (2009) reported that plant growth-promoting bacteria play a crucial role in producing IAA, which stimulates cell elongation, division, and differentiation. *Burkholderia* sp. and *Enterobacter* sp. in this experiment were found to produce IAA, leading to noticeable differences in plant height after 28 days.

After 45 days, seeds pelleted with *Burkholderia* sp. and *Enterobacter* sp. at concentrations of $1\times10^8$ CFU/mL showed significantly higher fresh shoot weight, dry shoot weight, fresh root weight, and dry root weight compared to unpelleted and pelleting material only. *Stenotrophomonas* sp. at $1\times10^7$ CFU/mL also resulted in higher fresh root weight and dry root weight (Table 5). Studies indicated that *Burkholderia* sp. and *Enterobacter* sp. have the potential to promote lettuce growth. The success of *Burkholderia* sp. and *Enterobacter* sp. in producing IAA contributed to consistent changes in plant height throughout the 45-day test period. *Burkholderia* sp. was particularly effective due to its reported role in fixing atmospheric nitrogen, providing essential components for plant development, and increasing nitrogen

availability, leading to enhanced photosynthesis and increased yield of lettuce plants (Coenye and Vandamme, 2003; Ghosh et al., 2016; Zhang et al., 2021). Similarities between *Enterobacter* sp. and *Burkholderia* sp. in producing growth-promoting substances, including IAA and cytokinins, were noted. These substances play a crucial role in stimulating root growth and overall plant development, affecting both root and leaf biomass. Inoculating *Enterobacter cloacae* MSR1 in *Pisum sativum* seeds, as reported by Khalifa et al. (2016), resulted in increased shoot and root length. *Enterobacter* sp. also shares similarities with *Burkholderia* sp. in promoting plant growth. Consistent with this, the inoculation with *Enterobacter* sp. J49 was observed to enhance the yield of maize crops (Anzuay et al., 2023).

**Table 5.** Fresh leaf weight, dry leaf weight, fresh root weight, and dry root weight of lettuce seeds after pelleting seeds with *Stenotrophomonas* sp., *Burkholderia* sp., and *Enterobacter* sp. tested under non-circulating hydroponic conditions.

| Treatment | Fresh leaf weight (g) | Dry leaf weight (g) | Fresh root weight (g) | Dry root weight (g) |
|---|---|---|---|---|
| Unpelleted seeds | 6.26$^{c1}$ | 0.41$^{b}$ | 3.87$^{bc}$ | 0.19$^{c}$ |
| $CaSO_4$-zeolite (P) | 6.21$^{c}$ | 0.44$^{b}$ | 3.73$^{c}$ | 0.35$^{bc}$ |
| (P) + $1\times10^7$ CFU/mL *Stenotrophomonas* sp. | 7.94$^{b}$ | 0.57$^{b}$ | 4.44$^{b}$ | 0.43$^{b}$ |
| (P) + $1\times10^8$ CFU/mL *Burkholderia* sp. | 8.54$^{a}$ | 0.62$^{a}$ | 4.49$^{a}$ | 0.49$^{a}$ |
| (P) + $1\times10^8$ CFU/mL *Enterobacter* sp. | 8.48$^{a}$ | 0.60$^{a}$ | 4.51$^{a}$ | 0.50$^{a}$ |
| F-test | ** | ** | ** | ** |
| CV (%) | 4.41 | 10.59 | 5.24 | 6.21 |

**: Significantly different at $p\leq0.01$

[1] Means within a column followed by the same letter are not significantly at $p\leq0.05$ by DMRT.

## 4. CONCLUSION

This study showed that *Enterobacter* sp. strain 4-RB05, which had the highest IAA production and PSI levels among the three tested strains, perform best in improving the germination rate in both laboratory and greenhouse conditions. When tested in a non-circulating hydroponic system for 45 days, seeds pelleting with $1\times10^8$ CFU/mL *Enterobacter* sp. resulted in higher plant height, fresh leaf weight, dry leaf weight, fresh root weight, and dry root weight compared to unpelleted seeds. It can be concluded that *Enterobacter* sp. at $1\times10^8$ CFU/mL has the potential to enhance the germination, vigor, and growth of red oak leaf plants. This resulted in higher plant height, fresh leaf weight, dry leaf weight, fresh root weight, and dry root weight compared to unpelleted seeds. Additional recommendations from this experiment include the possibility of seed pelleting with *Stenotrophomonas* sp. at $1\times10^7$ CFU/mL and *Burkholderia* sp. at $1\times10^8$ CFU/mL with lettuce seeds as alternative options. This is because the quality of germination and the yield of lettuce significantly increased compared to unpelleted seeds.

## ACKNOWLEDGEMENTS

We would like to thank The National Research Council of Thailand (NRCT), for the financial support for this research. This project was conducting under the Research and Researcher for industries (RRI) project, 2021, [grant number: N41A640243]. The author would like to offer particular thanks to the Division of Agronomy, Faculty of Agricultural Production, Maejo University for materials and the use of laboratories and research sites.

## REFERENCES

Anzuay MS, Prenollio A, Ludueña LM, Morla FD, Cerliani C, Lucero C, et al. *Enterobacter* sp. J49: A native plant growth-promoting bacteria as alternative to the application of chemical fertilizers on peanut and maize crops. Current Microbiology 2023;80(3):Article No. 85.

Baki AA, Anderson JD. Vigor determination in soybean seed by multiple criteria. Crop Science 1973;13(6):630-3.

Coenye T, Vandamme P. Diversity and significance of *Burkholderia* species occupying diverse ecological niches. Environmental Microbiology 2003;5(9):719-29.

Colmer TD, Cox MCH, Voesenek LACJ. Root aeration in rice (*Oryza sativa*): Evaluation of oxygen, carbon dioxide, and ethylene as possible regulators of root acclimatizations. New Phytologist 2006;170(4):767-78.

Czabator FJ. Germination value: An index combining speed and completeness of pine seed germination. Forest Science 1962;8:386-96.

Contreras S, Bennett MA, Metzger JD, Tay D. Maternal light environment during seed development affects lettuce seed weight, germinability, and storability. HortScience 2008;43:845-52.

Cosgrove DJ. Loosening of plant cell walls by expansins. Nature 2000;407(6802):321-6.

Damrosch B. Why you should try pelleted seeds [Internet]. 2016 [cited 2016 Aug 18]. Available from: https://goo.gl/XgvEMS.

dos Santos IB, Pereira APDA, de Souza AJ, Cardoso EJBN, da Silva FG, Oliveira JTC, et al. Selection and characterization of *Burkholderia* spp. for their plant-growth promoting effects and influence on maize seed germination. Frontiers in Soil Science 2022;1:e805094.

Gholami A, Shahsavan S, Nezarat S. The effect of plant growth promoting rhizobacteria (PGPR) on germination, seedling growth and yield of maize. World Academy of Science, Engineering and Technology 2009;37:19-24.

Ghosh R, Barman S, Mukherjee R, Mandal NC. Role of phosphate solubilizing *Burkholderia* spp. for successful colonization and growth promotion of *Lycopodium cernuum* L. (*Lycopodiaceae*) in lateritic belt of Birbhum district of West Bengal, India. Microbiological Research 2016;183:80-91.

Glick BR. Plant growth-promoting bacteria: Mechanisms and applications. Scientifica 2012;2012:Article No. 963401.

Hao Y, Hong Y, Guo H, Qin P, Huang A, Yang X, et al. Transcriptomic and metabolomic landscape of quinoa during seed germination. BMC Plant Biology 2022;22(1):1-13.

International Seed Testing Association (ISTA). International Rules for Seed Testing. Bassersdorf, Switzerland: ISTA; 2013.

Jeephet P. Effect of Seed Pelleting Formulas with Plant Growth Promoting Bacteria on Lettuce Seed's Quality and Longevity. [dissertation]. Chiang Mai, Maejo University; 2022.

Jeephet P, Atnaseo C, Hermhuk S, Kangsopa J. Effect of seed pelleting with different matrices on physical characteristics and seed quality of lettuce (*Lactuca sativa*). International Journal of Agricultural Technology 2022;18(5):2009-20.

Jomkhame S, Atnaseo C. Effectiveness of PGPB from different origins on enhancing germination and seedling growth of *Oryza sativa* L. cv. KDML105. Khon Kaen Agriculture Journal 2021;1:1011-7.

Khalifa AY, Alsyeeh AM, Almalki MA, Saleh FA. Characterization of the plant growth promoting bacterium, *Enterobacter cloacae* MSR1, isolated from roots of non-nodulating *Medicago sativa*. Saudi Journal of Biological Sciences 2016;23(1):79-86.

Kim MJ, Moon Y, Tou JC, Mou B, Waterland NL. Nutritional value, bioactive compounds and health benefits of lettuce (*Lactuca sativa* L.). Journal of Food Composition and Analysis 2016;49:19-34.

Kumar A, Rithesh L, Kumar V, Raghuvanshi N, Chaudhary K, Pandey AK. Stenotrophomonas in diversified cropping systems: friend or foe? Frontiers in Microbiology 2023;3(14):Article No. 1214680.

Kundan R, Pant G, Jadon N, Agrawal PK. Plant growth promoting rhizobacteria: Mechanisms and current prospects. Journal of Fertilizers and Pesticides 2015;6(2):Article No. 155.

Liu J, Li S, Li X, Luo Y, Chen L. Isolation, characterization, and evaluation of phosphate-solubilizing bacteria from wheat rhizosphere. Journal of Soil Science and Plant Nutrition 2018;18(4):1007-19.

Mis S, Ermis S, Powell AA, Demir I. Radicle emergence (RE) test identifies differences in normal germination percentages (NG) of watermelon, lettuce and carrot seed lots. Seed Science and Technology 2022;50(2):257-67.

Pal G, Saxena S, Kumar K, Verma A, Sahu PK, Pandey A, et al. Endophytic *Burkholderia*: Multifunctional roles in plant growth promotion and stress tolerance. Microbiological Research 2022;265:e127201.

Paul D, Sinha SN. Isolation and characterization of phosphate solubilizing bacterium *Pseudomonas aeruginosa* KUPSB12 with antibacterial potential from river Ganga, India. Annals of Agrarian Science 2017;15(1):130-6.

Pedrini S, Merritt David J, Stevens J, Dixon K. Seed coating: science or marketing spin? Trends in Plant Science 2017;22(2):106-16.

Rocha I, Ma Y, Vosátka M, Freitas H, Oliveira RS. Growth and nutrition of cowpea (*Vigna unguiculata*) under water deficit as influenced by microbial inoculation via seed coating. Journal of Agronomy and Crop Science 2019;205(5):447-59.

Roslan MAM, Zulkifli NN, Sobri ZM, Zuan ATK, Cheak SC, Abdul Rahman NA. Seed biopriming with P-and K-solubilizing *Enterobacter hormaechei* sp. improves the early vegetative growth and the P and K uptake of okra (*Abelmoschus esculentus*) seedling. PloS One 2020; 15(7):e0232860.

Shahab S, Ahmed N, Khan NS. Indole acetic acid production and enhanced plant growth promotion by indigenous PSBs. African Journal of Agricultural Research 2009;4(11):1312-6.

Siri B. Seed Conditioning and Seed Enhancements. Khon Kaen, Thailand: Klungnanawitthaya Priting; 2015.

Taylor AG, Harman GE. Concepts and technologies of selected seed treatments. Annual Review of Phytopathology 1990;28:321-39.

Weber H, Borisjuk L, Wobus U. Sugar import and metabolism during seed development. Trends in Plant Science 1997;2(5):169-74.

Weyens N, Vander Lelie D, Taghavi S, Newman L, Vangronsveld J. Exploiting plant-microbe partnerships to improve biomass production and remediation. Trends in Biotechnology 2009;27:591-8.

Wurr DCE, Fellows JR. A determination of the seed vigour and field performance of crisp lettuce seedstocks. Seed Science and Technology 1985;13:11-7.

Xu F, Tan X, Wang Z. Effects of sucrose on germination and seedling development of *Brassica napus*. International Journal of Biology 2010;2(1):150-4.

Zhang J, Xiao Q, Wang P. Phosphate-solubilizing bacterium *Burkholderia* sp. strain N3 facilitates the regulation of gene expression and improves tomato seedling growth under cadmium stress. Ecotoxicology and Environmental Safety 2021;217:e112268.

Zhao T, Deng X, Xiao Q, Han Y, Zhu S, Chen J. IAA priming improves the germination and seedling growth in cotton (*Gossypium hirsutum* L.) via regulating the endogenous phytohormones and enhancing the sucrose metabolism. Industrial Crops and Products 2020;155:Article No.112788.

# Feasible Application of PCLake Model to Predict Water Quality in Tropical Reservoirs

**Pongsakorn Wongpipun[1], Sanya Sirivithayapakorn[1*], and Narumol Vongthanasunthorn[2]**

*[1]Department of Environmental Engineering, Faculty of Engineering, Kasetsart University, Bangkok 10900, Thailand*
*[2]Faculty of Science and Engineering, Saga University, Saga City, Japan*

**ARTICLE INFO**

Received: 15 Sep 2023
Received in revised: 18 Nov 2023
Accepted: 22 Nov 2023
Published online: 5 Jan 2024
DOI: 10.32526/ennrj/22/20230251

**Keywords:**
PCLake/ Algae/ Eutrophication/ Lake/ Nutrient/ Reservoir

*** Corresponding author:**
E-mail: fengsys@ku.ac.th

**ABSTRACT**

The PCLake model has not previously been used for tropical reservoirs. This study attempted to apply the PCLake model to predict the chlorophyll a concentrations (Chl-a) in a tropical reservoir in Thailand. Sensitivity analyses were performed for the constants affecting the prediction of Chl-a in the phytoplankton module. The model calibration was performed by using the adjusted value of the most sensitive constant with the observed data from July to December 2020. The effects of the initial trophic state of the reservoir on the simulated Chl-a were evaluated. The results showed that Chl-a were sensitive to six constants. Among these constants, the value of the specific extinction of detritus (cExtSpDet) was adjusted using the calculated values from the typical limnological parameters of the studied reservoir. Statistical analyses of the results of calibration and the subsequent validation with the observed data from February to September 2022 were listed as follows: NSE=0.55 and 0.37, RSR=0.67 and 0.79, and PBIAS=27% and 9%, respectively. The initial trophic state of the reservoir had no influence on the long-term prediction of Chl-a. This preliminary effort indicates that the PCLake model can be used to predict Chl-a, which is representative of algal biomass in tropical reservoirs and is essential to water quality models, without complex modifications.

## 1. INTRODUCTION

Eutrophication has many negative effects on aquatic ecosystems. Perhaps the most obvious consequence is the increased growth of algae and aquatic weeds that interfere with water use for fishing, recreational, industrial, agricultural and drinking purposes (Carpenter et al., 1998). Therefore, predictive model of eutrophication, such as the PCLake model, were used to predict and control eutrophication in various reservoirs. The model can estimate the temporal impacts of different reservoir operating policies, point/nonpoint sources of pollution, and land use management planning.

PCLake used in this study is a freely distributed OSIRIS version released under the GNU Lesser General Public License (Mooij et al., 2010). PCLake was created for non-stratified temperate lakes in Northwestern Europe and has been applied effectively to several temperate lakes (Kuzyaka, 2015; Rolighed et al., 2016; Zhao et al., 2020; Zhang et al., 2022) including those in the Mediterranean (Mellios et al., 2015; Laspidou et al., 2017; Coppens et al., 2020) and subtropical (Fragoso et al., 2011; Kong et al., 2017) regions. However, it has never been used in the tropical areas. Most parameter values have been taken from much earlier studies with the model on a phytoplankton-dominated lake (Janse and Aldenberg, 1990; Janse et al., 1992; Aldenberg et al., 1995), while other values were derived from experimental data and field research in a temperate Dutch lake and the remaining values were derived from literature reviews and from calibration based on the combined data of several lakes in the Netherlands (Janse et al., 1992; Janse et al., 1995).

Anthropogenic eutrophication is increasingly recognized as a major threat to inland and coastal water quality in Thailand, with frequent reports of increases in the frequency, duration and severity (Rayan et al., 2021; Thaipichitburapa and Mek-

**Citation:** Wongpipun P, Sirivithayapakorn S, Vongthanasunthorn N. Feasible application of PCLake model to predict water quality in tropical reservoirs. Environ. Nat. Resour. J. 2024;22(1):34-43. (https://doi.org/10.32526/ennrj/22/20230251)

sumpun, 2021; Pinmongkhonkul et al., 2022; Saetang and Jakmunee, 2022).

Although the PCLake model was mainly applied for natural lakes (Kuzyaka, 2015; Rolighed et al., 2016; Coppens et al., 2020; Zhang et al., 2022), this model can also be applied to artificial reservoirs (Mellios et al., 2015; Kong et al., 2017; Laspidou et al., 2017), as it has flexibility regarding the input constants or time series for variables. This means that extreme fluctuations in the variable can be captured throughout the year, especially in reservoirs.

Algae play a key role in the eutrophication process and are essential for water quality modeling. In practice, total algal biomass is often represented by chlorophyll a (Chl-a), which is much easier to measure and provides a reasonable estimate of algal biomass (Zhen-Gang, 2017). This study attempted to demonstrate the potential application of the phytoplankton module of PCLake to predict the Chl-a in a tropical reservoir.

## 2. METHODOLOGY

Study area

The Khlong Luang Ratchalothorn (KLR) Reservoir is a reservoir providing water for agriculture, aquaculture, and water supply. The reservoir has a mean depth of 3.67 m, a surface area of 27 $km^2$ and a volume of 99 million $m^3$. The average water retention time is 355 days. The reservoir is in a sub-basin of the Bang Pakong basin, located at 13°23’00” N and 101°22’40” E in Ban Khlong sub-district, Tha Boon Mi district, Koh Chan, Chonburi province, Thailand at 35.5 m above sea level. The climate is tropical with annual mean precipitation of 1,302.3 mm (during 1993-2022), with the lowest mean monthly air temperature being in December (23°C) and the highest in April (35°C). The watershed areas (525 $km^2$) are mostly mountains. The potential wavelengths in this reservoir calculated from the reservoir fetch was 15.10 m, half of which was greater than the average water depth in the reservoir, indicating complete mixing of the water (Dodson, 2005; Blottiere, 2015).

Model set-up

From Figure 1, a monthly sampling campaign was conducted at the KLR Reservoir. Ten sampling stations were chosen, six in the reservoir (S1-S6) and four at the inlet (S7-S10). Surface water samples were collected based on grab sampling according to APHA et al. (1992). Originally, it was planned to collect samples once a month throughout the years 2020 until 2022, but due to the outbreak of the coronavirus (COVID-19), the locked down was declared for certain periods of those years. Therefore, samples could not be collected continuously. As a result, water quality data obtained from two time periods, July-December 2020 and February-September 2022, were used in the calibration and validation processes respectively. The analyzed water quality parameters were total phosphorus (TP), phosphate ($PO_4$), ammonium ($NH_4$), nitrate ($NO_3$), Kjeldahl nitrogen (TKN), chlorophyll a, and suspended solids (SS). The standard methods from APHA et al. (1992) were used to measure TP, $PO_4$, $NH_4$, $NO_3$, TKN, Chlorophyll a, and SS. A bulb thermometer was used to measure the water temperature. The clarity of the water was measured by Secchi disk.

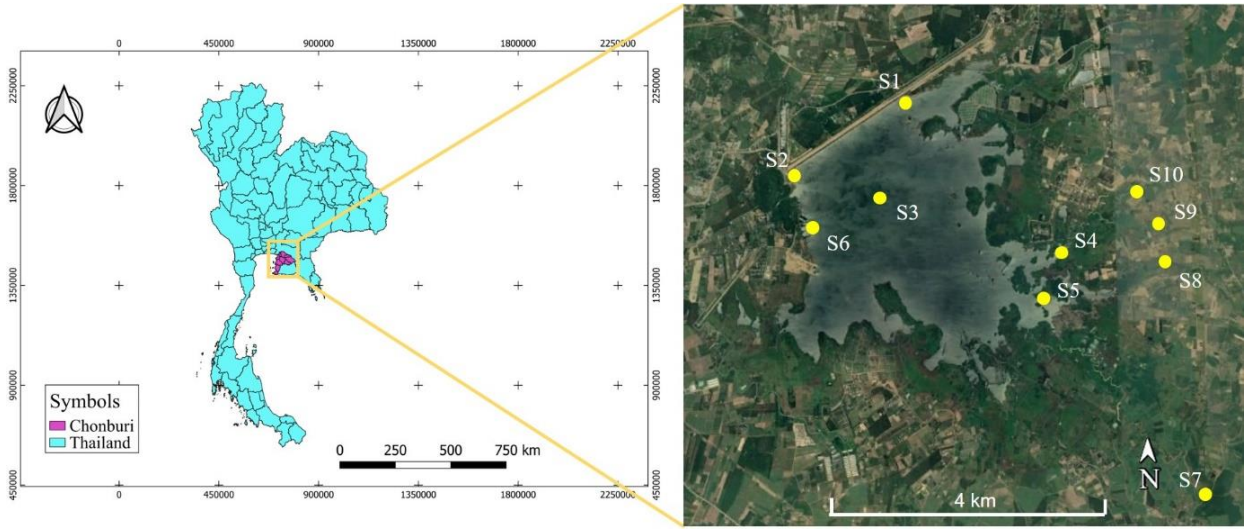


**Figure 1.** Location of sampling points (S1-S10) in Khlong Luang Ratchalothorn (KLR) Reservoir, Chonburi Province, Thailand.

The reservoir water level was recorded on a daily basis as part of the KLR Water Transmission and Maintenance Project of the Royal Irrigation Department. Meteorological data (mean daily wind speed and precipitation) was obtained from the Chonburi meteorological station of the Meteorological Department. The average daily global radiation was provided by the Department of Alternative Energy Development and Efficiency.

The average load of suspended solids leached from the soil surrounding the reservoir was calculated using the universal soil loss equation (Thitirojanawat and Chareonsuk, 1995). The nutrient load from the soil surface was determined by analyzing the soluble nutrients of different surface soils classified by land use types.

The PCLake model consists of seven comprehensive modules: phytoplankton (suspension), sedimentary phytoplankton, transport processes, vegetation, food webs, wetland zone (marsh zone), and seasonality. Current research requires the model to maintain mass balance of dissolved matter and particles in the water layer according to the amount of water flowing into and out of the reservoir. There is also a focus on simulating suspended phytoplankton in the form of Chl-a, therefore only the phytoplankton module and the transfer process module are used. Time step of calculation is 1 day.

### 2.1 Sensitivity and model performance testing

The constants affecting the Chl-a were identified in the phytoplankton module of the PCLake model. The sensitivity test determined the effect of changing the constant in the governing equation on the model output, based on the sensitivity coefficient (SC), as shown in Equation 1 (Rangel-Peraza et al., 2016):

$$SC = \frac{(\%\ \text{Change in output variables})}{(\%\ \text{Change in input constants})} \quad (1)$$

In the current study, the constant was doubled from the default value in the model (to represent extreme physical, chemical, or biological condition), except for maximum reduction factor of phosphorus adsorption affinity (fRedMax) that was increased only 1.2 times because the model could not be run with higher values. For each simulation run (365 days), only one constant was changed, while the other constants used the model defaults. The model default initial values, input factors, and time-series data of the variables were also used for model initialization in the sensitivity tests. Constant values accounting for the top-10% of the most significant change in Chl-a output were identified.

The Nash-Sutcliffe efficiency coefficient (NSE), the root-mean-square error (RMSE)-observations standard deviation ratio (RSR), and percentage bias (PBIAS) were used to evaluate model performance based on the general performance ratings (Table 1) (Moriasi et al., 2007).

NSE is a normalized measurement that assesses how much the residual variance differs from the measured data variance. NSE can be calculated using Equation 2:

$$NSE = 1 - \left[\frac{\sum_{i=1}^{n}(Yi^{obs} - Yi^{sim})^2}{\sum_{i=1}^{n}(Yi^{obs} - Y^{mean,obs})^2}\right] \quad (2)$$

Where; $Yi^{obs}$ is the $i^{th}$ observation for the constituent being evaluated, $Yi^{sim}$ is the $i^{th}$ simulated value for the constituent being evaluated, $Y^{mean,obs}$ is the mean of observed data for the constituent being evaluated and n is the total number of observations. NSE ranges from -∞ to 1.0. If the value is equal to or less than 0, it is considered unacceptable.

RSR is the RMSE normalized by the observed standard deviation. It is calculated as the ratio of the RMSE and the standard deviation of the measured data as shown in Equation 3:

$$RSR = \frac{RMSE}{STDEV_{obs}} = \frac{\left[\sqrt{\sum_{i=1}^{n}(Yi^{obs} - Yi^{sim})^2}\right]}{\left[\sqrt{\sum_{i=1}^{n}(Yi^{obs} - Y^{mean,obs})^2}\right]} \quad (3)$$

RSR is greater than or equal to zero. The lower the RSR (the lower the RMSE), the better the model simulation performance. If RSR is equal to 0, the model simulation is perfect.

PBIAS measures the average tendency of the simulated data to be larger or smaller than their observed counterparts. PBIAS is calculated with Equation 4:

$$PBIAS = \left[\frac{\sum_{i=1}^{n}(Yi^{obs} - Yi^{sim})}{\sum_{i=1}^{n}(Yi^{obs})} \times 100\right] \quad (4)$$

The optimal value of PBIAS is 0; positive values indicate a model bias toward underestimation, whereas negative values indicate a bias toward overestimation.

**Table 1.** General performance ratings for recommended statistics for monthly time step[1]

| Performance Rating | NSE | RSR | PBIAS (%) |
|---|---|---|---|
| Very good | $0.75 < NSE \leq 1.00$ | $0.00 \leq RSR \leq 0.50$ | $PBIAS < \pm 25$ |
| Good | $0.65 < NSE \leq 0.75$ | $0.50 < RSR \leq 0.60$ | $\pm 25 \leq PBIAS < \pm 40$ |
| Satisfactory | $0.50 < NSE \leq 0.65$ | $0.60 < RSR \leq 0.70$ | $\pm 40 \leq PBIAS < \pm 70$ |
| Acceptable/Unsatisfactory | $NSE \leq 0.50$ | $RSR > 0.70$ | $PBIAS \geq \pm 70$ |
| Unacceptable | $NSE < 0$ | – | – |

NSE=Nash-Sutcliffe efficiency coefficient; RSR=RMSE-observations standard deviation ratio; PBIAS=Percentage bias.
[1]Moriasi et al. (2007)

## 2.2 The effect of using a field sensitive constant as a computational constant in the PCLake model

*2.2.1 Calibration and validation*

In the calibration process, values of the top-10% sensitive constants in the phytoplankton module were adjusted using either calculated or literature values. The default initial concentration of each phytoplankton species, which was set in eutrophic state, was used in the calibration since the observed Chl-a in the field from the beginning of July to December 2020 indicated that the reservoir was in eutrophic state.

The results (scenario 2) were compared with the simulation that used all constants as the model default (scenario 1). The validation of the model with the chosen constants in the calibration process was performed using the dataset of February to September 2022 (scenario 3). The initial concentrations of each phytoplankton species in model validation were obtained from the output of the calibration based on the Chl-a. The initial values, input factors and time-series data from actual field observations in calibration and validation are shown in Table 2.

*2.2.2 Effect of initial concentrations of individual phytoplankton species*

The effects of initial concentrations of diatoms, green algae, and blue-green algae were investigated. The concentration of each phytoplankton species varied with the trophic state of the reservoir. The studied reservoir, Khlong Luang Ratchalothorn (KLR) Reservoir (Figure 1) has the possibility to switch between 3 states: mesotrophic, eutrophic and hyper-eutrophic (Boondao et al., 2019). Because field data on the concentrations of individual phytoplankton species were not available, data from the literature were used for each state as shown in Table 3.

**Table 2.** Initial values, input factors and time-series data of variables used for calibration and validation in PCLake model

| Description | Variable | Value (calibration step) from Jul to Dec 2020 | Value (validation step) from Feb to Sep 2022 | Unit |
|---|---|---|---|---|
| Initial value | Lake depth | 2.25 | 2.97 | m |
| | Initial concentration of diatoms in lake water | 0.5 (default) | 0.0171 (from calibration process) | g of dry-weight/$m^3$ |
| | Initial concentration of green algae in lake water | 0.5 (default) | 0.0209 (from calibration process) | g of dry-weight/$m^3$ |
| | Initial concentration of blue-green algae in lake water | 3.0 (default) | 0.4095 (from calibration process) | g of dry-weight/$m^3$ |
| | Dry-weight fraction of solid in sediment | 0.246 | 0.172 | g of dry-weight/g of sediment |
| | Organic fraction of dry-weight sediment | 0.102 | 0.073 | g of dry-weight/g of dry-weight sediment |
| Input factors | Lake size, expressed as fetch | 5,168 | 5,168 | m |
| | Iron content of inorganic matter | 0.032 | 0.016 | g of iron/g of dry-weight |
| | Oxygen concentration in inflow | 2.14 | 3.90 | mg of oxygen/L |
| | Aluminum content of inorganic matter | 0.021 | 0.019 | g of aluminum/g of dry-weight |

**Table 2.** Initial values, input factors and time-series data of variables used for calibration and validation in PCLake model (cont.)

| Description | Variable | Value (calibration step) from Jul to Dec 2020 | Value (validation step) from Feb to Sep 2022 | Unit |
|---|---|---|---|---|
| Time-series | Water temperature | Monthly time-series; Values ranging from 24 to 30 (28±2)[1] | Monthly time-series; Values ranging from 28 to 32 (30±2) | $^{o}$C |
| | Light | Daily time-series; Values ranging from 519.722 to 7,548.889 (4,719.991±1,493.247) | Daily time-series; Values ranging from 1,868.0711 to 7,590.625 (5,405.128±1,373.210) | W/m$^2$ |
| | Wind | Daily time-series; Values ranging from 0.5631 to 3.3786 (1.4314±0.6489) | Daily time-series; Values ranging from 5.068 to 20.272 (8.762±2.881) | m/s |
| | Inflow | Daily time-series; Values ranging from 0.192 to 302.061 (30.084±44.477) | Daily time-series; Values ranging from 0.008 to 321.953 (33.586±43.908) | mm/d |
| | Outflow | Daily time-series; Values ranging from 0 to 22.688 (4.051±5.950) | Daily time-series; Values ranging from 1.685 to 74.654 (22.408±20.187) | mm/d |
| Time-series | Phosphorus loading | Monthly time-series; Values ranging from 0 to 0.225 (0.036±0.084) | Monthly time-series; Values ranging from 0 to 0.096 (0.032±0.038) | g of phosphorus/ m$^2$·d |
| | Phosphate loading | Monthly time-series; Values ranging from 0 to 0.089 (0.014±0.033) | Monthly time-series; Values ranging from 0 to 0.046 (0.015±0.019) | g of phosphorus/ m$^2$·d |
| | Phosphorus bound to organic matter | Monthly time-series; Values ranging from 0 to 0.062 (0.010±0.023) | Monthly time-series; Values ranging from 0 to 0.050 (0.017±0.019) | g of phosphorus/ m$^2$·d |
| | Nitrogen loading | Monthly time-series; Values ranging from 0 to 0.706 (0.113±0.262) | Monthly time-series; Values ranging from 0 to 0.357 (0.116±0.141) | g of nitrogen/m$^2$·d |
| | Ammonium loading | Monthly time-series; Values ranging from 0 to 0.09 (0.02±0.03) | Monthly time-series; Values ranging from 0 to 0.01 (0.01±0.01) | g of nitrogen/m$^2$·d |
| Time-series | Nitrate loading | Monthly time-series; Values ranging from 0 to 0.24 (0.04±0.09) | Monthly time-series; Values ranging from 0 to 0.14 (0.05±0.06) | g of nitrogen/ m$^2$·d |
| | Nitrogen bound to organic matter | Monthly time-series; Values ranging from 0 to 0.147 (0.023±0.055) | Monthly time-series; Values ranging from 0 to 0.213 (0.065±0.085) | g of nitrogen/ m$^2$·d |
| | Inorganic matter loading | Monthly time-series; Values ranging from 0.002 to 11.733 (1.745±4.406) | Monthly time-series; Values ranging from 0.002 to 8.186 (2.245±3.390) | g of dry-weight/ m$^2$·d |

[1]mean±SD

**Table 3.** Initial concentration scenarios for each species of phytoplankton

| Scenario | Initial concentration of phytoplankton in lake water (gDW/m$^3$) | | | Sources |
|---|---|---|---|---|
| | Diatoms | Green algae | Blue-green algae | |
| 4 (eutrophic) | 0.50 | 0.50 | 3.00 | PCLake model's default values |
| 5 (mesotrophic) | 1.47 | 0.09 | 0.81 | Napiórkowska-Krzebietke et al. (2013) |
| 6 (hyper-eutrophic) | 4.29 | 0.95 | 39.81 | Dantas et al. (2008) |

## 3. RESULTS AND DISCUSSION

### 3.1 Sensitivity and model performance testing

In total, there are 59 constants related to the Chl-a in the phytoplankton module of the PCLake model (except those in the Arrhenius equation and an optimum function). Only the sensitivity coefficients results of the top-10% sensitive constants are listed in Table 4.

The sensitivity coefficients indicated that the top-10% sensitive constants of variation in the Chl-a output were: cChDBlueMax (maximum chlorophyll-to-carbon ratio of blue-green algae), cTmOptBlue (optimum temperature of blue-green algae), cExtSpBlue (specific extinction of blue-green algae), kMortBlueW (mortality constant of blue-green algae in water), fPAR (fraction of photosynthetically active radiation), and cExtSpDet (specific extinction of detritus).

Because the composition of phytoplankton in tropical lakes is generally similar to that of temperate lakes (Nilssen, 1984; Sarmento, 2012), default values were given to the following model constants: cChDBlueMax, cTmOptBlue, cExtSpBlue and kMortBlueW. The value of fPAR was also given by default because it corresponded to those measured in tropical regions (Noriega et al., 2021).

The value of cExtSpDet is measured in $m^2$/gDW. This constant may vary depending on the size and on the light-absorption and light-scattering properties of the detritus. The value is the reciprocal of the amount of detritus per square meter in the water column above the Secchi disk and can be calculated using Equation 5 (Carlson, 1977):

$$\text{cExtSpDet} = \frac{K_{det}}{(SS - Chla)} \quad (5)$$

Where; SS is suspended solids, defined as organic solids (in $g/m^3$). Chla is the chlorophyll a concentration (in $g/m^3$). $K_{det}$ is light extinction from detritus (in $m^{-1}$), calculated from Equation 6:

$$K_{det} = K - K_{pure} - K_{phyt} \quad (6)$$

Where; K is total light extinction (in $m^{-1}$), calculated from Equation 7, $K_{pure}$ and $K_{phyt}$ are light extinctions from pure water and phytoplankton, respectively. $K_{pure}$ was set to be 0.1 $m^{-1}$ (Lewis, 1987). $K_{phyt}$ can be calculated according to Equations 8:

$$K = -1 \times \frac{\ln(SD_{light})}{SD} \quad (7)$$

Where; $SD_{light}$ is the fraction of surface light penetration at the SD and is generally reported as 0.1 of SD (Huszar et al., 2006). SD is Secchi disk (in m).

$$K_{phyt} = \left(\frac{cExtSpDiat + cExtSpGren + cExtSpBlue}{3}\right) \times Chla \quad (8)$$

Where; cExtSpDiat, cExtSpGren, and cExtSpBlue are the specific extinction of diatoms, green algae, and blue-green algae, respectively (Huszar et al., 2006).

The values of SD, SS, and Chla were known from field surveys on November 26, 2020 (Table 5), while cExtSpDiat, cExtSpGren, and cExtSpBlue were obtained from the literatures (Riemann et al., 1989; Lee et al., 2000; Fujiki and Taguchi, 2002; Reynolds, 2006; Zhang et al., 2012; Vendruscolo et al., 2019). From Equations 5-8, the value of cExtSpDet would be 2.538 $m^2$/gDW.

### 3.2 The effect of using a calculated constant as a computational constant in the PCLake model

The simulated Chl-a from scenario 1 (all default constants) and scenario 2 (cExtSpDet, calculated from field data with a value of 2.538 $m^2$/gDW and other constants as model default values) were compared with the observed data in the period from July to December 2020 are shown in Figure 2.

The results show that scenario 2 (NSE=0.55, RSR=0.67, PBIAS=27%) is more consistent with the observed data than scenario 1 (NSE=-0.005, RSR=1.00, PBIAS=-75%). That is, the PCLake model satisfactorily predicted the Chl-a in the KLR Reservoir with only the cExtSpDet being changed from the model default (other constants were default values in the model) (NSE=0.55, RSR=0.67), but good and bias toward underestimated (PBIAS=27%). In the validation (scenario 3) with the observed data between February and September 2022, the performance was found to be acceptable (Figure 3, with NSE=0.37, RSR=0.79), but very good and bias toward underestimated (PBIAS=9%).

### 3.3 Effect of initial concentrations of individual phytoplankton species

The results of the simulation in reservoir with different initial trophic state are shown in Figure 4.

**Table 4.** The top 10% sensitivity constants relate to the chlorophyll a concentrations in the phytoplankton module of the PCLake model

| Constant | Unit | Description | Default constant | Increased constant | Simulated mean chlorophyll a concentrations calculated from the default constant simulation ($mg/m^3$) | Simulated mean chlorophyll a concentrations calculated from the increased constant simulation ($mg/m^3$) | Sensitivity coefficient |
|---|---|---|---|---|---|---|---|
| cChDBlueMax | mg Chl/ mg DW | Maximum chlorophyll-to-carbon ratio of blue-green algae | 0.015 | 0.030 | 51.599 | 92.321 | -0.790 |
| cTmOptBlue | ºC | Optimum temperature of blue-green algae | 25 | 50 | 51.599 | 11.693 | 0.770 |
| cExtSpBlue | $m^2/g$ DW | Specific extinction of blue-green algae | 0.35 | 0.70 | 51.599 | 34.524 | 0.330 |
| kMortBlueW | $d^{-1}$ | Mortality constant of blue-green algae in water | 0.01 | 0.02 | 51.599 | 37.278 | 0.280 |
| fPAR | – | Fraction of photosynthetically active radiation (PAR) | 0.48 | 0.96 | 51.599 | 39.304 | 0.238 |
| cExtSpDet | $m^2/g$ DW | Specific extinction of detritus | 0.15 | 0.30 | 51.599 | 39.423 | 0.236 |

**Table 5.** Secchi disk (SD), suspended solid (SS) and chlorophyll a concentration from field surveys on November 26, 2020

| Variable | Value | Unit |
|---|---|---|
| Secchi disk | 0.22 | m |
| Suspended solid | 6.8 | $g/m^3$ |
| Chlorophyll a concentration | 0.0034 | $g/m^3$ |

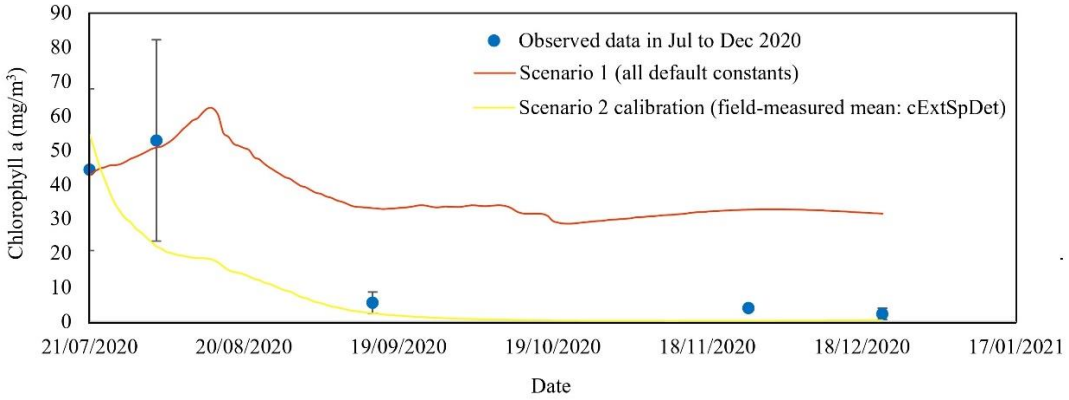


**Figure 2.** Simulated time-series of chlorophyll a concentrations using default and calculated cExtSpDet and observed chlorophyll a concentrations data in Jul to Dec 2020

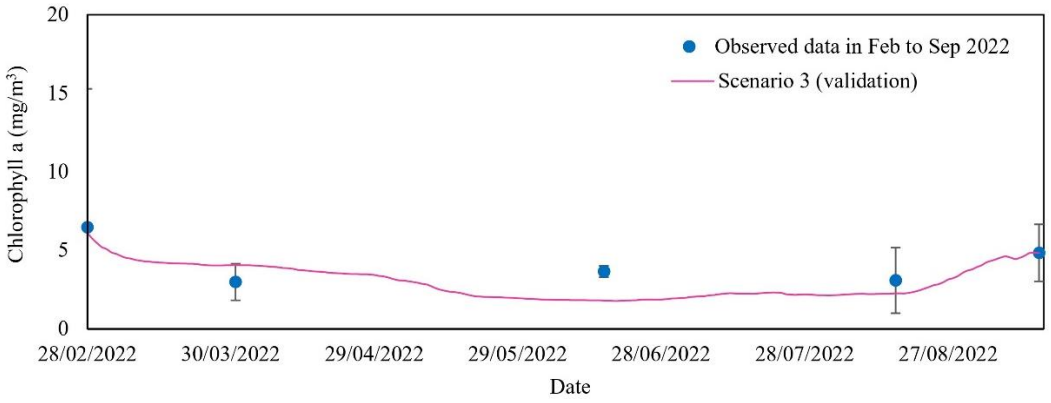


**Figure 3.** Simulated time-series of chlorophyll a concentrations against the observed data in the validation

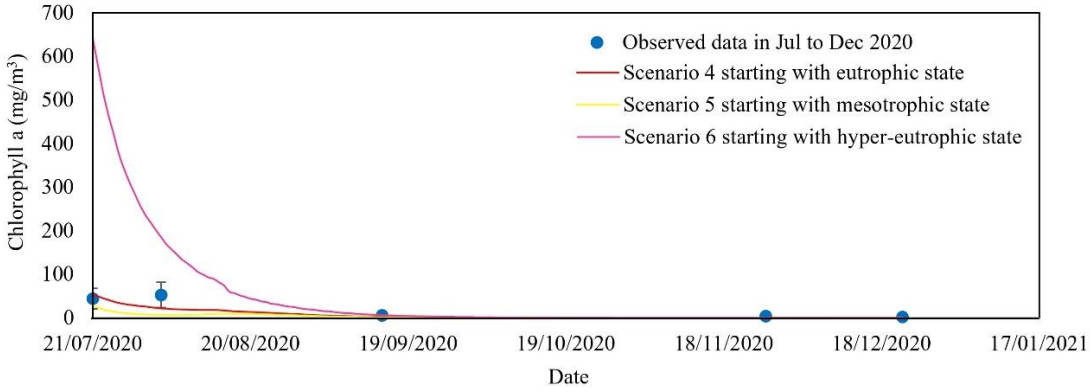


**Figure 4.** Simulated time-series of chlorophyll a concentrations with different initial trophic status

The results indicated that regardless of the initial trophic status of the KLR Reservoir, the simulated Chl-a were similar from day 60 onwards. In other words, the initial concentrations of diatoms, green algae, and blue-green algae in the reservoir had no influence on the long-term prediction of Chl-a.

Thus far, the PCLake model has been successful in simulating Chl-a and phytoplankton biomass in natural lakes located in the Mediterranean region (Coppens et al., 2020) and temperate regions (Zhao et al., 2020; Zhang et al., 2022), but has never been used in tropical areas. Therefore, the present research is the first attempt to apply such a model to a tropical area. The findings from this preliminary study indicated that the PCLake model could be applied to predict the Chl-a in this reservoir. The modification on one of the most sensitive constant, cExtSpDet, was made based on typical limnological parameters of the studied reservoir. Therefore, this model could potentially be applied to the tropical reservoir without complicated modifications. The potential usage of this model provides crucial support to the prospective water quality management programs for the existing reservoirs in Thailand. There is also an opportunity to apply for additional budget to extend the study period for more accurate simulation results.

## 4. CONCLUSION

The performance of the phytoplankton module in the PCLake model was examined for its application in tropical reservoir (i.e., the KLR Reservoir), in terms of its ability to predict Chl-a. The results show that six constants were sensitive to Chl-a: cChDBlueMax, cTmOptBlue, cExtSpBlue, kMortBlueW, fPAR, and cExtSpDet. To Apply the PCLake model to the KLR Reservoir, only the cExtSpDet was selected for calibration to best fit the observed Chl-a for the period July-December 2020 by using the calculated value from the typical limnological parameters of this reservoir. The performance results of the model were satisfactory to good and acceptable to very good in the calibration and validation process, respectively. The initial trophic status of the reservoir had no influence on the long-term prediction of Chl-a. The results demonstrated the potential usage of PCLake model to predict Chl-a in tropical reservoir with uncomplicated modification.

Until now, long-term field data related to the sensitive parameters in the calculation of Chl-a as well as the concentration of each species of phytoplankton were not available in the Khlong Luang Ratchalothorn Reservoir. It is suggested that monitoring plan for water quality simulation is necessary for water quality management in this and other reservoirs.

## ACKNOWLEDGEMENTS

This research was supported by a Ph.D. Scholarship for the Chalermprakiat 70 Years of Reign (fiscal year 2020), Agricultural Research Development Agency (ARDA; Public Organization) (Grant number: HRD6401055).

## REFERENCES

American Public Health Association (APHA), American Water Works Association (AWWA), Water Pollution Control Federation (WPCF). Standard Methods for the Examination of Water and Wastewater. Washington DC: American Public Health Association Inc.; 1992.

Aldenberg T, Janse JH, Kramer PRG. Fitting the dynamic model PCLake to a multi-lake survey through Bayesian statistics. Ecological Modelling 1995;78(1-2):83-99.

Blottiere L. The Effects of Wind-Induced Mixing on the Structure and Functioning of Shallow Freshwater Lakes in a Context of Global Change [dissertation]. Paris, Université Paris Saclay (COmUE); 2015.

Boondao S, Pengphit U, Klaikaew A. Study of Nutrient Content Affecting to Algae Growth: A Case Study of Khlong Luang Rachalothorn Reservoir, Chonburi Province: 25/2018.

Nonthaburi, Thailand: Bureau of Research and Development; 2019.

Carlson RE. A trophic state index for lakes. Limnology and Oceanography 1977;22(2):361-9.

Carpenter SR, Caraco NF, Correll DL, Howarth RW, Sharpley AN, Smith VH. Nonpoint pollution of surface waters with phosphorus and nitrogen. Ecological Applications 1998; 8(3):559-68.

Coppens J, Trolle D, Jeppesen E, Beklioğlu M. The impact of climate change on a Mediterranean shallow lake: Insights based on catchment and lake modelling. Regional Environmental Change 2020;20(62):1-13.

Dantas ÊW, Moura AN, Bittencourt-Oliveira MC, Arruda-Neto JDT, Cavalcanti ADC. Cavalcanti A. Temporal variation of the phytoplankton community at short sampling intervals in the Mundaú reservoir, Northeastern Brazil. Acta Botanica Brasilica 2008;22(4):970-82.

Dodson SI. Introduction to Limnology, 1st ed. New York, NY, USA: McGraw-Hill; 2005.

Fragoso CR, Motta Marques DML, Finkler Ferreira T, Janse JH, van Nes EH. Potential effects of climate change and eutrophication on a large subtropical shallow lake. Environmental Modelling and Software 2011;26(11):1337-48.

Fujiki T, Taguchi S. Variability in chlorophyll a specific absorption coefficient in marine phytoplankton as a function of cell size and irradiance. Journal of Plankton Research 2002;24(9):859-74.

Huszar VL, Caraco NF, Roland F, Cole J. Nutrient-chlorophyll relationships in tropical-subtropical lakes: Do temperate models fit? Biogeochemistry 2006;79:239-50.

Janse JH, Aldenberg T. Modelling phosphorus fluxes in the hypertrophic Loosdrecht lakes. Hydrobiological Bulletin 1990;24:69-89.

Janse JH, Aldenberg T, Kramer PRG. A mathematical model of the phosphorus cycle in Lake Loosdrecht and simulation of additional measures. Hydrobiologia 1992;233:119-36.

Janse JH, Van Donk E, Gulati RD. Modelling nutrient cycles in relation to food web structure in a biomanipulated shallow lake. Netherland Journal of Aquatic Ecology 1995;29:67-79.

Kong X, He Q, Yang B, He W, Xu F, Janssen ABG, et al. Hydrological regulation drives regime shifts: Evidence from paleolimnology and ecosystem modeling of a large shallow Chinese lake. Global Change Biology 2017;23(2):737-54.

Kuzyaka E. Modeling Impacts of Eutrophication and Climate Change in Lake Eymir using PCLake Model [dissertation]. Ankara, Middle East Technical University; 2015.

Laspidou C, Kofinas D, Mellios N, Latinopoulos D, Papadimitriou T. Investigation of factors affecting the trophic state of a shallow Mediterranean reconstructed lake. Ecological Engineering 2017;103:154-63.

Lee SJ, Jang MH, Kim HS, Yoon BD, Oh HM. Variation of microcystin content of *Microcystis aeruginosa* relative to medium N:P ratio and growth stage. Journal of Applied Microbiology 2000;89(2):323-9.

Lewis WM. Tropical limnology. Annual Review of Ecology and Systematics 1987;18(1):159-84.

Mellios N, Kofinas D, Laspidou C, Papadimitriou T. Mathematical modeling of trophic state and nutrient flows of Lake Karla using the PCLake model. Environmental Processes 2015;2(S1):85-100.

Mooij WM, Trolle D, Jeppesen E, Arhonditsis G, Belolipetsky PV, Chitamwebwa DBR, et al. Challenges and opportunities for integrating lake ecosystem modelling approaches. Aquatic Ecology 2010;44(3):633-67.

Moriasi DN, Arnold JG, Van Liew MW, Bingner RL, Harmel RD, Veith TL. Model evaluation guidelines for systematic quantification of accuracy in watershed simulations. Transactions of the ASABE 2007;50(3):885-900.

Napiórkowska-Krzebietke A, Stawecki K, Pyka JP, Hutorowicz J, Zdanowski B. Phytoplankton in relation to water quality of a mesotrophic lake. Polish Journal of Environmental Studies 2013;22(3):793-800.

Nilssen JP. Tropical lakes - functional ecology and future development: The need for a process-orientated approach. Hydrobiologia 1984;113:231-42.

Noriega Gardea MMÁ, Corral Martínez LF, Anguiano Morales M, Trujillo Schiaffino G, Salas Peimbert DP. Modeling photosynthetically active radiation: A review. Atmósfera 2021;34(3):357-70.

Pinmongkhonkul S, Prommana R, Khamkhunmuang T, Singkurt S, Sukcharoen A, Madhyamapurush W. The water quality assessment and biodiversity of phytoplankton in Phayao Lake, Phayao province, Thailand. The Journal of Agrobiotechnology Management and Economics 2022;24(2):65-72.

Rayan SB, Kaewdonree S, Rangsiwiwat A, Chartchumni B. Distribution of aquatic plants in Nong Han Wetland, Thailand. Songklanakarin Journal of Science and Technology 2021;43(1):195-202.

Rangel-Peraza JG, De Anda J, González-Farías FA, Rode M. Sensitivity and uncertainty analysis on water quality modelling of Aguamilpa Reservoir. Journal of Limnology 2016;75(s1):81-92.

Reynolds CS. The Ecology of Phytoplankton (Ecology, Biodiversity and Conservation). Cambridge: Cambridge University Press; 2006.

Riemann B, Simonsen P, Stensgaard L. The carbon and chlorophyll content of phytoplankton from various nutrient regimes. Journal of Plankton Research 1989;11(5):1037-45.

Rolighed J, Jeppesen E, Søndergaard M, Bjerring R, Janse JH, Mooij WM, et al. Climate change will make recovery from eutrophication more difficult in shallow Danish Lake Søbygaard. Water 2016;8(10):Article No. 459.

Saetang S, Jakmunee J. Evaluation of eutrophication state of Mae Kuang Reservoir, Chiang Mai, Thailand by using Carlson's trophic state index. Applied Science and Engineering Progress 2022;15(3):Article No. 4012.

Sarmento H. New paradigms in tropical limnology: The importance of the microbial food web. Hydrobiologia 2012;686(1):1-14.

Thaipichitburapa P, Meksumpun C. The effects of dissolved inorganic nutrients on eutrophication situations of Trat Bay, Trat Province. Burapha Science Journal 2021;26(2):770-82.

Thitirojanawat P, Chareonsuk S. Comparative study of rainfall erosivity factor (R-factor) to estimate of soil loss by using the Universal Soil Loss Equation (USLE). Proceedings of the 1995 Annual Forestry Conference; 1995 Nov 20-24; Kasetsart university, Bangkok: Thailand; 1995.

Vendruscolo RG, Fagundes MB, Maroneze MM, do Nascimento TC, de Menezes CR, Barin JS, et al. *Scenedesmus obliquus* metabolomics: Effect of photoperiods and cell growth phases. Bioprocess and Biosystems Engineering 2019;42(5):727-39.

Zhang C, Zhu Z, Špoljar M, Kuczyńska-Kippen N, Dražina T, Cvetnić M, et al. Ecosystem models indicate zooplankton biomass response to nutrient input and climate warming is

related to lake size. Ecological Modelling 2022;464:Article No. 109837.

Zhang Y, Yin Y, Wang M, Liu X. Effect of phytoplankton community composition and cell size on absorption properties in eutrophic shallow lakes: Field and experimental evidence. Optics Express 2012;20(11):11882-98.

Zhao G, Gao X, Zhang C, Sang G. The effects of turbulence on phytoplankton and implications for energy transfer with an integrated water quality-ecosystem model in a shallow lake. Journal of Environmental Management 2020;256:Article No. 109954.

Zhen-Gang J. Hydrodynamics and Water Quality: Modeling Rivers, Lakes and Estuaries. New Jersey, USA: John Wiley and Sons Inc.; 2017.

# Wood Substitute Material from Coconut Shell Waste and Green Adhesive

**Ariya Watcharawitthaya[1], Natee Srisawat[2], and Siriluk Chiarakorn[1*]**

[1]*Environmental Technology Program, School of Energy, Environment and Materials, King Mongkut's University of Technology Thonburi, Thailand*

[2]*Department of Textile Engineering Program, Faculty of Engineering, Rajamangala University of Technology Thanyaburi, Pathumthani, Thailand*

**ARTICLE INFO**

Received: 13 Jul 2023
Received in revised: 13 Nov 2023
Accepted: 27 Nov 2023
Published online: 8 Jan 2024
DOI: 10.32526/ennrj/22/20230182

**Keywords:**
Coconut shell/ Tapioca starch/ Epoxidized natural rubber/ Adhesive/ Hydraulic compression/ Wood substituted materials

*** Corresponding author:**
E-mail: siriluk.chi@kmutt.ac.th

**ABSTRACT**

This research aimed to utilise coconut shell waste as a raw material to produce compressed coconut shell sheets by using environmentally friendly adhesive from epoxidized natural latex and gelatinized tapioca starch. The coconut shells were cut into 1-mm particles and mixed with the adhesive. The mixture was then compressed in a 30×30×0.5 cm mould using a hydraulic compression machine at 5 MPa and 170°C for 5 minutes to form a compressed coconut shell sheet. The different ratios of adhesive to coconut shell particles (30, 40, and 50 g) per 100 g of coconut shell and the different ratios of gelatinized tapioca starch and epoxidized natural rubber (ranging from 1:0, 1:1, 2:1, 3:1, to 4:1 by weight) were examined. Scanning Electron Microscopy (SEM) and Fourier Transform Infrared Spectroscopy (FTIR) were employed to analyse the morphology and chemical composition of the coconut shell sheets, respectively. The physical and mechanical properties of the compressed coconut shell sheets were evaluated based on the Thai Industrial Standard (TIS) number 876-2547 for flat pressed particleboards. The results demonstrate successful production of compressed coconut shell sheets from coconut shell waste using the environmentally friendly adhesive. ENR played a role in networking between lignin and cellulose. While GTS improved the strength of the composite using hydrogen bonding. The optimal ratio of adhesive to coconut shell particles was 40 g of the green adhesive per 100 g of coconut shell. The optimal ratio of gelatinized tapioca starch to epoxidized natural rubber was 2:1 by weight. The coconut shell sheets produced from this study were uniform in shape, had unique textures, and met industry standards for wood substitute materials.

## 1. INTRODUCTION

Wood substitute materials (WSM) is wood that is substituted by various materials such as plastics, concrete, biomass etc. (Strykowski, 2013). The main wood substitute materials found in Thailand can be classified as flat-pressed (FP) particle board and plywood. Flat-pressed (FP) particle board is a sheet product manufactured by compressing wood or lignocellulosic materials in a hot press and bonding them with adhesive (Agnantopoulou et al., 2012). Plywood is a composite material manufactured from thin layers of wood veneer, typically bonded together with resin glue (Roumeli et al., 2012). Urea-formaldehyde adhesive is a common adhesive used for wood substituted materials, but it is toxic to the environment and human health (Naya and Nakanishi, 2005). Short-term effects of formaldehyde exposure include headache, runny nose, nausea and difficulty breathing. While long-term effects of formaldehyde exposure can lead to lung cancer. The World Health Organization (WHO) has developed a guideline for formaldehyde in non-occupational settings at 100 ppb (0.1 mg/m$^3$) for 30 minutes (Kaden et al., 2010). In Thailand, the Indoor Air Quality Association recommends the concentration of formaldehyde should not more than 0.1 ppm or 120 µg/m$^3$ (Bureau of Environmental Health, 2016). According to the European formaldehyde emission standard,

**Citation:** Watcharawitthaya A, Srisawat N, Chiarakorn S. Wood substitute material from coconut shell waste and green adhesive. Environ. Nat. Resour. J. 2024;22(1):44-54. (https://doi.org/10.32526/ennrj/22/20230182)

engineered wood products classified as E1 have the limit of formaldehyde emission to be equal to or less than 0.07 ppm. Thus, many researchers have explored environmentally friendly and non-toxic adhesive alternatives for wood substitute materials.

Thuraisingam et al. (2016) investigated the potential of natural rubber latex (NRL) in combination with rice flour as a binding agent to replace harmful urea-formaldehyde adhesives in the production of wood-based medium-density fibreboard (MDF) in the wood assembly industry. The study examined various ratios of natural latex mixed with rice flour and concluded that this combination produced an effective adhesive. Similarly, Agnantopoulou et al. (2012) conducted research on wood-based substitutes made from sawdust generated by lumber mills, using starch as a binder. The study highlights that while starch can effectively increase load-bearing capacity of the materials, wood substitute materials made from biomass particles and starch are often rigid and brittle, with low water resistance. To circumvent these limitations, this study utilises natural latex as a binding agent, given that natural rubber molecules can enhance the resiliency of wood substitute materials.

Starch is a macromolecular glucose polymer with the general formula $(C_6H_{10}O_5)_n$, in which anhydro-glucose units are connected by α-glycosidic linkage bonds. However, compared to monosaccharides, starch molecules are chemically non-reactive, and thus require a gelatinization pretreatment to increase hydroxyl functional groups. This gelatinization process breaks down intermolecular bonds in starch molecules in the presence of water and heat, allowing for increased water engagement and easier reaction with other functional groups. Rattanavilai (2007) used gelatinized sticky rice flour mixed with epoxidized natural rubber as a binder for rubber wood substitute materials. The binder significantly improved the water resistance and mechanical strength of the wood substitute materials. The combination of gelatinized starch and epoxidized natural rubber has many advantages. In addition to gelatinized starch and epoxidized natural rubber producing an effective binding agent, both are also able to decompose naturally, and thus the combination is non-toxic to the environment. Moreover, the processing and use of these two substances as wood substitute materials do not release formaldehyde.

Coconut shells are agricultural waste products from coconut-processing industries, which account for 23% of each coconut (Husseinsyah and Mostapha, 2011). In Thailand, the quantity of coconuts used for coconut milk production reached approximately 858,000 tons in 2018 alone, which resulted in nearly 200,000 tons of coconut shell waste (Junmee et al., 2021). While some coconut shell waste is used as fuel, a significant portion often goes directly to open dumps and landfills, causing adverse environmental impacts. Consequently, the transformation of coconut shell waste to value-added products has gained significant interest in Thailand in recent years.

Rubber production also plays a significant role in Thailand's industries. In fact, with over 1.8 million hectares of *Hevea brasiliensis* (commonly known as para rubber) cultivated in the southern Thailand, the country is the world's largest producer and exporter of natural rubber (Simon et al., 2021). Due to its affordability and abundant availability, natural rubber provides a desirable alternative to producing adhesives in wood substitute materials.

The goal of this study is to produce a wood substitute material using coconut shell waste and an adhesive made from epoxidized natural rubber and low-cost starch, such as tapioca starch. The study investigates the optimal ratios of coconut shell to adhesive and examines the ratio of tapioca starch to epoxidized natural rubber in the adhesive. The physical and mechanical properties of the compressed coconut shell sheets are evaluated according to the Thai Industrial Standard (TIS) No. 876-2547.

## 2. METHODOLOGY

### 2.1 Materials

The coconut shell waste for this study was obtained from local enterprises in Ban Thung Pradu Community, located in Thap Sakae District of Prachuap Khiri Khan Province, Thailand. The raw materials and chemicals used in this study include tapioca starch, hydrochloric acid (HCl) 37% (w/w), formic acid (85%), hydrogen peroxide ($H_2O_2$) 37%, methanol, Triton X-100 surfactant, potassium hydroxide (KOH) 10%, high-ammonia type latex with dry rubber content (DRC) of 60%, instant tapioca starch, and coconut shell particles.

### 2.2 Crushing coconut shells

Coconut shell waste was dried overnight in an oven and subsequently shredded and ground into smaller particles. The ground coconut shell particles were then filtered through a sieve with 1 mm openings.

### 2.3 Preparation of epoxidized natural rubber

The epoxidation process involved mixing 60% of dry rubber content (DRC) with 10% Triton X and stirring it at 170 rpm at 60°C for 20 min. Hydrogen peroxide was then added to the mixture, followed by formic acid. The mixture was continuously stirred at 300 rpm at 60°C for 3 h. The process resulted in Epoxidized Natural Rubber (ENR).

### 2.4 Preparation of gelatinized tapioca starch

The gelatinization process entailed combining 250 g of tapioca starch with 250 mL of distilled water (1:1 w/v). The mixture was stirred at 60°C for 30-45 min until the starch formed a viscous and transparent texture. The outcome was named Gelatinized Tapioca Starch (GTS).

### 2.5 Preparation of coconut shell sheets

The first step to make coconut shell sheets was to prepare an adhesive, which was achieved by mixing ENR and GTS in a 1:1 weight ratio, following the method outlined by Akbari et al. (2014). The mixture was stirred at room temperature for 15 min at a speed of 170 rpm. The adhesive was then combined with 100 g of coconut shell particles using different adhesive portions of 30, 40, and 50 g. For each adhesive ratio, the mixture was stirred at 2,000 rpm for 15 sec. The mixture of each adhesive ratio was later poured into a 30×30×0.5 cm square mould, as depicted in Figure 1. The mixture was then compressed using a hydraulic compression machine at a mould temperature of 170°C under pressure of 5 MPa for 5 min, following the method outlined by Lim et al. (2021).

The study also examined the effect of GTS and ENR content on mechanical strength. This was done by comparing five different weight ratios of GTS: ENR at 1:0, 1:1, 2:1, 3:1, and 4:1.

**Figure 1.** A 30×30×0.5 cm square mold with a mixture of coconut shell particles and the adhesive

### 2.6 Characterization of coconut shell sheets

The surface morphology of the coconut shell sheets was observed using scanning electron microscopy (SEM) at a magnification of 500X. The chemical composition of the coconut shell sheets was examined using the Fourier Transform Infrared Spectroscopy (FTIR) technique. FTIR spectra were recorded in transmission mode, ranging from 500 to 4,000 $cm^{-1}$.

### 2.7 Mechanical testing of coconut shell sheets

The mechanical testing conducted in this study adhered to the guidelines outlined in the Thai Industrial Standard (TIS) No. 876-2547 for Flat Pressed Particleboards. The details of the testing procedure are described as follows.

#### *2.7.1 Density*

The specimens were cut to a size of 50 mm × 50 mm and weighed with an accuracy of ±0.01 g. The thickness of each specimen was measured at its center using a vernier caliper, along with the width and length of the specimen. The density of each specimen was calculated using Equation (1).

$$\text{Density (kg/m}^3\text{)} = \frac{M}{V} \times 10^6 \quad (1)$$

Where; M is the mass of the specimen (g); V is the volume of the specimen ($mm^3$).

#### *2.7.2 Moisture content testing*

The specimens were weighed (with an accuracy of ±0.01 g) before being dried in an oven at (103±2°C) until the weight did not deviate by more than 0.1%. The moisture content (%) was calculated using Equation (2).

$$\text{Moisture content (\%)} = \frac{(m_1 - m_2)}{m_2} \times 100 \quad (2)$$

Where; $m_1$ is the initial weight of the specimen before drying (g); $m_2$ is the weight of the specimen after drying (g).

#### *2.7.3 Swelling analysis*

Firstly the thickness of the specimens was measured at the center. Secondly, the specimens were submerged in clean water at a temperature of 20±2°C for 1 h lastly, the specimens were removed from the water and dried at room temperature for another 1 h before being measured at the center position. The swelling thickness was calculated using Equation (3).

$$\text{Swelling according to thickness (\%)} = (t_2 - t_1) / t_1 \times 100 \quad (3)$$

Where; $t_1$ is the thickness of the specimen before immersion in water (mm); $t_2$ is the thickness of the specimen after immersion in water (mm).

*2.7.4 Flexural strength and elastic modulus testing*

The specimens were cut to a size of 20 cm × 5 cm and placed in the Universal Testing Machine. A load was applied at the center of the specimens until they fractured. The maximum force (in N) recorded by the machine was used to calculate the flexural strength in MPa using Equation (4). The elastic modulus was calculated using Equation (5).

$$f_m = \frac{3\,F_{max} \times l_1}{2\,bt^2} \quad (4)$$

Where; $f_m$ is the flexural strength (MPa); $F_{max}$ is the maximum force that the specimen can withstand (N); $l_1$ is the length of the support span (mm); b is the width of the specimen (mm); t is the thickness at the center of the specimen (mm).

$$E_m = \frac{{l_1}^3 (F_2 - F_1)}{4\,bt^2 (a_2 - a_1)} \quad (5)$$

Where; $E_m$ is the elastic modulus [N/mm]; $F_2$-$F_1$ is the force applied during the initial straight-line portion of the load-deflection curve (N); $a_2$-$a_1$ is the strain during the initial straight-line portion of the load-deflection curve (mm).

*2.7.5 Tensile strength testing*

The specimens (25 mm × 100 mm) were positioned in the grips of a Universal Test Machine and subjected to tension until failure. A typical test speed of 2 mm/min was employed for standard test specimens. The tensile strength was calculated using Equation (6).

$$\text{Tensile strength (MPa)} = \frac{F}{W \times L} \quad (6)$$

Where; F is the maximum pulling force (N); W is the width of the specimen (mm); L is the length of the test piece (mm).

## 3. RESULTS AND DISCUSSION

### 3.1 Effect of the ratio between adhesive and coconut shell particles

Figure 2 shows the white and homogeneous adhesive prepared as a mixture of ENR and GTS in a ratio of 1:1 by weight, as shown in Figure 2. Figure 3 presents a comparison of coconut shell sheets prepared using three different adhesive ratios: (a) 30 g, (b) 40 g, and (c) 50 g with 100 g of coconut shell particles.


**Figure 2.** (a) ENR (b) GTS and (c) Adhesive (1:1 weight ratio)

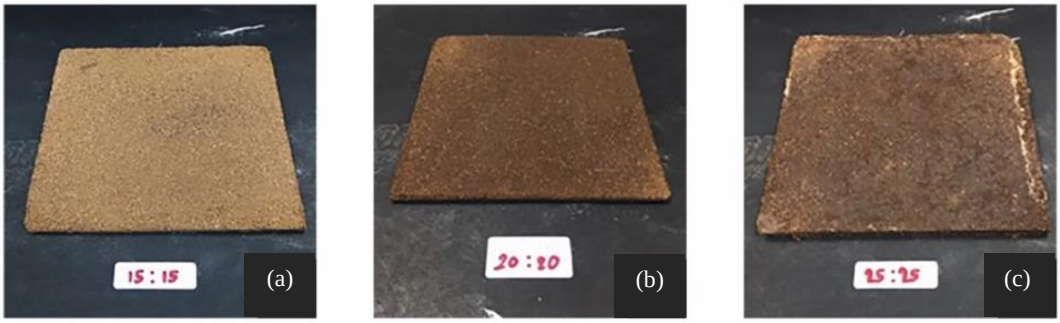


**Figure 3.** The coconut shell sheets prepared from three different adhesive ratios: (a) 30 g, (b) 40 g, and (c) 50 g with 100 g of coconut shell particles

As shown in Figure 3, the surfaces of samples (b) and (c) are dark brown in colour. This colouration occurred because the excess adhesive on the surface was burnt during compression at 170°C. Since the adhesive contained tapioca starch, the starch decomposed when heated above its decomposition temperature of 169.2°C (Lacerda et al., 2009). The experiment also revealed that that the greater the amount of adhesive used, the more deformation occurred. Meanwhile, the surface of sample (a) was not burnt, but it was brittle and could be broken easily by hand. This brittleness was due to an insufficient amount of adhesive to completely bind the coconut shell particles (Olumuyiwa et al., 2012). Consequently, a ratio of 40:100 (adhesive to coconut shell particles by weight) was chosen to investigate the optimal ratio of ENR to GTS in the next section.

### 3.2 Effect of the ratio between the GTS and ENR in adhesive

Based on the previous findings, the optimal adhesive content was set at 40 g, which comprised of 20 g of GTS and 20 g of ENR. To further investigate the impact of GTS and ENR content on the mechanical properties of the coconut shell sheets, samples were set up using adhesives with five varying weight ratios of GTS to ENR: 1:0, 1:1, 2:1, 3:1, and 4:1, as indicated in Table 1.

Figure 4 illustrates the surface morphologies of all five samples with different adhesive formulas. All samples were successfully formed through hydraulic compression without experiencing high-temperature deformation. Sample (a) (without ENR) was very rigid, but brittle and could be easily broken by hand. However, with the addition of ENR in the adhesive, the compressive strength of the samples improved significantly. Figure 5 presents the test results of the samples with five different adhesive formulas (a), (b), (c), (d), and (e) according to TIS 876-2547.

**Table 1.** The adhesive formulas with different ratios between the GTS and ENR (the ratio of adhesive to coconut shell was fixed at 40 g:100 g)

| Samples | GTS (g) | ENR (g) | Weight Ratio |
|---|---|---|---|
| (a) | 40 | 0 | 1:0 |
| (b) | 20 | 20 | 1:1 |
| (c) | 26.7 | 13.3 | 2:1 |
| (d) | 30 | 10 | 3:1 |
| (e) | 32 | 8 | 4:1 |

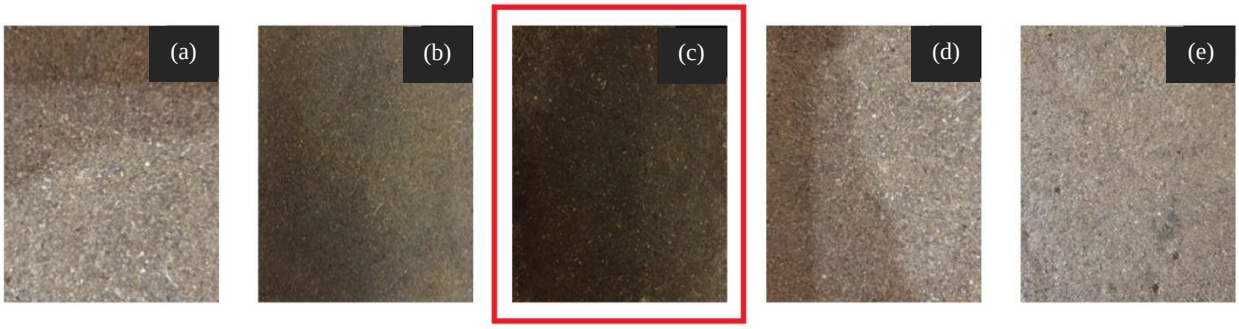


**Figure 4.** The photographs of samples with different adhesive formulas: (a), (b), (c), (d), and (e)

When the moisture content of the samples was analysed, all samples fell within the range of 4-7%, while the standard values of the moisture content are in a range of 4-13% hence a satisfactory result. However, when considering the density values, only samples (b), (c), and (d) met the standard requirements which are in a range of 400-900 kg/m$^3$, while samples (a) and (e), which contained higher proportions of GTS, exhibited very high density that exceeded the standard limit (900 kg/m$^3$). This was attributed to the high density of tapioca starch.

The swelling tests indicated that samples (a), (b), (c), and (e) had swelling values below 12%, which was in line with the standard. Sample (e), however, failed this test due to its high GTS content, which increased high water absorption capacity. The trend of the swelling test was consistent with the moisture absorption results. The tensile testing results revealed that all samples met the standard tensile strength requirement of 0.45 MPa, with sample (c) exhibiting the highest tensile strength among all samples. In terms of flexural strength, only samples (c) and (d) passed the standard threshold of 15 MPa. When comparing samples (c) and (d), sample (c) demonstrated higher flexural strength.

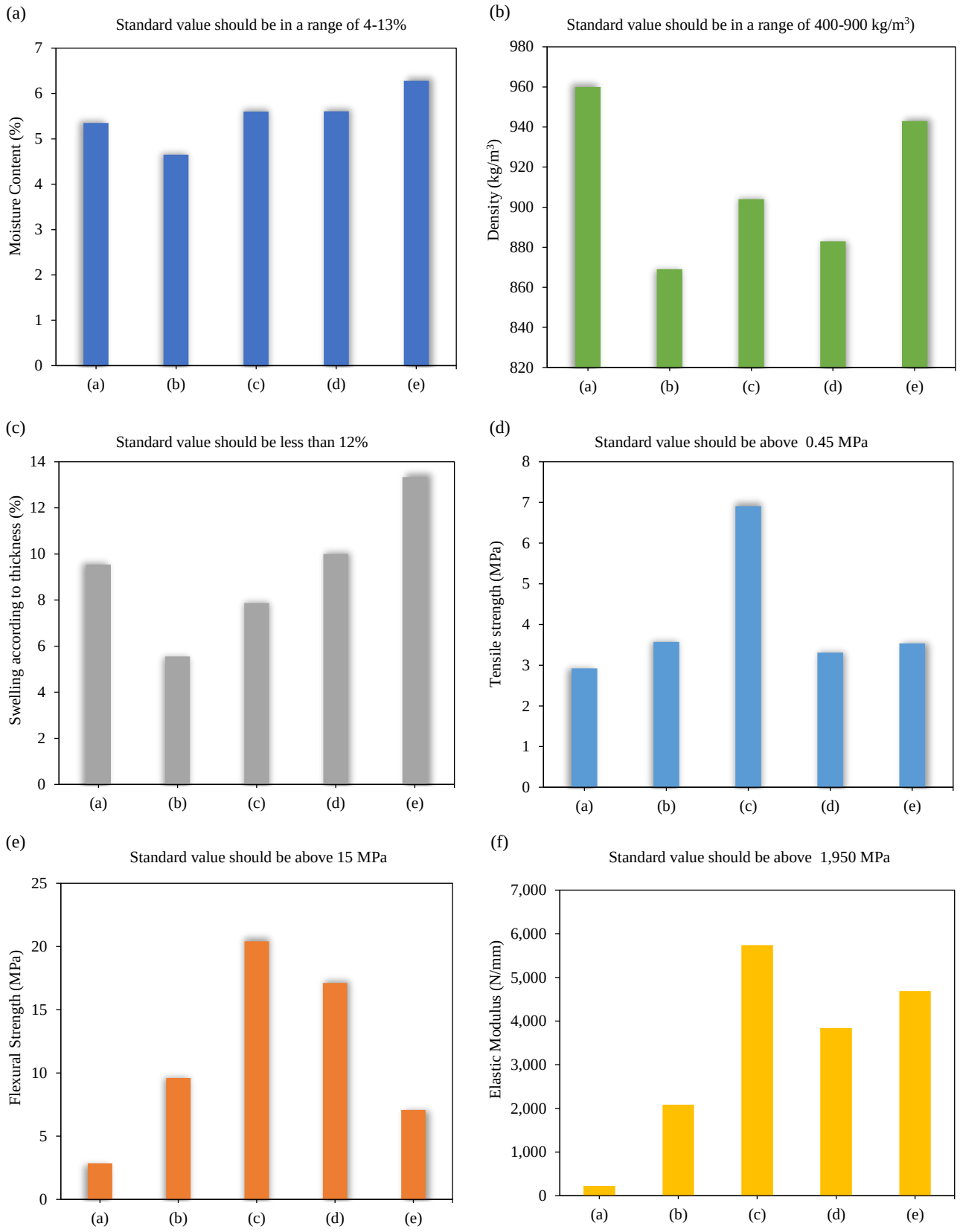


**Figure 5.** Testing results of the samples with different adhesive formulas (a), (b), (c), (d), and (e) according to the TIS standards 876-2547

All samples containing ENR (b)-(e) met the standard elastic modulus requirement of 1,950 N/mm. Notably, the addition of GTS significantly improved flexural strength and elastic modulus. Nonetheless, higher ratios of GTS i.e., ratios that exceeded 2:1 had a negative impact on mechanical strength, leading to a decrease in tensile and flexural strength. This finding is consistent with Bhaskar and Singh (2013) and Wronka and Kowaluk (2022). According to the TIS 876-2547 criteria, both samples (c) (2:1) and (d) (3:1) passed the standard requirement, although sample (c) exhibited better mechanical strength. Therefore, the promising adhesive ratio of GTS to ENR in order to produce coconut shell sheets was determined to be 2:1 (26.7 g of GTS and 13.3 g of ENR). Table 2 summarises the test results of sample (c), according to TIS standards (876-2547). It shows that sample (c) meets all criteria of TIS standards (876-2547).

**Table 2.** The test results of sample (c), according to TIS standards (876-2547)

| Criteria | Unit | Characteristics | TIS standard thresholds | Passed/Failed |
|---|---|---|---|---|
| Moisture content | % | 5.60 | 4-13 | P |
| Density | kg/m$^3$ | 904 | 400-900 | P |
| Swelling | % | 7.87 | ≤ 12 | P |
| Tensile strength | MPa | 6.91 | ≥ 0.45 | P |
| Flexural strength | MPa | 20.42 | ≥ 15 | P |
| Elastic modulus | N/mm | 5,741 | ≥ 1,950 | P |

### 3.3 Morphology of adhesive and coconut shell sheets

The morphology of the adhesive and coconut shell sheets obtained from SEM (500x) is illustrated in Figure 6. In Figure 6(a), starch granules were observed as round particles, covering some of the porous coconut shell surfaces, although the GTS was not completely coated on the coconut shell surfaces. Figure 6(b) shows coconut shells partially coated with ENR. Figure 6(c) illustrates that the adhesive made from GTS and ENR could penetrate into the pores of the coconut shells and thoroughly cover the shell surface. These findings reflect those of Owodunni et al. (2020) who produced particleboards made from coconut fibers and used modified potato starch as a binder, in which the starch granules could be melted to fill the open pores, which increased the compactness of the panels. The SEM images also suggested that the combination of GTS and ENR enhanced the binding ability of the coconut shell surfaces. During gelatinization, water and heat hydrolysed the starch granules, resulting in increased flowability and the presence of reactive hydroxyl groups. The hydroxyl groups in the starch could react with the epoxy groups in the ENR, and some of the epoxy groups in the ENR could also react with the hydroxyl groups in the cellulose molecules on the coconut shell surface. This resulted in a strong bond between the coconut shell particles. These findings are consistent with the analysis of functional groups in the adhesives FTIR, as discussed in the following section.

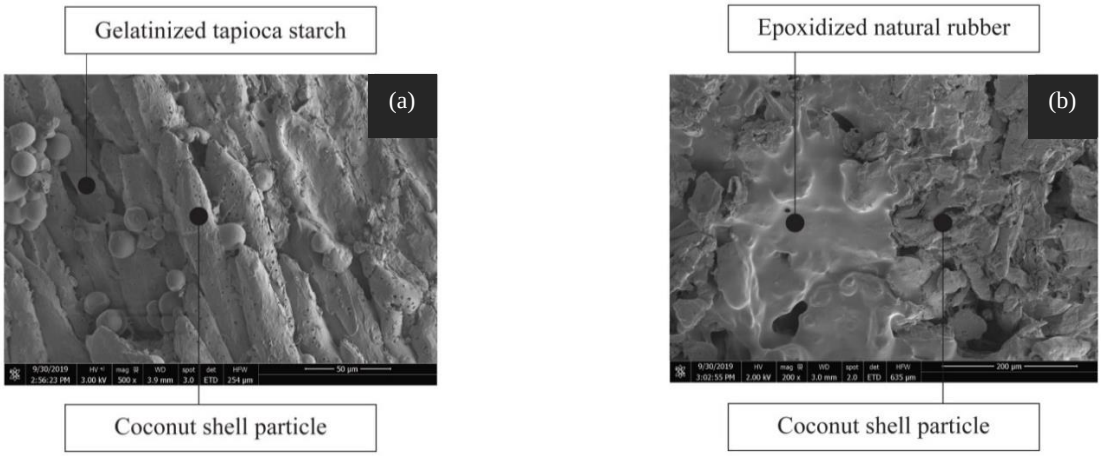


**Figure 6.** The surface morphology (500x) of (a) GTS mixed with coconut shell sample, (b) ENR with coconut shell sample, and (c) GTS mixed with ENR and coconut shell sample (40 g adhesive: 100 g coconut shell particles)

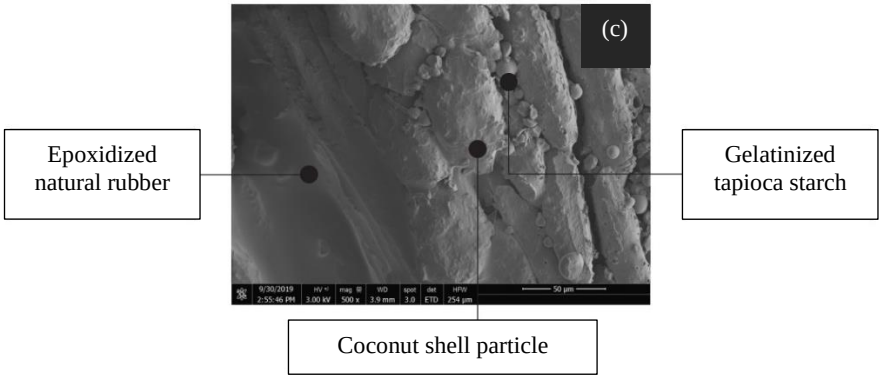


**Figure 6.** The surface morphology (500x) of (a) GTS mixed with coconut shell sample, (b) ENR with coconut shell sample, and (c) GTS mixed with ENR and coconut shell sample (40 g adhesive: 100 g coconut shell particles) (cont.)

### 3.4 Chemical Composition of the adhesive and the coconut shell sheets

Figure 7 presents the chemical compositions of ENR, the adhesive made from GTS and ENR (2:1), and the coconut shell sheet as analysed by FTIR analysis. The main structural molecules of ENR were identified at 1,665 $cm^{-1}$ and 3,070 $cm^{-1}$, corresponding to -C=C- and =CH stretching, respectively (Ibrahim et al., 2014; Yoksan, 2008). Figure 8 shows the presence of epoxide bonds as a result of the epoxidation of natural rubber latex with peracid, as shown in Figure 8. These bonds appeared at 871 $cm^{-1}$ and 1,251 $cm^{-1}$, consistent with Rattanavilai (2007). Epoxide bonds were also detected in the adhesive. Nonetheless, the epoxide bond at 871 $cm^{-1}$ was absent from the coconut shell sheets, since some epoxide bonds broke off and bonded with the carboxyl groups of lignin during hydraulic compression at 170°C. The hydrogen bonds between epoxide bonds and cellulose molecules were also present, as shown in Figure 9. In both the adhesive and the coconut shell sheets, C-O-C bonds were at 1,149 $cm^{-1}$, which is attributed to carbon and oxygen bonds in amylase and amylopectin found in the GTS. This finding is in agreement with Colussi et al. (2014).

Both the C=C and epoxide bonds present in the ENR played crucial roles in binding the coconut shell particles (Bijarimi et al., 2014). When the ENR was mixed with GTS, the epoxidized groups in the ENR formed hydrogen bonds with the hydroxyl groups on the tapioca starch molecules, resulting in a homogeneous solution (Yoksan, 2008). During hydraulic compression at 170°C, the epoxidized groups crosslinked with the carboxyl groups in the lignin molecules, leading to strong adhesion between the coconut shell particles and tapioca starch.

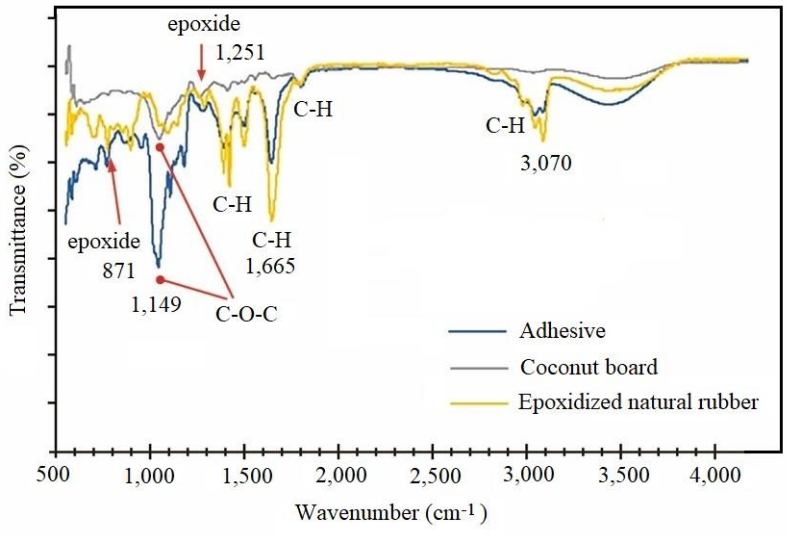


**Figure 7.** FTIR spectra of ENR, adhesive made from the GTS and ENR (2:1), and the coconut shell sheet

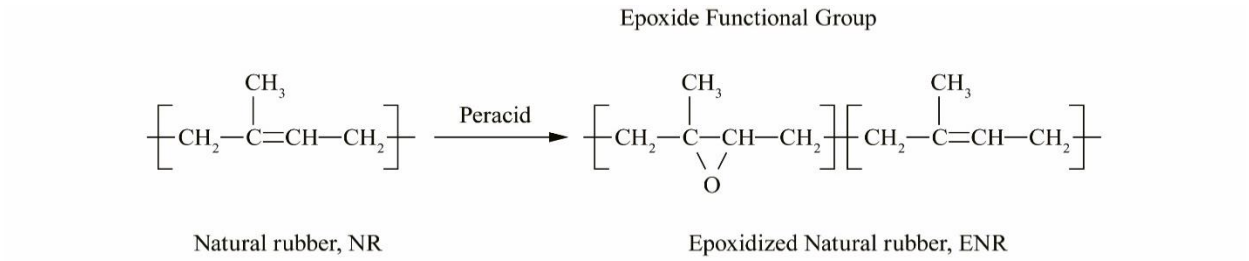


**Figure 8.** ENR from the epoxidation of natural rubber (modified from Yoksan, 2008)

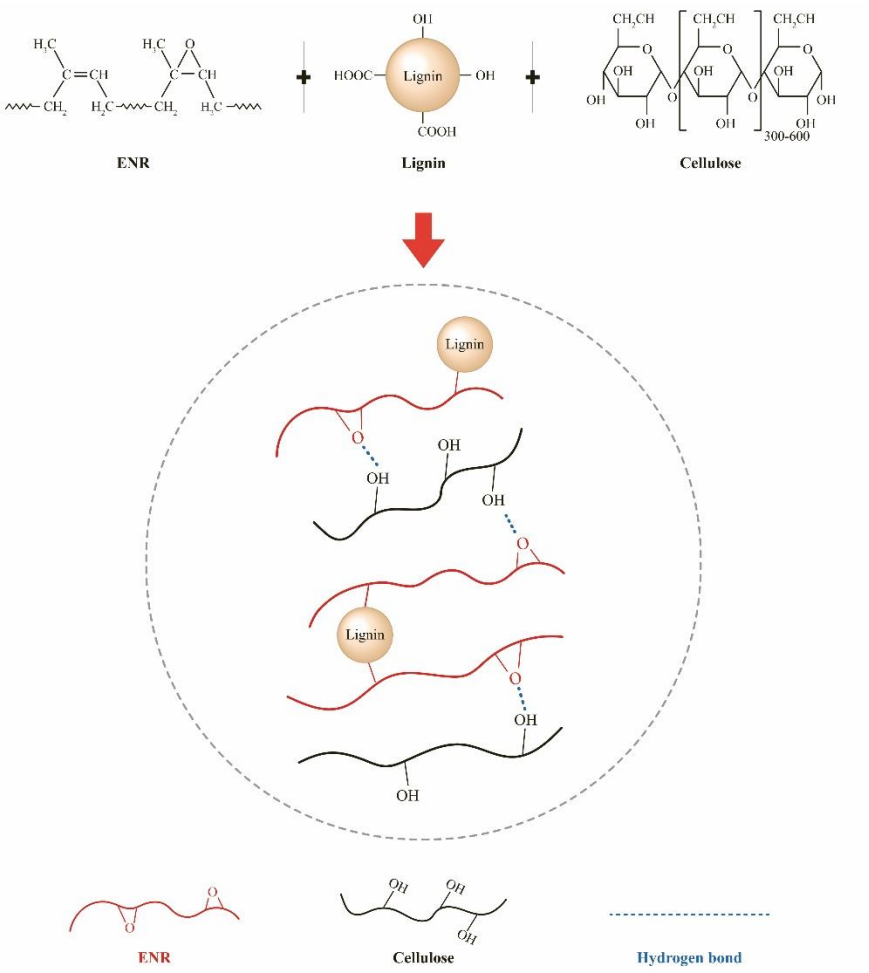


**Figure 9.** Reaction between ENR, cellulose in GTS and lignin in coconut shell

Based on the results of the physical, chemical, and mechanical analysis, it is evident that the combination of GTS and ENR produces effective adhesive that enhances the adhesion ability between coconut shell particles. The chemical reactions shown in Figure 9 indicated the roles of GTS and ENR on the adhesion improvement of coconut shell. The ENR could react with lignin molecules resulting in networking between ENR and lignin (Jiang et al., 2014). While GTS played a role in reinforcing of the composite material. If the portion of ENR increases, the composite material will behave like rubber. As a result, GTS was added to fix the ENR molecules by hydrogen bonding, making it more rigid and improve the mechanical strength of the composite material (Cai et al., 2022; Lim et al., 2021). However, an excessive amount of the starch can cause moisture absorption and swelling. The addition of ENR contributes to the improvement of flexural strength and elastic modulus in the coconut shell sheets. Lim et al. (2021) also reported that ENR latex-based binder can improve the modulus of rupture (MOR) of coconut fibre-based particleboards. From this study, the optimal adhesive ratio between GTS and ENR is

determined to be 2:1 by weight. Coconut shell sheets prepared with 40 g of adhesive and 100 g of coconut shell particles meet the requirements of TIS No. 876-2547. The economic study indicated that the total cost of a coconut shell sheet (30×30 cm) was about 25 THB/piece. The processing contributed to 50% of the total cost, followed by labor (25%) and raw materials (25%).

## 4. CONCLUSION

This study successfully produced a wood substitute material using coconut shell waste and an environmental-friendly adhesive made from ENR and GTS. The synergistic effects of using ENR and GTS on adhesion ability to produce coconut shell sheet were observed. ENR played a role in networking between lignin and cellulose. While GTS improved the strength of the composite using hydrogen bonding. The optimal weight ratio of binder to coconut shell was 40 g: 100 g and the optimal weight ratio of GTS to ENR was 2:1. The coconut shell sheet was formed by a hydraulic compression at 170°C for 5 min. The properties of the produced coconut shell sheets meet the standard requirements of TIS No. 876-2547 for flat pressed particleboards. With its unique patterns, low cost, and use of nontoxic adhesive, the produced coconut shell sheets could be applied as an alternative to wood.

## ACKNOWLEDGEMENTS

The author was supported by the Petch Pra Jom Klao Master's Degree Research Scholarship from King Mongkut's University of Technology Thonburi Contract No. 5/2560. The authors express their gratitude to the Electricity Generating Authority of Thailand (EGAT) for their kind supports. Special thanks are extended to Mr. Wittaya Santisukpaiboon, the Head of Thung Pradu Community, for providing raw materials used in this research.

## REFERENCES

Akbari S, Gupta A, Khan TA, Jamari SS, Ani NBC, Poddar P. Synthesis and characterization of medium density fiber board by using mixture of natural rubber latex and starch as an adhesive. Journal of the Indian Academy of Wood Science 2014;11(2):109-15.

Agnantopoulou E, Tserki V, Marras S, Philippou J, Panayiotou C. Development of biodegradable composites based on wood waste flour and thermoplastic starch. Journal of Applied Polymer Science 2012;126(1):273-81.

Bhaskar J, Singh VK. Physical and mechanical properties of coconut shell particle reinforced-epoxy composite. Journal of Materials and Environmental Science 2013;4(2):227-32.

Bijarimi M, Ahmad S, Rasid R. Mechanical, thermal and morphological properties of poly (lactic acid) epoxidized natural rubber blends. Journal of Elastomers and Plastics 2014;46(4):338-54.

Bureau of Environmental Health, Department of Health, Ministry of Public Health. Guidelines of Indoor Air Management and Evaluation in Public Building. Bangkok, Thailand: Bureau of Environmental Health, Department of Health, Ministry of Public Health; 2016. (in Thai)

Cai Z, Cadek D, Jindrova M, Kaderabkova A, Kuta A. Physical properties and biodegradability evaluation of vulcanized epoxidized natural rubber/thermoplastic potato starch blends. Materials 2022;15(21):1-16.

Colussi R, Pinto VZ, Halal SLME, Vanier NL, Villanova FA, Silva RM, et al. Structural, morphological, and physicchemical properties of acetylated high-, medium-, and low-amylose rice starches. Carbohydrate Polymer 2014;103:405-13.

Husseinsyah S, Mostapha M. The effect of filler content on properties of coconut shell filled polyester composites. Malaysian Polymer Journal 2011;6(1):87-97.

Ibrahim S, Daik R, Abdullah I. Functionalization of liquid natural rubber via oxidative degradation of natural rubber. Polymers 2014;6:2928-41.

Jiang C, He H, Yao X, Yu P, Zhou L, Jia D. Self-crosslinkable lignin/ epoxidized natural rubber composites. Journai of Applied Polymer Science 2014;131(23):1-9.

Junmee S, Sittha H, Chusinuan N, Twishsri W. The study of supply chain model of coconut Production in Prachuap Khiri Khan Chumphon and Surat Thani Provinces. Thai Agricultural Research Journal 2021;39(2):202-14.

Kaden DA, Corinne M, Gunnar DN, Wolkoff P. WHO Guidelines for Indoor Air Quality: Selected Pollutants: Formaldehyde. [Internet]. 2010 [cited 2023 Nov 11]. Available from: https://www.ncbi.nlm.nih.gov/books/NBK138711/.

Lacerda LG, Almerida RR, Demiate IM, Filho MASC, Vasconcelos EC, Woiciechowski AL, et al. Thermoanalytical and starch content evaiuation of cassava bagasse as agro-industrial residue. Brazilian Archives of Biogy and Technology 2009;52:143-50.

Lim JX, Ong TK, Ng CK, Chua IW, Lee YB, Yap ZY, et al. Development of particleboard from green coconut waste. Proceedings of the 15th International Engineering and Computing Research Conference (EURECA 2021); 2021 Jun 30; School of Computer Science and Engineering, Taylor's University, Malaysia, Subang Jaya, Selangor: Malaysia; 2021.

Naya M, Nakanishi J. Risk assessment of formaldehyde for the general population in Japan. Regulatory Toxicology and Pharmacology 2005;43:232-48.

Olumuyiwa AJ, Isaac TS, Samuel SO. Study of mechanical behavior of coconut shell reinforced polymer matrix composite. Journal of Minerals and Materials Characterization and Engineering 2012;11:774-9.

Owodunni AA, Lamaming J, Hashim R, Folahan O, Taiwo A, Hussin MH, et al. Properties of green particleboard manufactured from coconut fiber using a potato starch based adhesive. BioResources 2020;15(2):2279-92.

Rattanavilai S. Adhesive Development for Rubber Wood from Epoxide Natural Latex. Songkhla, Thailand: Faculty of Engineering Prince of Songkla University; 2007. p. 1-111.

Roumeli E, Papadopoulou E, Pavlidou E, Vourlias G, Bikiaris D, Paraskevopoulos KM, et al. Synthesis, characterization and

thermal analysis of urea-formaldehyde/nano$SiO_2$ resins. Thermochimica Acta 2012;527:33-9.

Strykowski W. Wood - A substitute or a raw material substituted for. Annals of Warsaw University of Life Sciences-SGGW, Forestry and Wood Technology 2013;84:194-200.

Simon JN, Nuthammachot N, Titseesang T, Okpara KE, Techato K. Spatial assessment of para rubber (*Hevea brasiliensis*) above ground biomass potentials in Songkhla Province, Southern Thailand. Sustainability 2021;13(16):Article No. 9344.

Thuraisingam J, Gupta A, Subramaniam M. Natural rubber latex (NRL) and rice starch as an alternative binder in wood composite industry. Australian Journal of Basic and Applied Sciences 2016;10(17):101-6.

Wronka A, Kowaluk G. The influence of multiple mechanical recycling of particleboards on their selected mechanical and physical properties. Materials 2022;15:1-18.

Yoksan R. Epoxidized natural rubber for adhesive application. Kasetsart Journal (Natural Science). 2008;42:325-32.

# Microplastics in the Water of Batang Anai Estuary, Padang Pariaman Regency, Indonesia: Assessing Effects on Riverine Plastic Load in the Marine Environment

**Suparno Suparno[1*], Deswati Deswati[2], Wiya Elsa Fitri[3], Hilfi Pardi[4], and Adewirli Putra[5]**

[1]*Departement of Fisheries Resources Utilization, Faculty of Fisheries and Marine Sciences, Universitas Bung Hatta, Padang 25133, Indonesia*
[2]*Department of Chemistry, Faculty of Mathematics and Natural Science, Andalas University, Padang 25163, Indonesia*
[3]*Department of Public Health, Syedza Saintika College of Health Sciences, Padang 25132, Indonesia*
[4]*Department of Chemistry Education, Faculty of Teacher Training and Education Raja Ali Haji Maritime University, Tanjungpinang 29115, Indonesia*
[5]*Department of Medical Laboratory Technology, Syedza Saintika College of Health Sciences, Padang 25132, Indonesia*

**ARTICLE INFO**

Received: 20 Jul 2023
Received in revised: 21 Nov 2023
Accepted: 30 Nov 2023
Published online: 9 Jan 2024
DOI: 10.32526/ennrj/22/20230191

**Keywords:**
Ecotoxicological impact/ Batang Anai River/ Microplastic polymers/ Pariaman Regency

*** Corresponding author:**
E-mail:
suparnopranoto@bunghatta.ac.id

**ABSTRACT**

Microplastic (MP) is one of the most dangerous contaminants due to its ecotoxicological impact on the aquatic environment, aquatic biota, and human health. Defined as particles less than 5 mm, these contaminants originates from either primary or secondary source. Therefore, this study aimed to analyze the abundance, shape, color, size, and type of microplastic (MP) polymers. In the process, water samples were collected from 3 distinct points in the Batang Anai River, to obtain MP. Subsequently, analysis was conducted using a microscope and Attenuated Total Reflection-Fourier Transform Infrared Spectroscopy (ATR-FTIR). The results showed that the abundance of MP in the water samples ranged from 37-77 particles/L, and the most dominant shapes, colors, and sizes identified were fragments (49.44%), black (48%), and sizes >1,000 µm (33%), respectively. Characterization and interpretation of functional groups in the FTIR spectrum indicated the presence of cellulose polymer, ethylene-propylene copolymer, neoprene, and polyester. In conclusion, this report can be used as initial information to help control plastic waste pollution.

## 1. INTRODUCTION

Plastic waste is a global environmental pollutant, posing a threat to ecosystems (GESAMP, 2015), aquatic biodiversity (Urbina et al., 2021), air quality (Lopez-Rojo et al., 2020), and human health (Sutherland et al., 2011). The exponential growth in this material is anticipated to persist, with disposal and accumulation in landfills affecting aquatic ecosystems (Geyer et al., 2017). Currently, plastic constitutes 54% of the world's human waste by mass (Hoellein et al., 2014). This is because it can last a very long time before being degraded (Barboza et al., 2019) due to weathering which breaks down long chain polymers into smaller pieces (Rodrigues et al., 2018; Zhang et al., 2021), facilitating digestion by aquatic biota and integration into food web (Da Costa et al., 2017).

MP pollution is as a focal point of investigations into plastic waste. These minutes plastic particles are globally available in oceans, rivers, lakes, soil, and organisms (Du et al., 2021). Both densely populated cities and remote region face threat from MP pollution (Feng et al., 2021; Sekudewicz et al., 2021). While slow-flow areas, such as oceans, lakes, and reservoirs can become dumping grounds, rivers serve as conduits connecting the waste to terrestrial environment (Ho et al., 2020). The Batang Anai River spanning 54.6 km passes through 2x11 sub-districts of Anam Lingkuang, Lubuak Aluang, and Batang Anai in Padang Pariaman Regency, Indonesia (CSA, 2016). Furthermore, it originates in Tanah Datar District and empties into Muara Anai in Padang Pariaman District. This river plays a crucial role in supporting agriculture, forestry,

**Citation:** Suparno S, Deswati D, Fitri WE, Pardi H, Putra A. Microplastics in the water of Batang Anai Estuary, Padang Pariaman Regency, Indonesia: Assessing effects on riverine plastic load in the marine environment. Environ. Nat. Resour. J. 2024;22(1):55-64. (https://doi.org/10.32526/ennrj/22/20230191)

fish farming, sand mining, settlement, and industrial activities. However, increased human activities, particularly deforestation and the construction of flood control canals and settlements, have negatively impacted the water quality.

No study or publication addresses the content of MP in the Batang Anai River. Therefore, it is necessary to conduct an investigation to (1) systematically examine the incidence of MP pollution in the Batang Anai River as well as (2) explain and analyze the distribution characteristics of the particles in the Batang River. The results of this investigation will contribute to the understanding of MP pollution in freshwater environments, serving as a primary reference for future studies. This can inform initiatives aimed at reducing plastic usage, improving recycling practices, and enhancing overall environmental protection.

## 2. METHODOLOGY

### 2.1 Description of the study site

The study was conducted on the Batang Anai River, Padang Pariaman Regency, West Sumatera, Indonesia, from January-February 2023. Samples of river water was collected 3 times (January 1, January 30, and February 28) from 3 different stations, namely ST 1, ST 2, and ST 3, which were upstream waters Anai Trunks, water on the Tidal Bridge, and water body at the mouth of the Batang Anai River, respectively. The selection of these stations was based on consideration of regional conditions and characteristics of the study area, aw presented in Figure 1 and Table 1.

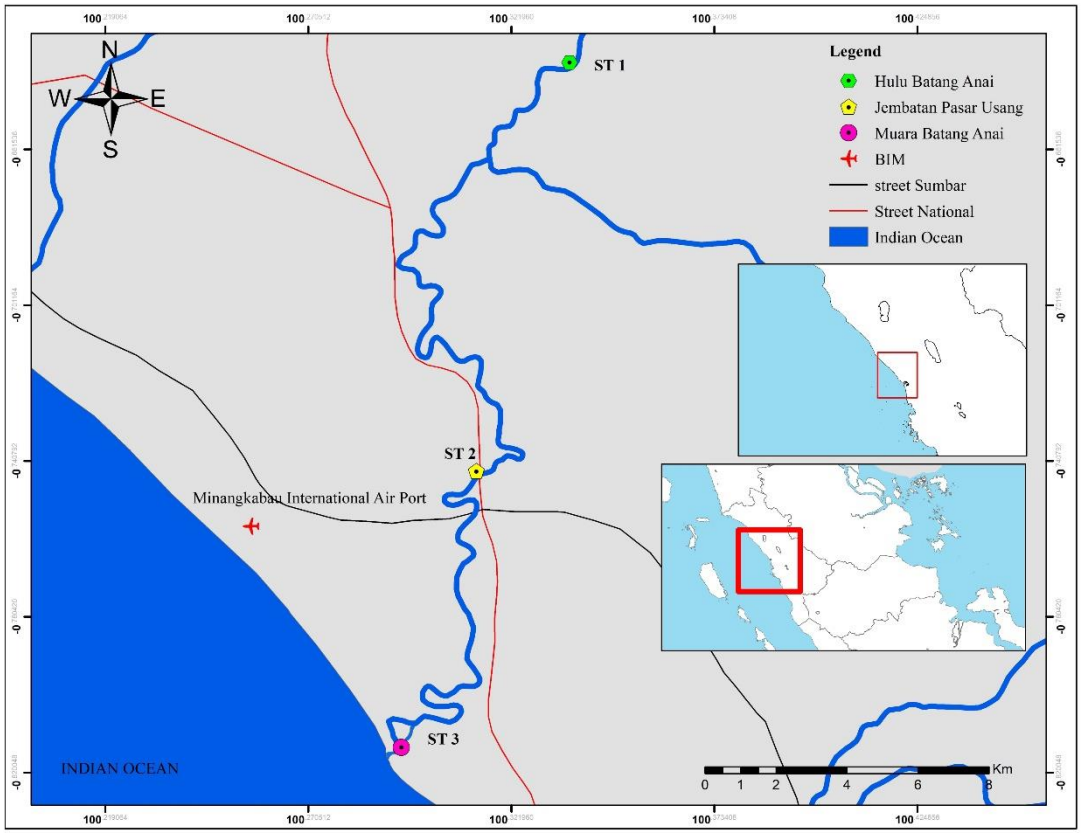


**Figure 1.** Batang Anai Research Locations [Source: Geospatial Agency of Special Region of Pariaman Regency (2020)]

### 2.2 Sampling of water

River water was collected using a 5 L bucket and filtered 20 times through a plankton net No. 25. Subsequently, the filtered samples were transferred into HDPE sample bottles to prevent particle contamination and stored in a cool box (Cordova et al., 2019; Deswati et al., 2023a; Deswati et al., 2023b).

### 2.3 MP extraction

Approximately 20 mL of 30% $H_2O_2$ was added to the water samples, and the mixture was homogenized with a magnetic stirrer for 5 min. The samples were then covered with aluminum foil to avoid environmental pollution and left undisturbed for 24 h. An extra 30% $H_2O_2$ was added until impurity

disappeared. Furthermore, filteration was performed using Whatman filter paper no 42 with the help of a vacuum pump. The filtered particles were identified visually under a microscope, and the suspected MP was counted (Cordova et al., 2019; Deswati et al., 2023a; Deswati et al., 2023b).

**Table 1.** Sampling locations

| Station/Coordinate | Description |
|---|---|
| Station 1 (ST 1)<br>0º 38' 22.03" S<br>100º 20' 12.24" E | This location is characterized by clear river water, large boulders, sandy bottom substrate, fast water, and no pollution. Activities in the dam: water tourism, the forest is still dense, the activity of the population is still tiny, and there are no macrobenthos. |
| Station 2 (ST 2)<br>0º 44' 36.00" S<br>100º 18' 47.20" E | The waters of the middle part of the Batang Anai River are characterized by high sedimentation, turbid water, slow water flow, sandy mud bottom substrate, high residential activity, community sand mining, and lots of macro-zoobenthos. |
| Station 3 (ST 3)<br>0º 48' 49.08" S<br>100º 17' 38.66" E | The Batang Anai estuary is characterized by high pollution, high residential activity, ship activity at the Muara Anai Fishery Port, Cooking Oil Factory, sand mining activities, sandy mud bottom substrate, turbid water, lots of macrozoobenthos, and brackish water. |

### 2.4 MP identification

Visual inspection was conducted to obtain MP based on the characteristics. The particles were observed, photographed, and marked using a camera-equipped trinocular microscope (B-350 Optika). MP was determined using Moticplus 3.0 software, and the parameters recorded were size, shape, and color. Its forms are categorized into fibers, fragments, films, and granules. Furthermore, size categories included <100 µm, 101-300 µm, 301-500 µm, 501-1,000 µm, and >1,000 µm (Cordova et al., 2019; Deswati et al., 2023c).

### 2.5 MP analysis

All tagged items were confirmed using a PerkinElmer Spectrum Spotlight 400 micro-Fourier transshape infrared spectroscope (µ-FT-IR; Perkin-Elmer Inc., U.S.A.) (Ding et al., 2018). Attenuated total reflection mode (ATR) was used, and germanium (Ge) crystals in the ATR imaging attachment were in direct contact with the MP. Spectra were obtained from spectral and spatial resolution of 8/cm and 6.25 µm (the highest spatial resolution was 1.56 µm), respectively, within the spectral range of 4,000 to 750/cm with 16 Coscans for each measurement. This enabled the identification of MP diameters up to 6.25 µm. The resulting spectra were compared with the database from Sadltler to confirm polymers, with spectra matches exceeding 70% considered reliable (Su et al., 2020). Non-plastics were removed from the MP count and recalculation was conducted.

### 2.6 Quality control

To minimize contamination, MP extraction and observation procedures adhered procedures, including the use of latex gloves, 100% cotton laboratory clothing, and working in a clean and enclosed environment (Falahudin et al., 2020; Mai et al., 2018). All laboratory equipment, such as sample bottles, test tubes, tweezers, and filters, was made from non-plastic materials and was sterilized before application. Samples were kept covered when not under analysis, and double-distilled water was used during all processes (Cordova et al., 2019; Mai et al., 2018). Additionally, to control contamination from air, especially from synthetic fiber materials (Chen et al., 2020; Dris et al., 2016), a blank procedure was implemented during laboratory analysis (Falahudin et al., 2020). Post-laboratory processes, the filter paper was observed under a microscope to confirm the absence of MP, indicating no contamination throughout the procedures.

MP Abundance Calculation. MP abundance analysis in water was conducted using the following formula (Masura et al., 2015).

$$K = \frac{n}{v}$$

Where; K=abundance of MP (particle/L); n=number of MP; v=sample volume (L).

## 3. RESULTS AND DISCUSSION

### 3.1 MP abundance

The abundance of MP in Batang Anai River water samples ranged from 37-77 particles/L, and it was predominant at ST 2, followed by ST 3 and ST 1 (Figure 2).

The abundance of MP in the water at the ST 2 can be attributed to factors such as high population density, sand mining activities, elevated sedimentation, turbid water, slow water flow, and sandy mud

riverbeds. This was in accordance with the study of Ding et al. (2019) who reported a high abundance of MP in water near densely populated areas with increased community activity. ST 3, as the second highest abundance location, is characterized by high pollution, intense residential activity, ship activity at the Muara Anai Fishing Harbor, cooking oil factories, sand mining activities, and sandy mud bottom substrate. In contrast, ST 1, with the lowest MP abundance, was situated in clear river water with large rocks, a Sandy river bed, fast flowing water, minimal pollution, and limited population activity.

The abundance of MP in this study was lower compared to previous investigations, such as conducted in the Estuary of the Yellow River, China (Han et al., 2019), the Dutch River, Amsterdam Canal, Netherlands, and Germany (Leslie et al., 2017), as detailed in Table 2.

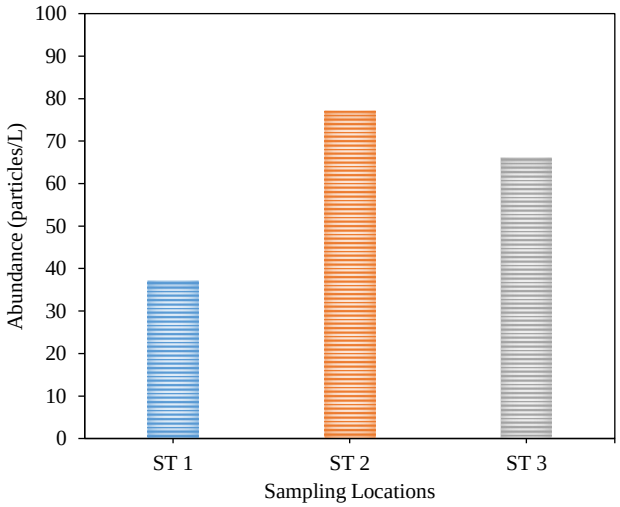


**Figure 2.** MP Abundance at different sampling locations of water (particles/L)

**Table 2.** Comparison of MP abundance in river water from several countries

| Location | Sampling equipment | Abundance (particle/L) | References |
|---|---|---|---|
| Yellow River Estuary, China | Stainless-steel bucket, 5 L | 930 | Han et al. (2019) |
| Dutch River and Amsterdam Canals | Bulk, 2 L | 48-187 | Leslie et al. (2017) |
| Danube River, Austria | Net | 0.32±4.66 | Lechner et al. (2014) |
| Seine River, France | Net | 0.003-0.11 | Dris et al. (2015) |
| Ciwalengke River, Indonesia | Bulk, 1 L; 1.2 µm | 5.85±3.28 | Alam et al. (2019) |
| Pearl River, China | Net, 160 µm | 0.57±0.71 | Fan et al. (2019) |
| Batang Anai River, Indonesia | Mini manta trawl net, 300 µm, 0.35 L | 37-77 | This study |

The high abundance of MP in river water can be attributed to 2 primary factors. Firstly, high levels of pollution play significant role. This was in line with the study by Jambeck et al. (2015) who stated that China is the largest contributor of plastic waste from land to sea. The results of investigation conducted on Batang Anai river water show higher MP content (37-77 particles/liter) compared to the report by Alam et al. (2019), where the content in Ciwalengke river water, Indonesia was 5.85±3.28 particles/L, as presented in Table 1. The difference in MP density between these locations were influenced by variations in sampling time, population activity and population density. The second factor was the sampling tool used, as shown in Table 1. Areas with high MP abundance do not use separate pumps, plankton nets, or manta nets, but instead use separate Niskin bottles, Van Dorn water sampling tools, buckets, or pails. Mesh size also determined the effectiveness of nondiscrete devices for filtering. Finer mesh sizes were generally applied in pumping methods (Cutroneo et al., 2020). Non-discrete tools allow particles smaller than the mesh size to escape during field sampling, while the discrete counterpart will collect all MP sizes and shapes (Cutroneo et al., 2020; Wu et al., 2020).

### 3.2 Shape abundance

The results showed 3 shapes of MP, namely fragments, films, and fibers (Figure 3). The shape in water was dominated by fragments with the order being 89 particles/L (49.44%) > fiber 86 particles/L (47.78%) > film six particles/L (3.33%).

In the Pearl River of China, abundant types of fragments were discovered (Fan et al., 2019), while in the Yellow River, China (Han et al., 2019), Ciwalengke River, Indonesia (Alam et al., 2019), Sein River, France (Dris et al., 2015) several forms of fiber were reported. Variations in the abundance of MP forms across different locations were attributed to differences in sampling methods, processing and analysis techniques, oceanography (tides and currents), and meteorology (Abayomi et al., 2017;

Kanhai et al., 2017). The MP fragments entering rivers was thought to originate from 1) Larger plastics subjected to physical degradation over time due to exposure to sunlight, heat, and mechanical action such as crushing by waves at sea or erosion on land; 2) Synthetic clothing and textiles, such as polyester or nylon, shedding small fibers during washing; 3) Disintegration of personal care products containing small plastic particles as abrasives; 4) MP fragmentation through maintenance and painting activities, dispersing small plastic particles into the air or leaching them into the aquatic system; 5) The plastic processing industry releasing MP fragments into the environment through improperly managed industrial waste or production processes.

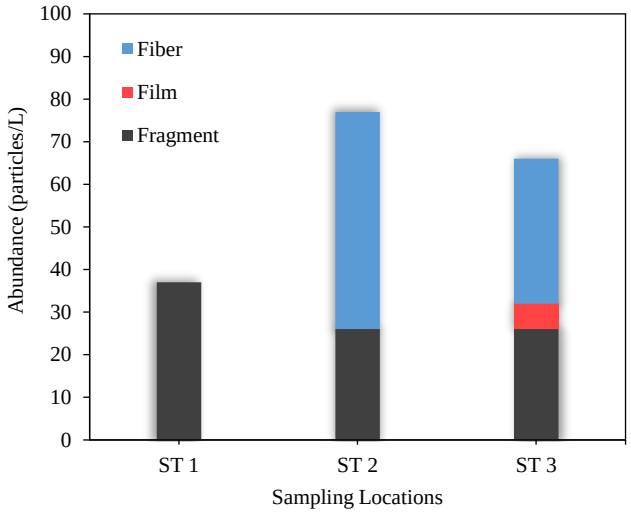


**Figure 3.** The abundance of MP forms in water (particles/L)

The abundance of MP in the form of fiber entering the river originates from: 1) Clothing made of synthetic fibers such as polyester, nylon, acrylic, or polyamide, releasing MP fibers during washing, reaching the environment through household wastewater or inadequately filtered sewage treatment systems; 2) Other textile products such as furniture fabrics, carpets, towels, or linen containing plastic fibers that break down into particles when used and washed; 3) Textile production processes generating plastic fiber waste that enters the environment as MP; 4) Consumer goods such as toothbrushes, makeup brushes, cleaning brushes, or other household tools made of plastic fibers can become a source of MP when damaged or disposed of improperly; 5) Industries, such as plastic processing or textile production, causing the release of MP fibers into the environment through poorly managed waste or production processes.

Plastic film is one of the most common forms of MP in water due to its high mobility, easily dispersing throughout ecosystems by water, wind, or human activities. To address the MP film problem, it is essential to reduce the usage of single-use plastic films, develope environmentally friendly substitutes, and better-managing plastic waste.

### 3.3 Size abundance

MP sizes identified in this study were classified into 5 categories, namely <100 µm, 101-300 µm, 301-500 µm, 501-1,000 µm, and >1,000 µm, as presented in Figure 4. The dominant size category in water was >1,000 µm (33%). This predominance may be attributed to the 300 µm sampling equipment (net) used, allowing MPs smaller than this size to eacape during water sampling (Suteja et al., 2021).

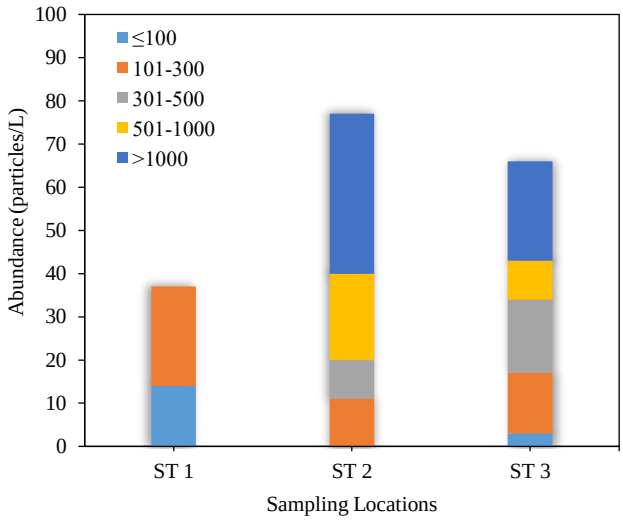


**Figure 4.** MP abundance based on different sizes of water sampling locations

The size of MP entering rivers can affect the environment and aquatic organisms. This influence was evident in several ways including: 1) The size affect the ability to spread and move in the environment. Smaller MP have tend to dissolve more easily in water, get moved by ocean currents or wind, and spread widely. Conversely, the sizes tend to be confined to areas closer to the source; 2) The ability of MP to enter into living organisms and move through food webs was affected. Smaller particles can easily be ingested by small organisms such as plankton, potentially accumulating and biomagnifying through the food chain; 3) The health of exposed organisms was impacted. Smaller MP had a higher ability to enter into the tissues and organs of the body, including the respiratory and digestive systems. This intrusion can

lead to inflammation, oxidative stress, immune system disorders, and organ damage; 4) The size has effect on chemical interactions and potential toxicity. A larger MP surface can provide more surface area to interact with hazardous chemicals and become an absorption medium for contaminants in the environment. However, the smaller particle can precipitate more efficiently and produce a more significant toxic effect on living organisms.

### 3.4 Color abundance

The MP identified in this study varied from transparent, black, blue, and red to yellow. Meanwhile, the black color dominated in each river water, namely black, constituting 48% of the total, as presented in Figure 5. This prevalence of black MP is primarily attributed to the breakdown of black plastic, a material extensively used in diverse sectors such as food packaging, cooking utensils, trays, toys, household electronics, and car components. Due to lower recycling rates, more significant quantities of this color of material are likely to end up as environmental waste (Huang and Xu, 2022).

Transparent MP may come from packaging products such as disposable plastic bags, cups, and bottles. The colored forms can be derived from packaged products and other durable plastic consumer goods (Zhang et al., 2018). Blue, yellow, and red MP result from the inherent color of the plastic and from photoaging processes. Photoaging induces discoloration, providing a visual indicator of the duration of plastic particle exposure in the environment (Zhao et al., 2022).

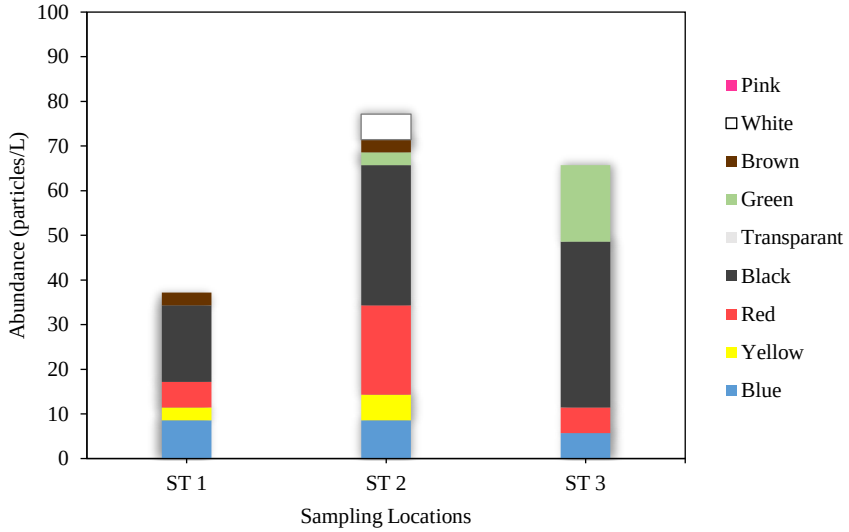


**Figure 5.** MP abundance based on different color water sampling locations

### 3.5 Identification of MP polymer types

Polymer identification was not conducted for all MP particles, but a random selection was made from the total pool of particles. Among the 63 MP particles obtained from water samples, 9.5% were randomly chosen for identification. The polymers identified in this study, confirmed through FTIR, include cellulose (Figure 6), ethylene propylene copolymer (Figure 7), neoprene (Figure 8), and polyester (Figure 9).

The interpretation of the FTIR spectrum (Figure 6) for the fiber extracted from water at ST 1 indicated that the fiber was a reinforced cellulose polymer. The identity of the absorption band include the broad peak at 3,331 $cm^{-1}$ which is a function of the stretching vibration of the hydroxyl institution (-OH) in polysaccharides. The band at 2,894 $cm^{-1}$ was related to the C-H stretching vibrations of all hydrocarbon components inside the polysaccharide. The absorption bands at 1,367-1,334 $cm^{-1}$, and 1,027 $cm^{-1}$ comprise bending vibrations of -$CH_2$ and C-O bonds in cellulose (Hospodarova et al., 2018).

Based on Figure 7, the fragment and fiber indicated the presence of ethylene-propylene copolymer, which is reinforced by the advent of absorption at 1,465 $cm^{-1}$ ($CH_2$ bending vibration). At 1,378 $cm^{-1}$, symmetrical bending of the $CH_3$ bond was observed. Additionally, the spectrum demonstrate absorption peaks at 1,155 $cm^{-1}$, corresponding to the stretching vibration of C-C($CH_3$)-C. At 970 $cm^{-1}$, it was indicative of the rocking vibration of the $CH_3$ bond (Koenig, 1999).

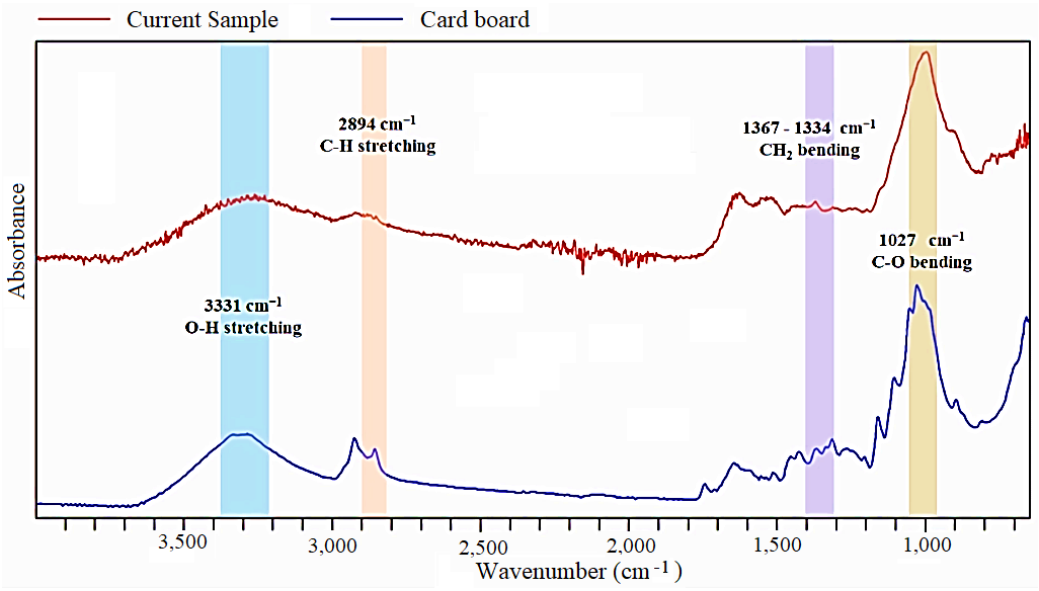


**Figure 6.** Fiber FTIR spectrum from water (ST 1)

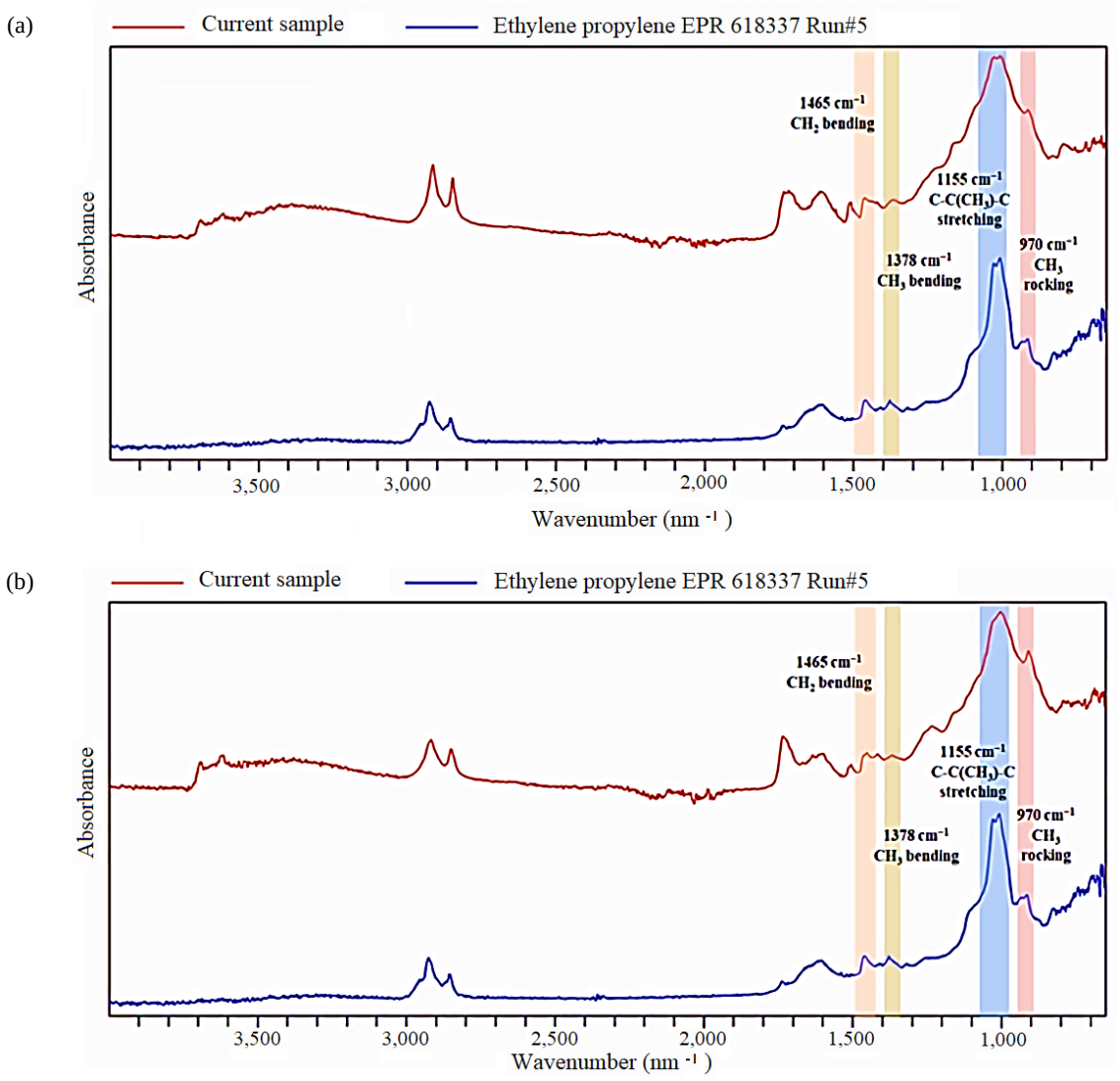


**Figure 7.** FTIR spectrum (a) Fragment from water ST 1 and (b) Fiber from water ST 2

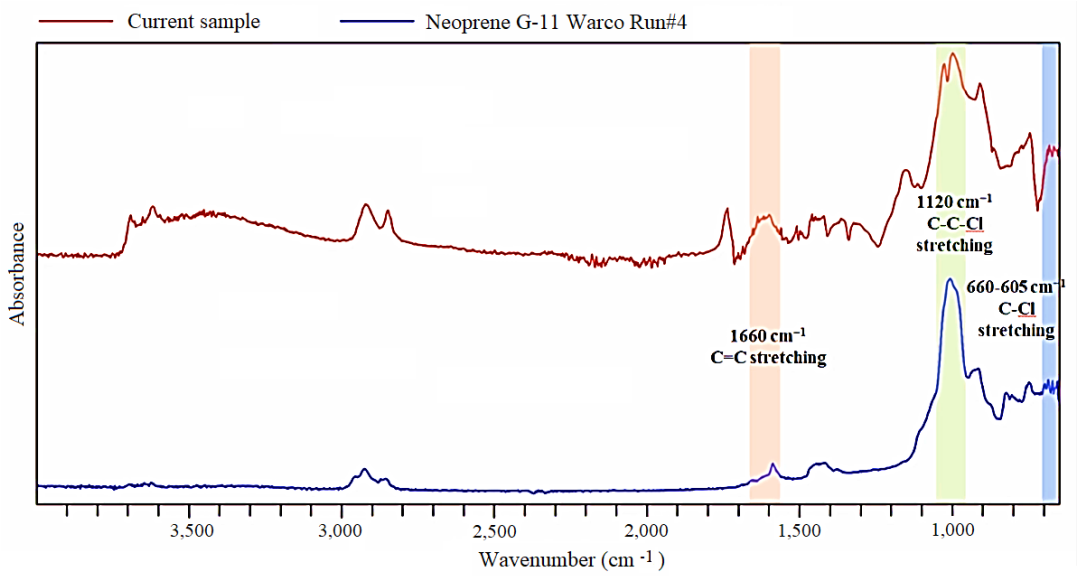


**Figure 8.** Fragment FTIR spectrum from water ST 2

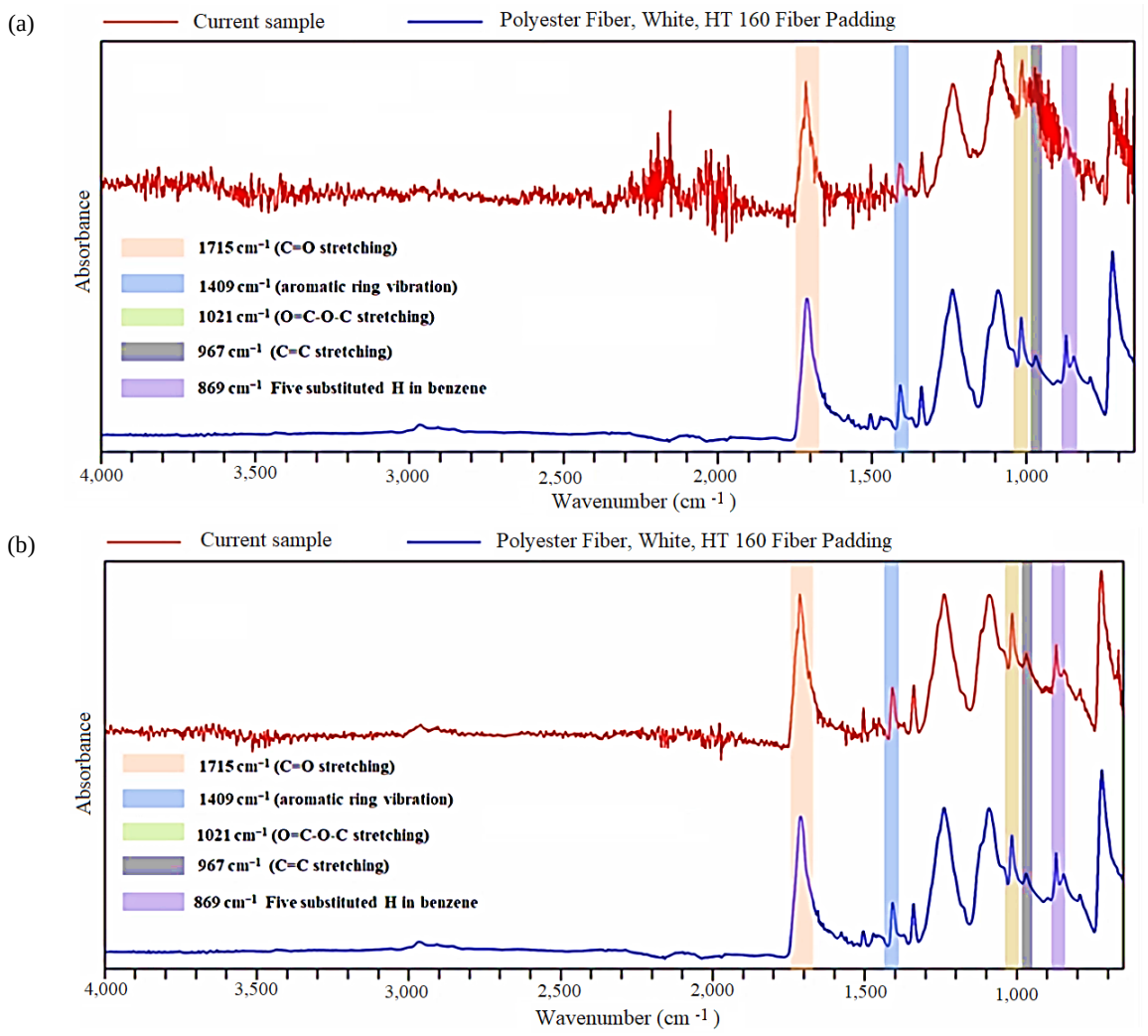


**Figure 9.** The two-fiber FTIR spectrum of Water ST 3

Based on Figure 8, the fragment extracted from ST 2 water indicated the presence of neoprene polymer, which is reinforced through the appearance of absorption at 1,660 $cm^{-1}$, 1,120 $cm^{-1}$, and 660-605 $cm^{-1}$, namely C=C stretching vibrations, C-C stretching at C-C-Cl, and C-Cl stretching vibration (Koenig, 1999).

The results of the translation of the FTIR spectrum on 2 fibers extracted from ST 3 water were polyester polymers, bolstered through the appearance of absorption at 1,715 $cm^{-1}$, 1,409 $cm^{-1}$, 1,021 $cm^{-1}$, 967 $cm^{-1}$, and top 869 $cm^{-1}$, indicating C=O stretching vibrations, aromatic ring vibrations, O=C-O-C stretching, C=C stretching, and 5 H substituted in benzene, respectively (Bhattacharya, 2014).

## 4. CONCLUSION

In conclusion, the utilization of plastic materials in everyday led to the introduction of MP into the waters of Batang Anai River, attracting considerable attention for its impact on humans and organisms that absorb organic contaminants and pathogens from the surrounding media. This study was in accordance with the aim of analyzing the abundance of microplastics (MP), shape, color, size and characteristics of polymers. The abundance in Batang Anai River water samples ranged from 37-77 particles/L, with the dominant form being fractional. Furthermore, MP in water were dominated by sizes >1,000 µm (33%), while the most appeared color was black. Based on the identification of polymer using the FTIR test, it was suspected that the detected types were cellulose, ethylene-propylene copolymer, neoprene, and polyester. Therefore, it was hoped that the results of this study can be a reference to better understand of MP pollution in Batang Anai river water.

## REFERENCES


Abayomi OA, Range P, Al-Ghouti MA, Obbard JP, Almeer SH, Ben-Hamadou R. Microplastics in coastal environments of the Arabian Gulf. Marine Pollution Bulletin 2017;124(1):181-8.

Alam FC, Sembiring E, Muntalif BS, Suendo V. Microplastic distribution in surface water and sediment river around slums and industrial areas (Case study: Ciwalengke River, Majalaya district, Indonesia). Chemosphere 2019;224:637-45.

Barboza LGA, Cozar A, Gimenez BC, Barros TL, Kershaw PJ, Guilhermino L. Microplastics Pollution in the Marine Environment. In: World Seas An Environmental Evaluation. Cambridge, MA, USA: Academic Press; 2019. p. 305-28.

Bhattacharya S. Study on structural, mechanical, and functional properties of polyester silica nanocomposite fabric. International Journal of Pure and Applied Sciences and Technology 2014;21(1):24-33.

Central Statistics Agency (CSA). Pariaman Regency, West Sumatera Province, Indonesia. River Name, Area Passed and Length in 2015 [Internet]. 2016 [cited 2023 Sept 25]. Available from: https://padangpariamankab.bps.go.id/statictable/2016/07/27/365/nama-sungai-daerah-yang-dilalui-dan-panjangnya-tahun-2015.html.

Chen G, Feng Q, Wang J. Mini-review of microplastics in the atmosphere and their risks to humans. Science of the Total Environment 2020;703:Article No. 135504.

Cordova MR, Purwiyanto AIS, Suteja Y. Abundance and characteristics of microplastics in the northern coastal waters of Surabaya, Indonesia. Marine Pollution Bulletin 2019; 142:183-8.

Cutroneo L, Reboa A, Besio G, Borgogno F, Canesi L, Canuto S, et al. Microplastics in seawater: Sampling strategies, laboratory methodologies, and identification techniques applied to the port environment. Environmental Science and Pollution Research 2020;27:8938-52.

Da Costa JP, da Costa Duarte A, Rocha-Santos TAP. Microplastics-occurrence, Fate and Behaviour in the Environment. Comprehensive Analytical Chemistry. Elsevier; 2017. p. 1-24.

Deswati D, Tetra ON, Hayati M, Putra A, Fitri WE, Suparno S, et al. Preliminary detection of microplastics in surface water of Maninjau Lake in Agam, Indonesia. AACL Bioflux 2023a;16(5):2601-14.

Deswati D, Wisna ND, Zein R, Tetra ON, Suparno S, Pardi H, et al. Preliminary study on microplastic pollution in water and sediment at the Beaches of Pariaman City, West Sumatra, Indonesia. AACL Bioflux 2023b;16(1):381-97.

Deswati D, Tetra ON, Febriani U, Suparno S, Pardi H, Putra A. Detection of microplastic in sediments at beach tourism area of Muaro Lasak, Padang City, West Sumatra, Indonesia. AACL Bioflux 2023c;16(5):2765-80.

Ding J, Li J, Sun C, Jiang F, Ju P, Qu L, et al. Detection of microplastics in local marine organisms using a multi-technology system. Analytical Methods Journal 2018;11:78-87.

Ding L, Guo X, Yang X, Zhang Q, Yang C. Science of the total environment microplastics in surface waters and sediments of the Wei River, in the northwest of China. Science of the Total Environment 2019;667:427-34.

Dris R, Gasperi J, Saad M, Mirande C, Tassin B. Synthetic fibers in atmospheric fallout: A source of microplastics in the environment. Marine Pollution Bulletin 2016;104:290-3.

Dris R, Gasperi J, Rocher V, Saad M, Renault N, Tassin B. Microplastic contamination in an urban area: A case study in Greater Paris. Environmental Chemistry 2015;12(5):592-9.

Du J, Zhou Q, Li H, Xu S, Wang C, Fu L, et al. Environmental distribution, transport and ecotoxicity of microplastics: A review. Journal of Applied Toxicology 2021;41(1):52-64.

Falahudin D, Cordova MR, Sun X, Yogaswara D, Wulandari I, Hindarti D, et al. The first occurrence, spatial distribution, and characteristics of microplastic particles in sediments from Banten Bay, Indonesia. Science of the Total Environment 2020;705:Article No. 135304.

Fan Y, Zheng K, Zhu Z, Chen G, Peng X. Distribution, sedimentary record, and persistence of microplastics in the Pearl River catchment, China. Environmental Pollution 2019;251:862-70.

Feng S, Lu H, Yao T, Liu Y, Tian P, Lu J. Microplastic footprints in the Qinghai-Tibet Plateau and their implications to the

Yangtze River Basin. Journal of Hazardous Materials 2021;407:Article No. 124776.

Geyer R, Jambeck JR, Law KL. Production, use, and fate of all plastics ever made. Science Advances 2017;3:e1700782.

Joint Group of Experts on the Scientific Aspects of Marine Environmental Protection (GESAMP). Sources, Fate and Effects of Microplastics in the Marine Environment: Part Two of a Global Assessment, A report to inform the Second United Nations Environment Assembly. London: International Maritime Organization; 2015. p. 96.

Han M, Niu X, Tang M, Zhang B, Wang G, Yue W, et al. Distribution of microplastics in surface water of the lower Yellow River near estuary. Science of the Total Environment 2019;707:Article No.135601.

Ho WK, Law JF, Zhang T, Leung KY. Effects of weathering on the sorption behavior and toxicity of polystyrene microplastics in multi-solute systems. Water Research 2020;187:Article No. 116419.

Hoellein T, Rojas M, Pink A, Gasior J, Kelly J. Anthropogenic litter in urban freshwater ecosystems: Distribution and microbial interactions. PLoS One 2014;9(6):e98485.

Hospodarova V, Singovszka E, Stevulova N. Characterization of cellulosic fibers by FTIR Spectroscopy for their further implementation to building materials. American Journal of Analytical Chemistry 2018;3:303-10.

Huang Y, Xu EG. Black microplastic in plastic pollution: Undetected and underestimated. Water Emerging Contaminants and Nanoplastics 2022;1(3):14-28.

Jambeck JR, Geyer R, Wilcox C, Siegler TR, Perryman M, Andrady A, et al. Plastic waste inputs from land into the ocean. Ciencia 2015;347(6223):768-71.

Kanhai LDK, Officer R, Lyashevska O, Thompson RC, O'Connor I. Microplastic abundance, distribution, and composition along a latitudinal gradient in the Atlantic Ocean. Marine Pollution Bulletin 2017;115(1-2):307-14.

Koenig JL. Spectroscopy of Polymers. New York: Elsevier; 1999. p. 77-145.

Lechner A, Keckeis H, Lumesberger-local F, Zens B, Krusch R, Tritthart M, et al. The Danube so colorful: A potpourri of plastic litter outnumbers fish larvae in Europe's second largest river. Environmental Pollution 2014;188:177-81.

Leslie HA, Brandsma SH, van Velzen MJM, Vethaak AD. Microplastics en route: Field measurements in the Dutch river delta and Amsterdam canals, wastewater treatment plants, North Sea sediments, and biota. Environment International 2017;101:133-42.

Lopez-Rojo N, Perez J, Alonso A, Correa-Araneda F, Boyero L. Microplastics have lethal and sublethal effects on stream invertebrates and affect stream ecosystem functioning. Environmental Pollution 2020;259:Article No. 113898.

Mai L, Bao LJ, Shi L, Wong CS, Zeng EY. A review of methods for measuring microplastics in aquatic environments. Environmental Science and Pollution Research 2018;25:11319-32.

Masura J, Baker J, Foster G, Arthur C. Laboratory Methods for the Analysis of Microplastics in the Marine Environment: Recommendations for Quantifying Synthetic Particles in Waters and Sediments. USA: NOAA Marine Debris Division; 2015. p. 31.

Rodrigues MO, Abrantes N, Gonçalves FJM, Nogueira H, Marques JC, Gonçalves AMM. Spatial and temporal distribution of microplastics in water and sediments of a freshwater system (Antua˜ River, Portugal). Science of the Total Environment 2018;633:1549-59.

Sekudewicz I, Da¸browska AM, Syczewski MD. Microplastic pollution in surface water and sediments in the urban section of the Vistula River (Poland). Science of the Total Environment 2021;762:Article No. 143111.

Su L, Sharp SM, Pettigrove VJ, Craig NJ, Nan B, Du F, et al. Superimposed microplastic pollution in a coastal metropolis. Water Research 2020;168:Article No. 115140.

Suteja Y, Atmadipoera AS, Riani E, Nurjaya IW, Nugroho D, Cordova MR. Spatial and temporal distribution of microplastic in surface water of tropical estuary: A case study in Benoa Bay, Bali, Indonesia. Marine Pollution Bulletin 2021; 163(1):111979-93.

Sutherland WJ, Bardsley S, Bennun L, Clout M, Cote IM, Depledge MH, et al. Horizon scan of global conservation issues for 2011. Trends in Ecology and Evolution 2011;26:10-6.

Urbina MA, Luna-Jorquera G, Thiel M, Acuña-Ruz T, Cristi MA, Andrade C, et al. A country's response to tackling plastic pollution in aquatic ecosystems: The Chilean way. Aquatic Conservation: Marine and Freshwater Ecosystems 2021;31:420-40.

Wu M, Yang C, Du C, Liu H. Microplastics in waters and soils: Occurrence, analytical methods, and ecotoxicological effects. Ecotoxicology and Environmental Safety 2020;202(3): 110910-22.

Zhang K, Hamidian AH, Tubic A, Zhang Y, Fang JK, Wu C, et al. Understanding plastic degradation and microplastic formation in the environment: A review. Environmental Pollution 2021;274:Article No. 116554.

Zhang K, Shi H, Peng J, Wang Y, Xiong X, Wu C, et al. Microplastic pollution in China's inland water systems: A review of findings, methods, characteristics, effects, and management. Science of the Total Environment 2018; 630:1641-53.

Zhao X, Wang J, Mei K, Leung Y, Wu F. Color: An important but overlooked factor for plastic photoaging and microplastic formation. Environmental Science and Technology 2022; 402:9161-3.

# Effect of Farming Systems on Soil Carbon Sequestration and Crop Yield of Paddy (*Oryza sativa* L.) in Irrigated Rice Field

**Mujiyo Mujiyo*, Suciati Dwi Nuraeni, Jauhari Syamsiyah, and Aktavia Herawati**

*Department of Soil Science, Faculty of Agriculture, Universitas Sebelas Maret, Surakarta, Indonesia*

**ARTICLE INFO**

Received: 10 Jul 2023
Received in revised: 28 Nov 2023
Accepted: 12 Dec 2023
Published online: 10 Jan 2024
DOI: 10.32526/ennrj/22/20230179

**Keywords:**
Carbon stock/ Conventional farming/ Greenhouse gas emissions/ Organic farming/ Plant biomass/ Semi-organic

*** Corresponding author:**
E-mail: mujiyo@staff.uns.ac.id

**ABSTRACT**

Carbon sequestration is obtained from the total accumulation of the element in both soil and plants. The enhancement has the capacity to reduce greenhouse gas emissions and influence soil quality and fertility, thereby affecting plant biomass and crop yield. Therefore, this research aimed to compare the total carbon sequestration in rice field with different farming systems, determine soil characteristics, and identify the correlation between the total carbon sequestration and impact on rice yield. An exploratory-descriptive method was used through field survey and laboratory analysis. The locations were mapped by overlaying the Indonesian landform map of the Girimarto District with various rice field systems, soil types, and slopes. Furthermore, the 12 Land Mapping Units (LMU) with 3-time repetitions resulted in 36 sampling points. Data were processed by calculating total carbon sequestration and statistical tests such as one-way ANOVA and Pearson's correlation. The results showed that rice field farming systems affected the total carbon sequestration. Organic farming had the highest total carbon sequestration value of 72.49 Mg/ha and the increase had a strongly positive correlation with crop yield of paddy. Crop yield in organic farming were higher than in semi-organic and conventional systems by 8.92 tons/ha. Factors that determined total carbon sequestration were soil C-organic and microbial biomass C. The suggested improvement recommendations were the transition of conventional and semi-organic farming as well as adding a variety of organic fertilizers such as biofertilizers.

## 1. INTRODUCTION

The amount of carbon in the atmosphere is reported to increase due to various living activities, such as respiration, forest fires, and fossil fuel production (Welsby et al., 2021; Gonsamo et al., 2017). This can cause greenhouse gases (GHG), which increases the temperature of the earth. Therefore, different efforts are needed to reduce GHG through carbon storage by adding organic materials (Pratama, 2019). High soil organic carbon (SOC) content leads to a solid soil structure, reduces erosion risk, and maintains nutrient availability to increase soil fertility. Fertile soil due to organic additions can increase plant biomass and rice yield by 18% (Arunrat et al., 2017; Liu et al., 2021). Carbon storage occurs through sequestration, which $CO_2$ is absorbed from the atmosphere during photosynthesis and transferred to soil through the roots (Losada et al., 2011). As a result, $CO_2$ gas in the atmosphere decreases, and increased carbon sequestration can reduce GHG emissions (Takakai et al., 2020). Controlling the rate of photosynthesis increases soil carbon input. Plants that absorb high concentrations of $CO_2$ will fix a lot of carbon during photosynthesis. However, several challenges can be encountered due to increasing temperatures. Water availability and the rate of photosynthesis become limited during the dry season or drought conditions. Furthermore, soil carbon stores are also easily lost due to plant root respiration and the decomposition of organic matter by microbial activity. An alternative strategy used to regulate carbon uptake includes a deliberate response to rising temperatures. This comprises the introduction of organic matter into soil through land processing before planting and post-harvest. The rationale behind this method is to elevate the decomposition of SOC, leading to an increased

**Citation:** Mujiyo M, Nuraeni SN, Syamsiyah J, Herawati A. Effect of farming systems on soil carbon sequestration and crop yield of paddy (*Oryza sativa* L.) in irrigated rice field. Environ. Nat. Resour. J. 2024;22(1):65-75. (https://doi.org/10.32526/ennrj/22/20230179)

production of $CO_2$. Subsequently, this augmented $CO_2$ production becomes an integral component of the ensuing photosynthesis process.

Most carbon sequestration research has been carried out in forests with tree cover on agricultural land. Rice field is notorious for emitting carbon dioxide into the atmosphere, accounting for a quarter of all anthropogenic GHG emissions (Jaiswal and Agrawal, 2020). By the last 50 years of scientific research, the agricultural sector has been exposed to climate changes in the dynamics of temperature and rainfall, causing plant stresses and decreases in production yield (Sengupta and Thangavel, 2023). Farming systems affects carbon sequestration, both adverse and beneficial impacts on the ecosystem. Arunrat et al. (2021) explained that conventional farming systems had higher GHG emissions level than organic due to excessive chemical fertilizer inputs. The intensive use of chemical fertilizers is the highest cause of soil degradation and results in poor soil carbon storage (Pahalvi et al., 2021). Conventional farming systems subjected to soil degradation often incur significant carbon losses, ranging from 25 to 75%, equivalent to approximately 10 to 30 Mg/ha (Lal, 2013). Meanwhile, organic fertilizers can increase soil carbon stock (Waqas et al., 2020). Organic farming systems enhance soil pH and hasten decomposition in humic compounds (Fitria and Soemarno, 2022). Leifeld and Fuhrer (2010) mentioned that this systems had higher soil organic carbon storage than conventional farming. Rice field with proper management practices can increase SOC by 4.85%, and support carbon sequestration in soil.

Carbon sequestration is important to improve soil quality, and fertility as well as reduce GHG emissions. Furthermore, carbon sequestration and soil fertility play an important role in the sustainability of agricultural land use. Soil captures and stores carbon dioxide from the atmosphere to reduce GHG emissions. In addition, SOC can promote the growth of aerobic microorganisms, which can consume $CH_4$ and reduce emissions. The presence can also influence other GHG emissions, such as nitrous oxide ($N_2O$) and methane ($CH_4$). SOC can increase the capacity to hold and convert nitrogen, reducing the production and release of $N_2O$, a potent GHG (Wiesmeier et al., 2019).

In the last two decades, climate and soil analyses have been looking at organic carbon as a strategy to minimize GHG emissions. However, many research have been conducted to identify carbon sequestration in forests, cropland, grassland, or land conversion. Agricultural land in the research area is included in the humid tropics. Basu (2014) stated that tropical areas such as Southeast Asia, specifically the humid tropics, have carbon storage capacity of 12-228 MgC/ha. Meanwhile, soil with anaerobic conditions, such as rice field, has a different amount of sequestration and depends on how systems are applied. Rice field soil conditions treated with flooding and drying affect environmental conditions in the anaerobic period. Within this context, anaerobic conditions contribute to an increased susceptibility of carbon decomposition rates to losses. The object of observation focuses on carbon sequestration in irrigated rice field with different farming systems. In addition, the defining factor concept was used to find soil characteristics (physical, chemical, and biological aspects) associated with carbon sequestration in rice field. The defining factor concept aims to formulate targeted land management strategies to maintain soil organic and carbon sequestration values, focusing on irrigated rice field. Each farming systems produce a different total carbon value related to the production of paddy crop. Land management using organic inputs shows better conditions and reduces GHG emissions. The objectives of this research were to compare total carbon sequestration in rice field with different farming systems, namely organic, semi-organic, and conventional rice field, to determine the characteristics of soil used as a basis for result determinants. Furthermore, the correlation between total soil carbon sequestration and its impact on rice yield was identified. The implications included updating data in rice field and increasing total carbon sequestration through appropriate and effective management of the defining factors to achieve optimal crop yield and sustain future agricultural land use sustainability.

## 2. METHODOLOGY

### 2.1 Research area

The research was conducted in Girimarto District, Wonogiri Regency, Central Java, Indonesia (Figure 1). The geographical location of Girimarto District is 7°45'51.4"-7°48'49.0" S and 111°01'47.6" -111°09'48.3" E with an altitude of 400 meters above sea level (m.a.s.l.), high rainfall (2,105 mm/year) at an area of 6,236.68 ha, composed of 111 hamlets. The total population is 45,569 people, with the largest livelihood in agriculture. The research was conducted on land use in rice field with organic, semi-organic, and

conventional farming systems. There are two types of soil, namely Alfisols and Inceptisols, on slopes of 0 to 8% and 8 to 15%, respectively. The analysis included biological, physical, and chemical analysis of soil and plants at Soil Chemistry and Fertility Laboratory, Faculty of Agriculture, Universitas Sebelas Maret.

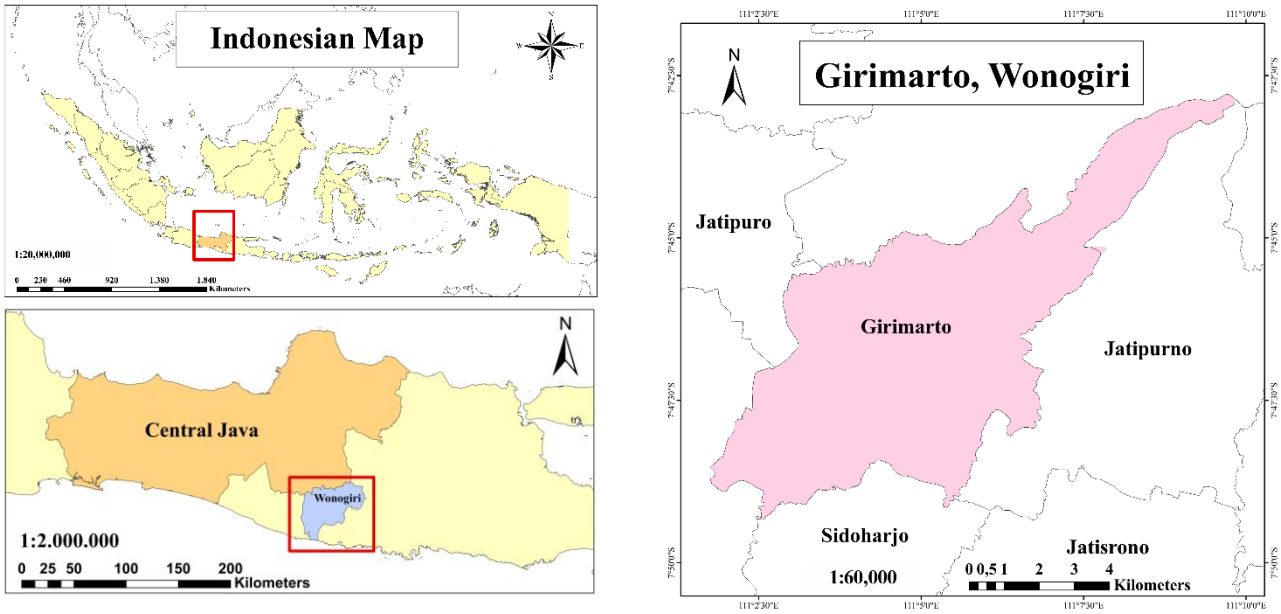


**Figure 1.** Research area

### 2.2 Soil and plant sampling

This research used an exploratory-descriptive method through field survey and laboratory analysis. Furthermore, the survey was conducted using the purposive sampling method. The land mapping unit (LMU) was carried out by overlaying the Indonesian land map (RBI) of Girimarto District, Wonogiri Regency, with a map of diverse land sources, including the type of rice field systems, soil type, and slope. The different rice field systems consist of organic, semi-organic, and conventional rice field. Soil types in the research location are Alfisols and Inceptisols, while the slope is 0-8% and 8-15%. The map overlay consists of 12 LMU, with 3 times repetitions, resulting in 36 sampling points, as shown in Figure 2. Soil samples were taken at 0 to 20 cm depth and a drill was used to carry out sampling during the maturation phase. Meanwhile, the samples taken were analyzed in the laboratory according to the method of each observation parameter during the maturation phase. The samples were oven-dried and weighed before further analysis to reduce the water content and inhibit the reaction process (Yadav et al., 2018).

### 2.3 Sample analysis

The parameters researched included soil volume weight by paraffin-clod method (Negro et al., 2018), texture by pipette method (Igaz et al., 2020), pH by potentiometric method (Lisak et al., 2015), soil C-organic by Walkley and Black method (Harahap et al., 2020), microbial biomass C by fumigation-extraction method (Heuck et al., 2015), C-organic of rice plants by Walkley and Black method (Gunamantha et al., 2021), rice yield (Nyamai et al., 2012) in Indonesia. This was conducted with observations of 1,000 grain weight, productive tillers, number of clumps per hectare, and number of grains per panicle (Sari, 2023), root volume by volumetric method, and root weight by gravimetric method. The calculation of total carbon sequestration was obtained from the accumulation of soil C-stock with plant C-stock. Meanwhile, soil C-stock (Bastia et al., 2013) and plant C-stock were obtained by equation (National Standardizations Agency of Indonesia, 2011).

$$Ct = BD \times \%C \times DP \quad (1)$$

$$Cm = Bo \times \%C \quad (2)$$

Where; Ct: soil C-stock (g/cm$^3$); BD: bulk density (g/cm$^3$); %C: soil organic carbon content (%); DP: soil depth (cm); Cm: plant C-stock; Bo: total plant biomass (kg). Total carbon sequestration was obtained from the sum of equation (1) and (2).

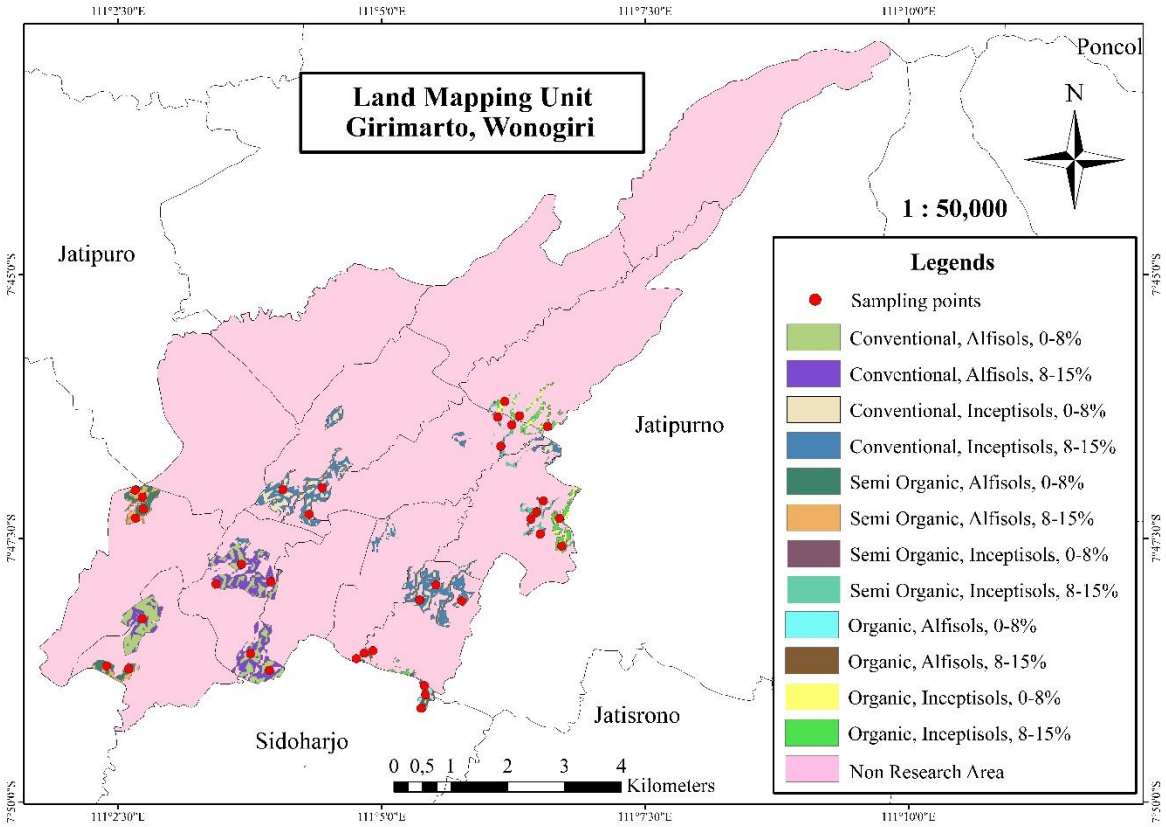


**Figure 2.** Observation and sampling point

### 2.4 Statistical analysis

Statistical tests were conducted using One-way Analysis of Variance (ANOVA) to determine effect of rice field farming systems on carbon sequestration and then Duncan's Multiple Range Test (DMRT) to determine differences in the impact of rice field farming systems. Defining factors were obtained by testing the correlation between parameters and total carbon sequestration. Defining factors were described as the most dominant factors influencing carbon sequestration and used as reference material for preparing appropriate land management recommendations to maintain soil organic carbon and sequestration.

## 3. RESULTS AND DISCUSSION

### 3.1 Soil C-stock, plant C-stock, carbon total sequestration

The C-organic at the research site is included in the medium category (2.09-2.81%), where the higher the content, the lower the bulk density. Soil C-stock content, plant C-stock, and total carbon sequestration at the research site ranged from 54.27-67.57 Mg/ha, 2.03-4.92 Mg/ha, and 56.30-72.49 Mg/ha, as shown in Table 1. The value of total carbon sequestration was highly dependent on various rice field farming systems. The results showed that rice field farming systems affected the total carbon sequestration value, as shown in Table 2.

**Table 1.** Value of soil C-stock, plant C-stock, and carbon total sequestration

| Farming systems | | C-Org (%) | BD (g/cm$^3$) | Soil c-tock (Mg/ha) | Biomass weight (g) | | | Plant C-Org (%) | | | Plant C-stock (Mg/ha) | Carbon total sequestration (Mg/ha) |
|---|---|---|---|---|---|---|---|---|---|---|---|---|
| | | | | | Stems | Root | Grain | Stems | Root | Grain | | |
| FS | C | 2.09 | 1.30 | 54.27 | 23.44 | 13.48 | 32.18 | 43.78 | 5.60 | 5.39 | 2.03 | 56.30 |
| | SO | 2.49 | 1.23 | 61.41 | 29.87 | 13.72 | 41.62 | 48.49 | 6.47 | 6.16 | 2.88 | 64.29 |
| | O | 2.81 | 1.20 | 67.57 | 44.27 | 27.06 | 53.54 | 55.51 | 6.81 | 7.93 | 4.92 | 72.49 |

Remark: FS=Farming systems; C=Conventional; SO=Semi organic

**Table 2.** Effect of farming systems on total soil carbon sequestration

| | Farming systems |
|---|---|
| Carbon total sequestration p-value (sig.) | 0.000** |

Remark: **=highly significant (p-value<0.01)

Soil C-stock, plant C-stock, and total carbon sequestration in organic rice field farming systems had higher values than in conventional and semi-organic rice field farming systems (Figure 3).

### 3.2 Rice productivity

Rice yield was obtained by observing the weight of 1,000 grains, productive tillers, number of clumps/ha, and number of grains/ha of rice yield (22). Yield of rice crop at the research location ranged from 4.14 to 8.92 tons/ha (Table 3).

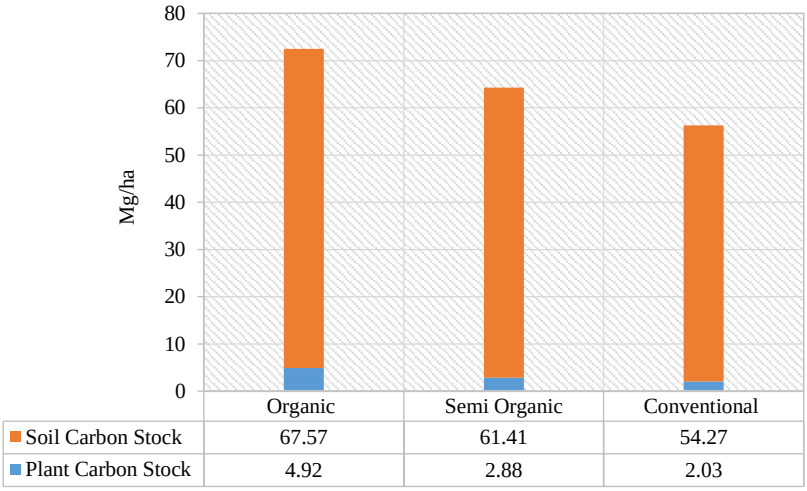


**Figure 3.** The average of C-stock soil, carbon of paddy crop, and carbon total sequestration under different farming systems

**Table 3.** Rice productivity

| Land characteristics | | 1,000 grain weight (g) | Productive tiller | Number of clumps/ha | Number of grains/ panicle | Rice yield (tons/ha) | Carbon total sequestration (Mg/ha) |
|---|---|---|---|---|---|---|---|
| Farming systems | Conventional | 32.50 | 8.67 | 160,000 | 91.75 | 4.14 | 56.30 |
| | Semi Organic | 32.75 | 9.92 | 160,000 | 100.42 | 5.22 | 64.29 |
| | Organic | 33.08 | 15.17 | 160,000 | 111.08 | 8.92 | 72.49 |
| Soil type | Alfisols | 32.50 | 10.94 | 160,000 | 100.61 | 5.64 | 63.04 |
| | Inceptisols | 32.75 | 11.56 | 160,000 | 101,56 | 6.15 | 65.68 |
| Slope | 0-8% | 32.59 | 11.83 | 160,000 | 101.33 | 6.25 | 65.04 |
| | 8-15% | 32.96 | 10.67 | 160,000 | 100.83 | 5.67 | 63.67 |

The results showed that rice field farming systems affected yield. Conventional, semi-organic, and organic farming systems have significantly different results, where organic systems has the highest yield at 8.92 tons/ha (Figure 4).

### 3.3 Defining factor of total C sequestration and the correlation between carbon sequestration and rice productivity in farming systems

Defining factors are important to provide recommendations for improving carbon sequestration in the research area. These factors are obtained through correlation tests between carbon total sequestration and various parameters (Table 4).

**Table 4.** Defining factor of carbon total sequestration

| Parameter | Carbon total sequestration |
|---|---|
| Bulk density (g/cm$^3$) | -0.272$^{ns}$ |
| pH | 0.136$^{ns}$ |
| Sand (%) | 0.053$^{ns}$ |
| Silt (%) | -0.096$^{ns}$ |
| Clay (%) | 0.035$^{ns}$ |
| Soil C-organic (%) | 0.923** |
| Microbial biomass C (µg/g) | 0.829** |

Remark: ns=not correlated; *=significantly correlated at p-value≤0.05; **=significantly correlated p-value≤0.01

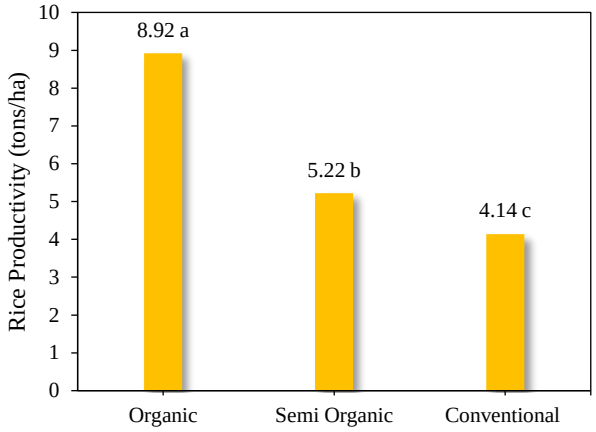


**Figure 4.** The average rice productivity under different farming systems

There are two defining factors of total carbon sequestration (Table 4), namely soil C-organic (r=0.923**) and microbial biomass C (r=0.829**). Figure 5 shows that organic rice field farming systems have the highest soil C-organic and microbial C biomass.

The results (Figure 6) of carbon total sequestration correlation test with rice yield showed a significant positive relationship (r=0.759**). Organic rice field farming systems had the highest root volume (113.33 mL) and weight (27.06 g).

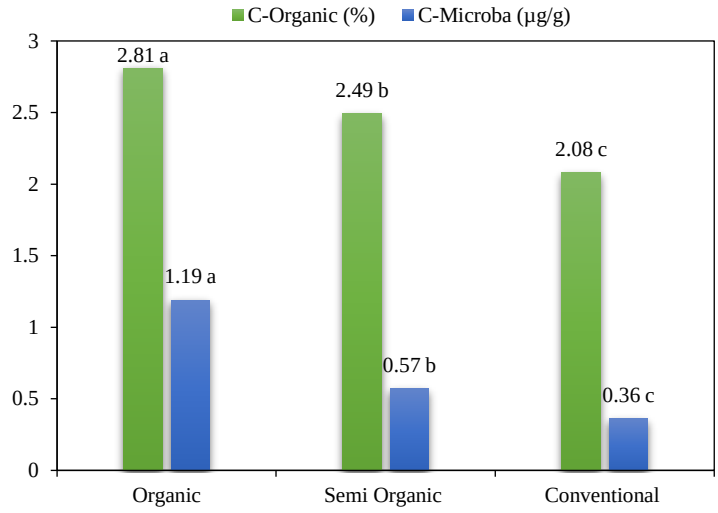


**Figure 5.** Defining factor of carbon total sequestration

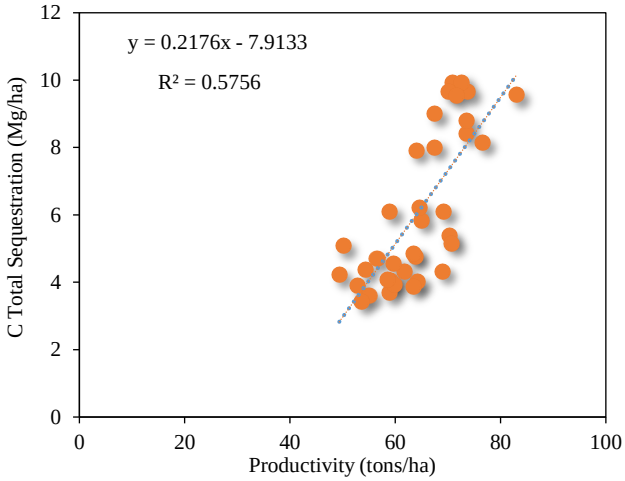


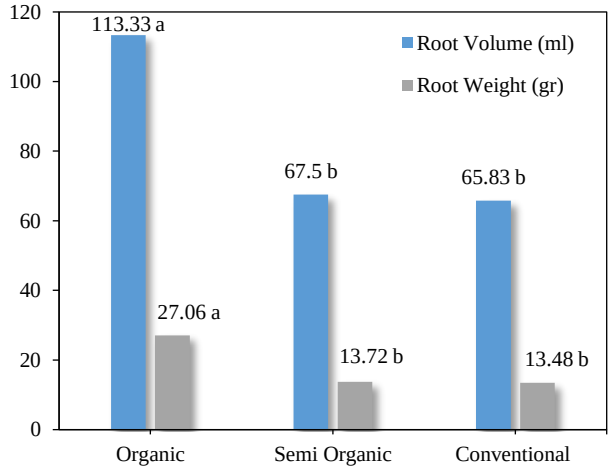


**Figure 6.** Correlation between C total sequestration and rice productivity

## 4. DISCUSSION

### 4.1 Carbon total sequestration

Carbon sequestration (Table 2) was influenced by farming systems (p-value<0.01) and rice field was a significant source of methane. Therefore, management practices such as water management (wetting and drying), fertilizer application, and tillage methods play a crucial role in reducing methane

emissions and enhancing carbon sequestration. Meanwhile, rice field cropping affects total carbon sequestration due to tillage. Before and after planting, soil tillage disturbs soil aggregates, causing organic carbon loss during soil mineralization. Different dosages and fertilizer types in each rice field farming method affect total carbon sequestration (Singh et al., 2018). Organic rice field is managed using fertilizer such as compost during tillage, where $CH_4$ and $N_2O$ emissions decrease by up to 50% compared to rice field with urea fertilizer (conventional rice field) (Gupta et al., 2021).

Carbon total sequestration (Figure 3) in conventional farming has the lowest value compared to other systems. This is because conventional agriculture does not use organic fertilizer, but has the lowest soil organic C content (Table 1) compared to organic and semi-organic rice, namely 2.09%. Furthermore, organic C content in semi-organic farming systems is 2.49%, and the total carbon absorption is higher than in conventional systems. Soil carbon levels are determined by the balance between inputs, such as plant residues and organic matter, and C losses owing to organic matter decomposition. To enhance SOC, carbon must be added to soil and this can be accomplished by improving crop yield to increase crop residue or retaining more residue in cropping systems (Hu et al., 2018). A previous research by Gupta et al. (2021) stated that rice field was the main contributor to $CH_4$, and flooded soil conditions increased $N_2O$ emissions in large amounts. The results from nitrification activities by microbes contribute to up to 70% of total $N_2O$ emissions. Synthetic N fertilization produces up to 77% $N_2O$, and the application of synthetic NPK fertilizer produces high total NO emissions. Meanwhile, organic fertilization such as compost, green manure, and plant litter only produces $N_2O$ ranging from 1% to 6% (Bordoloi et al., 2018; Gupta et al., 2021).

Carbon total sequestration in organic rice field farming systems is significantly different and has the highest value compared to semi-organic and conventional rice field farming systems (Figure 3). This is because organic rice field farming can improve soil fertility and increase plant biomass to enhance carbon sequestration. Applying organic fertilizers enhances the physical, biological, and chemical conditions of soil by improving aggregates that facilitate root penetration and provide a place for microorganisms. Therefore, nutrients and organic carbon are efficiently circulated among soil aggregates (Anshori et al., 2016; Wicaksono et al., 2014). Nutrients are used by plants for growth, including their roots. Growing and developing roots can optimally absorb water as photosynthetic material (Hodge, 2014). Increased photosynthesis can increase the results of photosynthesis in the form of acylates translocated to grain and all parts of the plant to increase biomass (Khoerunnisa et al., 2022). The amount of carbon stored in plant biomass shows carbon dioxide ($CO_2$) absorbed from the atmosphere. The dynamics of climate, such as increasing temperatures in rice field, affect the microbial activity of soil and the number of organic matter decompositions, as well as alter methane production and oxidation balance. High temperatures lead to higher methane emissions, reducing the potential carbon sinks of rice field. According to Keenan et al. (2014), carbon uptake from photosynthetic activity shows an increase and a higher value compared to plant respiration in some areas. In addition, high photosynthesis leads to increased uptake and storage of carbon in plants and soil, balancing methane emissions. Water management conservation measures and soil cover in organic rice field farming systems can prevent organic carbon loss (Meena et al., 2020). High levels of soil and plant organic carbon result in increased total carbon sequestration.

### 4.2 Rice productivity

Farming systems affected rice yield (p-value<0.01**) due to the provision of organic fertilizer with different doses. Fertilization aims to improve soil conditions by adding nutrients to support plant growth and development (Ekawati et al., 2021). Yield of rice crop in various rice field farming systems was significantly different, with the value of yield in organic rice field farming being higher (8.92 tons/ha) compared to conventional (4.14 tons/ha) and semi-organic (5.22 tons/ha) (Figure 4) systems. Applying organic fertilizer in cow manure can increase nutrients completely and improve soil structure, enhancing the capacity to hold nutrients and water. Meanwhile, cow manure provides soil nitrogen, phosphorus, potassium, and calcium nutrients. Organic fertilizers also increase microbial activity, resulting in the release of nutrients into soil (Tashi and Wangchuk, 2015). Conventional farming systems that continuously apply inorganic fertilizers can degrade soil and reduce yield (Chen et al., 2017).

Field management significantly affected productive tillers and the number of grains per panicle.

The number of productive tillers and grains per panicle of rice crop in organic rice field was higher than in semi-organic and conventional field farming systems. This is consistent with Siavoshi et al. (2011), where organic fertilizers give balanced nutrients, such as micronutrients, to enhance tillers, grains per panicle, and 1,000-grain weight. Micronutrients function as activators of the enzyme systems in the photosynthesis process to increase the conversion of carbon dioxide into carbohydrates (Sherefu and Zewide, 2021).

The pH ranged from 6.47 to 6.89 at the research location, which is slightly acidic to neutral. The increase in pH value in organic rice field farming is due to the application of organic fertilizers and the inundation process. In addition, inundation causes an increase in pH due to a change in oxidation to reduction, where the $Fe(OH)_3$ compound is reduced to $Fe(OH)_2$ and liberates $OH^-$ ions. A neutral pH reaction is an optimum condition for the availability of macronutrients needed for plant growth (Supriyadi et al., 2020).

### 4.3 Defining factor of carbon total sequestration

Understanding the determinants for formulating recommendations aimed at enhancing carbon sequestration in the Girimarto District is important. There are two determinants of carbon sequestration (Table 4), namely soil C-organic and microbial C-biomass. Rice field farming systems significantly affected both determinants (p-value<0.01**) due to the application of different types and doses of fertilizers. Fertilization activities aim to add macro and micronutrients needed by plants (Hayati et al., 2012).

The use of inorganic fertilizers offers a substantial quantity of specific nutrients. Due to their water-solubility, these fertilizers facilitate rapid absorption. However, prolonged and consistent use leads to soil degradation since the nutrients are prone to be fixed and leached, resulting in a gradual reduction in fertility. Meanwhile, applying organic fertilizers improves the physical, chemical, and biological conditions of soil (Nurmalasari et al., 2021). Organic fertilizers improve soil structure and have a more balanced macro and micronutrient content, resulting in increased soil fertility but require a larger input volume (Bhatt et al., 2019).

The lowest C-organic content in conventional rice field was 2.08%, as shown in Figure 5. The low level was due to the continuous application of inorganic without being balanced by the application of organic fertilizers. The reduction in soil fertility inhibits the regeneration of crop, leading to the unsustainability of agricultural practices (Agegnehu et al., 2017). Low levels of C-organic matter in field will affect the physical, chemical, and biological properties of soil, inhibiting plant growth and production (Rina, 2020). Low organic matter causes high soil density, making it difficult for roots to penetrate soil and causing microorganisms to decline due to the lack of organic matter (Costantini and Mocali, 2022). Carbon sequestration in conventional rice field farming systems was lowest at 56.30 Mg/ha. The lower soil C-organic content resulted in a decrease in soil C-stock.

Soil microbial C biomass plays an important role in fertility acting as an agent of biochemical processes and nutrient cycling, determining soil quality and yield (Brar et al., 2015). Decreased microbial C biomass reduces the rate of nutrient cycling in soil. Therefore, nutrient uptake by plant roots is disrupted to inhibit photosynthesis. Conventional rice field farming had the lowest microbial C biomass at 0.36 µg/g. There was a significant positive correlation between microbial biomass C and C-organic (r=0.837**). Micro-organisms use C-organic as a food source, and with a decrease in this variable also inhibit the activity.

### 4.4 Correlation of C total sequestration with rice yield

Statistical test results show that carbon sequestration has a very significant positive correlation with rice yield (r=0.759**). Based on Figure 6, organic rice field farming has the highest carbon sequestration and rice yield of 72.49 Mg/ha and 8.90 tons/ha. Photosynthesis is the process of converting carbon dioxide ($CO_2$) from the atmosphere and water ($H_2O$) from soil and water vapor into oxygen ($O_2$) and glucose ($C_6H_{12}O_6$) (Nagy et al., 2010). This process increases the need for photosynthetic materials by absorbing carbon dioxide (Daud et al., 2021). The increased photosynthesis followed by nutrient uptake by plants can improve products in glucose, which is translocated and accumulated into the grain (Hidayati et al., 2016).

In conventional rice field farming, the total carbon sequestration value and rice yield are 56.30 Mg/ha and 4.14 tons/ha. The lower carbon sequestration result, the lower rice yield. This is because the use of inorganic fertilizers causes soil C-organic to be lower than in other management systems. The low soil C-organic makes soil C-stock also low. High doses of chemical fertilizers containing certain

nutrients do not meet the needs of others, specifically micro-nutrients required by plants. The role of micronutrients in plants functions for protein synthesis, chlorophyll formation, and enzyme activators in the photosynthesis process. Therefore, the lack of micronutrients inhibits plant metabolism, such as photosynthesis, decreasing the absorption of $CO_2$ from the atmosphere.

Root weight and volume play an important role in plant carbon content. In the research location, conventional and semi-organic rice field used the IR 64 rice variety, while organic rice field used the Menthik Wangi variety. Root characteristics play an important role in dealing with drought stress conditions. This means that IR 64 rice is more sensitive to drought stress than Menthik Wangi rice. In conventional rice field farming systems, the variety has a lower root weight than the Menthik Wangi rice (Maisura et al., 2017). In contrast, Menthik Wangi varieties are better able to absorb water than IR 64 because the roots have better growth and elongation to reach deeper layers. In organic management systems, the variety has higher root weight and volume than conventional rice field, resulting in increased carbon sequestration. The observation results (Table 3) show that Menthik Wangi has a higher number of tillers, grain weight per panicle, and total grain number per panicle than the IR 64 variety.

## 5. CONCLUSION

In conclusion, farming systems was reported to influence carbon total sequestration due to differences in applying organic fertilizers. Organic rice field had higher carbon total sequestration than semi-organic and conventional rice field systems, which amounted to 72.49 Mg/ha. These results showed that carbon total sequestration significantly correlated with rice yield. Furthermore, organic rice field farming systems had the highest rice yield of 8.92 tons/ha. Soil characteristics that determined the total carbon sequestration in soil were soil C-organic, microbial biomass C, root volume, and root weight. Based on the results, the most feasible alternative to be implemented was converting conventional rice field to organic with a gradual reduction in the application of chemical fertilizers according to the conservation stage. Improvement could be given by using other variations of organic fertilizers to increase C-organic levels and total carbon sequestration, as well as reduce carbon dioxides in the atmosphere. The long-term impact of implementing this recommendation was an increase in carbon storage in soil and a contribution to the preservation of sustainable agriculture. This was due to the non-use of chemicals in agricultural businesses, as well as increased soil fertility and quality to increase rice productivity. Future research was also expected to compare carbon sequestration with the calculation of emissions released by agricultural businesses in organic, semi-organic, and conventional rice field.

## ACKNOWLEDGEMENTS

The authors are grateful to the P2M research grant from Universitas Sebelas Maret Surakarta, the Wonoagung Wonogiri Organic Farming Association (PPOWW), and Girimarto District, Wonogiri for facilitating the location. Furthermore, the authors thank Mohammad Rizki R, Nanda Mei I, Viviana I, Tiara Hardian, Akas Anggita, and Khalyfah Hasanah for their paper elaboration.

## REFERENCES

Agegnehu G, Srivastava AK, Bird MI. The role of biochar and biochar-compost in improving soil quality and crop performance: A review. Applied Soil Ecology 2017;119: 156-70.

Anshori A, Sunarminto BH, Haryono E. Flow of the organic matter on the organic paddy field in Jayan Sub-village, Kebonagung Village, Imogiri Sub-District, Bantul District, Yogyakarta. Caraka Tani: Journal of Sustainable Agriculture 2016;31(1):45-50.

Arunrat N, Pumijumnong N, Hatano R. Practices sustaining soil organic matter and rice yield in a tropical monsoon region. Soil Science and Plant Nutrition 2017;63(3):274-87.

Arunrat N, Sereenonchai S, Wang C. Carbon footprint and predicting the impact of climate change on carbon sequestration ecosystem services of organic rice farming and conventional rice farming: A case study in Phichit Province, Thailand. Journal of Environmental Management 2021; 289(1):1-11.

Bastia DK, Tripathy S, Barik T, Kar CS, Raha S, Tripathy A. Yield and soil organic carbon sequestration under organic nutrient management in rice-rice system. Journal of Crop and Weed 2013;9(1):52-5.

Basu JP. Agroforestry, climate change mitigation and livelihood security in India. New Zeal Journal of Forestry Science 2014;44(1):1-10.

Bhatt MK, Labanya R, Joshi HC. Influence of long-term chemical fertilizers and organic manures on soil fertility: A review. Univers Journal of Agriculture Research 2019;7(5):177-88.

Bordoloi N, Baruah KK, Thakur AJ. Effectiveness of plant growth regulators on emission reduction of greenhouse gas (Nitrous oxide): An approach for cleaner environment. Journal of Cleaner Production 2017;171:333-44.

Brar BS, Singh J, Singh G, Kaur G. Effects of long term application of inorganic and organic fertilizers on soil organic carbon and physical properties in maize-wheat rotation. Agronomy 2015;5(2):220-38.

Chen D, Yuan L, Liu Y, Ji J, Hou H. Long-term application of manures plus chemical fertilizers sustained high rice yield and improved soil chemical and bacterial properties. European Journal of Agronomy 2017;90:34-42.

Costantini EAC, Mocali S. Soil health, soil genetic horizons and biodiversity. Journal of Plant Nutrition and Soil Science 2022;185(1):24-34.

Daud M, Bustam BM, Harnelly E, Dharma W. Carbon absorption capability of single-leaf and compound-leaf plants in the BNI urban forest, Banda Aceh. Proceedings of the 1st Earth and Environtment Science; 2021 June 21-22; (Virtual) Bogor: Indonesia; 2021.

Ekawati R, Saputri LH, Kusumawati A, Paonganan L, Ingesti PSVR. Optimizing yard land by cultivating vegetable crops as an alternative in achieving food independence strategies. PRIMA: Journal Community Empowering and Service 2021;5(1):19-28.

Fitria L, Soemarno. Effects of lime and compost on chemical characteristics and soil hydraulic conductivity of Alfisols at ATP Jatikerto coffee plantation. Caraka Tani: Journal of Sustainable Agriculture 2022;37(1):48-61.

Gonsamo A, Chen JM, Colombo SJ, Ter-Mikaelian MT, Chen J. Global change induced biomass growth offsets carbon released via increased forest fire and respiration of the central Canadian boreal forest. Journal of Geophysical Research Biogeosciences 2017;122(5):1275-93.

Gunamantha IM, Oviantari MV, Suryaputra IGN, Sudiana IK, Sastrawidana IDK, Armatini K, et al. Nitrogen content and C-Organic in the field for tropical fruit plantation in Jinengdalem Village, Bali, Indonesia. Proccedings of the 6th International Conference on Climate Change; 2021 May 25; (Virtual) Surakarta: Indonesia; 2021.

Gupta K, Kumar R, Baruah KK, Hazarika S, Karmakar S, Bordoloi N. Greenhouse gas emission from rice fields: A review from Indian context. Environmental Science and Pollution Research 2021;28(24):30551-72.

Harahap FS, Rahmaniah, Oesman R, Arman I. Supply liquid organic fertilizer NASA and rice husk ash to the chemical properties of the soil on the tomato plant. International Journal of Science, Technology and Management 2020;1(3):185-9.

Hayati M, Marliah A, Fajri H. The effect of varieties and dosages of SP-36 fertilizer on the growth and yield of peanut crop (*Arachis hypogaea* L.). Jurnal Agrista Unsyiah 2012;16(1):7-13.

Heuck C, Weig A, Spohn M. Soil microbial biomass C:N:P stoichiometry and microbial use oforganic phosphorus. Soil Biology and Biochemistry 2015;85:119-29.

Hidayati N, Triadiati, Anas I. Photosynthesis and transpiration rates of rice cultivated under the system of rice intensification and the effects on growth and yield. Hayati Journal Bioscience 2016;23(2):67-72.

Hodge A. Interactions Between Arbuscular Mycorrhizal Fungi and Organic Material Substrates. Waltham, United State: Elsevier; 2014.

Hu T, Sørensen P, Olesen JE. Soil carbon varies between different organic and conventional management schemes in arable agriculture. European Journal of Agronomy 2018;94:79-88.

Igaz D, Aydin E, Šinkovičová M, Šimanský V, Tall A, Horák J. Laser diffraction as an innovative alternative to standard pipette method for determination of soil texture classes in central Europe. Water (Switzerland) 2020;12(5):1-16.

Jaiswal B, Agrawal M. Carbon footprints of agriculture sector. In: Muth SS, editor. Environmental Footprints and Eco-Design of Products and Processes. Varanasi: India; Springer Nature; 2020.

Keenan TF, Gray J, Friedl MA, Toomey M, Bohrer G, Hollinger DY, et al. Net carbon uptake has increased through warming-induced changes in temperate forest phenology. Nature Climate Change 2014;4(7):598-604.

Khoerunnisa, Putry RRH, Salsabila SA, Darmawan MR, Nahdatulia Y, Budisantoso I. Growth and flavonoids content of black rice (*Oryza sativa* L. indica) with compost tea of oyster mushroom waste. Caraka Tani: Journal of Sustainable Agriculture 2022;37(2):289-98.

Lal R. Intensive agriculture and the soil carbon pool. Journal of Crop Improvement 2013;27:735-51.

Leifeld J, Fuhrer J. Organic farming and soil carbon sequestration: What do we really know about the benefits? Ambio 2010;39(8):585-99.

Lisak G, Cui J, Bobacka J. Paper-based microfluidic sampling for potentiometric determination of ions. Sensors Actuators, B Chemical 2015;207(PB):933-9.

Liu Y, Ge T, van Groenigen KJ, Yang Y, Wang P, Cheng K, et al. Rice paddy soils are a quantitatively important carbon store according to a global synthesis. Communications Earth and Environment 2021;2(1):1-9.

Losada MRM, Freese D, Rodriguez AR. Carbon sequestration in agroforestry systems. In: Kumar BM, Nair PKR, editors. Carbon Sequestration Potential of Agroforestry Systems: Opportunities and Challenges. Lugo, Spain: Springer; 2011. p. 43-59.

Maisura M, Chozin MA, Lubis I, Junaidi A, Ehara H. Study of morphological and physiological characters of rice varieties tolerant to drought stress in paddy fields. Jurnal of Agrium 2017;14(1):8-16.

Meena RS, Kumar S, Yadav GS. Nitrogen footprint: A useful indicator of agricultural sustainability. In: Meena RS, editor. Nutrient Dynamics for Sustainable Crop Production. Uttar Pradesh, India: Springer; 2020.

Nagy L, Hajdu K, Fisher B, Hernandi K, Nagy K, Vincze J. Photosynthetic reaction centres-from basic research to application possibilities. Notulae Scientia Biologicae 2010; 2(2):7-13.

National Standardizations Agency of Indonesia. Measurement and Calculating of Carbon Stocks-Field Measurements for Estimating Forest Carbon Stocks (Ground Based Forest Carbon Accounting). Jakarta, Indonesia: National Standardizations Agency of Indonesia; 2011.

Negro SRL, Pereira D dos S, Montanari R, Dalchiavon FC, Oliveira CF. Correlations of soybean yield with soil porosity and bulk density of an Oxisol. Pesquisa Agropecuaria Tropical 2018;48(4):476-85.

Nurmalasari AI, Supriyono S, Budiastuti MTS, Nyoto S, Sulistyo TD. Composting rice straw for organic fertilizer and making husk charcoal as a planting medium in soybean demonstration plots. PRIMA: Journal of Community Empowering and Services 2021;5(2):102-9.

Nyamai M, Mati BM, Home PG, Odongo B, Wanjogu R, Thuranira EG. Improving land and water productivity in basin rice cultivation in Kenya through system of rice intensification (SRI). Agricultural Engineering International CIGR Journal 2012;14(2):1-9.

Pahalvi HN, Rashid S, Nisar B, Rafiya L, Kamili AN. Microbiota and Biofertilizers, Vol 2: Ecofriendly Tools for Reclamation of Degraded Soil Environs. Cham, Switzerland: Springer International Publishing; 2021.

Pratama R. The greenhouse effect on the earth. Buletin Utama Teknik 2019;14(2):120-6.

Rina W. Study of macro nutrients on agricultural land in Waiheru Village RT 06 RW 008 Baguala District, Ambon City in 2017. Global Health Science 2020;5(1):5-9

Sari SK. Production of Intani 602 hybird rice at various planting distances. Jurnal Suluh Tani 2023;1(1):44-9.

Sengupta A, Thangavel M. Analysis of the effects of climate change on cotton production in Maharashtra State of India using statistical model and GIS mapping. Caraka Tani: Journal of Sustainable Agriculture 2023;38(1):152-62.

Sherefu A, Zewide I. Review paper on effect of micronutrients for crop production. Nutrition and Food Processing 2021;4(7):1-8.

Siavoshi M, Laware SL, Laware S. Effect of organic fertilizer on growth and yield components in rice (*Oryza sativa* L.). Journal of Agricultural Science 2011;3(3):217-24.

Singh BP, Setia R, Wiesmeier M, Kunhikrishnan A. Agricultural management practices and soil organic carbon storage. In: Singh B, editor. Soil Carbon Storage: Modulators, Mechanisms and Modeling. Freising, Germany: Elsevier; 2018. p. 207-44.

Supriyadi S, Pratiwi MK, Minardi S, Prastiyaningsih NL. Carbon organic content under organic and conventional paddy field and its effect on biological activities (A case study in Pati Regency, Indonesia). Caraka Tani: Journal of Sustainable Agriculture 2020;35(1):Article No. 108.

Takakai F, Kominami Y, Ohno S, Nagata O. Effect of the long-term application of organic matter on soil carbon accumulation and GHG emissions from a rice paddy field in a cool-temperate region, Japan. -I. comparison of rice straw and rice straw compost-. Soil Science and Plant Nutrition 2020; 66(1):84-95.

Tashi S, Wangchuk K. Organic vs. conventional rice production: Comparative assessment under farmers' condition in Bhutan. Organic Agriculture 2015;6(4):255-65.

Waqas MA, Li Y, Smith P, Wang X, Ashraf MN, Noor MA, et al. The influence of nutrient management on soil organic carbon storage, crop production, and yield stability varies under different climates. Journal of Cleaner Production 2020; 268:1-12.

Welsby D, Price J, Pye S, Ekins P. Unextractable fossil fuels in a 1.5°C world. Nature 2021;597(7875):230-4.

Wicaksono MI, Rahayu M, Samanhudi S. Effect of mycorrhiza and organic fertilizer on garlic growth. Caraka Tani: Journal of Sustainable Agriculture 2014;29(1):35-44.

Wiesmeier M, Urbanski L, Hobley E, Lang B, Lützow MV, Spiotta EM, et al. Soil organic carbon storage as a key function of soils: A review of drivers and indicators at various scales. Geoderma 2019;333:149-62.

Yadav GS, Das A, Lal R, Babu S, Meena RS, Patil SB, et al. Conservation tillage and mulching effects on the adaptive capacity of direct-seeded upland rice (*Oryza sativa* L.) to alleviate weed and moisture stresses in the North Eastern Himalayan Region of India. Archives of Agronomy and Soil Science 2018;64(9):1254-67.

# Spatial Green Space Assessment in Suburbia: Implications for Urban Development

**Sura Pattanakiat[1,2], Sirasit Vongvassana[1,2*], Thamarat Phutthai[1,2], Pisut Nakmuenwai[1,2], Theerawut Chiyanon[1,2], Voravart Ratanadilok Na Bhuket[1], Thunyapat Sattraburut[1], Pathomphot Chinsawadphan[1], and Kajornsak Khincharung[1]**

*[1]Faculty of Environment and Resource Studies, Mahidol University, Nakhon Pathom 73170, Thailand*
*[2]Central and Western Regional Centre for Geo-Informatics and Space Technology, Mahidol University, Nakhon Pathom 73170, Thailand*

**ARTICLE INFO**

Received: 14 Jun 2023
Received in revised: 12 Dec 2023
Accepted: 19 Dec 2023
Published online: 11 Jan 2024
DOI: 10.32526/ennrj/22/20230153

**Keywords:**
Green space/ Classification/ Geoinformatics/ Urban planning/ Nonthaburi Province

*** Corresponding author:**
E-mail: sirasit.von@mahidol.ac.th

**ABSTRACT**

Nonthaburi, a suburban province adjacent to the Bangkok Metropolis, has experienced a reduction in green spaces due to urban expansion. This study quantified Nonthaburi's green space through visual interpretation of land use and land cover (LULC) using THEOS and Sentinel-2. Areas of green space were extracted using remote sensing indices and pixel-based classification based on THEOS. The extracted green area was then integrated with the existing LULC patterns to align with the green space characteristic established by Thailand's Office of Natural Resource and Environmental Policy and Planning. This includes public services, functional utility, median strips, community economics, fallow, and natural green space. The analysis of green space management and planning utilized the Urban Green Space Index (UGSI), Per Capita Green Space (PCGS), and accessibility to public green space. The results revealed that Nonthaburi comprises a green space area of 465.29 $km^2$ or 73.06%, exhibiting a higher prevalence within its western region while displaying a relatively lower extent in the urban zone adjacent to the Bangkok Metropolis. The per capita green space is 367.71 $m^2$ but decreases to 255.82 $m^2$ when accounting for the latent population, meaning it still meets the World Health Organization (WHO) criteria. Currently, only six parks (single and clusters) meet the criteria for public green space. Additionally, both fallow and median strip green spaces (at road interchanges) need to be considered for their potential use in new public service. Furthermore, very high-resolution imagery from unmanned aerial vehicles (UAVs) should be used for green space planning by the organization.

## 1. INTRODUCTION

Green space refers to any open piece of land that is partly or completely covered with vegetation, such as grass, trees, shrubs, or other vegetation (Lachowycz and Jones, 2013; US EPA, 2017). In both urban and rural environments, green space includes woodlands, parks, gardens, grassy areas, cemeteries, allotments, golf courses, and green corridors such as paths, empty railway lines, rivers, and canals (Carbó-Ramírez and Zuria, 2011; White et al., 2013; Petersen, 2013). Urban green spaces provide a wide range of ecosystem services for city residents (Bastian et al., 2012; Pinto et al., 2022). They serve as settings that promote mental and physical health for all the people living in an urban community. Additionally, they contribute to the maintenance and protection of urban biodiversity, reduce and regulate environmental hazards such as air, water and noise pollution, and mitigate the impacts of extreme weather events (Haq, 2011; Heinze, 2011; Krisdianto et al., 2012; WHO Regional Office for Europe, 2017).

According to guidelines intended to drive sustainable green space management in Thailand, green space refers to natural or human-made areas in cities or communities covered with vegetation as a primary component. It benefits the environment,

**Citation:** Pattanakiat S, Vongvassana S, Phutthai T, Nakmuenwai P, Chiyanon T, Bhuket VRN, Sattraburut T, Chinsawadphan P, Khincharung K. Spatial green space assessment in Suburbia: Implications for urban development. Environ. Nat. Resour. J. 2024;22(1):76-92. (https://doi.org/10.32526/ennrj/22/20230153)

sustains ecosystems, and enhances people's quality of life (ONEP, 2019). This concept is similar to the definition for "vegetated areas" used in most papers according to the terminology and definition reviewed by Taylor and Hochuli (2017). The Office of Natural Resource and Environmental Policy and Planning (ONEP) (2019) established a classification scheme based on utilization patterns divided into six categories as follows: 1) public service with green space such as parks, botanical gardens, playgrounds, and sports fields; 2) functional utility green space such as personal areas, institutional areas, and utility areas; 3) strip green space such as roads, railways and street isles; 4) community economic green space such as paddy fields, field crops, and orchards; 5) natural green space such as wetlands, and bodies of water; and 6) fallow green space such as abandoned land. This coincides with the two different interpretations of green space including green space as nature and green space as urban vegetated space (Taylor and Hochuli, 2017).

The standard for per capita green space is set at a minimum of 9 $m^2$ per individual (Deloya, 1993; Kuchelmeister, 1998; WHO, 2010; WHO, 2012). The ONEP (2017) suggests that urban communities in Thailand should provide at least 20,000 $m^2$ of public service green space serving, a minimum of 2,000 people and ensuring not less than 5 $m^2$ per individual. Further, these spaces should be easily accessible or walkable within a 500 m distance. The ONEP (2019) also suggests that public service green space should not be less than 15 $m^2$ per individual. The overall green space type coverage for small, medium, and large communities is 25%, 20%, and 15%, respectively.

Due to various factors including mass communication, residential investment, commuting, and infrastructure services, urban growth is affected (Lu et al., 2013). Therefore, urban green space planning is important and necessary. Approaches suggested for urban policymakers and practitioners include clarifying the targets and objectives of green space planning, considering the urban/local planning context and frameworks, adopting a long-term perspective while remaining flexible, and viewing green space projects as investments in public health and social well-being (WHO Regional Office for Europe, 2017). The Twelfth National Economic and Social Development Plan (2017-2021), under the strategic development of urban and metropolitan areas, specifically aims to increase urban green space for recreation and air pollution control services (NESDC, 2017). Abandoned green spaces have the potential to be transformed into public-service green spaces for recreation (Park and Guldmann, 2020). Furthermore, the Twentieth National Strategy proposes that Thailand should consist of green space covering approximately 55% of the total area of the country, with 5% located in urban and rural communities.

Studies tend to focus on general green space extraction using medium-resolution satellite data and overlook the classification of green space patterns by integrating remote sensing techniques, especially in the Southeast Asia region (Richards et al., 2017; Nor et al., 2021). Although some studies incorporate high-resolution satellite imagery for green space pattern classification and planning, they often fail to address the issue of green space accessibility, particularly concerning public service green spaces that can be directly utilized by people. Furthermore, most studies concentrate predominantly on urban and metropolitan areas (Senanayake et al., 2013; Shekhar and Aryal, 2019; Chinnabut et al., 2021; Wirayuda et al., 2023), thereby neglecting the suburban areas that are undergoing urbanization and will be significantly impacted by future urban expansion.

Nonthaburi is one of the central provinces of Thailand and is experiencing high levels of expansion due to its proximity to the extended Bangkok metropolitan region (EBMR) (Kalawong et al., 2018; Nathalang, 2019). This situation is similar to that of another location in Southeast Asia (Xu et al., 2019; Zhao et al., 2020). Consequently, Nonthaburi is facing a complex range of problems arising from a development perspective. The main issues include inadequate waste and wastewater treatment, air pollution, particularly the expansion and distribution of PM2.5, severe traffic congestion and accidents, and the destruction of green spaces (Nonthaburi Provincial Office, 2019).

The Five-Year Nonthaburi Development Plan (2018-2022) proposes the provision of 5 $m^2$ of urban green space per individual and 30-50% of the total area of government, academic, and religious places designated as environmental green space. Nonetheless, the spatially explicit assessment of the current green space pattern, its quantity, and its compliance with predefined criteria remains an ongoing inquiry essential for effective management and planning purposes. Thus, the objective is to investigate the current state of green space in Nonthaburi, utilizing geoinformatics technologies

such as remote sensing (RS) and geographic information systems (GIS). These valuable tools can support and implement appropriate management strategies in this investigation.

## 2. METHODOLOGY

### 2.1 Study area

Nonthaburi is located at latitude 13°47'19.63" N to 14°8'25.14" N and longitude 100°15'44.12" E to 100°34'4.09" E, in the low-lying floodplain of the Chao Phraya River, covering an area of 636.82 km$^2$. It is one of the provinces neighboring the Bangkok Metropolitan area and is divided into two parts by the Chao Phraya River. Nonthaburi consists of six districts and 22 municipalities (Figure 1). The climate in the region is influenced by the north-east and south-west monsoons. The soil texture is predominantly clay and silty clay. Due to the high soil fertility, a significant portion of the area has been utilized for agricultural activities. The registered population in 2019 was 1,265,387 (Department of Provincial Administration, 2019) and the latent population was 553,457 (Nonthaburi Provincial Statistical Office, 2020).

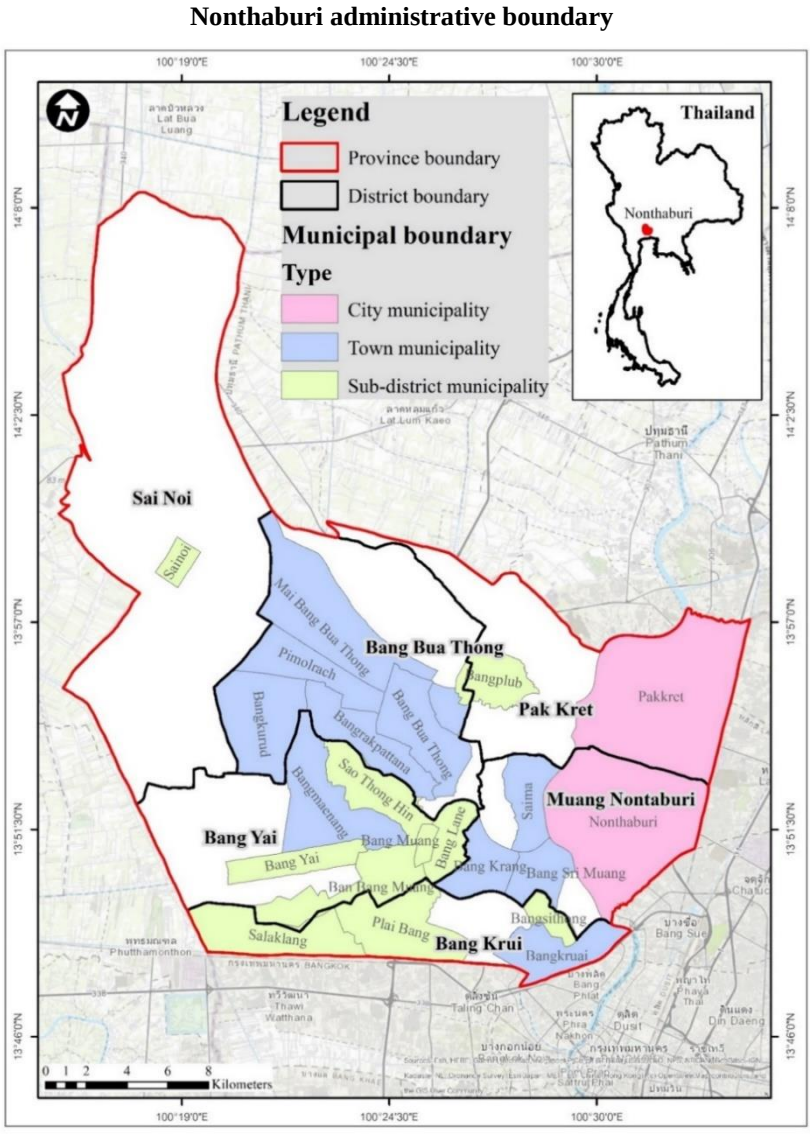


**Figure 1.** Location of the study site and the province and municipality boundary of Nonthaburi Province, Thailand

### 2.2 Material and methods

The methodology consists of three major phases (Figure 2) using ArcGIS (ESRI, Redlands, CA, USA) and Sentinel Application Platform (SNAP) (European Space Agency: ESA) software. Firstly, THEOS and Sentinel-2 satellite imagery were processed. Next, land use and land cover (LULC) were interpreted visually. Finally, green space classification and further

analysis were conducted using auxiliary data such as road networks obtained from the Ministry of Transportation of Thailand, and public area data derived from Google Maps and NOSTRA Maps. Several indices were applied to highlight critical green space coverage for proposed management planning.

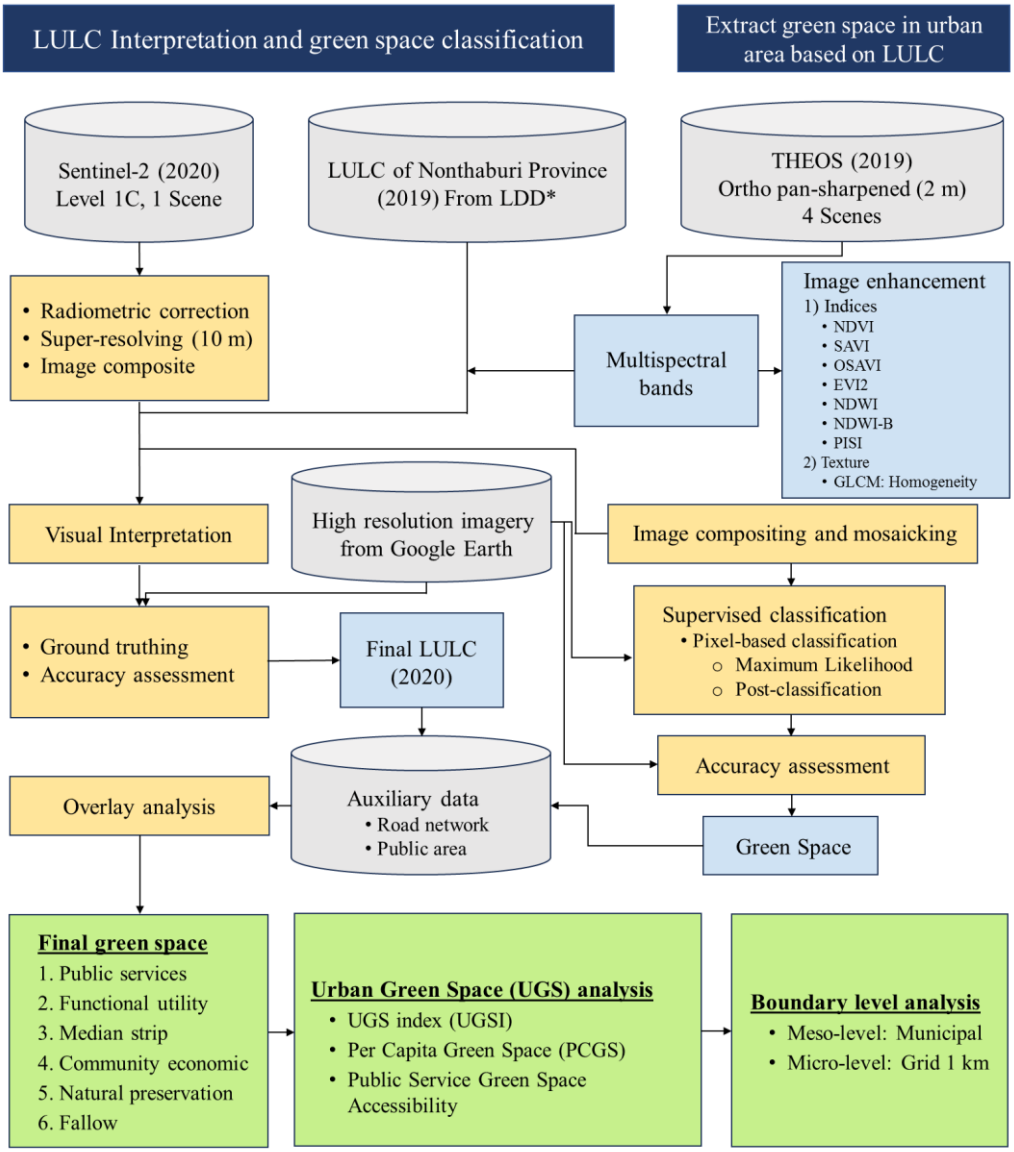


**Figure 2.** Overall methodology workflow [*LDD=Land Development Department of Thailand]

*2.2.1 Satellite data processing*

The pan-sharpened THEOS ortho imagery, consisting of four scenes, supported by the Geo-Informatics and Space Technology Development Agency of Thailand (GISTDA), was acquired in May and July 2019. These images had already undergone radiometric and geometric corrections, including ortho-rectification using a digital elevation model (DEM).

The Sentinel-2 imagery, acquired in January 2020, was obtained from the European Space Agency (ESA) Copernicus Open Access Hub. The digital numbers were then converted to top-of-atmosphere reflectance using quantification values proposed by the ESA (ESA, 2015). Additionally, a super-resolving multiresolution with band-independent geometry of multispectral pixels method (Brodu, 2017) was applied to enhance the spatial resolution of all spectral bands up to 10 m. compensating for the lack of a panchromatic band compared to THEOS.

The pan-sharpened multispectral image with its high spatial resolution, allows for the use of automated classification approaches (Sangpradid and Sarapirome, 2014; Abutaleb et al., 2021; Vigneshwaran and Kumar, 2021; Alcaras et al., 2022). Thus, spectral enhancement using pan-sharpened

THEOS data was applied with multi-index models representing vegetation, water, and impervious surfaces, along with grey-level co-occurrence matrix (GLCM) measures of texture to improve classification accuracy (Krefis et al., 2011; Li et al., 2011; Lane et al., 2014). These indices include the Normalized Difference Vegetation Index (NDVI) (Rouse et al., 1973), Soil Adjusted Vegetation Index (SAVI) (Huete, 1988), Optimized Soil-Adjusted Vegetation Index (OSAVI) (Rondeaux et al., 1996), Enhanced Vegetation Index (2-band) (EVI2) (Jiang et al., 2008), Normalized Difference Water Index (NDWI) (McFeeters, 1996), NDWI-B (Qu et al., 2011), Perpendicular Impervious Surface Index (PISI) (Tian et al., 2018), and GLCM homogeneity texture (Haralick et al., 1973) (Table 1).

**Table 1.** Remotely sensed indices and textural feature used for pan-sharpened THEOS data

| Index | Formula | Source |
|---|---|---|
| Normalized Difference Vegetation Index (NDVI) | $\frac{NIR - RED}{NIR + RED}$ | Rouse et al. (1973) |
| Soil Adjusted Vegetation Index (SAVI) | $(1 + L) * \left(\frac{NIR - RED}{NIR + RED + L}\right)$ L=0.5 (work well in most situation) | Huete (1988) |
| Optimized Soil-Adjusted Vegetation Index (OSAVI) | $\frac{NIR - RED}{NIR + RED + 0.16}$ | Rondeaux et al. (1996) |
| Enhanced Vegetation Index (2-band) (EVI2) | $2.5 * \left(\frac{NIR - RED}{NIR + (2.4 * RED) + 1}\right)$ | Jiang et al. (2008) |
| Normalized Difference Water Index ($NDWI_{McFeeters}$) | $\frac{GREEN - NIR}{GREEN + NIR}$ | McFeeters (1996) |
| Normalized Difference Water Index – B (NDWI-B) | $\frac{BLUE - NIR}{BLUE + NIR}$ | Qu et al. (2011) |
| Perpendicular Impervious Surface Index (PISI) | $0.8192 * BLUE - 0.5735 * NIR + 0.0750$ | Tian et al. (2018) |
| Grey-level co-occurrence matrix (GLCM): Homogeneity texture of NIR band with 9 × 9 windows | $\sum_{i=0}^{N-1} * \sum_{j=0}^{N-1} \frac{P(i,j)}{1 + (i - j)^2}$ N denotes the number of gray levels, while P(i, j) is the normalized value of the gray-scale at position i and j | Haralick et al. (1973) |

*2.2.2 Land use and land cover interpretation*

Land use and land cover (LULC) for Nonthaburi in 2019, derived from the Land Development Department of Thailand (LDD), was visually interpreted to create the 2020 LULC. The LULC nomenclature was modified into 13 classes based on the LDD, including paddy fields, field crops and horticulture, perennial and orchard, aquatic plants, aquaculture, urban and built-up areas, roads, recreation areas, golf courses, rangeland and scrub, marshes and swamps, bare land, and water bodies. Subsequently, an intensive ground survey was conducted in April 2020. The sample size was determined using the cumulative binomial probability distribution (Fitpatricks-Lins, 1981) as shown in formula 1.

$$N = \frac{Z^2 pq}{E^2}, Z = 2 \quad (1)$$

Where; N is the minimum sample size, p is the expected percent accuracy, q = 100 − p, and E is the allowable error. Finally, an accuracy assessment was performed, with an overall accuracy of more than 85% accepted (Congalton and Green, 1999). The Kappa coefficient (Landis and Koch, 1977; Congalton, 1991) was analyzed to generate the final LULC map. The overall accuracy and kappa coefficient were 85.59% and 0.83, respectively (Table S1).

*2.2.3 Green space classification and analysis*

Since remote spectral indices models are widely used in conjunction with multispectral images and the GLCM measures of texture to improve the accuracy of classified data (Li et al., 2011; Lane et al., 2014; Thakkar et al., 2014; Qu et al., 2021), the extraction of green spaces was performed using a combination of multi-indices models, homogeneity texture, and multispectral images derived from pan-sharpened THEOS data. This was archived through the commonly used pixel-based supervised classification approach known as the maximum likelihood algorithm (ML). Additionally, the spectral indices were rescaled

to match the range of the pan-sharpened multispectral images before stacking and using them in the ML algorithm (Lane et al., 2014).

The high-resolution imagery from Google Earth Pro proved to be a powerful resource and was utilized to select the training and verification sites using a grid sampling method (Ghorbanian et al., 2020; Nawar et al., 2022; Adorno et al., 2023; Kruasilp et al., 2023). Subsequently, post-classification analysis was conducted to eliminate the salt and pepper effect from the classified data, followed by an accuracy assessment (Campbell, 1987) (Table S2).

Next, the green space derived from pixel-based classification was overlaid with the LULC data, with particular emphasis on the urban and built-up patterns that fall under the category of functional utility green space. As a result, the final classification of green space was categorized into six classes: public service, functional utility, median strip, community economic, natural, and fallow (Table 2).

**Table 2.** Typology of green space used in this study

| Green space | Land use | Data manipulation |
|---|---|---|
| Functional utility | Green area in urban and built-up land, and golf course | Visually interpret urban and built-up and golf course, then extract green space in urban and built-up land using pan-sharpened THEOS based multi-indices model |
| Public services | Recreation area | Visual interpretation based on Sentinel-2, THEOS, and Google Earth Pro |
| Median strip | Green area in road island and interchange | |
| Community economic | Agricultural area | |
| Natural | Marsh and swamp and water bodies | |
| Fallow | Rangeland and scrub | |

Furthermore, urban green space analysis techniques such as the Urban Green Space Index (UGSI) (formula 2) (Nowak et al., 1996) and Per Capital Green Space (PCGS) (formula 3) were employed to highlight the critical coverage of green space, particularly at the meso-level (municipal area) and micro-level (1 km grid zone) (Alavipanah et al., 2015), which represent the fine-grained distribution of population and economic agglomeration (Jin et al., 2023).

$$UGSI_i = \frac{G_i}{A_i} \times 100 \quad (2)$$

$$PCGS_i = \frac{G_i}{PN_i} \quad (3)$$

Where; $G_i$=Green space in spatial unit i; $A_i$=Area of the i spatial unit; $PN_i$=Population in spatial unit i.

Finally, a proximity analysis was conducted to access walkability to public service green spaces within a 500 m radius (ONEP, 2017; de Sousa Silva, 2018). This analysis was complemented by utilizing the 100 m gridded population count data from 2020 obtained from WorldPop (Bondarenko et al., 2020). The overall workflow is illustrated in Figure 2.

## 3. RESULTS AND DISCUSSION

### 3.1 Land use and land cover

Nonthaburi's LULC has been classified visually into 4 major categories with 13 classes based on the nomenclature proposed by the Land Development Department. These classes include: 1) agricultural area (paddy fields (26.91%), field crops and horticulture (5.41%), perennial and orchard (8.13%), aquatic plants (0.85%), and aquaculture (0.68%)); 2) urban area (urban and built-up land (43.94%), roads (1.53%), recreation areas (0.14%), and golf courses (0.10%)); 3) miscellaneous area (rangeland and scrub (2.68%), marsh and swamp (4.54%), and bare land (0.98%)); and 4) water bodies (4.10%) (Figure 3).

### 3.2 Green space discriminations

The classified LULC, high-resolution satellite images from Google Earth Pro, and intensive ground surveys were used to determine the green space areas based on the definition provided by the ONEP (2019). The total area of classified green space in Nonthaburi Province is approximately 465.29 $km^2$, which can be categorized as follows: green space for public service (recreation areas) covering about 0.9 $km^2$, functional utility green space (green areas in urban and built-up land and golf courses) covering about 124.10 $km^2$,

median strip green space (green areas in road islands and interchanges) covering about 0.79 km$^2$, community economic green space (agricultural areas) covering about 267.41 km$^2$, natural green space (wetlands and water bodies) covering about 55.01 km$^2$, and fallow green space (rangeland and scrub) covering about 17.07 km$^2$ (Figure 4 and Table S3).

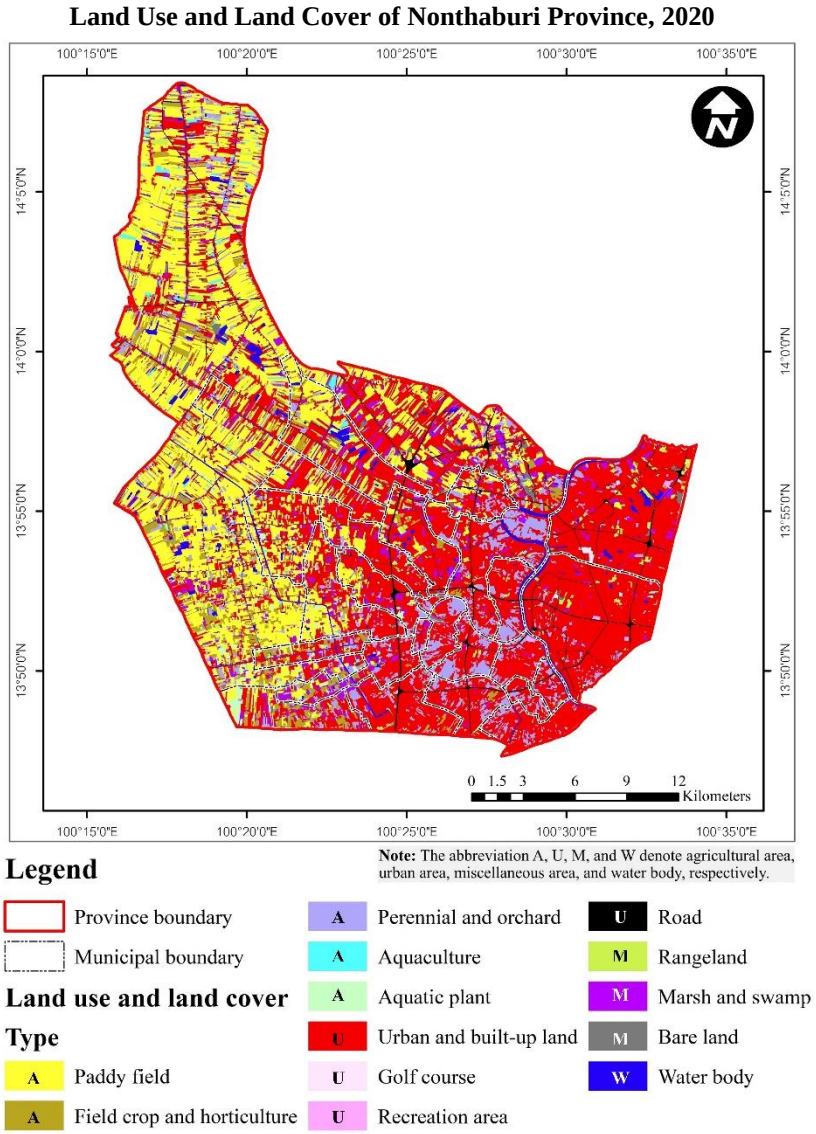


**Figure 3.** Land use and land cover of Nonthaburi Province, 2020

The Urban Green Space Index (UGSI) in Nonthaburi is 73.06% of the total provincial area. The Per Capita Green Space (PCGS), based on the registered population, is 367.71 m$^2$ per person. When considering the latent population data, the PCGS decreases to 255.82 m$^2$ per capita. However, it still exceeds the recommendation by the WHO, which suggests a minimum availability of 9 m$^2$ of green space per individual with an ideal UGS value of 50 m$^2$ per capita. Furthermore, it also surpasses the criteria set by the ONEP, which proposes a minimum of 15% UGS for metropolitan cities. Sai Noi district exhibits the highest UGSI and PCGS values of 92.58% and 2,703.24 m$^2$ per person, respectively, mainly due to the extensive agricultural activities in the area. It also demonstrates the highest UGSI and PCGS values for community economic green space (69.38% and 2,025.96 m$^2$ per individual), functional utility green space (11.83% and 345.40 m$^2$ per individual), natural green space (7.68% and 224.27 m$^2$ per individual), and fallow green space (3.57% and 104.27 m$^2$ per individual). Conversely, Muang Nonthaburi District, which is predominantly urbanized, has the lowest UGSI and PCGS located values of 44.58% and 89.53 m$^2$ per individual, respectively (Table S3).

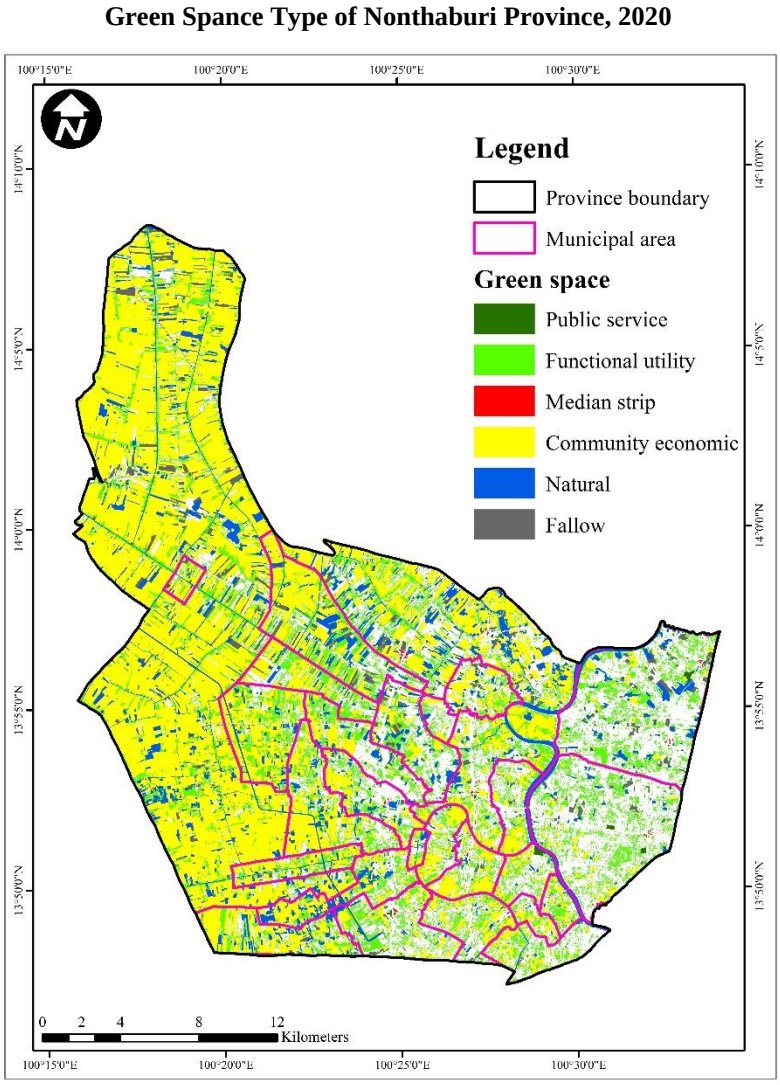


**Figure 4.** Green space type of Nonthaburi Province, 2020

Urban green space within municipal areas, which depicts the urban characteristics, decreases to 59.31% or 180.29 km$^2$ compared to the UGSI value of the province. The high UGSI group includes the Bangkurud, Bang Yai, and Salaklang municipalities (85.01%, 82.33%, and 81.92%, respectively). The low UGSI group includes Nonthaburi, Pak Kret, and Bangkruai municipalities (35.22%, 41.22%, and 46.40%, respectively). The high PCGS group includes Sai Noi, Salaklang, and Bang Yai municipalities (844.92, 639.91, and 525.48 m$^2$ per individual, respectively). The low PCGS group includes Nonthaburi, Pak Kret, and Bang Sri Muang municipalities (57.27, 99.48, and 104.73 m$^2$ per individual, respectively) (Figure 5). Out of 22 municipalities, 16 consist of green space for public services. Unfortunately, most of them have shown a PCGS lower than the recommended 15 m$^2$ per individual set by the ONEP (2019) (Tables S4, S5, and S6).

### 3.3 Grid-based green space

Grid-based analysis was employed to enhance the management approaches for green space. Proposed grids of 1 × 1 km were superimposed with the green space of Nonthaburi. According to the ONEP (2019), the range of green space coverage at the community level should not be less than 15-25%. The results revealed that most of the grids consisted of green space coverage of more than 25%, while 17 grids had less than 25% coverage. These grids were located in Muang Nonthaburi, Pak Kret, and Bang Kruai districts. Significantly, the percentage of green space decreased when adjacent to Bangkok, the capital city of Thailand (Figure 6).

**Urban Green Space Index of Municipal Area, 2020**

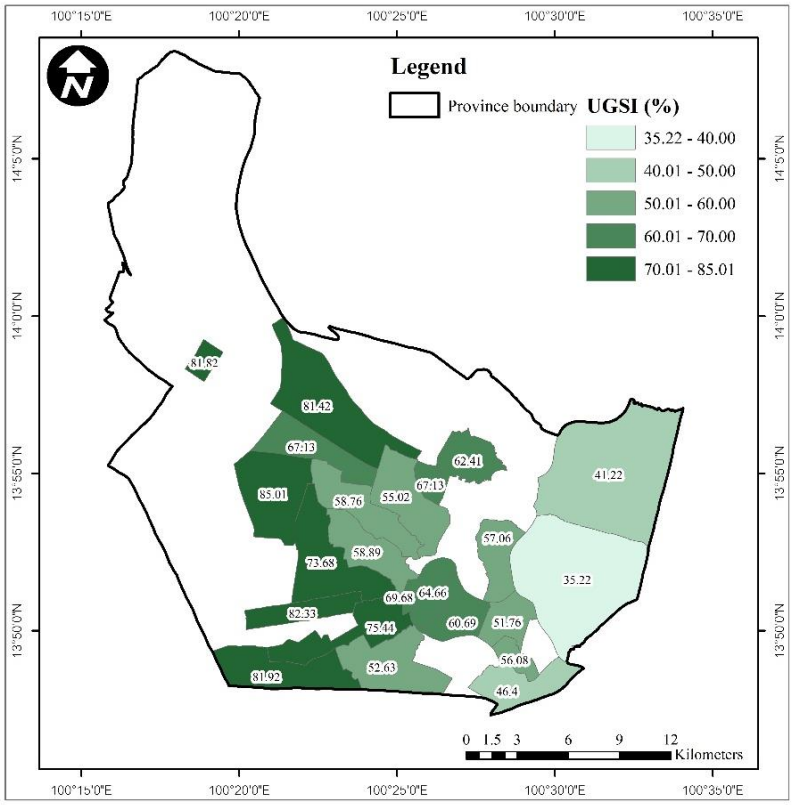


**Per Capita Green Space of Municipal Area, 2020**

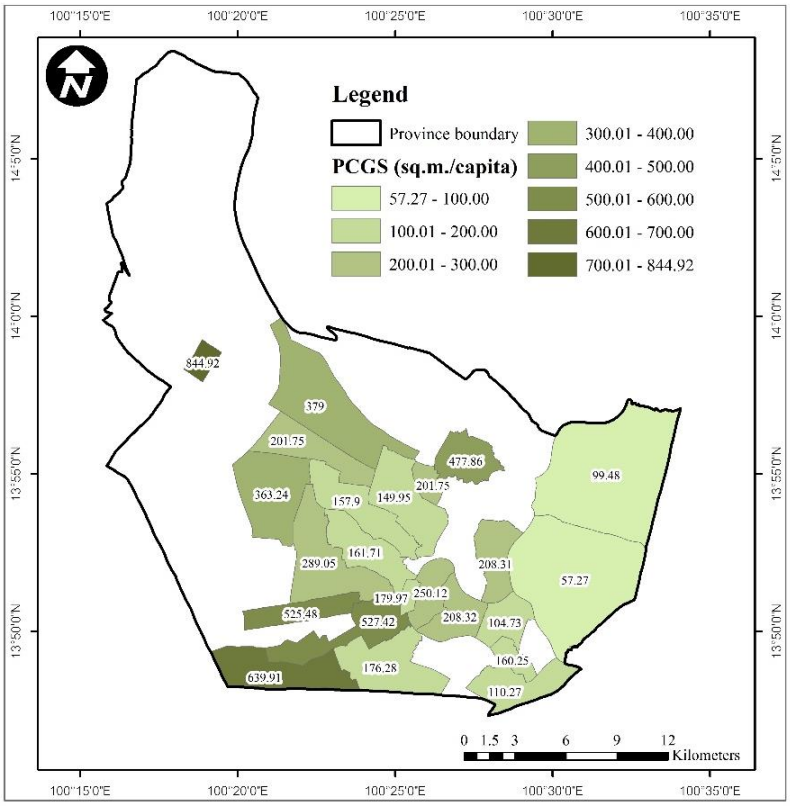


**Figure 5.** UGSI and PCGS of Nonthaburi municipal area, 2020

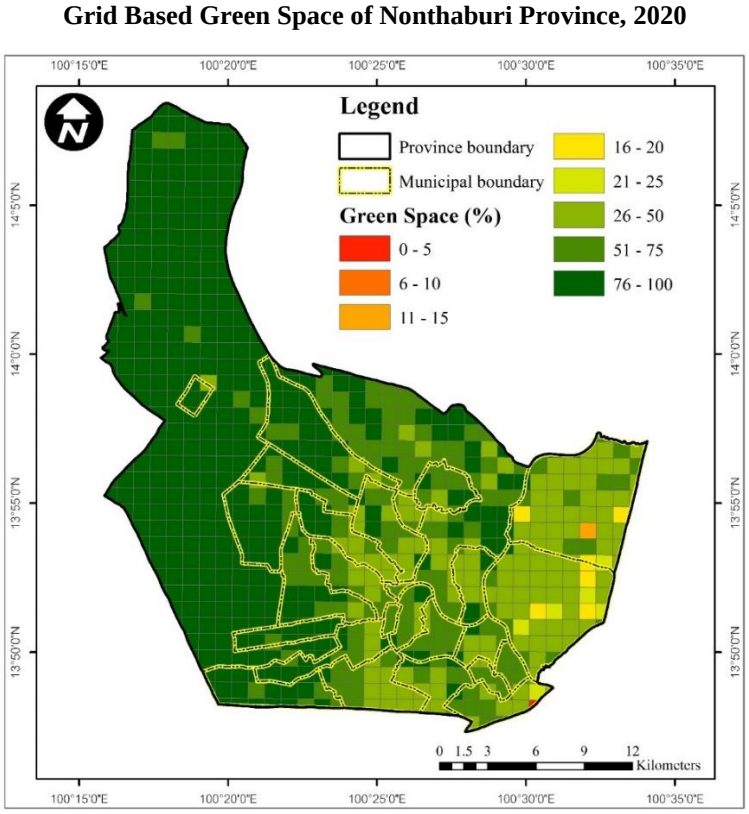


**Figure 6.** Grid based green space of Nonthaburi Province, 2020

### 3.4 Public service green space and its accessibility

All of the public service green space can be identified for 41 sites located in Muang Nonthaburi, Bang Yai, Pak Kret, Bang Bua Thong, Sai Noi, and Bang Kruai districts, consisting of 21, 7, 5, 4, 3, and 1 site(s), respectively. Unfortunately, most of them are smaller than 20,000 $m^2$. However, there are still public services green spaces larger than 20,000 $m^2$ with a service area of at least 5 $m^2$ per individual and easy accessibility or walkability within 500 m. These include the Nonthaburi sports stadium, with a total service area of 26,273.35 $m^2$ and 5.23 $m^2$ per individual, the park at Bang Khu Wieng interchange, with a total service area of 39,729.17 $m^2$ and 7.30 $m^2$ per individual, the park at Chaiyapruek road, with a total service area of 65,382.60 $m^2$ and 13.01 $m^2$ per individual, and Somdet Phra Srinagarindra Park, with a total service area of 155,470.01 $m^2$ and 19.82 $m^2$ per individual. Although there are parks with green spaces larger than 20,000 $m^2$, their population density is quite high, resulting in a green service area of less than 5 $m^2$ per individual. Additionally, some parks located closely within a 500 m range can be grouped as clusters, thus increasing the service area and service per capita, such as the parks at Bang Sri Muang municipality with a total service area of 148,361.12 $m^2$ and 14.84 $m^2$ per individual, and the sports field and park in Sai Noi municipality with a total service area of 34,547.31 $m^2$ and 8.65 $m^2$ per individual (Figure 7 and Table S7).

### 3.5 Suitable area for development into public service green space

The abandoned fallow green spaces have the potential to be developed into public service green spaces. Moreover, the green spaces at road interchanges can also serve the same purpose. Thus, these two types of green spaces located in grids with less than 25% green space were chosen. These areas were found within the Nonthaburi and Pak Kret municipalities.

For Nonthaburi municipality, the public service green space would increase from 0.23 $km^2$ to 0.32 $km^2$ (a 36% increase) if green spaces at Ngamwongwan interchange and other fallow green spaces were converted (Figures 8 and 9). Meanwhile, the transformation of fallow land in Pak Kret municipality would result in a gain of 25% (0.05 $km^2$) in the public service green space area.

Furthermore, both potentially fallow and interchange green spaces adjacent to Bangkok also create a new public service green space cluster (the big red 500-m buffer) with increased service area of 0.25 $km^2$ and 2.06 $m^2$ per capita (Figure 8).

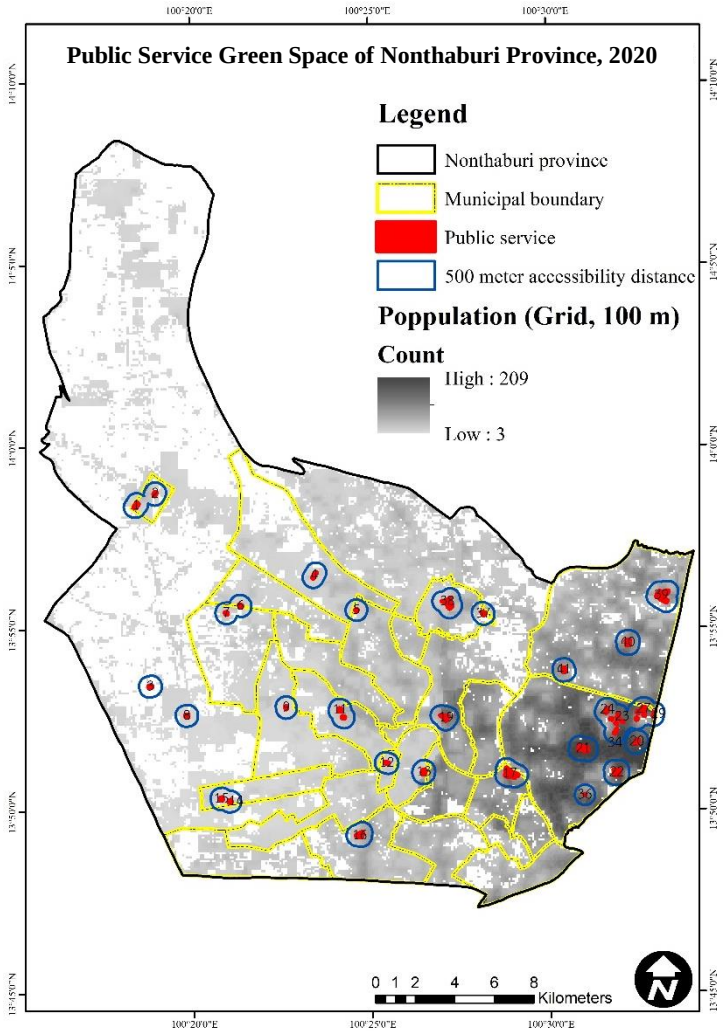


**Figure 7.** Public green space and accessibility distance of Nonthaburi Province, 2020

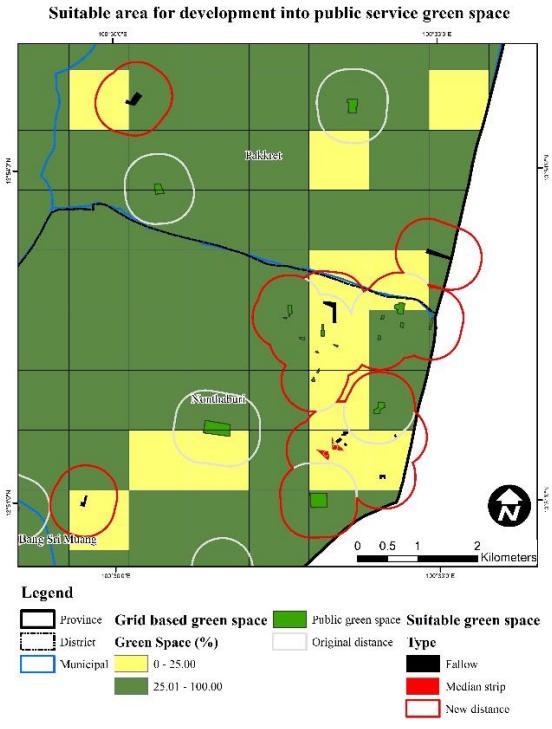


**Figure 8.** Suitable area for development into public service green space

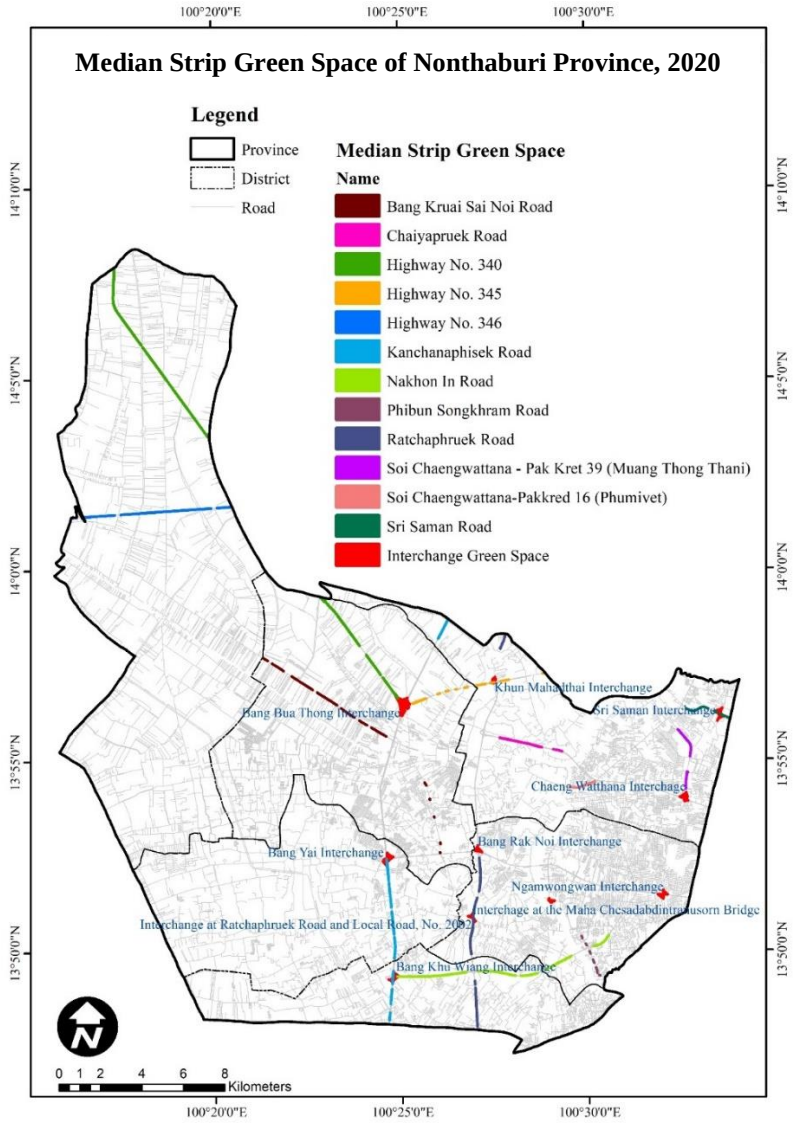


**Figure 9.** Median strip green space of Nonthaburi Province, 2020

### 3.6 UAV-based green space

The management of green space within specific locations requires more detailed information to initiate master planning. Higher-resolution data can improve decision-making accuracy. Therefore, UAVs are considered a useful tool to support urban space planning and management. They provide large-scale mapping and a three-dimensional perspective. The Nonthaburi Government Center area was selected for urban green space assessment using UAVs. It was found that green space covers approximately 80,972.30 $m^2$ or 40.30% of the provincial area (Figure 10). This meets the target set by the Nonthaburi provincial plan (2018-2022), which proposes green space covering about 30-50% of the organization's area.

## 4. DISCUSSION

This study integrated LULC classification with green space extraction using visual interpretation and computer-assisted classification, along with a multi-indices model, to identify and quantify green space in Nonthaburi Province to support decision-makers in terms of management and planning purposes.

Nonthaburi is identified as having a high-density and mixed-use pattern, similar to other modern compact cities (Russo and Cirella, 2018). Even though there is a significant amount of green space due to agricultural activity in the western part of the province, the UGSI and PCGS tend to decrease as the population increases, particularly in the districts of Muang Nonthaburi, Pak Kret, and Bang Kruai, where the municipalities of Nonthaburi, Pak Kret, and Bang

Kruai are located. The grid-based green space values also align with the UGSI and PCGS. This decrease can be attributed to the development of housing estates in the past, in line with the Fifth National Economic and Social Development Plan (1982-1986) (Sakulcharoenporn and Kiattisahakul, 2021).

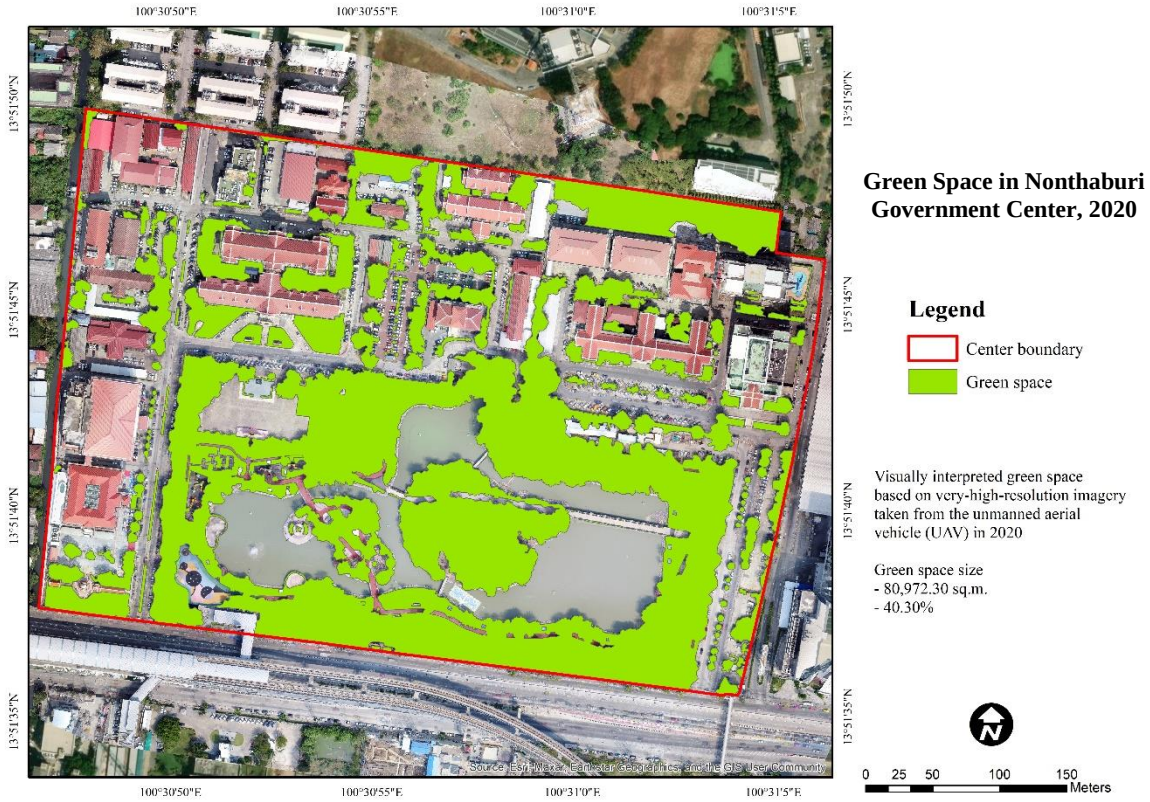


**Figure 10.** Green space in Nonthaburi Government Center, 2020

In terms of spatial distribution, green space in Nonthaburi is similar to cities in other countries, such as Colombo in Sri Lanka and Kalaburagi, and Mumbai in India, where areas located away from the city center tend to have more green space and better environmental quality, while areas closer to the center have less green space (Senanayake et al., 2013; Shekhar and Aryal, 2019; Sathyakumar et al., 2020). This pattern depends on population density, which affects green space coverage, with a higher population in municipal areas such as cities, towns, and sub-districts. However, Nonthaburi municipality differs in terms of urban green space characteristics compared to the municipality of Pattaya, a tourist destination with a UGSI of only 16.57% due to extensive urban and built-up land for tourism purposes (Chinnabut et al., 2021).

Unfortunately, green spaces in Nonthaburi have decreased significantly due to dynamic changes in physical development. The urban and semi-urban areas along the east side of Nonthaburi have experienced significant growth, particularly in the suburbs or urban fringe areas (Nathalang, 2019). Megaprojects for transportation, aimed at linking Nonthaburi with the Bangkok metropolitan area and neighboring provinces, are being developed continuously. These projects include the construction of ring roads, expressways, motorways, and sky trains. Major routes such as the Kanchanaphisek ring road have been expanded to 12 lanes, while Rattanathibeth road has been expanded to 10 lanes. Other development activities that contribute to the reduction of urban green spaces include the expansion of real estate, condominiums, department stores, hotels, and restaurants. Rapid urbanization without retaining adequate green space degrades the urban environment and livability (Song et al., 2021). Moreover, natural disasters such as flooding in 1995 and 2011 have also affected agricultural areas, especially mixed orchards and durian, the most famous fruit and a geographical indicator in Thailand (Thongdara et al., 2013).

According to the Nonthaburi development plan (2018-2022), there are some strategies such as "Developing the area of Nonthaburi Province into a

green city, comprising agricultural zones and green urban spaces". Moreover, there are some land use plan zones in Nonthaburi Province's principle city plan in 2023 (Government Gazette, 2023), such as green zone, white zone with green frame and diagonal lines, and light green zone, which represent rural and agricultural land, conservation area for rural and agricultural land, and open space for recreation and maintain environmental quality, respectively. However, the green space may fail to be kept due to gaps in the law regarding land (Chitchang and Cheyklinput, 2022).

Based on the aforementioned, authorities in developing cities should protect environmental resources such as remaining agricultural areas, remnant forest patches, and river corridors. These areas can be re-created as habitats at a later stage of development to maintain urban ecosystem services (Richards et al., 2017). Careful selection of tree species, especially deciduous and dry evergreen species, is important to ensure adaptation to the monsoonal dry season in Thailand, contributing to a more diverse aesthetic quality (Thaiutsa et al., 2008) and effectively mitigating the urban heat island phenomenon (Pan et al., 2023).

The inadequacy of public service green space in Nonthaburi is comparable to other cities that also face uneven distribution and the need for improvement (Oh and Jeong, 2007; Shahfahad et al., 2019; Vîlcea and Șoșea, 2020). As suggested by Park and Guldmann (2020), there is an opportunity to transform neglected fallow green spaces into public service green areas. Furthermore, greater consideration must be given to the development of median strip green spaces at road interchanges as public service green areas. Fortunately, the areas in Nonthaburi addressed in this research are still intact. One particularly promising location is the Ngamwongwan interchange, which is situated in an area with limited green space coverage and requires improvement and development. This is an indispensable component of the city's plan, requiring careful management and planning to ensure its preservation (Suthasupa, 1997). These endeavors play a crucial role in advancing human health and enhancing overall well-being within urban communities, as demonstrated by previous studies (Corley et al., 2021; Pouso et al., 2021; Lin et al., 2023).

Finally, very high-resolution imagery was applied to demonstrate the assessment of green space coverage assessment at a detailed scale, such as the Nonthaburi Government Complex, which requires the use of precise images from UAV sensors (Shahtahmassebi et al., 2021). However, further studies should be conducted using multi-spectral UAV sensors, which can automate classification and integrate with rapid delineation processes.

This study exhibited and emphasized the importance of promoting and enhancing the use of geoinformatics technology in environmental evaluations. Such technology plays a crucial role in achieving the Sustainable Development Goals, specifically SDG 3 (ensuring good health and well-being for all) and SDG 11 (creating sustainable cities and communities).

## 5. CONCLUSION

This study aimed to identify and quantify green space in Nonthaburi Province using geoinformatics, such as remote sensing and GIS. The green space patterns were modified to align with the nomenclature established by the Office of Natural Resource and Environmental Policy and Planning (ONEP). Due to the prevalence of agricultural land in the rural western areas of Nonthaburi, particularly paddy fields, the green space exhibited a high Urban Green Space Index (UGSI) value for the province. The Per Capita Green Space (PCGS) met the recommendations set by the World Health Organization (WHO). Green space distribution tended to decrease when adjacent to the Bangkok Metropolis. Only six parks or park clusters fulfilled the criteria for public green spaces. The potential for developing fallow green spaces and green spaces at road interchanges into public service areas should be considered. Lastly, the use of unmanned aerial vehicles (UAVs) is suggested for green space assessment at the organizational level.

## ACKNOWLEDGEMENTS

This research was supported by Geo-Informatics and Space Technology Development Agency (Public Organization) (GISTDA), Mahidol University, and Central and Western Regional Centre for Geo-Informatics and Space Technology, Mahidol University (GISTMU) through cooperation. We would also like to extend our thanks to the Nonthaburi Province for their collaboration in providing valuable data and feedback.

## DECLARATION OF COMPETING INTEREST

The authors declare that they have no known competing financial interests or personal relationships

that could have appeared to influence the work reported in this paper.

## APPENDIX A. SUPPLEMENTARY DATA

Supplementary material related to this article can be found starting from Tables S1 to S7.

## REFERENCES


Abutaleb K, Mudede MF, Nkongolo N, Newete SW. Estimating urban greenness index using remote sensing data: A case study of an affluent vs poor suburbs in the city of Johannesburg. Egyptian Journal of Remote Sensing and Space Sciences 2021;24(3):343-51.

Adorno BV, Körting TS, Amaral S. Contribution of time-series data cubes to classify urban vegetation types by remote sensing. Urban Forestry and Urban Greening 2023;79:Article No. 127817.

Alavipanah S, Wegmann M, Qureshi S, Weng Q, Koellner T. The role of vegetation in mitigating urban land surface temperatures: A case study of Munich, Germany during the warm season. Sustainability 2015;7(4):4689-706.

Alcaras E, Falchi U, Parente C, Vallario A. Accuracy evaluation for coastline extraction from Pléiades imagery based on NDWI and IHS pan-sharpening application. Applied Geomatics 2022;15(3):595-605.

Bastian O, Haase D, Grunewald K. Ecosystem properties, potentials, and services: The EPPS conceptual framework and an urban application example. Ecological Indicators 2012;21:7-16.

Bondarenko M, Kerr D, Sorichetta A, Tatem AJ. Census/Projection-Disaggregated Gridded Population Datasets, Adjusted to Match the Corresponding UNPD 2020 Estimates, for 183 Countries in 2020 Using Built-Settlement Growth Model (BSGM) Outputs. Hampshire: University of Southampton; 2020.

Brodu N. Super-resolving multiresolution images with band-independent geometry of multispectral pixels. IEEE Transactions on Geoscience and Remote Sensing 2017; 55(8):4610-7.

Campbell JB. Introduction to Remote Sensing. New York: The Guilford Press; 1987.

Carbó-Ramírez P, Zuria I. The value of small urban greenspaces for birds in a Mexican city. Landscape and Urban Planning 2011;100(3):213-22.

Chinnabut S, Chen N, Zhang H. Analysis urban green space classification using landscape pattern analysis based on GIS and remote sensing in Pattaya, Thailand. Proceeding of the 2nd Intercontinental Geoinformation Days (IGD); 2021 May 5-6; Mersin: Turkey; 2021.

Chitchang K, Cheyklinput K. Impact on green areas in Sao Thong Hin Sub-District and Bang Mae Nang Sub-district, Bang Yai District due to the expansion of Nonthaburi Province Between 1982 and 2021. Journal of Social Sciences and Humanities 2022;48(2):73-92 (in Thai).

Congalton RG, Green K. Assessing the Accuracy of Remotely Sensed Data: Principles and Practices. Washington DC: CRC Press; 1999.

Congalton RG. A review of assessing the accuracy of classifications of remotely sensed data. Remote Sensing of Environment 1991;37(1):35-46.

Corley J, Okely J, Taylor AM, Page DC, Welstead M, Skarabela B, et al. Home garden use during COVID-19: Associations with physical and mental wellbeing in older adults. Journal of Environmental Psychology 2021;73:Article No. 101545.

de Sousa Silva C, Viegas I, Panagopoulos T, Bell S. Environmental justice in accessibility to green infrastructure in two European Cities. Land 2018;7(4):Article No. 134.

Deloya MC. Urban forestry activities in Mexico. Unasylva 1993;173(44):28-32.

Department of Provincial Administration. Population number [Internet]. 2019 [cited 2020 Jun 24]. Available from: https://stat.bora.dopa.go.th/new_stat/webPage/statByYear.php (in Thai).

European Space Agency (ESA). Sentinel-2 User Handbook [Internet]. 2015 [cited 2021 Aug 30]. Available from: https://sentinel.esa.int/documents/247904/685211/Sentinel-2_User_Handbook.

Fitpatricks-Lins K. Comparison of sampling procedures and data analysis for a land-use and land-cover map. Photogrammetric Engineering and Remote Sensing 1981;47(3):343-51.

Ghorbanian A, Kakooei M, Amani M, Mahdavi S, Mohammadzadeh A, Hasanlou M. Improved land cover map of Iran using Sentinel imagery within Google Earth Engine and a novel automatic workflow for land cover classification using migrated training samples. ISPRS Journal of Photogrammetry and Remote Sensing 2020;167:276-88.

Haq S. Urban green spaces and an integrative approach to sustainable environment. Journal of Environmental Protection 2011;2(5):601-8.

Haralick RM, Shanmugan K, Dinstein I. Textural Features for Image Classification. IEEE Transactions on Systems, Man, and Cybernetics 1973;3(6):610-21.

Heinze J. Benefits of Green Space - Recent Research. Virginia: Environmental Health Research Foundation; 2011.

Huete AR. A soil-adjusted vegetation index (SAVI). Remote Sensing of Environment 1988;25(3):295-309.

Jiang Z, Huete AR, Didan K, Miura T. Development of a two-band enhanced vegetation index without a blue band. Remote Sensing of Environment 2008;112(10):3833-45.

Jin Y, Xu Y, Liu W. The green quality of urban spatial development: A multi-dimensional and multi-regional model using big data. Urban Forestry and Urban Greening 2023;85:Article No. 127953.

Kalawong S, Chainit A, Bongsebodhidhamma N. Local government collaboration model development in local development plan collaboration in Nonthaburi Province, Thailand. Asian Political Science Review 2018;2(2):60-71.

Krefis AC, Schwarz NG, Nkrumah B, Acquah S, Loag W, Oldeland J, et al. Spatial analysis of land cover determinants of malaria incidence in the Ashanti Region, Ghana. PloS ONE 2011;6(3):e17905.

Krisdianto, Soekarno, Udiansyah, Januwiadi B. Standing carbon in an urban green space and its contribution to the reduction of the thermal discomfort index: A case study in the City of Banjarbaru, Indonesia. International Journal of Scientific and Research Publications 2012;2(4):1-7.

Kruasilp J, Pattanakiat S, Phutthai T, Vardhanabindu P, Nakmuenwai P. Evaluation of land use land cover changes in Nan Province, Thailand, using multi-sensor satellite data and Google Earth Engine. Environment and Natural Resources Journal 2023;21(2):186-97.

Kuchelmeister G. Urban green for local needs - improving quality of life through multipurpose urban forestry in developing countries. Proceedings of the 1st International Conference on Quality of Life in Cities; 1998 Mar 4-6; Singapore; 1998.

Lachowycz K, Jones AP. Towards a better understanding of the relationship between greenspace and health: Development of a theoretical framework. Landscape and Urban Planning 2013;118:62-9.

Landis JR, Koch GG. The measurement of observer agreement for categorical data. Biometrics 1977;33:159-74.

Lane C, Liu H, Autrey B, Anenkhonov O, Chepinoga V, Wu Q. Improved wetland classification using eight-band high resolution satellite imagery and a hybrid approach. Remote Sensing 2014;6(12):12187-216.

Li G, Lu D, Moran E, Hetrick S. Land-cover classification in a moist tropical region of Brazil with Landsat TM imagery. International Journal of Remote Sensing 2011;32(23): 8207-30.

Lin D, Sun Y, Yang Y, Han Y, Xu C. Urban park use and self-reported physical, mental, and social health during the COVID-19 pandemic: An on-site survey in Beijing, China. Urban Forestry and Urban Greening 2023;79:Article No. 127804.

Lu C, Wu Y, Shen Q, Wang H. Driving force of urban growth and regional planning: A case study of China, Guangdong Province. Habitat International 2013;40:35-41.

McFeeters SK. The use of Normalized Difference Water Index (NDWI) in the delineation of open water features. International Journal of Remote Sensing 1996;17(7):1425-32.

Nathalang S. From the suburb communities to capitalist urbanism: The case study of Nonthaburi Area. Journal of Anthropology, Sirindhorn Anthropology Centre 2019;1(2):150-90.

National Economic and Social Development Council (NESDC). The Twelfth National Economic and Social Development Plan (2017-2021). Bangkok, Thailand: NESDC; 2017.

Nawar N, Sorker R, Chowdhury FJ, Rahman M. Present status and historical changes of urban green space in Dhaka City, Bangladesh: A remote sensing driven approach. Environmental Challenges 2022;6:Article No. 100425.

Nonthaburi Provincial Office. The Fifth Years Nonthaburi Development Plan (2018-2022). Nonthaburi, Thailand: Nonthaburi Provincial Office; 2019 (in Thai).

Nonthaburi Provincial Statistical Office. Nonthaburi Provincial Statistical Report: 2020. Bangkok, Thailand: National Statistical Office, Ministry of Digital Economy and Society; 2020 (in Thai).

Nor ANM, Aziz HA, Nawawi SA, Jamil RM, Abas MA, Hambali K, et al. Evolution of green space under rapid urban expansion in Southeast Asian Cities. Sustainability 2021;13(21):Article No. 12024.

Government Gazette. Notification of the Ministry of Interior Re: the enforcement of Town Planning of Nonthaburi 2023. Volume 140, Part 48 D, Dated 1 March B.E. 2566. Bangkok, Thailand: Office of the Council of State; 2023 (in Thai).

Nowak DJ, Rowntree RA, McPherson EG, Sisinni SM, Kerkmann ER, Stevens JC. Measuring and analyzing urban tree cover. Landscape and Urban Planning 1996;36(1):49-57.

Oh K, Jeong S. Assessing the spatial distribution of urban parks using GIS. Landscape Urban Plan 2007;82(1-2):25-32.

Office of Natural Resource and Environmental Policy and Planning (ONEP). Driving Sustainable Green Space Guideline. Bangkok, Thailand: ONEP; 2019 (in Thai).

Office of Natural Resource and Environmental Policy and Planning (ONEP). Management Guideline and Standard for Urban Green Space in Thailand. Bangkok, Thailand: Thailand Environment Institute (TEI); 2017 (in Thai).

Pan L, Lu L, Fu P, Nitivattananon V, Guo H, Li Q. Understanding spatiotemporal evolution of the surface urban heat island in the Bangkok metropolitan region from 2000 to 2020 using enhanced land surface temperature. Geomatics, Natural Hazards and Risk 2023;14(1):Article No. 2174904.

Park Y, Guldmann J. Understanding disparities in community green accessibility under alternative green measures: A metropolitan-wide analysis of Columbus, Ohio, and Atlanta, Georgia. Landscape and Urban Planning 2020;200:Article No. 103806.

Petersen LK. The materiality of everyday practices in urban greenspace. Journal of Environmental Policy and Planning 2013;15(3):353-70.

Pinto LV, Inácio M, Ferreira CS, Ferreira AD, Pereira P. Ecosystem Services and well-being dimensions related to urban green spaces: A systematic review. Sustainable Cities and Society 2022;85:Article No. 104072.

Pouso S, Borja Á, Fleming LE, Gómez-Baggethun E, White MP, Uyarra MC. Contact with blue-green spaces during the COVID-19 pandemic lockdown beneficial for mental health. Science of the Total Environment 2021;756:Article No. 143984.

Qu L, Chen Z, Li M, Zhi J, Wang H. Accuracy improvements to pixel-based and object-based LULC classification with auxiliary datasets from Google Earth Engine. Remote Sensing 2021;13(3):Article No. 453.

Qu W, Lu JX, Li L, Li XW. Research on automatic extraction of water bodies and wetlands on HJ Satellite CCD images. Remote Sensing Information 2011;4:28-33.

Richards DR, Passy P, Oh RRY. Impacts of population density and wealth on the quantity and structure of urban green space in tropical Southeast Asia. Landscape and Urban Planning 2017;157:553-60.

Rondeaux G, Steven M, Baret F. Optimization of soil-adjusted vegetation indices. Remote Sensing of Environment 1996; 55(2):95-107.

Rouse JW, Haas RH, Schell JA, Deering DW. Monitoring Vegetation Systems in the Great Plains with ERTS. Proceedings of the Third ERTS Symposium, NASA SP-351; 1973 Dec 10-14; Washington DC; 1973. p. 309-17.

Russo A, Cirella GT. Modern compact cities: How much greenery do we need? International Journal of Environmental Research and Public Health 2018;15(10):Article No. 2180.

Sakulcharoenporn S, Kiattisahakul P. Nonthaburi Province expansion of housing estates, 1982-1994. Journal of the Faculty of Arts, Silpakorn University 2021;43(1):133-54 (in Thai).

Sangpradid S, Sarapirome S. Road extraction from pan-sharpened THEOS images. Journal of Remote Sensing and GIS Association of Thailand 2014;15(2):12-7.

Sathyakumar V, Ramsankaran R, Bardhan R. Geospatial approach for assessing spatiotemporal dynamics of urban green space distribution among neighbourhoods: A demonstration in Mumbai. Urban Forestry and Urban Greening 2020;48:Article No. 126585.

Senanayake IP, Welivitiya WDDP, Nadeeka PM. Urban green spaces analysis for development planning in Colombo, Sri Lanka, utilizing THEOS satellite imagery: A remote sensing

and GIS approach. Urban Forestry and Urban Greening 2013;12(3):307-14.

Shahfahad, Kumari B, Tayyab M, Hang HT, Khan MM, Rahman A. Assessment of public open spaces (POS) and landscape quality based on per capita POS index in Delhi, India. SN Applied Sciences 2019;1:Article No. 368.

Shahtahmassebi AR, Li C, Fan Y, Wu Y, Lin Y, Gan M, et al. Remote sensing of urban green spaces: A review. Urban Forestry and Urban Greening 2021;57:Article No. 126946.

Shekhar S, Aryal J. Role of geospatial technology in understanding urban green space of Kalaburagi City for sustainable planning. Urban Forestry and Urban Greening 2019;46:Article No. 126450.

Song Y, Aryal J, Tan L, Jin L, Gao Z, Wang Y. Comparison of changes in vegetation and land cover types between Shenzhen and Bangkok. Land Degradation and Development 2021;32(3):1192-204.

Suthasupa S. Open space: Elements in the city plan. NAJUA: Architecture, Design and Built Environment 1997;15:121-8 (in Thai).

Taylor L, Hochuli DF. Defining greenspace: Multiple uses across multiple disciplines. Landscape and Urban Planning 2017; 158:25-38.

Thaiutsa B, Puangchit L, Kjelgren R, Arunpraparut W. Urban green space, street tree and heritage large tree assessment in Bangkok, Thailand. Urban Forestry and Urban Greening 2008;7(3):219-29.

Thakkar A, Desaic V, Patel A, Potdar M. Land use/land cover classification using remote sensing data and derived indices in a heterogeneous landscape of a Khan-Kali watershed, Gujarat. Asian Journal of Geoinformatics 2014;14(4):1-12.

Thongdara R, Tanachaikhan P, Kulpradit K, Tibkaew PA. The urban expansion to durian orchard in Nonthaburi. Proceedings of the 34th Asian Conference on Remote Sensing 2013; 2013 Oct 20-24; Bali: Indonesia; 2013.

Tian Y, Chen H, Song Q, Zheng K. A novel index for impervious surface area mapping: Development and validation. Remote Sensing 2018;10:Article No. 1521.

United States Environmental Protection Agency (US EPA). What is open space/green space [Internet]. 2017 [cited 2021 Aug 24]. Available from: https://www3.epa.gov/region1/eco/uep/openspace.html.

Vigneshwaran S, Kumar SV. Comparison of classification methods for urban green space extraction using very high resolution worldview-3 imagery. Geocarto International 2021;36(13):1429-42.

Vîlcea C, Șoșea C. A GIS-based analysis of the urban green space accessibility in Craiova City, Romania. Geografisk Tidsskrift-Danish Journal of Geography 2020;120(1):19-34.

White MP, Alcock I, Wheeler BW, Depledge MH. Coastal proximity, health, and well-being: Results from a longitudinal panel survey. Health and Place 2013;23:97-103.

Wirayuda IKAK, Widayani P, Sekaranom AB. Urban green space analysis and its effect on the surface urban heat island phenomenon in Denpasar City, Bali. Forest and Society 2023;7(1):150-68.

WHO Regional Office for Europe. Urban Green Spaces: A Brief for Action. Copenhagen: WHO Regional Office for Europe, Copenhagen; 2017.

World Health Organization (WHO). Health Indicators of sustainable cities in the Context of the Rio+20 UN Conference on Sustainable Development [Internet]. 2012 [cited 2021 Aug 24]. Available from: https://cdn.who.int/media/docs/default-source/environment-climate-change-and-health/sustainable-development-indicator-cities.pdf?sfvrsn=c005156b_2.

World Health Organization (WHO). Urban Planning, Environment and Health: From Evidence to Policy Action. Geneva: World Health Organization; 2010. p. 119.

Xu G, Jiao L, Liu J, Shi Z, Zeng C, Liu Y. Understanding urban expansion combining macro patterns and micro dynamics in three Southeast Asian megacities. Science of the Total Environment 2019;660:375-83.

Zhao M, Zhou Y, Li X, Cheng W, Zhou C, Ma T, et al. Mapping Urban Dynamics (1992-2018) in Southeast Asia using consistent nighttime light data from DMSP and Viirs. Remote Sensing of Environment 2020;248:Article No. 111980.

# INSTRUCTION FOR AUTHORS

**Publication and Peer-reviewing processes of Environment and Natural Resources Journal**

**Environment and Natural Resources Journal** is a peer reviewed and open access journal that is published in six issues per year. Manuscripts should be submitted online at https://ph02.tci-thaijo.org/index.php/ennrj/about/submissions by registering and logging into this website. Submitted manuscripts should not have been published previously, nor be under consideration for publication elsewhere (except conference proceedings papers). A guide for authors and relevant information for the submission of manuscripts are provided in this section and also online at: https://ph02.tci-thaijo.org/index.php/ennrj/author. All manuscripts are refereed through a **single-blind peer-review** process.

Submitted manuscripts are reviewed by outside experts or editorial board members of **Environment and Natural Resources Journal**. This journal uses double-blind review, which means that both the reviewer and author identities are concealed from the reviewers, and vice versa, throughout the review process. Steps in the process are as follows:

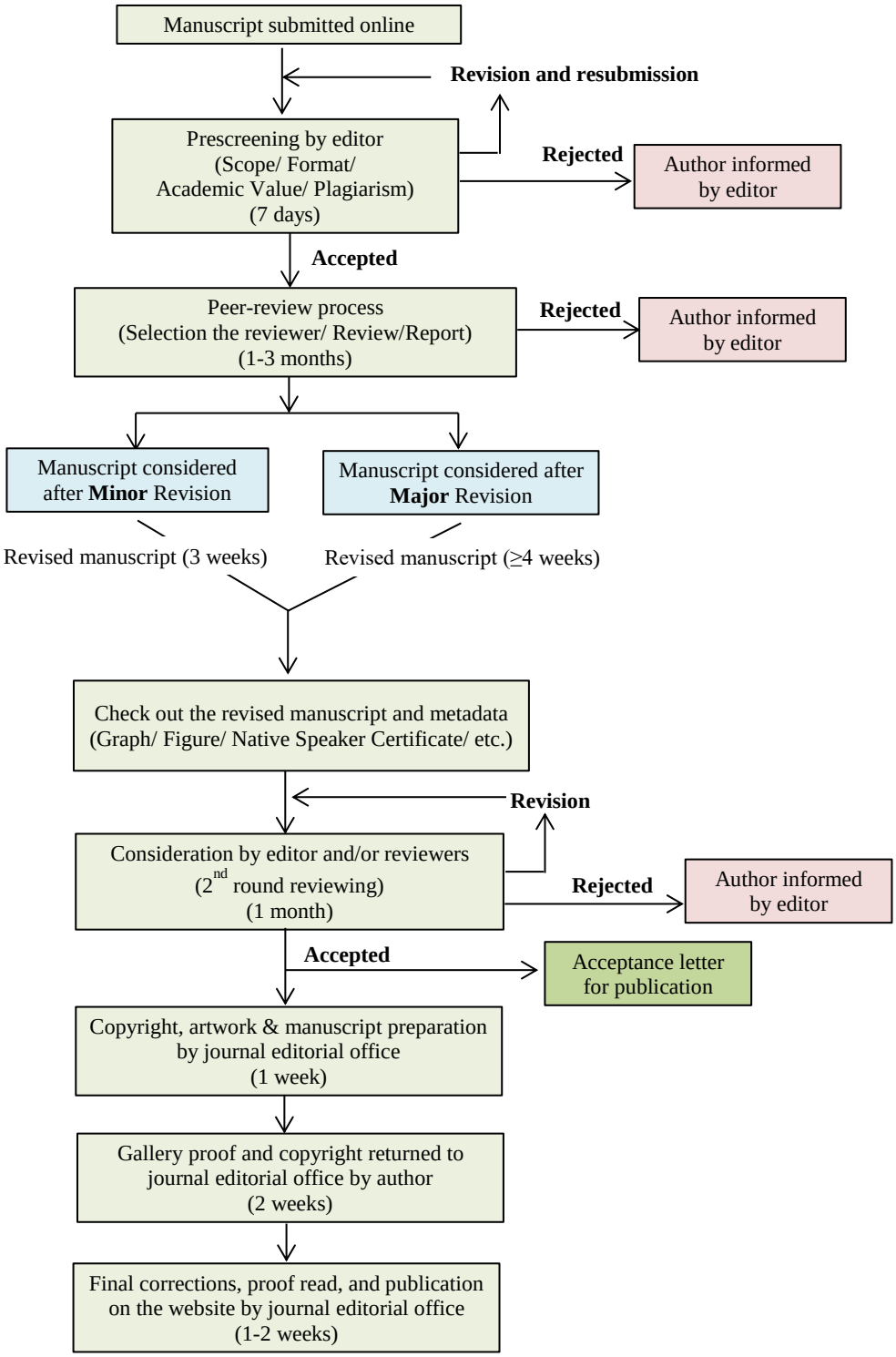

**The Environment and Natural Resources Journal** (EnNRJ) accepts 2 types of articles for consideration of publication as follows:

- *Original Research Article:* Manuscripts should not exceed 3,500 words (excluding references).
- *Review Article (by invitation):* This type of article focuses on the in-depth critical review of a special aspect in the environment and also provides a synthesis and critical evaluation of the state of the knowledge of the subject. Manuscripts should not exceed 6,000 words (excluding references).

**Submission of Manuscript**

Cover letter: Key points to include:

- Statement that your paper has not been previously published and is not currently under consideration by another journal
- Brief description of the research you are reporting in your paper, why it is important, and why you think the readers of the journal would be interested in it
- Contact information for you and any co-authors
- Confirmation that you have no competing interests to disclose

Manuscript-full: Manuscript (A4) must be submitted in Microsoft Word Files (.doc or .docx). Please make any identifying information of name(s) of the author(s), affiliation(s) of the author(s). Each affiliation should be indicated with superscripted Arabic numerals immediately after an author's name and before the appropriate address. Specify the Department/School/Faculty, University, Province/State, and Country of each affiliation.

Manuscript-anonymized: Manuscript (A4) must be submitted in Microsoft Word Files (.doc or .docx). Please remove any identifying information, such as authors' names or affiliations, from your manuscript before submission and give all information about authors at title page section.

Reviewers suggestion *(mandatory)*: Please provide the names of 3 potential reviewers with the information about their affiliations and email addresses. *The recommended reviewers should not have any conflict of interest with the authors. Each of the reviewers must come from a different affiliation and must not have the same nationality as the authors.* Please note that the editorial board retains the sole right to decide whether or not the recommended potential reviewers will be selected.

**Preparation of Manuscript**

**Manuscript** should be prepared strictly as per guidelines given below. The manuscript (A4 size page) must be submitted in Microsoft Word (.doc or .docx) with Times New Roman 12 point font and a line spacing of 1.5. *The manuscript that is not in the correct format will be returned and the corresponding author may have to resubmit*. The submitted manuscript must have the following parts:

Title should be concise and no longer than necessary. Capitalize first letters of all important words, in Times New Roman 12 point bold.

Author(s) name and affiliation must be given, especially the first and last names of all authors, in Times New Roman 11 point bold.

Affiliation of all author(s) must be given in Times New Roman 11 point italic.

Abstract should indicate the significant findings with data. A good abstract should have only one paragraph and be limited to 250 words. Do not include a table, figure or reference.

Keywords should adequately index the subject matter and up to six keywords are allowed.

Text body normally includes the following sections: 1. Introduction 2. Methodology 3. Results and Discussion 4. Conclusions 5. Acknowledgements 6. References

Reference style must be given in Vancouver style. Please follow the format of the sample references and citations as shown in this Guide below.

Unit: The use of abbreviation must be in accordance with the SI Unit.

**Format and Style**

**Paper Margins** must be 2.54 cm on the left and the right. The bottom and the top margin of each page must be 1.9 cm.

**Introduction** is critically important. It should include precisely the aims of the study. It should be as concise as possible with no sub headings. The significance of problem and the essential background should be given.

**Methodology** should be sufficiently detailed to enable the experiments to be reproduced. The techniques and methodology adopted should be supported with standard references.

**Headings** in Methodology section and Results and Discussion section, no more than three levels of headings should be used. Main headings should be typed (in bold letters) and secondary headings (in bold and italic letters). Third level headings should be typed in normal and no bold, for example;

**2. Methodology**
**2.1 Sub-heading**
*2.1.1 Sub-sub-heading*

**Results and Discussion** can be either combined or separated. This section is simply to present the key points of your findings in figures and tables, and explain additional findings in the text; no interpretation of findings is required. The results section is purely descriptive.
Tables Tables look best if all the cells are not bordered; place horizontal borders only under the legend, the column headings and the bottom.
Figures should be submitted in color; make sure that they are clear and understandable. Please adjust the font size to 9-10, no bold letters needed, and the border width of the graphs must be 0.75 pt. *(Do not directly cut and paste them from MS Excel.)* Regardless of the application used, when your electronic artwork is finalized, please 'save as' or convert the images to TIFF (or JPG) and separately send them to EnNRJ. The images require a resolution of at least 300 dpi (dots per inch). If a label needed in a figure, its font must be "Times New Roman" and its size needs to be adjusted to fit the figure without borderlines.

*All Figure(s) and Table(s) should be embedded in the text file.*

**Conclusions** should include the summary of the key findings, and key take-home message. This should not be too long or repetitive, but is worth having so that your argument is not left unfinished. Importantly, don't start any new thoughts in your conclusion.

**Acknowledgements** should include the names of those who contributed substantially to the work described in the manuscript but do not fulfill the requirements for authorship. It should also include any sponsor or funding agency that supported the work.

**References** should be cited in the text by the surname of the author(s), and the year. This journal uses the author-date method of citation: the last name of the author and date of publication are inserted in the text in the appropriate place. If there are more than two authors, "et al." after the first author' name must be added. Examples: (Frits, 1976; Pandey and Shukla, 2003; Kungsuwas et al., 1996). If the author's name is part of the sentence, only the date is placed in parentheses: "Frits (1976) argued that . . ."

*Please be ensured that every reference cited in the text is also present in the reference list (and vice versa).*

**In the list of references** at the end of the manuscript, full and complete references must be given in the following style and punctuation, arranged alphabetically by first author's surname. Examples of references as listed in the References section are given below.

*Book*
Tyree MT, Zimmermann MH. Xylem Structure and the Ascent of Sap. Heidelberg, Germany: Springer; 2002.

*Chapter in a book*
Kungsuwan A, Ittipong B, Chandrkrachang S. Preservative effect of chitosan on fish products. In: Steven WF, Rao MS, Chandrkachang S, editors. Chitin and Chitosan: Environmental and Friendly and Versatile Biomaterials. Bangkok: Asian Institute of Technology; 1996. p. 193-9.

*Journal article*
Muenmee S, Chiemchaisri W, Chiemchaisri C. Microbial consortium involving biological methane oxidation in relation to the biodegradation of waste plastics in a solid waste disposal open dump site. International Biodeterioration and Biodegradation 2015;102:172-81.

*Published in conference proceedings*
Wiwattanakantang P, To-im J. Tourist satisfaction on sustainable tourism development, amphawa floating marketSamut songkhram, Thailand. Proceedings of the 1st Environment and Natural Resources International Conference; 2014 Nov 6-7; The Sukosol hotel, Bangkok: Thailand; 2014.

*Ph.D./Master thesis*

Shrestha MK. Relative Ungulate Abundance in a Fragmented Landscape: Implications for Tiger Conservation [dissertation]. Saint Paul, University of Minnesota; 2004.

*Website*

Orzel C. Wind and temperature: why doesn't windy equal hot? [Internet]. 2010 [cited 2016 Jun 20]. Available from: http://scienceblogs.com/principles/2010/08/17/wind-and-temperature-why-doesn/.

*Report organization:*

Intergovernmental Panel on Climate Change (IPCC). IPCC Guidelines for National Greenhouse Gas Inventories: Volume 1-5. Hayama, Japan: Institute for Global Environmental Strategies; 2006.

**Remark**

** Please be note that manuscripts should usually contain at least 15 references and some of them must be up-to-date research articles.*

** Please strictly check all references cited in text, they should be added in the list of references. Our Journal does not publish papers with incomplete citations.*

**Changes to Authorship**

This policy of journal concerns the addition, removal, or rearrangement of author names in the authorship of accepted manuscripts:

*Before the accepted manuscript*

For all submissions, that request of authorship change during review process should be made to the form below and sent to the Editorial Office of EnNRJ. Approval of the change during revision is at the discretion of the Editor-in-Chief. The form that the corresponding author must fill out includes: (a) the reason for the change in author list and (b) written confirmation from all authors who have been added, removed, or reordered need to confirm that they agree to the change by signing the form. Requests form submitted must be consented by corresponding author only.

*After the accepted manuscript*

The journal does not accept the change request in all of the addition, removal, or rearrangement of author names in the authorship. Only in exceptional circumstances will the Editor consider the addition, deletion or rearrangement of authors after the manuscript has been accepted.

**Copyright transfer**

The copyright to the published article is transferred to Environment and Natural Resources Journal (EnNRJ) which is organized by Faculty of Environment and Resource Studies, Mahidol University. The accepted article cannot be published until the Journal Editorial Officer has received the appropriate signed copyright transfer.

**Online First Articles**

The article will be published online after receipt of the corrected proofs. This is the official first publication citable with the Digital Object Identifier (DOI). After release of the printed version, the paper can also be cited by issue and page numbers. DOI may be used to cite and link to electronic documents. The DOI consists of a unique alpha-numeric character string which is assigned to a document by the publisher upon the initial electronic publication. The assigned DOI never changes.

Mahidol University

Wisdom of the Land

Research and Academic Service Section, Faculty of Environment and Resource Studies, Mahidol University
999 Phutthamonthon 4 Rd, Salaya, Nakhon Pathom 73170, Phone +662 441-5000 ext. 2108 Fax. +662 441 9509-10
E-mail: ennrjournal@gmail.com Website: https://www.tci-thaijo.org/index.php/ennrj